Neo-Classical Control of Structures

Mark E. Campbell

B.S., Mechanical Engineering, Carnegie Mellon University
Pittsburgh, Pennsylvania (1990)

Submitted to the Department of Aeronautics and Astronautics
in Partial Fulfillment of the Requirements for the Degree of

MASTER OF SCIENCE in AERONAUTICS AND ASTRONAUTICS

at the

MASSACHUSETTS INSTITUTE OF TECHNOLOGY

February 1993

Signature of Author _____
Department of Aeronautics and Astronautics
February 5, 1993

Certified by _____
Professor Edward F. Crawley
Department of Aeronautics and Astronautics
MacVicar Faculty Fellow

Accepted by _____
Professor Harold Y. Wachman
Chairman, Department Graduate Committee

Neo-Classical Control of Structures

by

Mark E. Campbell

Submitted to the Department of Aeronautics and Astronautics
on February 5, 1993 in Partial Fulfillment of Requirements
for the Degree of Master of Science

An experimental and analytical comparison of Neo-Classical and optimal control design techniques for controlled structures is conducted. Neo-Classical control design is a control methodology which blends the loop assignments and complex topological design of Linear Quadratic Gaussian controllers, the robustness of Sensitivity Weighted Linear Quadratic Gaussian controllers, and the lower order, robustness and practical insight of the classical controllers into a control strategy for structures. The asymptotic properties of the SISO LQG compensator are presented. The SISO disturbance rejection topology is divided into three distinct topologies, depending upon the performance and output being analogs, and/or the disturbance and input being analogs. For each of these topologies, assuming collocated, dual, and complementary extreme input output pairs, LQG and SWLQG compensators are designed for a typical section model, and interpreted classically, with the results summarized in a set of design rules. Adaptations to noncollocated input output pairs, and MIMO topologies are also addressed, and summarized in additional design rules. Neo-Classical compensators are designed for the typical section, and compared with the optimal techniques. Optimal and Neo-Classical compensators are designed and experimentally implemented on the Middeck Active Control Experiment, a test article for Controlled Structures Technology.

Thesis Supervisor:

Dr. Edward F. Crawley

Professor of Aeronautics and Astronautics and MacVicar Faculty Fellow

Acknowledgements

I would like to express my sincere appreciation to Ed for his guidance and support not only as a thesis supervisor, but also as a confidant and close friend. The experience has been very challenging and rewarding, and the future looks just as bright.

I would like to thank all the people in SERC, for all their help and encouragement, especially the MACE team and Dave Miller and Erik Saarmaa for their assistance.

I would like to express my gratitude to John Sesak and Warren Hoskins for their technical expertise and support.

I would like to especially thank my boys here in Boston: Yew-Poh, Jose, Norm, and Dave. We've had some great times and I know we have a lifetime bond. I would also like to thank my friends Charrissa, Becky, Dave D., Pete, and Eric S, and I cannot forget my roommate Kishore. I am also indebted to my friends outside Boston, who always remind me of how wonderful the outside world is.

I would like to give a special acknowledgement to my family. Your love and support has been an inspiration all along. You have the unique ability to encourage me to achieve, without actually pushing.

And finally I want to express my sincere gratefulness to my best friend and love, Tanya. Your love, support, and companionship have helped me keep what little sanity I began with, and I thank you very much for being there every day. ILY.

Table of Contents

List of Figures

List of Tables and Design Rules

Tables

Neo-Classical Design Rules

Chapter 1

Introduction

With the evolution of controlled structures, a control design methodology is required which delivers required performance with minimum compensator size and maximum robustness. The literature of the last decade is replete with optimal solutions to this problem, but few shed practical insight into the "philosophy" embedded within them, or the relationship to classical approaches. All optimal approaches attempt (and succeed to a greater or lesser degree) to address the four main issues in Controlled Structures Technology (CST) [Crawley and Hall (1991)]: robustness, order, complex topologies, and practical insight.

The first issue is closed loop robustness to model errors. In lightly damped structures, the model is extremely sensitive to errors, such that small parameter variations can lead to large variations in the frequency response. Errors such as these pose closed loop stability concerns for the control designer, and must be dealt with in the control design process.

A second issue in the control design for structures is the dimension of the compensator. In many optimal compensation techniques, the order of the

compensator is equal or greater than the mathematical model of the plant. The model, however, because of the high number of modes in a lightly damped structure, tends to be very large.

A third issue is the development of controllers for complex system topologies. The most basic of these is the multiple input multiple output (MIMO) problem, with the possibility of several performances and disturbances. The MIMO problem is very important for controlled structures.

The fourth and often overlooked issue in the control strategy for structures is the practical insight into the control design. Many techniques design a compensator which solves the problem theoretically, or provides disturbance rejection in this case. However, the practical implementation of many of the resulting compensators is infeasible, thus creating another challenge to the designer.

The objective of this work is to develop a control methodology for controlled structures which addresses these four primary issues, namely robustness, reduced order, complex topologies, and practical insight. This methodology is called Neo-Classical control. A parallel objective of this work is to examine existing control strategies, to identify their strengths and weaknesses in these four areas. Extending our understanding of the design of controllers for structures will lead to new optimal control strategies.

Much research on these four areas has been done in the field of controlled structures. Optimal control techniques, such as Linear Quadratic Gaussian (LQG) compensators lack robustness to model errors [Doyle (1978)], which is especially true for lightly damped structures. How (1993) divides the techniques for developing robust compensators into six distinct categories: polynomial, state space, μ, multiple model, stochastic, and de-sensitizing techniques. Each approach represents a fundamentally different way of modeling uncertainty and determining how the changes in the system influence stability. In each of these approaches, the goal is to

develop a system uncertainty, without being overly conservative.

Polynomial techniques analyze the characteristic equation to determine the stability of an uncertain system, such as the Routh-Hurwitz criterion [D'Azzo and Houpis (1988)] and Kharitinov's Theorem [Kharitonov (1978)]. The $\mathcal{H}_\infty$ or small gain approach has been developed to test the stability of the system with a single, complex uncertainty block [Doyle *et al.* (1989)]. An extension of this work has been to couple the $\mathcal{H}_\infty$ uncertainty test with an $\mathcal{H}_2$ performance objective [Haddad and Bernstein (1990)]. In order to reduce the conservatism inherent in a single block, the μ-synthesis technique was developed [Doyle (1985)] which uses a structured complex uncertainty. However, these approaches are known to be conservative for systems with constant real parameter uncertainties. Therefore, real μ and mixed μ techniques have recently been developed for real parameter uncertainties [Doyle (1985)], [Morton and McAfoos (1985)], and [Fan *et al.* (1991)]. Recent work by How (1993) has introduced a combined $\mathcal{H}_2$/real μ approach to robust control. Where as before, there is an $\mathcal{H}_2$ performance objective, but a much tighter bound on the real parameter uncertainty.

Multiple model techniques have been used for many years [Ashkenazi and Bryson (1982)] and [Ly (1982)]. It is recently that they have been used to gain robustness to parametric uncertainty for the control of structures [MacMartin *et al.* (1991)] and [Grocott *et al.* (1992)]. The objective is to design a single compensator for several models of an uncertain system, consisting of the nominal system and the expected parameter variations. Hyland (1982) presents a stochastic technique called the Maximum Entropy approach, where a multiplicative white noise model is used to capture the parameter uncertainty of the system. The final technique, called de-sensitization, attempts to directly address the sensitivity problems of LQG compensators. For example, Blelloch and Mingori (1990) modify the state and noise weighting matrices in the LQG compensator to account for structured parametric

uncertainty, thus reducing the optimality. Sesak and Likins (1988) add sensitivity states, which penalize the variation of the performance objective with respect to parameter variations. These states can be eliminated from the model using a singular perturbation technique.

Although many of these techniques provide robust compensation, a tradeoff is usually a larger order compensator, leading to the second primary area of controlled structures.

Most of the work in compensator order reduction falls into three categories: full order model reduction followed by compensator design; compensator design on the full order model followed by compensator order reduction; and optimal, fixed order compensator Both reduction techniques can be accomplished by similar methods, such as the cost analysis approach [Skelton *et al.* (1982)] and [Yousuff and Skelton (1984)] or internal balancing [Moore (1981)]. Model reduction followed by compensator design suffers from observation and control spillover from unmodeled and higher frequency dynamics [Balas (1978)]. Optimal Projection techniques such as those developed by Bernstein and Hyland (1986), produce an optimal, fixed order compensator. A key difficulty with this, and other numerical techniques, is an initial guess is required. The numerical problem is difficult, and when it is solved, there is no guarantee that the solution is at the global minimum. Therefore, the most prominent compensator order reduction algorithm is compensator design on the full order model, followed by compensator reduction. A survey of the different controller reduction algorithms was done by Hyland and Richter (1990).

Techniques have also been developed which address both of these issues, robustness and controller reduction. Any of the robustness techniques that require a numerical solution can combine these two constraints. Bernstein and Haddad (1988) show how to incorporate real structured uncertainty into the Optimal Projection equations. Bernstein and Hyland (1988) combined the insights of

Maximum Entropy and Optimal Projection.

The third issue in the control strategies for structures is the development of compensators for complex topologies, such as MIMO control and noncollocated control. Fixed architecture control designs, such as sensor actuator loop assignments, however, can not be addressed by the original formulation of LQG. Mercadel (1990) addresses the fixed architecture $\mathcal{H}_2$ designs. In the classical framework, topologies such as the MIMO problem are a significant weakness.

SISO classical design techniques [D'Azzo and Houpis (1988)] are simple and easy to interpret. Wie and Byun (1989) developed SISO structural filters such as nonminimum phase notch filters for noncollocated control. Wie *et al.* (1991) also used classical design for disturbance rejection of narrow band disturbances.

A variety of techniques have been developed for the classical control of MIMO plants. Unfortunately, many of them, such as sequential loop closure [Maciejowski (1989)] are *ad hoc*. Techniques have been developed [Mayne (1979)] to decouple the problem into a series of SISO problems. However, in controlled structures, this decoupling destroys the pole zero patterns of certain loops, such as those with alternating poles and zeros. Characteristic locus methods have been developed [Kuvaritakis (1979)] which establish an approximate communitive compensator by manipulating the characteristic loci. Other methods include Nyquist array techniques [Rosenbrock (1970)] and reversed-frame normalization [Hung and MacFarlane (1982)], which is quite difficult to solve for the MIMO problem.

Although the MIMO problem and other complex topologies such as noncollocated control are still significant weaknesses in classical techniques, significant practical insights can be learned using these methods, leading to the final issue in control strategies for structures. In the classical design of SISO systems, the control designer uses practical insight which can be meaningful when experimentally implementing compensators. Often in the optimal or robust design

techniques, although the resulting compensator mathematically works, the implementation of the compensator is infeasible. Practical insight can be used in examining the compensator resulting from the optimal technique, and then changing the formulation of the problem to fit the designer's needs. The classical techniques allow the control designer more interaction throughout the control design process.

The approach of this work is to examine an optimal technique for the control design of certain SISO structural control topologies. Then, a robustfied optimal control technique will be used to show robust compensators for the same topologies. These optimal control techniques will then be interpreted using the practical insight of classical design, with the results presented in a set of design rules for low order, robust SISO compensators. Finally, compensators are designed and implemented experimentally, including both SISO systems and an adaptation to MIMO systems.

Compensators will be designed and examined on a smaller order model called a typical section [Miller *et al.* (1990)]. The typical section model encompasses all of the important details of a controlled structure, i.e. collocated and noncollocated control, and MIMO control, without the complexities of the experiment, i.e. sensor actuator dynamics, and computer processor lags.

In order to develop low order, robust MIMO controllers designed with the practical insight of the control designer, a variety of tools will be used. The Linear Quadratic Gaussian (LQG) compensator [Kwakernaak and Sivan (1972)] will be examined because of its ability to handle the MIMO problem, and other difficult topologies such as noncollocated inputs, outputs, disturbances, and performances. The Sensitivity Weighted LQG controller (SWLQG) [Grocott and Sesak (1992)] will be used as a robustification tool for the LQG compensator. Through changes in the weighting matrices, the SWLQG compensator robustifies the LQG compensator to changes in modal frequencies.

The LQG and SWLQG compensators, and a truncation of these compensators designed for SISO topologies, will be thoroughly examined to understand the optimal compensation techniques of the LQG compensators, the robustification techniques of the SWLQG compensators, and how truncation of different modes in the compensator affects the closed loop stability. All of the issues of control strategy for structures will be examined, namely robustness, order, complex topological design, and practical interpretation using classical insights. The results are summarized in a set of rules for the control design strategy called Neo-Classical control design. Neo-Classical Control blends the loop assignments and complex topological design of the LQG controllers, the robustness of the SWLQG controllers, and the lower order, robustness and practical insight of the classical controllers, into a control strategy for controlled structures.

Chapter 2 develops background information needed for the foundation of Neo-Classical control design. The problem format is presented, which is a disturbance rejection performance requirement. The optimal LQG and SWLQG controller designs are presented, along with their asymptotes, followed by a short discussion of classical control design techniques. The SISO topologies examined in the following chapters are presented, along with a discussion of the importance of the pole zero patterns of the input output pairs. The typical section used throughout the work is introduced. It is a four mode, Rayleigh-Ritz model of a cantilever beam. The Middeck Active Control Experiment (MACE) is also introduced. MACE is a NASA In-Step and Control Structure Interaction (CSI) Office funded Shuttle middeck experiment, with the launch expected in the summer of 1994. The MACE test article is used as a verification of the different control design techniques experimentally.

Chapters 3, 4, and 5 examine three SISO topologies of the disturbance rejection problem, which depend upon the relationships between the four variables,

the input, output, disturbance, and performance. If the performance and output are collocated and dual, then they are said to be *analogs*. If the disturbance and input are collocated and dual, then they are also said to be *analogs*. Chapter 3 examines the SISO disturbance rejection topology when the performance and output are analogs, *and* the disturbance and input are analogs. Chapter 4 examines the SISO disturbance rejection topology when the performance and output are analogs, *or* the disturbance and input are analogs. And Chapter 5 examines the SISO disturbance rejection topology when neither the output and performance are analogs, nor the input and disturbance are analogs.

The format of Chapters 3, 4, and 5 are very similar. The input output pairs are collocated, dual, and complementary extreme, creating an alternating pole zero pattern. LQG and SWLQG compensators designed on the typical section will be examined and interpreted classically. The results are presented in a Neo-Classical Design Rule. This rule is then used to design low order robust compensators for the typical section. Experimental closed loop results of LQG, SWLQG, truncated LQG, and Neo-Classical compensators designed and implemented on the MACE test article are the presented.

In Chapters 3, 4, and 5, an assumption of the pole zero pattern of the input output pair transfer function is made, i.e. alternating poles and zeros. This is a result of the input output pair being collocated, dual, and complementary extreme. Chapter 6 examines the implications on the control design when this is not the case, or when the input output pair is noncollocated. Similar topologies to those is the previous chapters are used, and the format of the chapter is also similar. Optimal controllers are designed and interpreted into another Neo-Classical Design Rule, and a closed loop experiment using a Neo-Classical compensator for a topology on the MACE test article with a noncollocated sensor actuator pair is presented.

Chapter 7 examines the MIMO problem, with two inputs, two outputs, one

disturbance, and one performance. The Neo-Classical Design Rules presented in the previous chapters are used to design MIMO compensators for implementation experimentally on the MACE test article using two techniques: High Authority Control/Low Authority Control (HAC/LAC) [Gupta *et al.* (1982)] and Sequential Loop Closure. LQG, and SWLQG compensators were also designed and implemented experimentally, for comparison to the classical MIMO compensators. The subject of MIMO topologies is a very large and complex issue, and this chapter is used to show the abilities of the Neo-Classical Control to adapt to the MIMO problem.

Chapter 2

Background

2.1 Introduction

This chapter describes tools and background information which will be used throughout this document to develop Neo-Classical control design for structures. Included in this chapter is the problem formulation for performance robustness and disturbance rejection. The optimal control techniques used such as Linear Quadratic Gaussian (LQG) and Sensitivity Weighted Linear Quadratic Gaussian (SWLQG) will be discussed, along with classical control techniques such as loop shaping, filtering, and PID control. Single input single output systems will be examined in more detail, including loop shaping for different control topologies, and pole zero patterns for actuator sensor pairs. A four mass typical section model is presented, which is used as a vehicle for illustrating the different control techniques. And finally, the Middeck Active Control Experiment (MACE) will be introduced as a platform for demonstrating control designs experimentally.

2.2 Problem Format

The primary objective in many control designs, especially for controlled structures, is disturbance rejection. For multibody space structures, disturbances may enter a structure at a variety of different points and with many different frequency contents. Figure 2.1 shows a typical control system with disturbances w, performances z, inputs u, and outputs y. The G block is the open loop system, while the designed compensator K is shown connecting the outputs to the inputs.

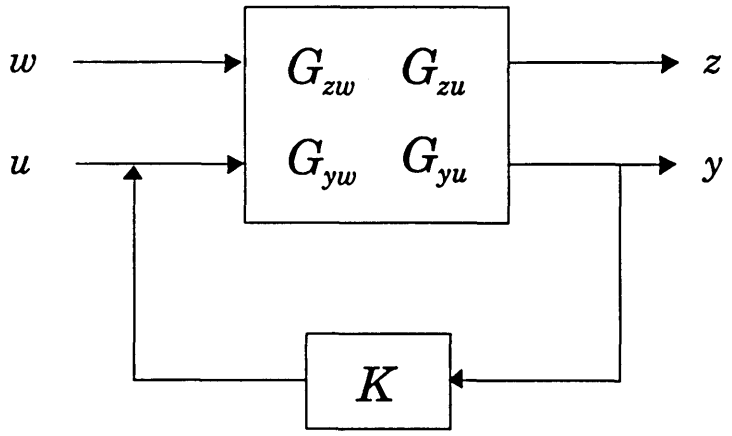

Figure 2.1. Standard control system with disturbances w, inputs u, performances z, and outputs y.

In multiple input, multiple output (MIMO) form, the above system is given by

$$\begin{Bmatrix} z \\ y \end{Bmatrix} = \begin{bmatrix} G_{zw} & G_{zu} \\ G_{yw} & G_{yu} \end{bmatrix} \begin{Bmatrix} w \\ u \end{Bmatrix} \tag{2.1}$$

For a control law

$$u = -Ky \tag{2.2}$$

the MIMO closed loop transfer function from the disturbances to the performances is

$$\frac{z}{w} = G_{zw} - G_{zu}K\left(I + G_{yu}K\right)^{-1}G_{yw} \tag{2.3}$$

and the stability of the closed loop system can be evaluated using the multivariable nyquist criterion: If a system $G_{yu}K$ has p unstable poles, then the closed loop system is stable if and only if the polar plot of $N(j\omega)$ encircles the (-1,0) point with p counterclockwise encirclements, where $N(j\omega)$ is given by

$$N(j\omega) = DET\left(I + G_{yu}(j\omega)K(j\omega)\right) - 1 \tag{2.4}$$

2.3 Optimal Controllers

Linear Quadratic Gaussian (LQG) controllers [Kwakernaak and Sivan (1972)] are the standard to which most control designs are compared, because of optimality and simplicity. In the control design for structures, the strengths of LQG design are its ability to develop MIMO compensators, including both multiple performances and disturbances, and to develop compensators for complex topologies, such as noncollocated input output pairs. LQG design, however, lacks robustness to model errors [Doyle (1978)]. For structural plants, a slight mismodeling could lead to a large phase difference between the model and the actual plant. These errors could easily lead to unstable closed loop systems, especially for relatively nonrobust LQG compensators. The dimension of the LQG compensator, equal to that of the plant, is also a weakness. The large dimension of models for structures could prevent the actual implementation of such large LQG compensators. Despite their known weaknesses, LQG compensators will be

used as a reference in this work.

LQG compensators are H_2 optimal compensators designed by solving two separate problems, the first of which is the Linear Quadratic Regulator (LQR) problem [Kalman (1960)]. Consider the following plant,

$$\dot{x} = Ax + B_u u + L_w w \tag{2.5}$$

$$y = C_y x + v \tag{2.6}$$

$$z = C_z x \tag{2.7}$$

where x represents the states, y the outputs, u the inputs, z the performances, w the disturbances, and v the sensor noise. In the LQR problem, a deterministic cost is given by

$$J = \int_0^\infty \left(z^T z + u^T R u\right) dt = \int_0^\infty \left(x^T Q x + u^T R u\right) dt \tag{2.8}$$

where Q and R are positive semidefinite and positive definite weighting matrices respectively, or

$$Q = C_z{}^T C_z \geq 0 \tag{2.9}$$

$$R > 0 \tag{2.10}$$

The result of the LQR problem is a matrix of optimal gains for state feedback

$$u = -Gx \tag{2.11}$$

which minimizes the cost given in Equation 2.8.

The second part of the LQG problem is the standard Kalman Filter [Kalman and Bucy (1961)], and is dual to the LQR problem. For the Kalman filter,

an estimate $\hat{x}$ of the states is made by using knowledge of the outputs of the system, corrupted by sensor noise, and knowledge of the previous estimates. The disturbance and sensor noise assumed to be zero mean, Gaussian processes that are uncorrelated in time, and have the following covariances

$$W = E\{ww^T\} \geq 0 \tag{2.12}$$

$$V = E\{vv^T\} > 0 \tag{2.13}$$

The optimal estimate $\hat{x}$ of the states x is found by minimizing the expected error

$$J_{KF} = E\{(x-\hat{x})^T(x-\hat{x})\} \tag{2.14}$$

The result of the Kalman Filter problem is a matrix of optimal gains H that produces an optimal estimate of the states $\hat{x}$, with the following estimator dynamics

$$\dot{\hat{x}} = A\hat{x} + B_u u + H(y - C_y\hat{x}) \tag{2.15}$$

The LQG compensator is formed by combining the LQR and Kalman Filter solutions into a model based compensator, by using the estimate of the states, $\hat{x}$, from the Kalman Filter problem as if these were the exact states, x, in the LQR problem. The LQG compensator then becomes

$$K(s) = G(sI - A + B_u G + HC_y)^{-1} H \tag{2.16}$$

In the LQG problem, the weighting matrices R and V are defined as

$$R = \rho R_o \tag{2.17}$$

$$V = \mu V_o \tag{2.18}$$

where ρ and μ are positive scalar weightings, and R_o and V_o are diagonal matrices in the LQR and Kalman Filter problems. The weighting ρ defines the relative importance between minimizing the performance z versus control effort u, while μ defines the relative importance between minimizing the disturbance w versus sensor noise v.

In this work, the single input single output (SISO) LQG compensator will be examined thoroughly. In order to show the locations of the compensator poles and zeros, a summary of the asymptotic properties of the SISO LQG compensator will be presented. The derivations are shown in Appendix A. For the general disturbance rejection problem, the SISO LQG compensator simplifies to

$$K(s) = \frac{G\Phi H}{1 + G\Phi B_u + C_y \Phi H} \tag{2.19}$$

where Φ is the state transition matrix $(sI\text{-}A)^{-1}$. In most cases, the Kalman Filter gain μ is smaller than the LQR gain ρ, in an effort to make the state estimator dynamics faster than the state feedback dynamics. Therefore, the relevant asymptotical limits of the SISO LQG compensator are for small values of the Kalman Filter weighting μ, and varying values of the LQR weighting ρ.

The SISO LQG compensator for low noise, or small values of μ, and expensive control, or large values of ρ, is given by

$$\underset{\substack{\mu \to 0 \\ \rho \to \infty}}{LIM}\, K(s) = \frac{G\Phi B_w}{C_y \Phi B_w} = \frac{G\Phi B_w}{g_{yw}} \tag{2.20}$$

Note: For the MIMO problem, this compensator can be written as

$$\underset{\substack{\mu \to 0 \\ \rho \to \infty}}{LIM}\, K(s) = G\Phi B_w \left[C_y \Phi B_w \right]^{-1} \tag{2.21}$$

This states that the zeros of the SISO LQG compensator for low noise and expensive control, tend to the zeros of the $G\Phi B_w$ transfer function, and the poles tend to the zeros of the g_{yw} transfer function. This compensator is dependent upon the assumption that the transfer function g_{yw} is minimum phase. Also, the rate in which the compensator converges to this asymptote is dependent upon the pole zero pattern of g_{yw}. For instance, the LQG compensator will approach the asymptote more quickly if g_{yw} has alternating poles and zeros, instead of poles and missing zeros.

The LQR gain matrix G was solved by MacMartin (1990) for the expensive LQR control case

$$\underset{\rho\to\infty}{LIM}\, G = \frac{1}{\sqrt{\rho}} \sum_i \sqrt{v_i^H Q v_i} \left[\frac{\left(w_i^H B_u\right)^H}{\left|w_i^H B_u\right|} \right] w_i^H \tag{2.22}$$

where v_i and w_i are the right and left eigenvectors of the system matrix A, and the superscript H denotes a complex conjugate transpose. For single input single output systems, the entire quantity is a constant, except for the last term, w_i^H. The optimal LQR feedback gains are seen from Equation 2.22 to be a weighted combination of the left eigenvectors. Lazarus (1991) showed that in the expensive control case, the gains are nonzero only for the rate states. The LQR compensator is equivalent to a rate feedback sensor.

For an undamped, single mode example, the LQG compensator, for low noise and expensive control, reduces to

$$\underset{\substack{\mu\to 0 \\ \rho\to\infty}}{LIM}\, K(s) = \frac{k_{LG}}{\sqrt{\rho}} \frac{s}{s^2+\omega^2} \left[g_{yw} \right]^{-1} \tag{2.23}$$

$$\underset{\substack{\mu\to 0\\ \rho\to\infty}}{LIM}\, K(s) = \frac{k_{LG}}{\sqrt{\rho}} \frac{s}{s^2+\omega^2}\left[\frac{s}{s^2+\omega^2}\right]^{-1} \tag{2.24}$$

$$\underset{\substack{\mu\to 0\\ \rho\to\infty}}{LIM}\, K(s) = \frac{k_{LG}}{\sqrt{\rho}} \frac{s}{s} = \frac{k_{LG}}{\sqrt{\rho}} \tag{2.25}$$

where k_{LG} is a scalar constant. The compensator in this case is a low gain, constant feedback of the rate state, which is the output y. Note that the compensator contains a pole zero cancellation at zero, and a pole zero cancellation at infinity. For a two undamped modes example, the compensator is given by

$$\underset{\substack{\mu\to 0\\ \rho\to\infty}}{LIM}\, K(s) = \frac{k_{LG}}{\sqrt{\rho}} \frac{s\left(r_1\left(s^2+\omega_{p2}^2\right)+r_2\left(s^2+\omega_{p1}^2\right)\right)}{\left(s^2+\omega_{p1}^2\right)\left(s^2+\omega_{p2}^2\right)}\left[g_{yw}\right]^{-1} \tag{2.26}$$

$$\underset{\substack{\mu\to 0\\ \rho\to\infty}}{LIM}\, K(s) = \frac{k_{LG}}{\sqrt{\rho}} \frac{s\left(r_1\left(s^2+\omega_{p2}^2\right)+r_2\left(s^2+\omega_{p1}^2\right)\right)}{\left(s^2+\omega_{p1}^2\right)\left(s^2+\omega_{p2}^2\right)}\left[\frac{s\left(s^2+\omega_{z1}^2\right)}{\left(s^2+\omega_{p1}^2\right)\left(s^2+\omega_{p2}^2\right)}\right]^{-1} \tag{2.27}$$

$$\underset{\substack{\mu\to 0\\ \rho\to\infty}}{LIM}\, K(s) = \frac{k_{LG}}{\sqrt{\rho}} \frac{s\left(r_1\left(s^2+\omega_{p2}^2\right)+r_2\left(s^2+\omega_{p1}^2\right)\right)}{s\left(s^2+\omega_{z1}^2\right)} \tag{2.28}$$

where r_1 is the residue of the first mode and r_2 is the residue of the second mode in the transfer function $G\Phi B_w$. For this case, the poles of the compensator are the zeros of the g_{yw} transfer function. The compensator zeros, however, have a zero at zero, and a pair of zeros which are a weighted average of the poles of the open loop system. For the case where the first mode is most dominant, or r_1 is much greater than r_2, the asymptote simplifies to

$$\underset{\substack{\mu\to 0\\ \rho\to\infty\\ r_1>r_2}}{LIM}\, K(s) = \frac{k_{LG} r_1}{\sqrt{\rho}} \frac{s\left(s^2+\omega_{p2}^2\right)}{s\left(s^2+\omega_{z1}^2\right)} \tag{2.29}$$

For the undamped, two mode example, with only one dominant mode, the low gain LQG compensator with small noise not only uses rate feedback, but the less dominant mode is also inverted. Note that the compensator also has a pole zero cancellation at zero, and a pole zero cancellation at infinity. This leads to a generalized statement for the SISO expensive control, low noise LQG asymptote

$$\underset{\substack{\mu\to 0\\ \rho\to\infty}}{LIM}\, K(s) = \frac{G\Phi B_w}{g_{yw}} = \frac{k_{LG}}{\sqrt{\rho}} \frac{s}{s^2 + 2\zeta_{dm}\omega_{dm}s + \omega_{dm}^2} \frac{1}{g_{yw}} \tag{2.30}$$

where ζ_{dm} and ω_{dm} are the damping ratio and frequency of the most dominant mode, and k_{LG} is a scalar constant. Note that the residue of the most dominant modes has been absorbed into the scalar constant k_{LG}. This compensator is called the low gain LQG asymptote. The poles of this compensator are the zeros of the disturbance to output transfer function g_{yw}, and the zeros include a zero at zero for rate feedback, and the poles of the g_{yw}, except for the dominant pole pair.

The SISO LQG compensator for low noise, or small values of μ, and cheap control, or small values of ρ, as shown in Appendix A to be

$$\underset{\substack{\mu\to 0\\ \rho\to 0}}{LIM}\, K(s) = \frac{\pm\frac{1}{\sqrt{\rho}}\frac{1}{\sqrt{\mu}} C_z\Phi B_w}{\pm\frac{1}{\sqrt{\rho}} C_z\Phi B_u \pm\frac{1}{\sqrt{\mu}} C_y\Phi B_w} = \frac{\pm\frac{1}{\sqrt{\rho}}\frac{1}{\sqrt{\mu}} g_{zw}}{\pm\frac{1}{\sqrt{\rho}} g_{zu} \pm\frac{1}{\sqrt{\mu}} g_{yw}} \tag{2.31}$$

This result states that the zeros of the low noise, cheap control SISO LQG compensator tend to the zeros of g_{zw}, and the poles tend to a weighted combination of the zeros of g_{zu} and g_{yw}. This compensator is dependent upon the assumptions that the transfer functions g_{yw} and g_{zu} are minimum phase. However, in addition to being minimum phase, the low noise, cheap control LQG asymptote is also dependent upon the actual pole zero structure of g_{yw} and g_{zu}, as was the low gain LQG asymptote. For instance, the convergence of the LQG compensator to the

asymptotical limit in Equation 2.31 is much faster if the pole zero patterns of g_{yw} and g_{zu} consist of alternating poles and zeros.

For the case where the Kalman Filter weighting is smaller than the LQR weighting, or the estimator dynamics are faster than the state feedback dynamics, the high gain LQG asymptote simplifies to

$$\underset{\substack{\mu\to 0\\ \rho\to 0\\ \rho>\mu}}{LIM}\, K(s) = \pm\frac{1}{\sqrt{\rho}}\frac{g_{zw}}{g_{yw}} \tag{2.32}$$

If g_{yw} and g_{zu} have alternating pole zero patterns, and the asymptotical limits in Equations 2.30 and 2.32 are valid, the poles of the LQG compensator remain constant, set at the zeros of the disturbance to output transfer function, g_{yw}. The zeros, however, range from a zero at zero, and the open loop poles except for the most dominant mode in the low gain LQG asymptote (Equation 2.30), to the zeros of the disturbance to performance transfer function, g_{zw}, in the high gain asymptote (Equation 2.32).

Many approaches have been attempted to address the principle weakness of the LQG compensator, robustness [Ashkenazi and Bryson (1982)] and [MacMartin *et al.* (1991)]. In order to examine a typical optimal compensator which is more robust compensator than LQG, the Sensitivity Weighted Linear Quadratic Gaussian (SWLQG) [Grocott and Sesak (1992)] will also be used as a reference. The SWLQG compensator *de-sensitizes* the original LQG compensator to changes in modal frequency. In SWLQG design, the open loop system, (Equations 2.5-2.7), is first transformed into modal form. The transformation is similar to the Jordan tranformation [Strang (1980)]. If the eigenvalues and eigenvectors of A are given by

$$(\lambda_i I - A)v_i = 0 \tag{2.33}$$

then the corresponding transform for a real eigenvalue is the corresponding eigenvector, or

$$T_{n\times i} = [v_{n\times i}] \tag{2.34}$$

And the corresponding transform for a complex conjugate set of eigenvalues is the real and imaginary part of the corresponding eigenvector, or

$$T_{n\times i} = [\mathrm{Re}(v_{n\times i}) \quad \mathrm{Im}(v_{n\times i})] \tag{2.35}$$

With this transformation, the A matrix will be diagonal for real eigenvalues, and a 2x2 block for complex eigenvalues. The 2x2 block for each structural mode in the model is then in modal form

$$A_{2\times 2} = T^{-1}AT = \begin{bmatrix} -\omega_n\sqrt{1-\zeta^2} & -\zeta\omega_n \\ \zeta\omega_n & -\omega_n\sqrt{1-\zeta^2} \end{bmatrix} \tag{2.36}$$

In modal form, the A matrix is block diagonal and there is a one degree of freedom set of equations for each mode. The states of the transformed system are called modal coordinates.

In the SWLQG procedure, the weighting matrices Q and W of the LQR and Kalman Filter problems are appended with another matrix

$$Q_{SW} = Q + \Delta Q \tag{2.37}$$

$$W_{SW} = W + \Delta W \tag{2.38}$$

The appended matrix is all zeros except for a 2x2 block corresponding to the mode being de-sensitized. This 2x2 block is the same block from the original matrix,

multiplied by a positive scalar factor for sensitivity.

As an example, for a 4x4 system in modal form, if the second mode of the system is de-sensitized, the A matrix, and the corresponding Q and W weighting matrices would be

$$A = \begin{bmatrix} a_{11} & 0 \\ 0 & a_{22} \end{bmatrix} \tag{2.39}$$

$$Q_{SW} = Q + \Delta Q = \begin{bmatrix} q_{11} & q_{12} \\ q_{21} & q_{22} \end{bmatrix} + \beta \begin{bmatrix} 0 & 0 \\ 0 & q_{22} \end{bmatrix} \tag{2.40}$$

$$W_{SW} = W + \Delta W = \begin{bmatrix} w_{11} & w_{12} \\ w_{21} & w_{22} \end{bmatrix} + \beta \begin{bmatrix} 0 & 0 \\ 0 & w_{22} \end{bmatrix} \tag{2.41}$$

where a_{ij}, q_{ij}, and w_{ij} are all 2 x2 blocks.

The de-sensitizing factor β is the choice of the control designer, as it is dependent on the mode, bandwidth of the system and other factors of the particular structural control problem. With the open loop system in this form, the SWLQG procedure *de-sensitizes* the compensator to frequency changes by increasing the apparent cost of the mode. This increase will prevent possible inversion of the mode, thus robustifying the standard LQG compensator for that particular mode. Other robustness issues such as changes in damping can also be addressed by SWLQG, but with a different appended matrix [Grocott and Sesak (1992)].

The large dimension of the compensators is another of weakness of LQG compensators [Yousuff and Skelton (1984)] and [Moore (1981)]. Model truncation followed by compensator design and compensator design followed by compensator truncation are two approaches to achieving a lower order compensator. In both truncation techniques, spillover is the dominant problem [Balas (1978)]. In this

work, the 40 state LQG compensators were truncated using a Hankel Singular Value analysis [Kaileth (1980)] and [Matlab (1990)]. The analysis ranks the modes based upon their residues, or combined controllability and observability of the modes. Those with modes with smaller Hankel Singular Values are discarded. The resulting compensator, however, will not be optimal in minimizing the performance metric.

2.4 Classical controllers

Classical control design has been applied successfully to many types of applications [D'Azzo and Houpis (1988)]. The benefits include controllers that are robust to model errors, and the dimension of the compensators are usually smaller than that of the plant. Classical compensators also capture the physical insight of the control designer. These benefits of classical control mirror the weaknesses of LQG compensators. The complement is also true. MIMO designs are difficult to derive and understand using classical control. The choice and sequence of loops to closed is a complex and iterative process. Nevertheless, the benefits of classical control design make it valuable as a reference as well.

For classical control design for disturbance rejection, a frequency domain analysis such as Bode or Nyquist is preferred. Time domain performance metrics such as step response or jitter requirements can be interpreted in the frequency domain.

The closed loop system of a SISO classical design can be shown as

$$z = \frac{G}{(1+GK)}w + \frac{GK}{(1+GK)}v = S(s)w + C(s)v \tag{2.42}$$

where z is the performance, w is the disturbance, and v is the sensor noise. The

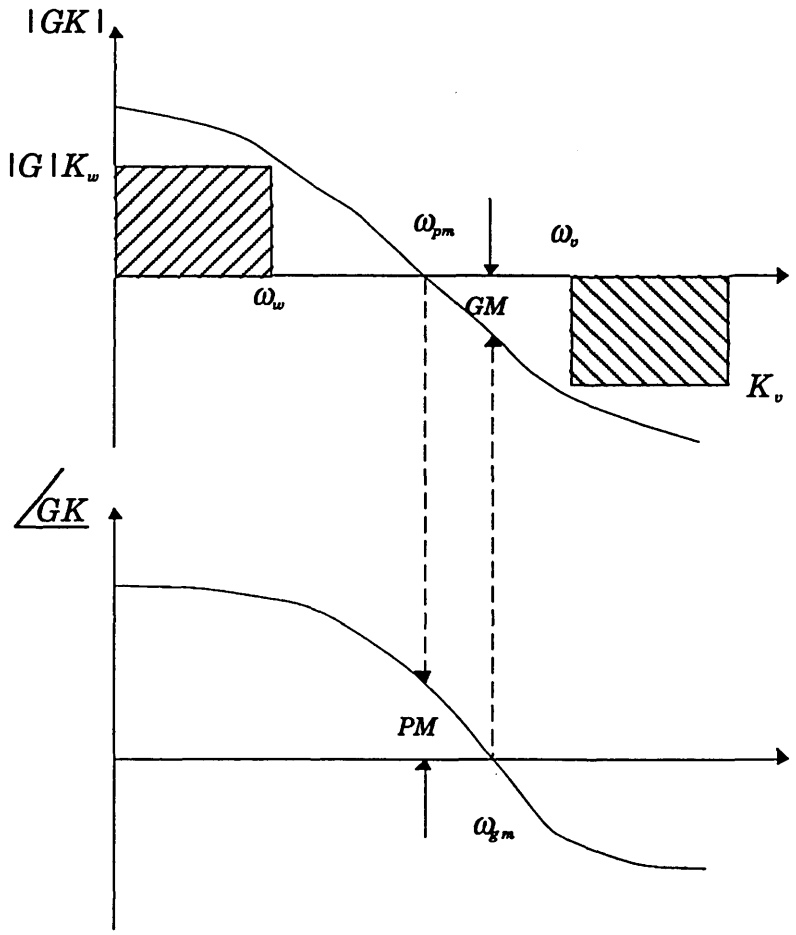

Figure 2.2. Classical design of control systems in the frequency domain for disturbance rejection and noise reduction.

open loop transfer function from the input u to the output y is G, and the compensator is K. For this system, the disturbance is equivalent to the input, and the performance is equivalent to the output. *S(s)* and *C(s)* are defined as the sensitivity and complementary sensitivity functions.

Typically, the disturbance has a low frequency content, while the noise has a high frequency content. Figure 2.2 shows a Bode plot of a typical loop transfer function *GK*, used to design the closed loop system with a disturbance w and noise v. At low frequency, when disturbance rejection is more important than the influence of sensor noise, the closed loop system becomes

$$z = \frac{G}{1+GK} w \tag{2.43}$$

In order to reduce the effect of the disturbance, the magnitude of GK is made large. If the closed loop design objective is to reduce the magnitude of the disturbance by a specified amount, over a specified frequency range, then the closed loop system can be given by

$$\left|\frac{z}{w}\right| = \left|\frac{G}{GK}\right| = \frac{1}{K_w} \tag{2.44}$$

K_w is used to represent how far and over what frequency range the disturbances are rejected in the design, and can be applied to the control design graphically, as shown in Figure 2.2.

Similarly, at high frequency, when the reduction of sensor noise is more important than the influence of the disturbance, the closed loop system becomes

$$\left|\frac{z}{v}\right| = |GK| = K_v \tag{2.45}$$

K_v is used to represent how far and over what frequency range the noises are rejected in the design, and is also shown as a graphical design tool in Figure 2.2. The design of the loop transfer function GK using these requirements is called loop shaping.

For structural control design, classical loop shaping achieves phase stabilization within the bandwidth, and gain stabilization beyond the bandwidth by employing techniques such as PID control and first and second order filters. Figure 2.3(a) shows a second order notch filter. The choice of damping ratio ζ_0 controls the *width* of the notch, while α controls the *depth* of the notch. Another type of notch filter, called a nonminimum phase notch filter, has been used as a

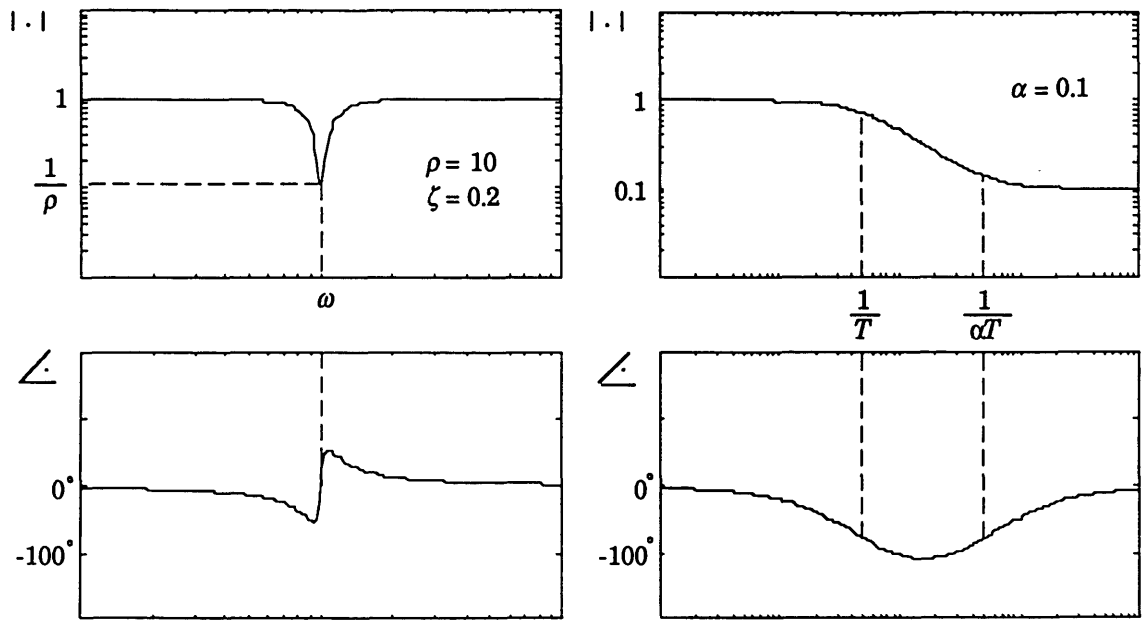

$$\frac{s^2 + 2\zeta_o \omega s + \omega^2}{s^2 + 2\alpha\zeta_o \omega s + \omega^2} \qquad k\frac{Ts+1}{\alpha Ts+1}$$

(a) (b)

Figure 2.3. Filtering techniques: (a) Second order notch filter (b) First order lag filter.

classical tool for noncollocated loops [Wie and Byun (1989)]. This notch filter is the same as that shown in Figure 2.3(a), except the zeros in the numerator are nonminimum phase. The magnitude for each is the same, while the phase drops rapidly because of the nonminimum phase zeros. This phase drop allows the designer to phase stabilize, or add damping, to certain modes. The nonminimum phase notch can be made by using negative values for both ζ_o and α.

Figure 2.3(b) shows a first order lag filter, which is used in loop shaping. The choices of T, k and α are utilized in the loop shaping process. They also can be used in root locus techniques, by adding a pole zero pair to shape the root locus.

Classical compensators also contain rolloff dynamics. These dynamics are used to ensure closed loop stability from modes above the bandwidth of the system,

and to reduce the effects of sensor noise, as shown in Figure 2.2. Types of rolloff include one real pole, and two heavily damped poles.

The clarity and simplicity of classical control design of SISO systems is not evident when moving to MIMO systems. A variety of classical control designs for MIMO systems has been developed [Maciejowski (1989)], but interactions between the loops, choices of loops and loop assignments, and designing compensators for multiple performance metrics and disturbances have accentuated the shortcoming of classical control design in the compensation of MIMO systems. One option for classical compensation of MIMO systems is sequential loop closure, shown in Figure 2.4. In this procedure, loops are designed and closed sequentially, beginning with the highest bandwidth loop. The second loop is closed around the new plant, which incorporates the first compensator. If the first loop closed is a high bandwidth, high gain loop, then the next loop closed with a lower bandwidth will not have harmful effects on the first closed loop. The resulting MIMO compensator is created by designing each loop independently.

A form of sequential loop closure is High Authority Control/Low Authority

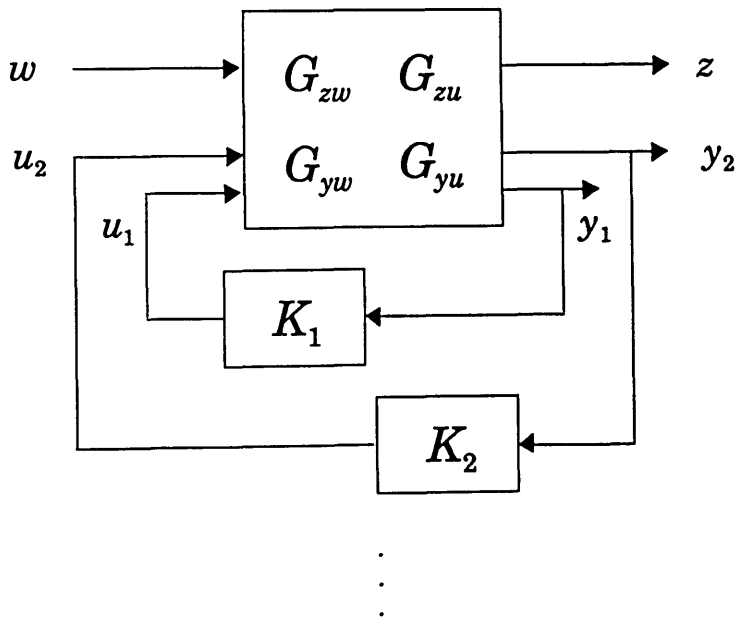

Figure 2.4. Sequential loop closing technique.

Control (HAC/LAC) [Gupta *et al.* (1982)]. In this procedure, low authority control loops, usually collocated rate feedback, are first closed on the controlled structure to add damping to critical modes. A new plant is created which is more robust to model errors when high authority control loops are closed.

2.5 SISO Disturbance Rejection Topologies

The single input single output disturbance rejection problem can be used not only for control design for SISO systems, but also for interpretation of other aspects of the control design process such as different topologies, input output loop assignments, and even MIMO compensator design insight. For the SISO problem, different simplifications in the topology of the system make the compensator design more intuitive.

If the general control system given in Equation 2.1 is simplified to a SISO system, the result is

$$\begin{Bmatrix} z \\ y \end{Bmatrix} = \begin{bmatrix} g_{zw} & g_{zu} \\ g_{yw} & g_{wu} \end{bmatrix} \begin{Bmatrix} w \\ u \end{Bmatrix} \tag{2.46}$$

The closed loop transfer function from the disturbance w to the performance z is given by

$$\frac{z}{w} = \frac{g_{zw} + \left(g_{zw} g_{yu} - g_{zu} g_{yw}\right) K}{1 + g_{yu} K} \tag{2.47}$$

where the compensator is

$$u = -Ky \tag{2.48}$$

Setting the closed loop transfer function from w to z equal to ε,

$$\frac{z}{w} = \frac{g_{zw} + \left(g_{zw} g_{yu} - g_{zu} g_{yw}\right) K}{1 + g_{yu} K} = \varepsilon \tag{2.49}$$

Disturbance rejection can be achieved by letting ε tend to zero.

The topology of the system given in Equation 2.46 is very important to the closed loop system. The relationship between u and y, is the association between the sensor and actuator of the control system. The resulting transfer function, g_{yu}, is dependent on location, duality, and impedance of the sensor actuator pair [Fleming (1990)] and [Fleming and Crawley (1991)]. Sensor actuator pairs are the most important relationships in the control design process because they create the plant around which the compensator is closed. This relationship will be explored more fully in Section 2.6.

Two other relationships, however, can be meaningful in simplifying the control design process and in gaining physical insight into designing the compensator. The relationship between z and y is the association between the performance and output. If z and y are collocated, or at the same spatial point in the structure, and they are the same type, i.e. direction, spatial distribution, and inertial or a relative based, then there is an explicit relation between the two

$$z(s) = \phi_{zy}(s) y(s) \tag{2.50}$$

If $\phi_{zy}(s)$ exists, then the performance and output are said to be *analogs*. An example of this type of topology is the feedback of an inertial rate gyro as the sensor output, with the integration of the rate gyro, or inertial angle as the performance.

A similar comparison can be made for the association between the disturbance w and the input u. If the w and u are collocated, or at the same spatial point in the structure, and they are the same type, i.e. direction, spatial

distribution, and have the same reaction characteristics, then the relation between the two is identical

$$w(s) = u(s) \tag{2.51}$$

If this is true, then the disturbance and input are said to be *analogs*. This type of disturbance is less common, but an example of this type of topology is the isolation of a mirror from a moving base. The relative motion between the base and the mirror is the disturbance, and the input can be a force actuator placed between the two in order to isolate the mirror.

If the measured output y and the performance z are analogs *and* the input u and the disturbance w are analogs, then the SISO system in Equation 2.46 simplifies to

$$\begin{Bmatrix} z \\ y \end{Bmatrix} = \begin{bmatrix} g_{zw} & g_{zu} \\ g_{yu} & g_{yu} \end{bmatrix} \begin{Bmatrix} w \\ u \end{Bmatrix} = \begin{bmatrix} \phi_{zy} g_{yu} & \phi_{zy} g_{yu} \\ g_{yu} & g_{yu} \end{bmatrix}_{\substack{z=\phi_{zy} y \\ w=u}} \begin{Bmatrix} w \\ u \end{Bmatrix} \tag{2.52}$$

And the closed loop transfer function from disturbance to performance is

$$\frac{z}{w} = \frac{g_{zw}}{1 + g_{yu} K} = \left. \frac{\phi_{zy} g_{yu}}{1 + g_{yu} K} \right|_{\substack{z=\phi_{zy} y \\ w=u}} \tag{2.53}$$

If the above transfer function is set equal to ε, and solved for the compensator K,

$$K = \frac{g_{zw} - \varepsilon}{\varepsilon g_{yu}} = \left. \frac{\phi_{zy} g_{yu} - \varepsilon}{\varepsilon g_{yu}} \right|_{\substack{z=\phi_{zy} y \\ w=u}} \tag{2.54}$$

Good disturbance rejection is achieved as ε tends to zero, giving the compensator

$$\underset{\varepsilon \to 0}{LIM}\, K = \frac{g_{zw}}{\varepsilon g_{yu}} = \left.\frac{\phi_{zy} g_{yu}}{\varepsilon g_{yu}}\right|_{\substack{z=\phi_{zy} y \\ w=u}} \tag{2.55}$$

This is the disturbance to performance transfer function minimizing compensator when the performance and output are analogous, *and* the disturbance and input are analogous. Equation 2.55 shows that disturbance rejection for this topology is achieved by using a compensator which is high gain, and contains the transformation ϕ_{zy}. This compensator can also be generalized into a magnitude only requirement, since disturbance rejection is desired for the magnitude only, and in loop shaping, only the magnitude of the loop transfer function is shaped. For loop shaping, using a high gain compensator, the magnitude of the closed loop system within the bandwidth reduces to

$$\left|\frac{z}{w}\right| = \left|\frac{\phi_{zy}}{K}\right| \qquad \text{for} \qquad \left|g_{yu} K\right| \gg 1 \tag{2.56}$$

The design of compensation for this form is relatively simple. Except for the transformation $\phi_{zy}(s)$, disturbance rejection performance is accomplished by setting the magnitude of K to be large. This is a valuable insight, but the pole zero structure of the plant g_{yu} will still be the most important factor in the compensator design because of the closed loop stability. This case is the subject of Chapter 3.

For the case where the output y and performance z are analogs, *but* the input u and the disturbance w are not, the SISO system simplifies to

$$\begin{Bmatrix} z \\ y \end{Bmatrix} = \begin{bmatrix} g_{zw} & g_{zu} \\ g_{yw} & g_{yu} \end{bmatrix} \begin{Bmatrix} w \\ u \end{Bmatrix} = \left[\begin{matrix} \phi_{zy} g_{yw} & \phi_{zy} g_{yu} \\ g_{yw} & g_{yu} \end{matrix}\right]_{z=\phi_{zy} y} \begin{Bmatrix} w \\ u \end{Bmatrix} \tag{2.57}$$

And the closed loop transfer function from disturbance to performance is

$$\frac{z}{w} = \frac{g_{zw}}{1 + g_{yu}K} = \left.\frac{\phi_{zy}g_{yw}}{1 + g_{yu}K}\right|_{z=\phi_{zy}y} \tag{2.58}$$

If the above transfer function is set equal to ε, and solved for the compensator K,

$$K = \frac{g_{zw} - \varepsilon}{\varepsilon g_{yu}} = \left.\frac{\phi_{zy}g_{yw} - \varepsilon}{\varepsilon g_{yu}}\right|_{z=\phi_{zy}y} \tag{2.59}$$

Good disturbance rejection is achieved as ε tends to zero, giving the disturbance to performance transfer function minimizing compensator

$$\underset{\varepsilon \to 0}{LIM}\, K = \frac{g_{zw}}{\varepsilon g_{yu}} = \left.\frac{\phi_{zy}g_{yw}}{\varepsilon g_{yu}}\right|_{z=\phi_{zy}y} \tag{2.60}$$

Disturbance rejection in this problem is accomplished in the same manner as in the previous problem, by setting the magnitude of K to be large. By comparison with the simplest case of Equation 2.55, there remains the transformation function $\phi_{zy}(s)$, but there is also a ratio of transfer functions, or *filter* g_{yw}/g_{yu}. The contrast of the compensators Equation 2.55 with 2.60 shows that if an input is moved away from the disturbance in a structure, and all other features are held constant, the compensator design task is the same, except for an added filter g_{yw}/g_{yu}, which contains the transfer function through the plant from u to w. In certain cases, the compensator design may need to convolve the dynamics of this filter into the compensator in order to sufficiently reduce the magnitude of the disturbance to performance transfer function.

For loop shaping, using a high gain compensator, the magnitude of the closed loop system within the bandwidth reduces to

$$\left|\frac{z}{w}\right| = \left|\frac{\phi_{zy} g_{yw}}{g_{yu} K}\right| \qquad \text{for} \qquad |g_{yu} K| \gg 1 \tag{2.61}$$

Similarly, for the less common case where the input u and the disturbance w are analogs, *but* the output y and the performance z are not, the SISO system simplifies to

$$\begin{Bmatrix} z \\ y \end{Bmatrix} = \begin{bmatrix} g_{zw} & g_{zu} \\ g_{yu} & g_{yu} \end{bmatrix} \begin{Bmatrix} w \\ u \end{Bmatrix} = \begin{bmatrix} g_{zu} & g_{zu} \\ g_{yu} & g_{yu} \end{bmatrix}_{w=u} \begin{Bmatrix} w \\ u \end{Bmatrix} \tag{2.62}$$

And the closed loop transfer function from disturbance to performance is

$$\frac{z}{w} = \frac{g_{zw}}{1 + g_{yu} K} = \left.\frac{g_{zu}}{1 + g_{yu} K}\right|_{w=u} \tag{2.63}$$

If the above transfer function is set equal to ε, and solved for the compensator K,

$$K = \frac{g_{zw} - \varepsilon}{\varepsilon g_{yu}} = \left.\frac{g_{zu} - \varepsilon}{\varepsilon g_{yu}}\right|_{w=u} \tag{2.64}$$

Good disturbance rejection is achieved as ε tends to zero, giving the disturbance to performance transfer function minimizing compensator

$$\underset{\varepsilon \to 0}{LIM}\, K = \frac{g_{zw}}{\varepsilon g_{yu}} = \left.\frac{g_{zu}}{\varepsilon g_{yu}}\right|_{w=u} \tag{2.65}$$

This case is dual to the system in Equations 2.57-2.61, however, the filter is now g_{zu}/g_{yu}, and there is no transformation function, ϕ_{zy}. Notice, however, the transformation between z and y is embedded in the filter, g_{zu}/g_{yu}. The contrast of the compensator in Equation 2.55 with 2.65 shows that if an output is moved away from the performance in a structure, and all other features are held constant, the

compensator design task is the same, except for an added filter g_{zu}/g_{yu}, which contains the transfer function through the plant from z to y. The compensator design may need to convolve the dynamics of this filter into the compensator order to sufficiently reduce the magnitude of the disturbance to performance transfer function.

For loop shaping, using a high gain compensator, the magnitude of the closed loop system within the bandwidth reduces to

$$\left|\frac{z}{w}\right| = \left|\frac{g_{zu}}{g_{yu}K}\right| \qquad \text{for} \qquad |g_{yu}K| \gg 1 \tag{2.66}$$

These two cases are the subject of Chapter 4.

The simplifications in leading to the closed loop transfer functions in Equations 2.56, 2.61, and 2.66, although different in many respects, contain a similarity

$$g_{zw}g_{yu} - g_{zu}g_{yw} = 0 \tag{2.67}$$

For the general SISO design case as in Equation 2.46, the simplification given in Equation 2.67, which leads to the closed loop systems in Equations 2.56, 2.61, and 2.66, does not occur. The control design is more complex and potentially limited in performance. In the previous simplified topologies, disturbance rejection could be accomplished by setting the magnitude of K to be large, i.e. loop shaping. However, for the general closed loop system given in Equation 2.46, the only simplification which occurs for the high gain compensator is

$$\left|\frac{z}{w}\right| = \left|\frac{g_{zw}g_{yu} - g_{zu}g_{yw}}{g_{yu}}\right| \qquad \text{for} \qquad |g_{yu}K| \gg 1 \tag{2.68}$$

In examining Equation 2.68, the disturbance rejection performance of the closed loop system does not tend to zero as the magnitude of K increased as it did in the simplified topologies. For the loop shaping concept to yield improved performance, then the large K closed loop limit for disturbance to performance must be smaller than the open loop disturbance to performance, or

$$\left| \frac{g_{zw} g_{yu} - g_{zu} g_{yw}}{g_{yu}} \right| \ll |g_{zw}| \tag{2.69}$$

In general, this will not be the case. Equation 2.69 may in some cases be useful as a tool for sensor actuator selection. Sensor outputs and actuator inputs can be designed to insure Equation 2.69 to be satisfied. In the case that Equation 2.69 is satisfied, then the closed loop transfer function from disturbance to performance simplifies to

$$\frac{z}{w} = \frac{g_{zw}}{1 + g_{yu} K} \tag{2.70}$$

If the above transfer function is set equal to ε, and solved for the compensator K,

$$K = \frac{g_{zw} - \varepsilon}{\varepsilon g_{yu}} \tag{2.71}$$

Good disturbance rejection is achieved as ε tends to zero, giving the disturbance to performance transfer function minimizing compensator

$$\underset{\varepsilon \to 0}{LIM}\, K = \frac{g_{zw}}{\varepsilon g_{yu}} \tag{2.72}$$

The closed loop system again contains a filter g_{zw}/g_{yu}, and the loop shaping concept of setting the magnitude of K to be large, in order to achieve disturbance rejection

applies. The compensator again may need to convolve the dynamics of the filter into the compensator in order to sufficiently reduce the magnitude of the closed loop disturbance to performance transfer function. For loop shaping, using a high gain compensator, the magnitude of the closed loop system within the bandwidth reduces to

$$\left|\frac{z}{w}\right| = \left|\frac{g_{zw}}{g_{yu}K}\right| \quad \text{for} \quad |g_{yu}K| \gg 1 \quad \text{and} \quad \left|\frac{g_{zw}g_{yu} - g_{zu}g_{yw}}{g_{yu}}\right| \ll |g_{zw}|, \quad (2.73)$$

For the general closed loop disturbance to performance transfer function given in Equation 2.47, when the test given in Equation 2.69 is not met, the alternative to loop shaping is to derive the dynamic compensator to drive the numerator of the closed loop disturbance to performance transfer function (Equation 2.47) to zero. Setting the closed loop transfer function from w to z equal to ε,

$$\frac{z}{w} = \frac{g_{zw} + \left(g_{zw}g_{yu} - g_{zu}g_{yw}\right)K}{1 + g_{yu}K} = \varepsilon \quad (2.74)$$

And solving for the compensator K yields

$$K = \frac{g_{zw} - \varepsilon}{\varepsilon g_{yu} - \left(g_{zw}g_{yu} - g_{zu}g_{yw}\right)} \quad (2.75)$$

Good disturbance rejection is achieved as ε tends to zero, giving the disturbance to performance transfer function minimizing compensator

$$\underset{\varepsilon \to 0}{LIM}\, K = \frac{-g_{zw}}{g_{zw}g_{yu} - g_{zu}g_{yw}} \quad (2.76)$$

In examining the resulting compensator, one can see that it inverts the second

term in the numerator of Equation 2.47, and cancels the first. Although, in principle, this accomplishes the disturbance rejection goal, in practice it will be very difficult to implement due to robustness concerns. This compensator does not fall into the loop shaping category, since the magnitude is a constant, and there are no simplifications such as in the magnitude only requirement. This may lead to a fundamental performance robustness limitation in the general case when u and w are not analogs, and y and z are not analogs. This case will be the subject of Chapter 5.

It must be stressed that compensator design for each of these topologies, Equations 2.52, 2.57, 2.62, and the general system in 2.47, is a combination of the simplification of the closed loop system *and* an accommodation of the pole zero structure of g_{yu}, which will be addressed next in Section 2.6.

2.6 Pole zero structure of loops

Control design for structures is greatly dependent on the pole zero structure of the input output pair. Lightly damped poles and zeros create large differences in the magnitude and phase of a transfer function, thus leading to small gain and phase margins, and concern for stability robustness in the closed loop system. For certain input output pairs, real minimum and nonminimum phase zeros may occur. Although a structure is passively stable, nonminimum phase zeros create possible limitations in achieving the performance objective [Freudenberg and Looze (1985)].

Fleming (1990) showed that the zeros of a transfer function are dependent on the type, impedance, and location of the sensors and actuators. For a SISO system, when a sensor and actuator are dual, complementary extremes, and collocated, the resulting pattern is alternating poles and zeros [Gavartner (1970)].

Duality implies the actuator and sensor are the same type, i.e. direction, spatial distribution, and the nature of the sensing or actuating as being inertial or relative measurement based. Complementary extreme pairs implies the sensor actuator pair have different impedances, such as a force actuator and a displacement sensor. And collocated implies the sensor actuator pair are located at the same spatial point in the structure. This pole zero pattern is desirable to control designers because the system is hyperstable [Steiber (1988)]. This hyperstable system is bounded-input-bounded-output (BIBO) stable, and ensures that the closed loop system is hyperstable if the feedback form around the system is hyperstable. This means a large subset of controllers will be closed loop stable on a system with a dual, complementary extreme, collocated sensor actuator pair.

Fleming studied the pole zero patterns of systems where the duality, impedance, and location of the sensor actuator pair were changed. A collocated, dual, and complementary extreme sensor actuator creates alternating poles and zeros, as shown in Figure 2.5(a). As the pair becomes noncollocated, the zeros increase in frequency. At a certain point, pole zero cancellations occur, and eventually, the zero moves to the other side of the pole, creating a *missing* zero between two poles. This is shown in Figure 2.5(b). Missing zeros usually occur at high frequencies first. Therefore, for slight noncollocation, an alternating pole zero pattern may be evident in the lower frequency range. As the sensor actuator pair becomes even more noncollocated, the zeros will become nonminimum phase in some structures, as shown in Figure 2.5(c). The nonminimum phase zeros diminish in frequency as the noncollocation distance is increased.

Nonminimum phase zeros place fundamental limitations on the frequency ranges over which control can be exerted. However, if there is a frequency range in which the poles and zeros are alternating, such as if the nonminimum phase zeros are before or after the bandwidth of interest, then the noncollocated sensor

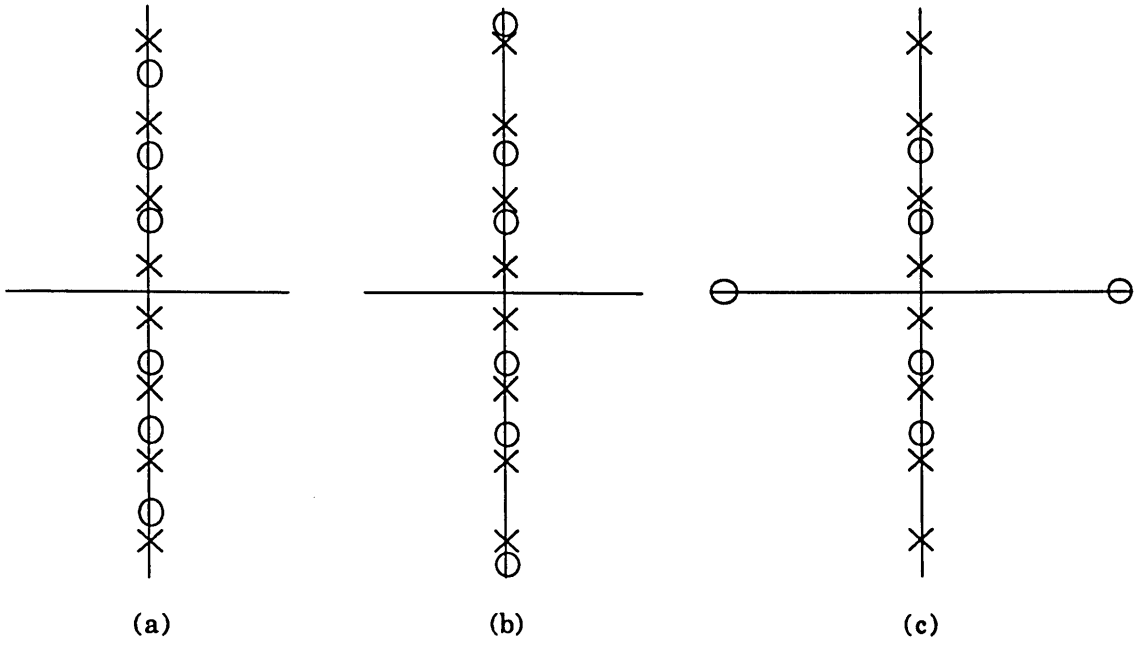

Figure 2.5. Typical pole zero patterns for sensor actuator pairs on a structure: (a) collocated (b) slightly noncollocated (c) noncollocated

and actuator pair may be adequate.

2.7 Typical section model

In order to examine trends in optimal controllers and demonstrate Neo-Classical design, a two dimensional typical section model will be used. Typical sections used in structural control are small order model used to gain insight necessary to design and interpret higher order problems [Miller *et al.* (1991)]. A typical section should be designed to be a simple, small order model that captures the fundamental physics of the problem.

Figure 2.6 shows a typical section model of a cantilever beam, which will be used in this study. The model is made up of four identical masses and rotary inertias and four springs. A four mode Rayleigh-Ritz representation [Bathe

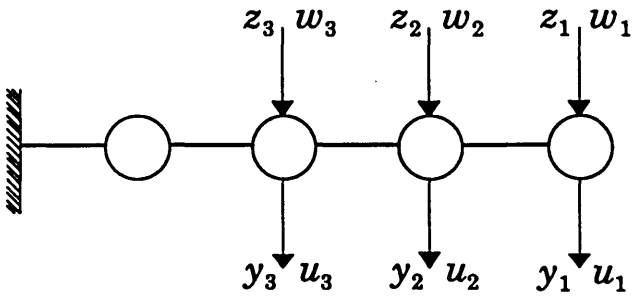

Figure 2.6. Four mass, typical section model of a cantilever beam.

(1982)] of a Bernoulli-Euler beam was made and an eight state model was constructed. Damping was added to the model, using 1% proportional damping. For control design, there are three inputs u, i.e. vertical forces on the first three masses, and three outputs y, i.e. the measured vertical velocity on the first three masses. There are also three disturbances w and performances z, i.e. the vertical forces and displacements on the first three masses. A summary of the typical section model is shown in Appendix B.

The typical section model shown in Figure 2.6 has all of the important features of a complex control design of a flexible structure, such as collocated and noncollocated control and relevant performance metrics and disturbances. However, it lacks some of the aspects of a control design that would be part of the experimental implementation of compensators such as time delays and sensor and actuator dynamics.

2.8 The Middeck Active Control Experiment (MACE)

The platform for experimental testing for each of the controllers designed as part of this study is the Middeck Active Control Experiment (MACE) [Miller *et al.* (1992)], a Shuttle middeck experiment tentatively scheduled for flight in the

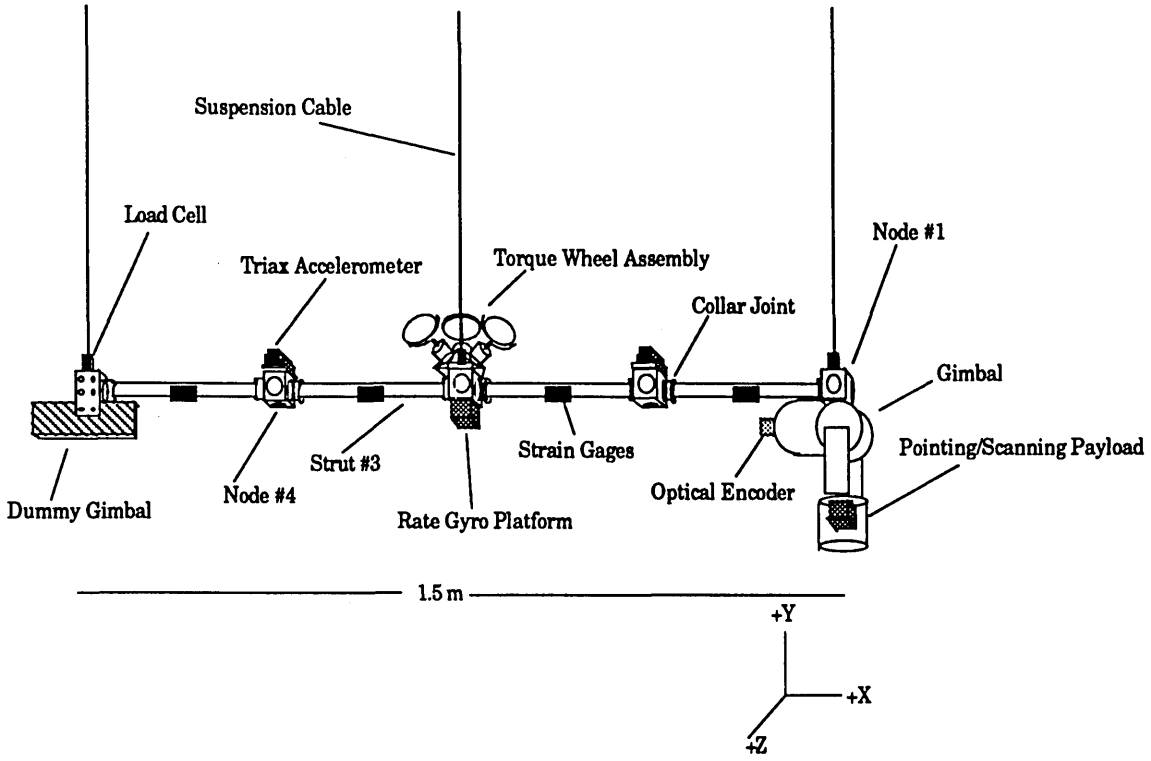

Figure 2.7. MACE Development Model test article.

summer of 1994. The Development Model, the first of three sets of hardware to be developed under the MACE program, is shown in Figure 2.7. The test article is designed to simulate flexible spacecraft with multiple pointing payloads. The objective of the experiment is to develop a qualification procedure for flexible precision spacecraft. For future vehicles which cannot be dynamically tested on the ground in a sufficiently realistic zero-gravity simulation, this procedure will increase confidence in the eventual orbital performance of such spacecraft [MACE-1-101 (1991)]. Specifically, the objective is to investigate the extent to which closed loop behavior of the MACE test article in zero gravity can be predicted. This prediction becomes particularly difficult when dynamic behavior during ground testing exhibits extensive suspension and direct gravity coupling.

The test article is a multiple input, multiple output (MIMO) system

Table 2.1. Description of the actuators on the MACE test article.

Inputs	Actuator	Location	Description
2	Gimbal	Node 1	Relative torque X & Z axis rotation only two DC torque motors
3	Torque Wheels	Node 3	Inertial torque three DC servo motors aluminum inertia wheels orthogonally mounted

[Saarmaa (1991)]. There are five inputs: a two axis gimbal exerting a relative torque between the pointing payload and the right end of the bus (Figure 2.7); and a three axis set of torque wheels, producing an inertial torque at the center of the bus. A summary of the actuators is given in Table 2.1. The are 12 outputs: a three axis rate gyro package at the center of the bus, and a two axis rate gyro in the payload, measuring inertial rotational velocity; two three axis accelerometers on nodes 2 and 4 measuring linear acceleration; and two rotary encoders measuring

Table 2.2. Description of the sensors on the MACE test article.

Outputs	Sensor	Location	Description
3	Rate Gyro	Node 3	Inertial rotational velocity Nominal 48 Hz natural frequency 0.35 of critical damping
2	Rate Gyro	Payload Can	Inertial rotational velocity Nominal 48 Hz natural frequency 0.35 of critical damping
2	Accelerometer	Node 2	Linear acceleration X & Y axes only Natural Frequency > 300 Hz 0.3-0.8 of critical damping
3	Accelerometer	Node 4	Linear acceleration Natural Frequency > 300 Hz 0.3-0.8 of critical damping
2	Encoder	Gimbal Axes	Relative gimbal angle Laser rotary encoders

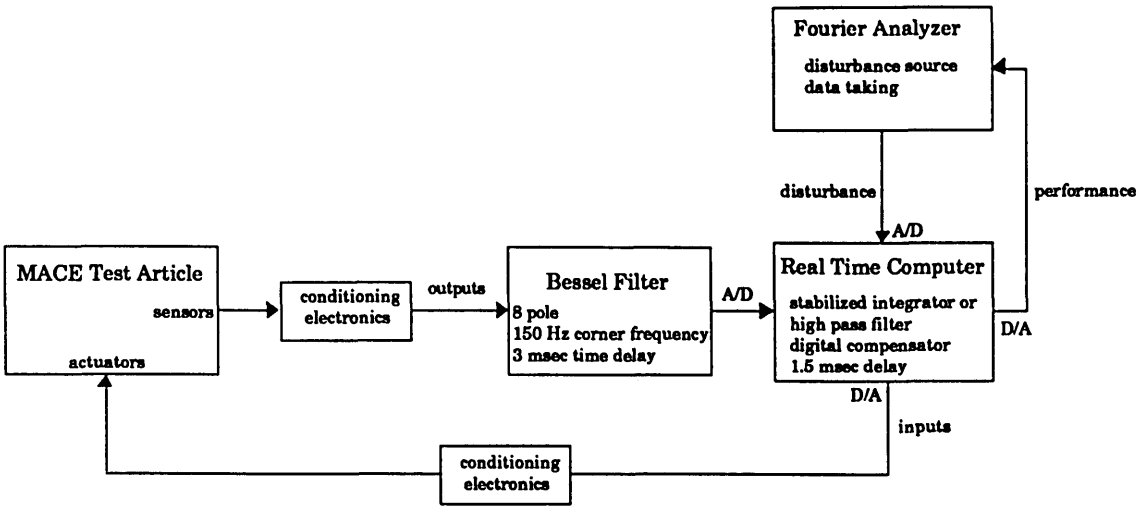

Figure 2.8. Block diagram of the experimental setup of the MACE test article.

the relative angle between the end of the bus and the payload. Table 2.2 summarizes the sensors on the MACE test article. Various signal conditioning and power amplification electronics are included for the sensors and actuators.

The bus is composed of flexible Lexan struts, interconnected by aluminum nodes. The 7 kg dummy mass on node 5 will be replaced in the future with another two axis gimbal. The test article is suspended by a pneumatic/electric low frequency suspension system [Kienholz (1990)].

Other equipment important to the experiment includes an 8-pole antialiasing Bessel Filter with a corner frequency of 150 Hz used in each control loop. The compensators are designed using Matlab [Pro-Matlab (1990)] or Matrixx [Matrixx (1990)], and the digitally implemented compensator is constructed in System Build of Matrixx. A real time control computer [AC-100 (1991)] is used to implement the compensator. The hardware channels include 16 inputs (A/D's), 6 encoder inputs, and 8 outputs (D/A's). A Fourier analyzer was also used as a disturbance source and for taking data. Figure 2.8 shows the experimental block diagram.

Table 2.3. Frequencies, damping ratios, and type of structural modes for each mode in the finite element model of the Development Model from 0-60 Hz.

Frequency (Hz)	Damping Ratio (%)	Type of Mode
0	1	Torque wheel #1
0	1	Torque wheel #2
0	1	Torque wheel #3
0.2001	0.150	Suspension - bounce
0.2198	0.150	Suspension - Y axis pendulum
0.2317	0.150	Suspension - X axis pendulum
0.2333	0.150	Suspension - Z axis pendulum
0.3339	0.0786	Suspension - tilt
1.0930	0.150	Suspension - 1st twist
1.2140	0.150	Outer gimbal pendulum
1.2870	0.0563	Inner gimbal pendulum
1.8620	0.03689	1st X-Y bending
3.1310	0.03723	1st X-Z bending
6.7190	0.01741	2nd X-Y bending
6.8690	0.01211	2nd X-Z bending
8.8500	0.01624	Suspension - 2nd twist
9.4000	0.0080	3rd X-Y bending
13.290	0.00660	3rd X-Z bending
14.000	0.00660	4th X-Y bending
14.250	0.00664	Suspension - 3rd twist
17.400	0.00588	4th X-Z bending
36.000	0.01180	Suspension - 4th twist
39.100	0.020	Suspension - 5th twist
42.500	0.0150	5th X-Y bending
64.120	0.010	5th X-Z bending
86.000	0.010	1st axial

Table 2.4. Additional dynamics appended to the finite element model

Component	Dynamics
Rate Gyros	rolloff: 2 poles: $\omega = 46$ Hz, $\zeta = 0.5$ 1 pole: $\omega = 70$ Hz
Time Delay	4th order PADE approximation: 4 stable poles 4 nonminimum phase zeros
Stabilized Integrator	2 poles: $\omega = 0.03$ Hz, $\zeta = 0.707$ 1 zero: $\omega = 0$ Hz
High Pass Filter	2 poles: $\omega = 0.03$ Hz, $\zeta = 0.707$ 2 zeros: $\omega = 0$ Hz for each

and assigned a nominal 1% value for all other modes. Appended to the finite element model are dynamics for additional components of the experiment. These are shown in Table 2.4. The rate gyros have three states for their rolloff characteristics. A fourth order PADE approximation is used to model the time delay. Time delays in the control computer, the Bessel Filters, and mismodeled dynamics figured significantly in the control design process. In order to avoid secular offsets due to integration of DC bias in any of the sensors, particularly the rate gyros and accelerometers, a two pole stabilized integrator or two pole high pass filter, both with a corner frequency of 0.03 Hz, were used in each control loop.

Appendix C shows the pertinent transfer functions of the model and data taken from the test article. Flexible modes such as those at 6.8 and 9.4 Hz were modelled well, with less than 5% error for all flexible modes at frequencies less than 50 Hz. The difficulty in modeling suspension effects, and the inability to reproduce the same suspension system for each experiment prevented accurate modeling of the suspension modes. These errors can be seen in Appendix C, where the finite element model does represent the actual suspension modes at low frequency. Nonlinearities also occurred in the experimental setup. Large gimbal

motions are the most obvious nonlinearity. An example of nonlinearities can be seen by comparing the transfer functions in Figures A.2 and A.4. In the z-axis gimbal to z-axis bus rate gyro transfer function, the model accurately represents the flexible mode at 6.8 Hz. But, in the z-axis torque wheels to Z-axis payload rate gyro transfer function, the mode is approximately 7.2 Hz. This model will be used for all control designs.

A finite element model was developed for the MACE test article [Rey and Glaese (1992)]. The model is a 40 mode model, which is truncated to a smaller number of states for control design. Table 2.3 shows the frequency, damping ratio, and type of mode for all modes below 60 Hz in the finite element model. Damping in the model was measured experimentally for all modes up to 50 Hz,

Chapter 3

SISO Topology I: Analogous Performance & Output *and* Analogous Disturbance & Input

3.1 Introduction

This chapter describes the first building block of the Neo-Classical design methodology, namely when the performance and output are collocated and dual, i.e. analogs, *and* the disturbance and input are collocated and dual, i.e. analogs. It is a simplified case of the general closed loop disturbance rejection problem, as described in Chapter 2. In the first section of this chapter, specific topologies of the typical section will be introduced as tools for compensator examination. The topologies have collocated, dual input output pairs only. Aspects of the LQG compensator and the robustified SWLQG compensator are analyzed such as dominant mode control, plant inversion, and truncation of compensator states. The benefits and weaknesses of the LQG and SWLQG compensators are then interpreted classically and presented in the format of a Neo-Classical Design Rule. Compensators are then designed using LQG, SWLQG, and the Neo-Classical design rule and implemented on the Middeck Active Control Experiment.

3.2 Topologies Examined

It was shown in Section 2.5 that when the performance z and output y are collocated and dual, or analogs, *and* the disturbance w and input u are collocated and dual, or analogs, the general single input single output disturbance rejection problem simplifies to

$$\begin{Bmatrix} z \\ y \end{Bmatrix} = \begin{bmatrix} g_{zw} & g_{zu} \\ g_{yu} & g_{yu} \end{bmatrix} \begin{Bmatrix} w \\ u \end{Bmatrix} = \begin{bmatrix} \phi_{zy} g_{yu} & \phi_{zy} g_{yu} \\ g_{yu} & g_{yu} \end{bmatrix}_{\substack{z=\phi_{zy} y \\ w=u}} \begin{Bmatrix} w \\ u \end{Bmatrix} \tag{3.1}$$

where ϕ_{zy} and is the temporal relationship between z and y,

$$z(s) = \phi_{zy}(s) y(s) \tag{3.2}$$

This type of topology is Topology I. The following relationships can be seen between the transfer functions.

$$g_{yw} = g_{yu} \tag{3.3}$$

$$g_{zu} = \phi_{zy} g_{yu} \tag{3.4}$$

$$g_{zw} = \phi_{zy} g_{yw} = \phi_{zy} g_{yu} \tag{3.5}$$

This is an important insight because disturbance rejection in the closed loop transfer function from disturbance to performance simplifies to

$$\frac{z}{w} = \frac{g_{zw}}{1 + g_{yu} K} = \left. \frac{\phi_{zy} g_{yu}}{1 + g_{yu} K} \right|_{\substack{z=\phi_{zy} y \\ w=u}} \tag{3.6}$$

If the above transfer function is set equal to ε, and solved for the compensator K,

$$K = \frac{g_{zw} - \varepsilon}{\varepsilon g_{yu}} = \left.\frac{\phi_{zy} g_{yu} - \varepsilon}{\varepsilon g_{yu}}\right|_{\substack{z=\phi_{zy} y \\ w=u}} \tag{3.7}$$

Good disturbance rejection is achieved as ε tends to zero, giving the compensator

$$\underset{\varepsilon \to 0}{LIM}\, K = \frac{g_{zw}}{\varepsilon g_{yu}} = \left.\frac{\phi_{zy} g_{yu}}{\varepsilon g_{yu}}\right|_{\substack{z=\phi_{zy} y \\ w=u}} \tag{3.8}$$

This is the disturbance to performance transfer function minimizing compensator when the performance and output are analogous, *and* the disturbance and input are analogous.

There are two important considerations in the design of the compensator for the above system. The first is the performance criterion, which is disturbance rejection in the closed loop system (Equation 3.6). This can be accomplished by increasing the magnitude of K, such that

$$\left|\frac{z}{w}\right| = \left|\frac{\phi_{zy}}{K}\right| \qquad \text{for} \qquad \left|g_{yu} K\right| \gg 1 \tag{3.9}$$

The second is the stability of the closed loop system, as opposed to the performance metric. Of course this must also be insured in the control design process.

In the SISO disturbance rejection case, there are three important relationships to consider in defining the topology, and therefore the difficulty of the compensation: The relationships between: z and y, w and u, and y and u. In Section 2.6, the importance of the relationship between u and y, and the benefits of a collocated, complementary extreme, and dual actuator sensor pair were presented. This input output pair produced an alternating pole zero pattern and a simple plant to compensate. The topologies examined in this chapter will have a collocated, dual, and complementary extreme, input output pairs, in addition to the performance and

output being analogs and the disturbance and input being analogs, and fall into the category of topologies called Topology I.

In Typical Section 1A in Figure 3.1(a), the performance z_1 is the vertical position of the tip mass, while the output y_1 is the vertical velocity of the tip mass. The relationship between z_1 and y_1 is then

$$z_1(s) = \frac{1}{s} y_1(s) \tag{3.10}$$

$$\text{therefore,} \qquad \phi_{zy}(s) = \frac{1}{s} \tag{3.11}$$

The disturbance w_1 is an inertial vertical force on the tip mass, as is the input u_1. Therefore, w_1 and u_1 are identical.

$$w_1(s) = u_1(s) \tag{3.12}$$

The closed loop system for Typical Section 1A then simplifies to

$$\frac{z_1}{w_1} = \frac{\frac{1}{s} g_{yu}}{1 + g_{yu} K} \tag{3.13}$$

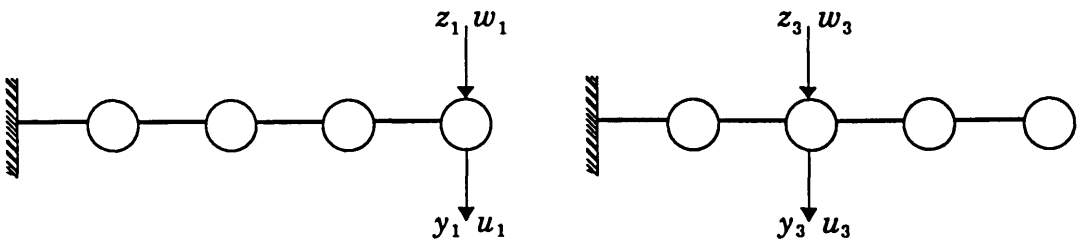

(a) Typical Section 1A (b) Typical Section 1B

Figure 3.1. Topology I: Typical Sections 1A and 1B with analogous performance and output, *and* analogous disturbance and input, and collocated, dual, *and* complementary extreme input and output.

Typical Section 1B, given in Figure 3.1(b), has the same type of topology and structural plant as Typical Section 1A, except the action is at the third mass. The temporal relationship between the performance z_3 and the output y_3 is the same as that given in Equation 3.11, and the disturbance w_3 and the input u_3 are identical.

Figures 3.2(a) and (b) show the open loop input output transfer functions for Typical Sections 1A and 1B. The features of the alternating pole zero pattern are evident. The performance for these topologies is the time integral of the output, and the disturbance is the same as the input. The disturbance to performance transfer functions, g_{zw}, are therefore, $1/s$ times the corresponding input output transfer functions, g_{yu}, shown in Figure 3.2.

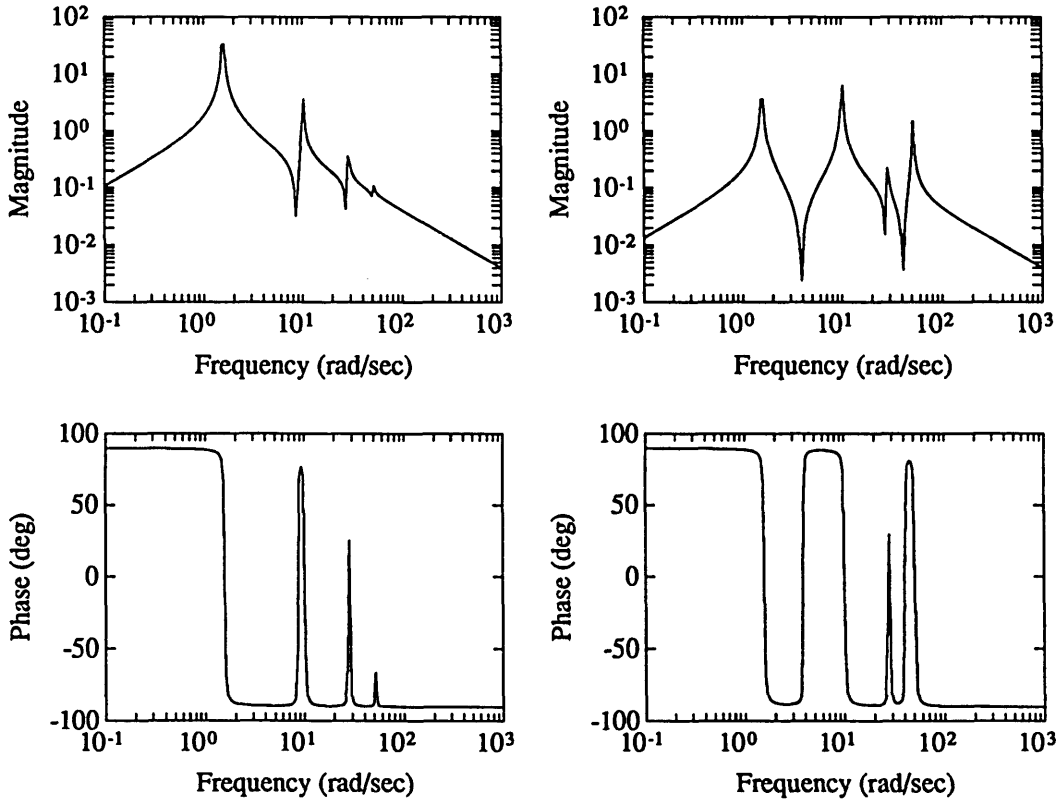

(a) g_{yu} for Typical Section 1A

(b) g_{yu} for Typical Section 1B

Figure 3.2. Input output transfer functions for Typical Sections 1A and 1B.

The two typical sections in Figure 3.1 are designed to illustrate several important issues in compensator design for the topology given, without adding to the complexity of a large model and experimental implementation. The first issue is the choice of the bandwidth of the system, which is governed by the performance requirements and input output nature of the plant. The term bandwidth in this work, is synonymous with the crossover of the dereverberated mobility of the loop transfer function $g_{yu}K$. MacMartin (1990) defined the *dereverberated* mobility to be the *backbone* of the transfer function. Once a bandwidth has been chosen in a control design, the loop transfer function can be separated into four regions. The first is the low frequency region far within the bandwidth of the loop. Another is the high frequency region far outside the bandwidth of the loop. The final two regions create the crossover region of the loop transfer function. The crossover region is a small frequency band before and after the crossover of the loop gain at 0 dB. The final two regions lie in this band, before and after the crossover.

The selection of a bandwidth, or loop crossover, will define the four regions, and subsequently which modes lie in each. The form of compensation for each mode will be seen to depend on which of the four regions the mode lies in. Figure 3.3 shows an example of a loop transfer function, with a crossover of 15 rad/sec. For this example, the mode at 1.6 rad/sec is within the bandwidth, at low frequency, and lies in Region 1, and the mode at 51 rad/sec is outside the bandwidth, at high frequency, and lies in Region 4. The modes at 10.1 and 28 rad/sec are both in the crossover region, with the mode at 10.1 rad/sec lying in Region 2, and the mode at 28 rad/sec lying in Region 3. Modes in Regions 3 are defined by having an additional loop gain greater that -3 dB after the crossover, for robustness. An example of a mode in Region 3 is the 28 rad/sec mode in Figure 3.3. The division between Regions 2 and 3 is the crossover of the loop transfer function. The boundaries between the other two regions are conceptual, and dependent upon the specific control design problem.

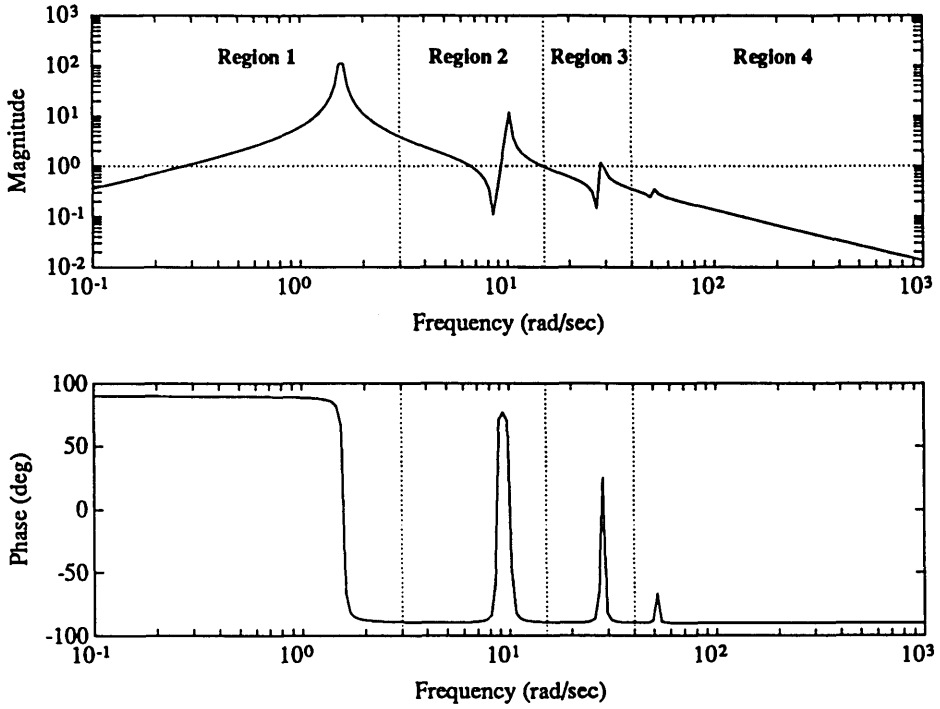

Figure 3.3. Typical loop transfer function, $g_{yu}K$, with a crossover of 15 rad/sec showing the four regions in which structural modes may lie.

Defining these will become more clear in the analysis of the compensators for the typical sections in Section 3.3.

The second issue contracted by the two typical sections is the presence or absence of a single dominant mode. Typical Section 1A has one dominant mode, at 1.6 rad/sec (as defined by its Hankel Singular Values, or residues). This system can be thought of as having the dominant dynamics of a second order resonance, with some additional higher frequency dynamics. Typical Section 1B, does not have one dominant mode. The first two modes at 1.6 and 10 rad/sec have equivalent Hankel Singular Values.

In order to determine the form of compensation required, LQG and other optimal compensation techniques will be examined for these topologies of the typical section models.

3.3 Optimal Compensation

Examination of Linear Quadratic Gaussian (LQG) and other optimal compensators for the topologies such as those given in Figures 3.1(a) and (b) will reveal dynamic optimal compensation techniques for structural modes far below, far above, or within the region of loop crossover, and dominant versus recessive mode control. For the control law

$$u(s) = -K(s)y(s) \tag{3.14}$$

the LQG compensator is given by

$$K(s) = G\left(sI - A + B_u G + HC_y\right)^{-1} H \tag{3.15}$$

where G and H are the Linear Quadratic Regulator (LQR) and Kalman Filter optimal gains respectively.

Asymptotic Properties of LQG Compensators

In order to determine the properties of the optimal dynamic compensator, the asymptotic properties of the LQG compensator are examined. In the problem definition, the LQG compensator is dependent on the choices of the LQR and Kalman Filter scalar weightings ρ and μ respectively. The Kalman Filter weighting is chosen to be smaller than the LQR weighting in order to make the estimation dynamics of the LQG compensator faster than the state feedback dynamics. The relevant asymptotical limits to examine, therefore, are as μ tends to zero, and varying ρ from infinity to zero. As ρ tends to infinity, the LQR problem is said to have *expensive* control, and as ρ tends to zero, the LQR problem is said to have *cheap* control.

It was shown in Equation 2.30 that as the sensor noise diminishes, and for the expensive LQR control problem, the LQG compensator simplifies to

$$\underset{\substack{\mu\to 0\\ \rho\to\infty}}{LIM}\, K(s) = \frac{G\Phi B_w}{g_{yw}} = \frac{k_{LG}}{\sqrt{\rho}} \frac{s}{s^2 + 2\zeta_{dm}\omega_{dm}s + \omega_{dm}^2} \frac{1}{g_{yw}} \tag{3.16}$$

Using the simplifications for Topology I, this reduces to

$$\underset{\substack{\mu\to 0\\ \rho\to\infty}}{LIM}\, K(s) = \frac{k_{LG}}{\sqrt{\rho}} \frac{s}{s^2 + 2\zeta_{dm}\omega_{dm}s + \omega_{dm}^2} \frac{1}{g_{yw}} = \frac{k_{LG}}{\sqrt{\rho}} \frac{s}{s^2 + 2\zeta_{dm}\omega_{dm}s + \omega_{dm}^2} \frac{1}{g_{yu}}\Bigg|_{\substack{z=\phi_{zy}y\\ w=u}} \tag{3.17}$$

where ζ_{dm} and ω_{dm} are the damping ratio and frequency of the most dominant mode, and k_{LG} is a scalar weighting. Note that the residue of the most dominant modes has been absorbed into the scalar constant k_{LG}. This compensator is called the low gain asymptote of LQG. The poles of this compensator are the zeros of the disturbance to output transfer function g_{yw}, or the input output transfer function, g_{yu}, in this case. And the zeros include a zero at zero for rate feedback, and the poles of the g_{yw}, or g_{yu}, except for the dominant pole pair.

The high gain LQG asymptotic compensator is given by letting both the Kalman Filter weighting μ and LQR weighting ρ tend to zero. It was shown in Equation 2.32 that as the sensor noise diminishes, and for the cheap LQR control problem, the LQG compensator simplifies to

$$\underset{\substack{\mu\to 0\\ \rho\to 0\\ \rho>\mu}}{LIM}\, K(s) = \pm\frac{1}{\sqrt{\rho}} \frac{g_{zw}}{g_{yw}} \tag{3.18}$$

Using the simplifications for Topology I, this reduces to

$$\underset{\substack{\mu\to 0\\ \rho\to 0\\ \rho>\mu}}{LIM}\, K(s) = \pm\frac{1}{\sqrt{\rho}} \frac{g_{zw}}{g_{yw}} = \pm\frac{1}{\sqrt{\rho}} \frac{\phi_{zy}g_{yu}}{g_{yu}}\Bigg|_{\substack{z=\phi_{zy}y\\ w=u}} \tag{3.19}$$

assuming that μ is smaller than ρ. This asymptotical compensator is formed by assuming the transfer functions g_{zu} and g_{yw} are minimum phase. The simplifications in Equations 3.3-3.5 show that these transfer functions contain alternating poles and zeros. This states that the SISO cheap control, low noise LQG asymptotic compensator is a high gain compensator, containing the temporal relationship between the performance and output. The poles and zeros of the compensator are identically the zeros of the open loop g_{yu} transfer function. This is the high gain LQG asymptote for Topology I. Notice how it identically matches the disturbance to performance transfer function minimizing compensator in Equation 3.8.

For Typical Sections 1A and 1B, given the relationship between z and y in Equation 3.11, the compensator simplifies to

$$\underset{\substack{\mu\to 0\\ \rho\to 0\\ \rho>\mu}}{LIM}\, K(s) = \frac{\pm 1}{\sqrt{\rho}} \frac{\phi_{zy} g_{yu}}{g_{yu}} = \frac{\pm 1}{s\sqrt{\rho}} \tag{3.20}$$

This states that the high gain LQG asymptotic compensator, is a high gain integration of the output velocity, or equivalently displacement feedback.

As shown in Equation 3.17 and 3.19, the poles of the LQG compensator are the open loop zeros of g_{yu}, regardless of the choice of ρ. The zeros of the compensator, however, range from a zero at zero and an inversion of the open loop poles of the g_{yu} transfer function (except for the most dominant pair of poles) in the expensive LQR control problem (Equation 3.17), to the open loop zeros of the g_{yu} transfer function in the cheap LQR control problem (Equation 3.19). The cheap control, low noise LQG asymptote results in compensator pole zero cancellations.

Equations 3.17 and 3.19 show the asymptotical limits of an LQG compensator, with no sensor noise. The actual LQG compensator, is one of a family of compensators whose bandwidth is set by the choice of the LQR weighting

parameter ρ. In the expensive control problem, the compensator has low gain, and thus there is no crossover, and no bandwidth. In the cheap control problem, the compensator increases proportional to $1/\sqrt{\rho}$. As ρ tends to zero, the gain increases, as does the crossover and closed loop bandwidth of the system. The bandwidth increases asymptotically to infinity.

Typical Section Results: LQG compensator

Typically, an intermediate ρ is chosen to set a finite bandwidth. For this intermediate case, the compensator is a blending of the compensators from the low gain and high gain LQG asymptotes, with the division between the two essentially the bandwidth or crossover of the system. At high frequencies, above the bandwidth, the compensator is similar to the low gain LQG asymptote given in Equation 3.16. At low frequencies, within the bandwidth, the compensator is similar to the high gain LQG controller given in Equation 3.19. The frequency range between these two controllers is the crossover region.

Figure 3.4 shows the open loop input output transfer function, g_{yu}, for Typical Section 1A (Figure 3.1(a)). Figure 3.5(a) shows an 8 state LQG compensator for low sensor noise (μ=1E-8) and an intermediate LQR weighting (ρ=1E-1), plotted with the low and high gain LQG asymptotes designed for Typical Section 1A. The crossover or bandwidth of the system is 4 rad/sec, as can be seen in the loop transfer function $g_{yu}K$ in Figure 3.5(b). Within the bandwidth of 4 rad/sec, the compensator is a high gain integrator, as in the high gain LQG asymptote (Equation 3.20). This corresponds to the low frequency Region 1, in Figure 3.3.

Well above the bandwidth of the system, as one can see by examining the loop transfer function in Figure 3.5(b), the modes at 28 and 55 rad/sec are exactly inverted, similar to the low gain, LQG asymptote (Equation 3.17). This corresponds to Region 4, in Figure 3.3.

In the crossover region, the integral control, or position feedback of the high gain LQG asymptote, changes to proportional or rate feedback of the low gain LQG asymptote. This change is made by the use of a zero, as in a proportional-integral (PI) controller. The characteristics of the PI controller are integral control (position feedback in this case) at low frequency, and proportional control (rate feedback in this case) at high frequency. The setting of the zero is such that the phase margin at crossover is approximately 60°. Although the phase margins of an LQG compensator are not guaranteed [Doyle (1978)], with the pole zero structure of g_{yw}, the Kalman Filter exactly estimates the states for small sensor noise, or small values of μ. Therefore, the guaranteed phase margins of 60° for the Linear Quadratic Regulator [Stein and Athens (1984)] are approximated in the LQG compensator. For this case, the zero is at 1.8 rad/sec.

The mode at 10 rad/sec is interesting because it is within the crossover

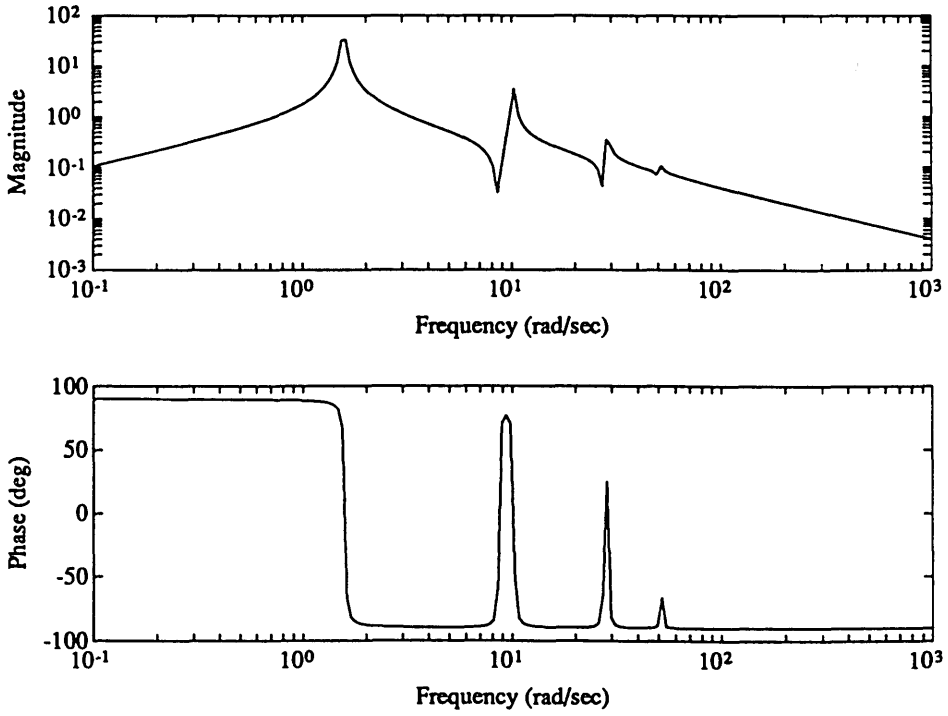

Figure 3.4. Open loop input output transfer function, g_{yu}, for Typical Section 1A.

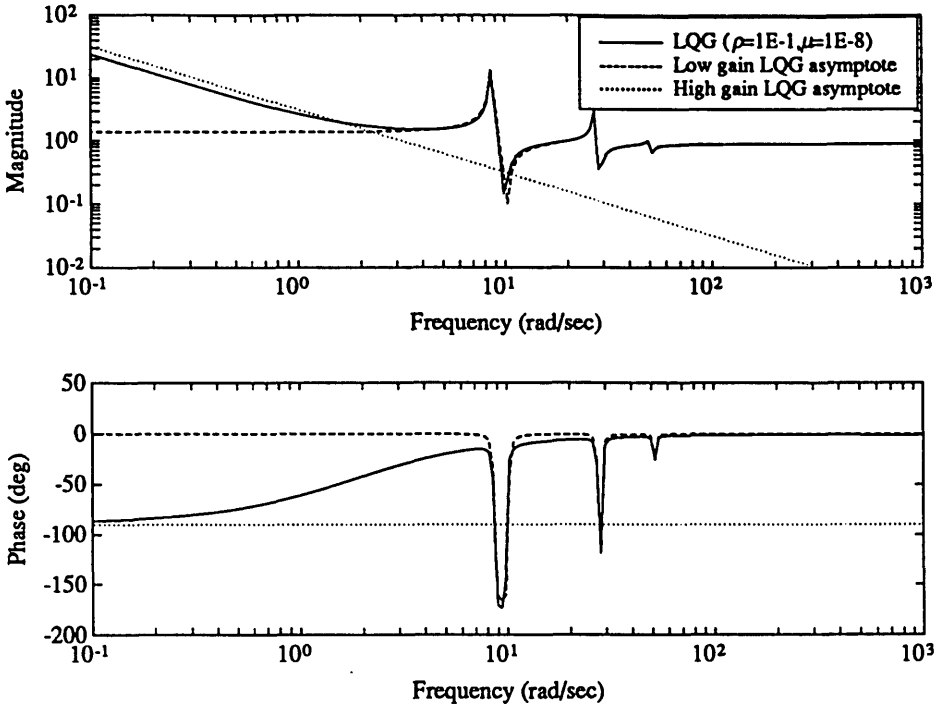

Figure 3.5(a). 8 state LQG compensator K (ρ=1E-1, μ=1E-8) for Typical Section 1A, and the low and high gain LQG asymptotes.

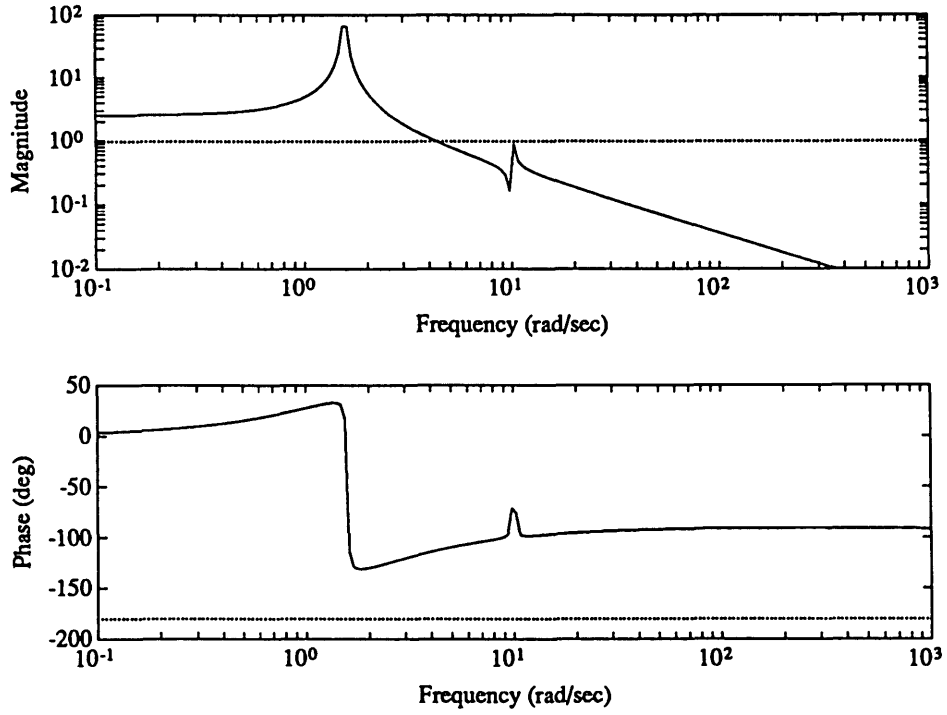

Figure 3.5(b). Loop transfer function $g_{y_u}K$ for the LQG compensator and the open loop transfer function.

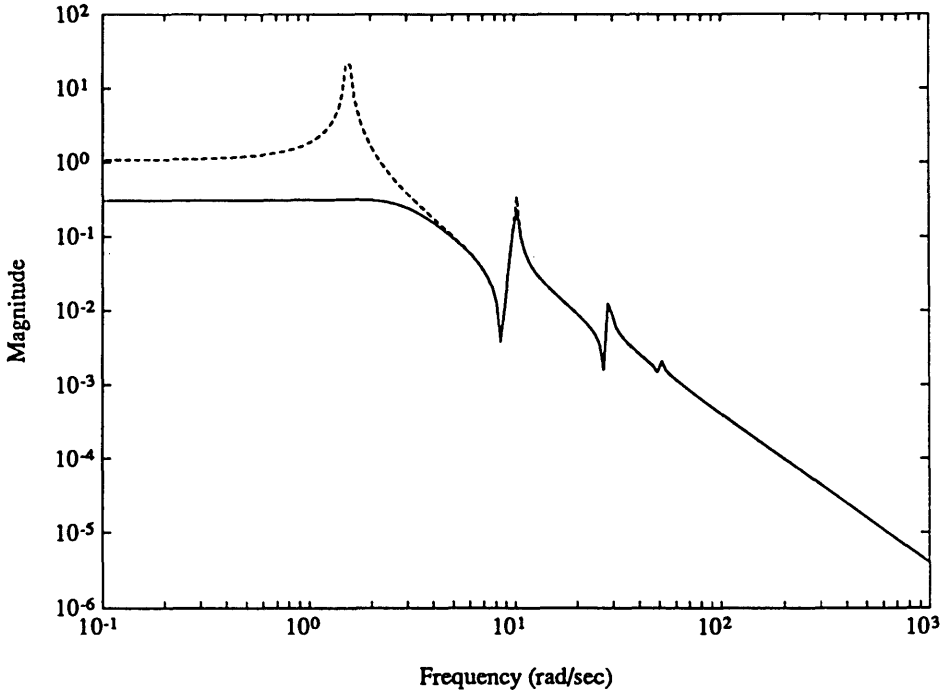

Figure 3.5(c). Open and closed loop disturbance to performance transfer functions for Typical Section 1A. Performance improvement with the LQG compensator is 27.7 dB.

region, and therefore does not fall clearly into the low or high gain LQG controller cases. This mode is in Region 3, as in Figure 3.3. Notice that the open loop zero is inverted by the compensator pole exactly. However, the open loop pole is not exactly inverted. The zero is inverted because the poles of the compensator, as given in Equations 3.17 and 3.19, are the zeros of the input output transfer function, and are not a function of the LQR weighting ρ. In contrast, the pole will be inverted if it is far above the bandwidth of the system, and not be inverted if it is well within the bandwidth. The resulting compensator zero is neither a compensator pole zero cancellation, as in the high gain LQG controller, or an open loop pole inversion, as in the low gain LQG controller. It is an intermediate case.

Also note that the dominant pole pair at 1.6 rad/sec is not inverted. The high gain asymptote (Equation 3.20) would not invert it, and neither would the low gain

asymptote (Equation 3.17), since it is the dominant mode.

Figure 3.5(c) shows the open and closed loop transfer functions from w to z. The performance metric used is

$$J = \sigma_z \tag{3.19}$$

where σ_z is the variance of the position z. For this LQG compensator, the performance improvement in the closed loop is 27.7 dB.

Figure 3.6 shows LQG compensators designed for Typical Section 1A for three values of the LQR control weighting ρ. The Kalman Filter weighting μ is held constant at 1E-8. Figure 3.6(b) shows the corresponding loop transfer functions, $g_{yu}K$, for the three LQG compensators. Notice that as ρ is decreased, i.e. as the bandwidth of the loop transfer function increases, the zero frequency of the PI controller increases, as does the gain of the compensator and loop transfer function. Thus, there is a larger frequency range which matches the high gain integral control of the LQG asymptote (Equation 3.20).

Notice how the poles of the compensator do not change. They are fixed at the zeros of the open loop input output transfer function, g_{yu}. The zeros of the compensator move from the poles of the open loop transfer function g_{yu} (Equation 3.17), to the zeros of the open loop transfer function g_{yu} (Equation 3.19). For instance, examining the compensator pole zero inversion for the mode at 10 rad/sec, as ρ decreases, the compensator zero moves toward the fixed compensator pole, thus decreasing the residue of the pole. If ρ were made smaller, the residue continue to decrease to zero, creating a compensator pole zero cancellation. This results in the compensator not inverting the modes within the bandwidth of the system, as ρ decreases, which can be seen in the loop transfer functions.

The most dominant mode at 1.6 rad/sec is never inverted. In the closed loop,

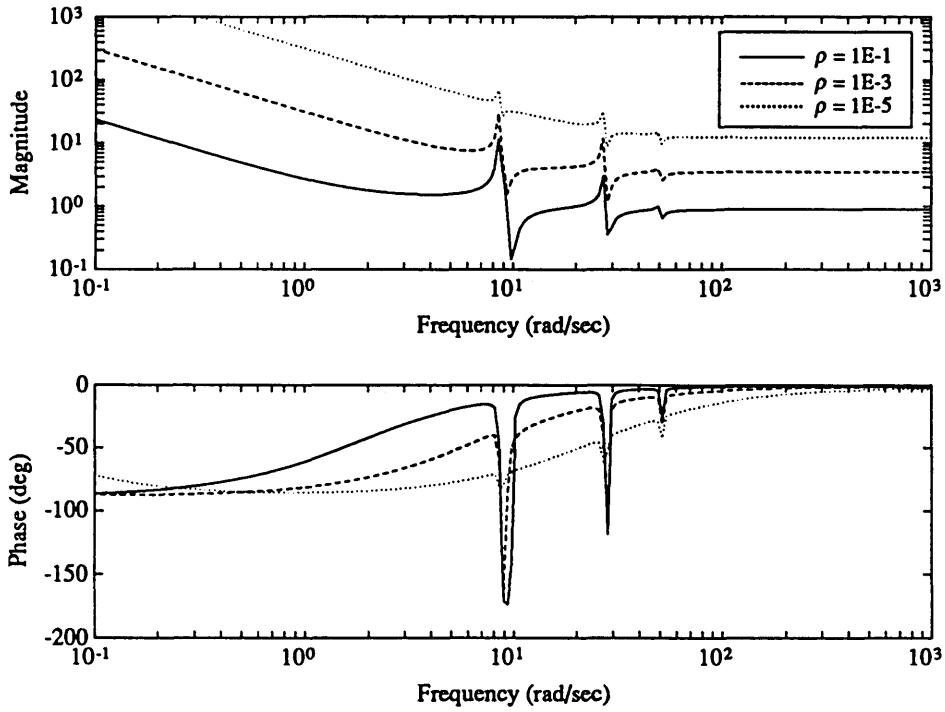

Figure 3.6(a). LQG compensators for Typical Section 1A for three values of ρ. μ=1E-8.

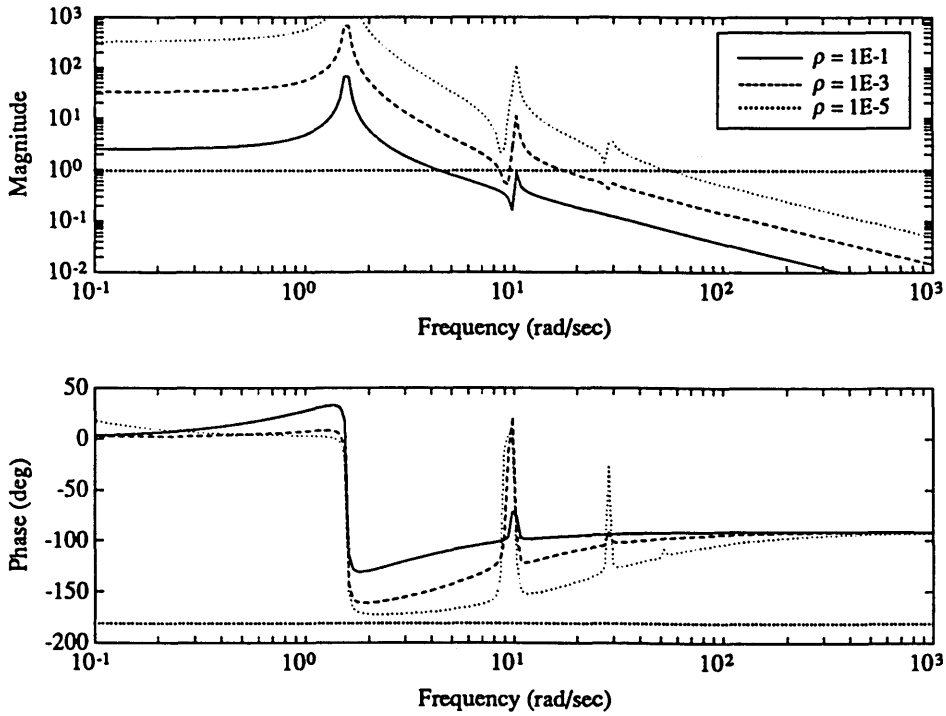

Figure 3.6(b). Loop transfer functions corresponding to the three LQG compensators in Figure 3.6(a).

these dominant poles essentially act as a second order mode, whose closed loop frequency becomes greater as the control weighting is decreased.

Now that the trends in optimal compensation are understood for low sensor noise weighting, and varying control effort weightings, the LQG compensators will be analyzed for changes in the Kalman Filter weighting μ. Figure 3.7(a) shows three LQG compensators for a constant LQR weighting (ρ=1E-1), but the Kalman Filter weighting is varied. Figure 3.7(b) shows the corresponding loop transfer functions, $g_{yu}K$, for the three LQG compensators. As μ is increased, representing an increasingly noisy sensor, the PI controller becomes a lag filter, as the frequency of the integrator pole rises. In the general high gain asymptote in Equation 2.31 if μ is not assumed to be less than ρ, then for Topology I asymptote, instead of an integrator, the high gain LQG controller resembles a high gain lag controller, with a pole at $\sqrt{\mu/\rho}$. Or, as the sensor becomes more noisy, pure integration of the output is not used. The zero of the PI controller does not move as μ is varied.

As μ is decreased, a high frequency, heavily damped pole pair decreases in frequency, thus creating a steeper rolloff in the compensator and loop transfer functions in Region 4. In Section 2.4, it was shown that to design for sensor noise minimization, a magnitude requirement should be placed on the closed loop transfer function at high frequency, or

$$\left|\frac{z}{v}\right| = |G(j\omega)K(j\omega)| = K_v \tag{3.22}$$

Increasing the value of μ is equivalent to the sensors becoming more noisy. A classical designer would decrease the value of the design criterion K_v in Equation 3.22, if the sensors became more noisy, thus decreasing the magnitude of the loop transfer function $g_{yu}K$ at higher frequency. In examining Figures 3.7(a) and (b), this is what the LQG compensator does.

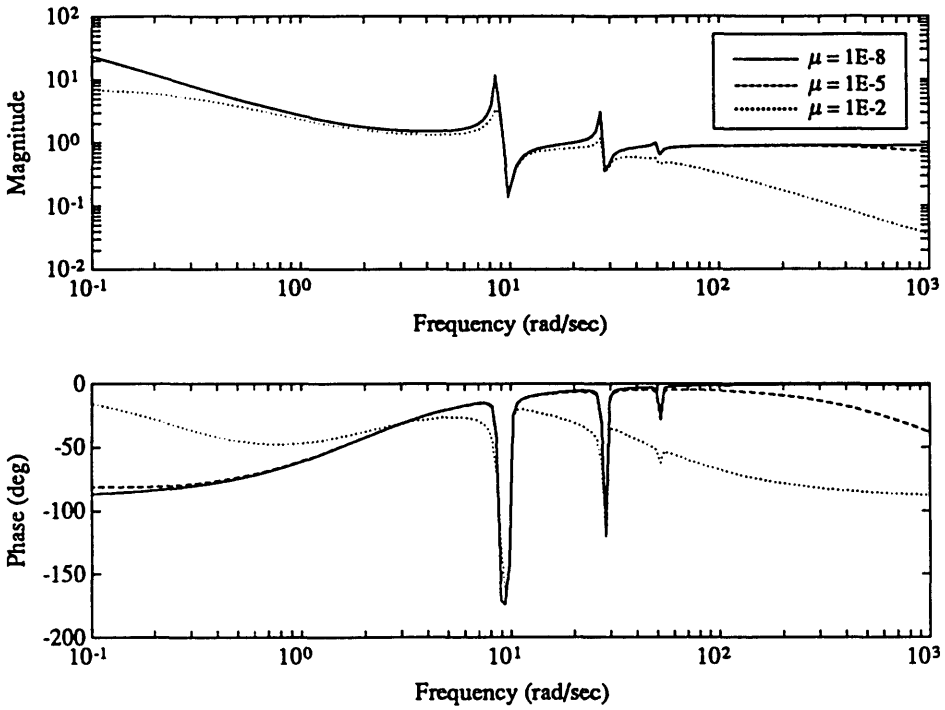

Figure 3.7(a). LQG compensators for Typical Section 1A for three values of μ. ρ=0.1.

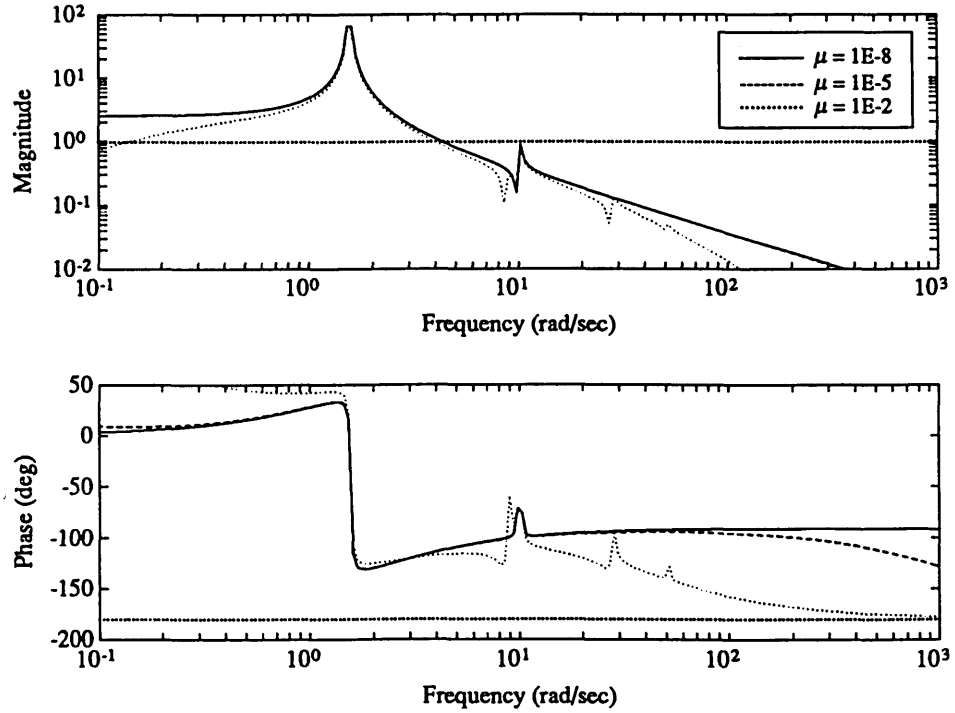

Figure 3.7(b). Loop transfer functions corresponding to the three LQG compensators in Figure 3.7(a).

Multiple Dominant Modes

Figure 3.8 shows the open loop input output transfer function g_{yu} for Typical Section 1B (Figure 3.1(b)). In this case, there are two dominant modes at 1.6 and 10 rad/sec. Figure 3.9(a) shows an 8 state LQG compensator and the low and high gain LQG asymptotes for Typical Section 1B. The Kalman Filter uses low sensor noise again (μ=1E-8), and the LQR weighting is set as an intermediate value (ρ=7E-4). The bandwidth is 15 rad/sec, as shown in the loop transfer function in Figure 3.9(b). The compensator once again contains a PI controller, with a zero at 7 rad/sec, used to create a phase margin at loop crossover of approximately 60°. At higher frequencies, the open loop dynamics, g_{yu}, are inverted by the compensator. At frequencies below crossover, the open loop zero pair at 4 rad/sec is inverted by a pole pair of the compensator, however, the two most dominant modes at 1.6 and 10

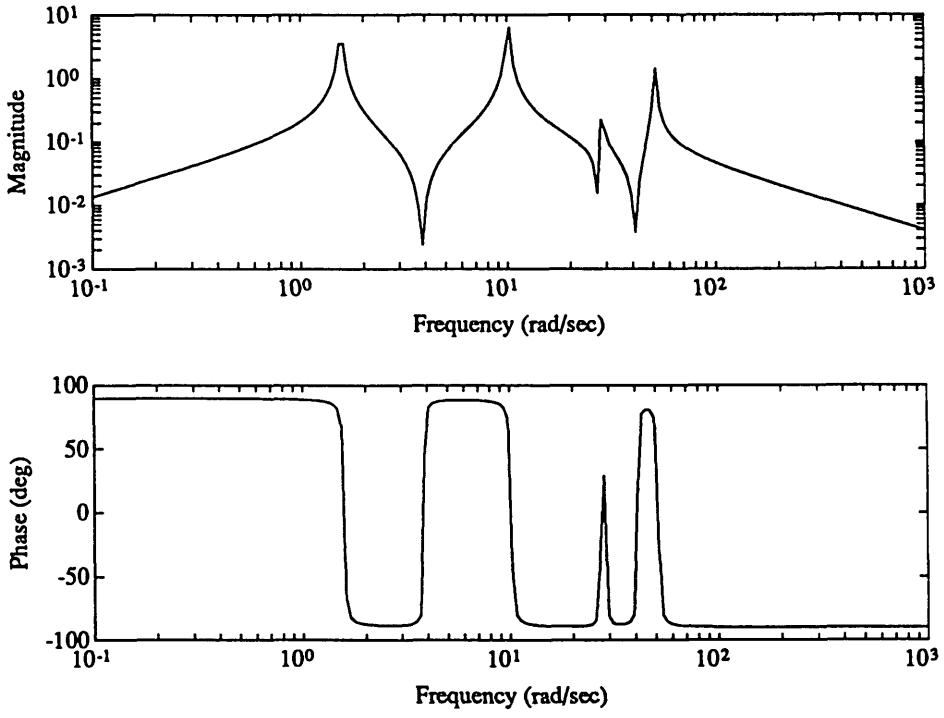

Figure 3.8. Open loop input output transfer function g_{yu} for Typical Section 1B.

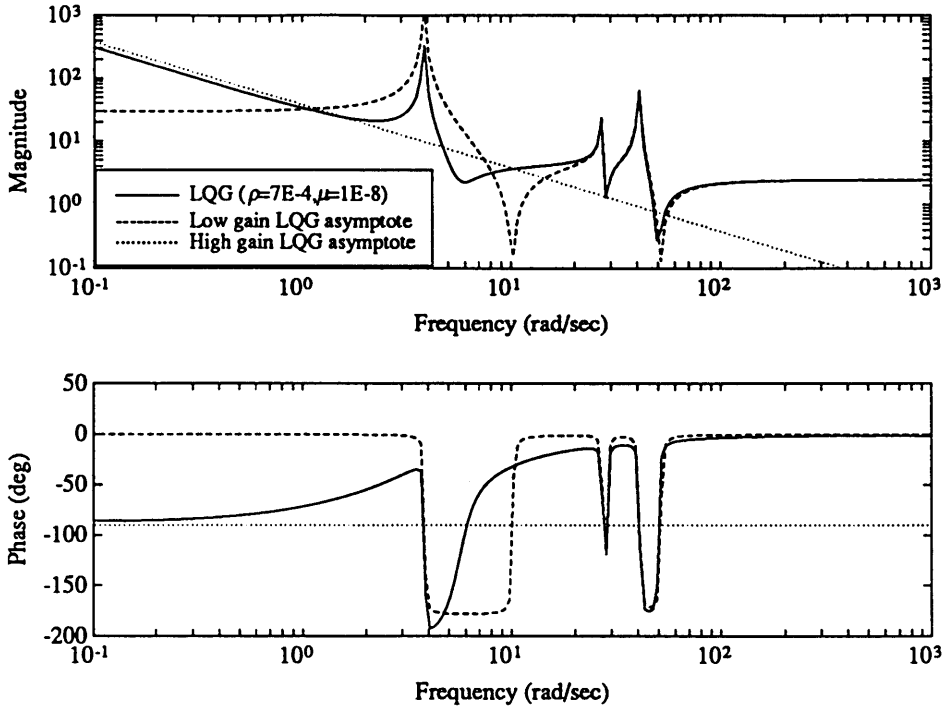

Figure 3.9(a). 8 state LQG compensator K (ρ=7E-4, μ=1E-8) for Typical Section 1B, and the low and high gain LQG asymptotes.

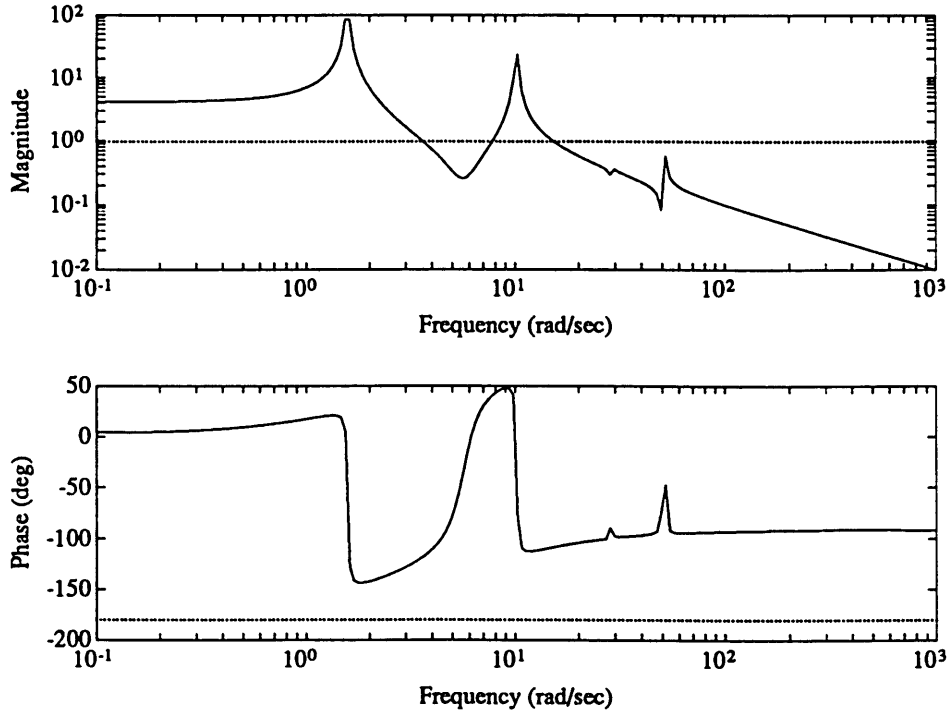

Figure 3.9(b). Loop transfer function $g_{yu}K$ for the LQG compensator and open loop transfer function.

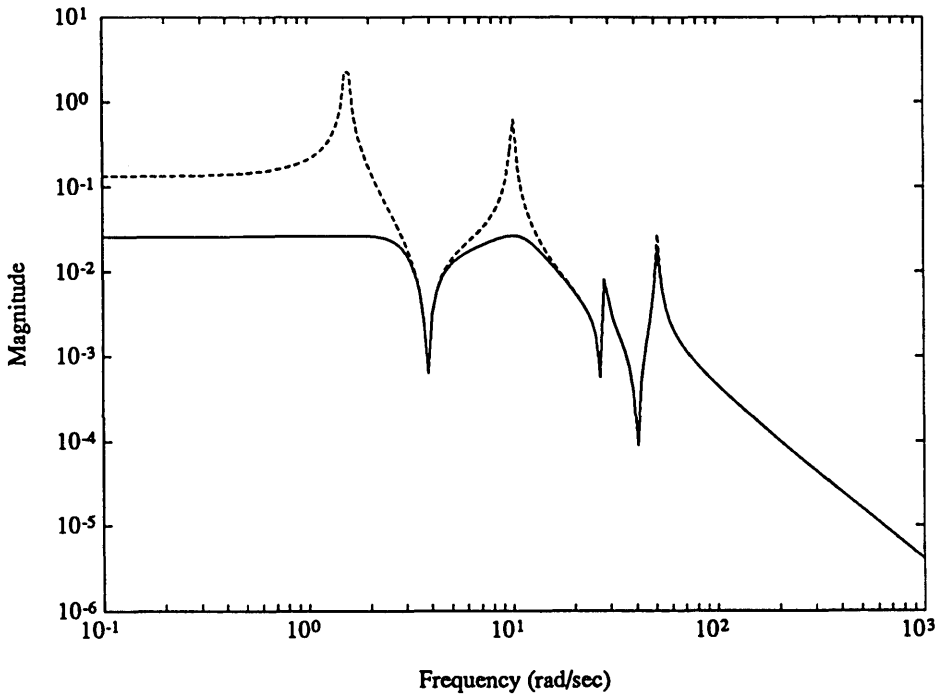

Figure 3.9(c). Open and closed loop disturbance to performance transfer functions for Typical Section 1B. Performance improvement with the LQG compensator is 31.1 dB.

rad/sec are not inverted.

The mode at 10 rad/sec is in the crossover region, as a result of the 15 rad/sec crossover frequency of the loop transfer function (Figure 3.9(b)). Equation 2.28 showed that for a two mode example, the low gain LQG asymptote will place a weighted zero pair between the two pole pairs, if both pole pairs are dominant. As ρ decreases, and the bandwidth increases, this weighted zero pair should migrate to a compensator pole pair, according to the high gain LQG asymptote, creating a compensator pole zero cancellation. For this compensator, there is a zero pair at 6 rad/sec and 30% damping ratio, and is migrating toward the pole pair at 4 rad/sec. If ρ were decreased further, the compensator zero pair cancel the pole pair at 4 rad/sec, and become a high gain integrator as in the high gain LQG asymptote. Note that this is the same result as for the single dominant modes case. Therefore, except

for the low gain LQG compensator which places a weighted zero pair between the two dominant poles, compensation of a system with two dominant modes is quite similar to compensation of a system with only one dominant mode. And if both dominant modes are far within the bandwidth, i.e. in Region 1, compensation is identical to a system with only one dominant mode.

Sensitivity Weighted LQG

One of the weaknesses of LQG compensators for controlled structures is lack of robustness. In compensators described previously, the pole zero inversions can create closed loop stability problems if there are small modelling errors in the open loop frequencies of the poles and zeros. Examining the phase of the compensators, the pole zero inversions have phase drops of at least 150° for some modes. If the open loop system has even slight modelling errors, this phase drop could de-stabilize the closed loop system very easily. The Sensitivity Weighted LQG compensator, as described in Section 2.3, will be seen to robustify these pole zero inversions.

Figure 3.10(a) show three SWLQG compensators designed for the Typical Section 1A, and Figure 3.10(b) shows the corresponding loop transfer functions $g_{yu}K$. The LQR and Kalman Filter weightings are the same as the LQG compensator in Figure 3.5(a). Notice that the crossover of the loop transfer function is approximately 4 rad/sec. The three compensators shown have increasing uncertainty in the mode at 10 rad/sec. This mode is chosen because it lies within the crossover region, and after the loop crossover, corresponding to Region 3 in Figure 3.3. As the uncertainty increases, or as the weighting factor β in the SWLQG compensator increases, the pole of the compensator pole zero inversion damps quickly, but the zero does not. The phase drop due to this pole zero inversion is not as large. As β increases, the pole zero inversion in the SWLQG compensator begins to resemble the notch filter shown in Figure 2.3(a).

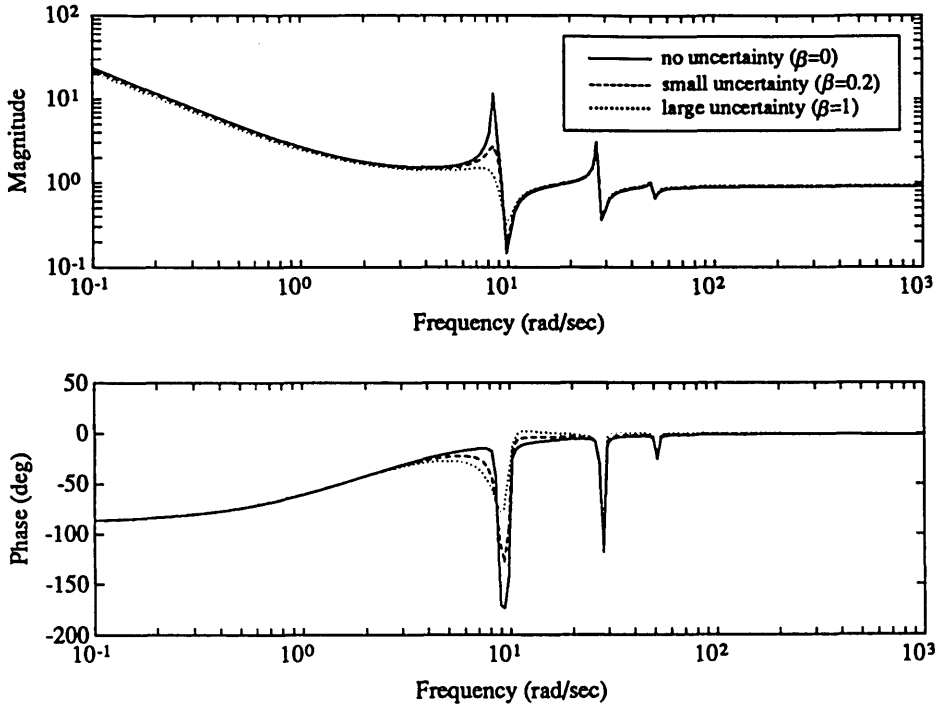

Figure 3.10(a). SWLQG compensators for Typical Section 1A for three different uncertainties in the mode at 10 rad/sec (Region 2).

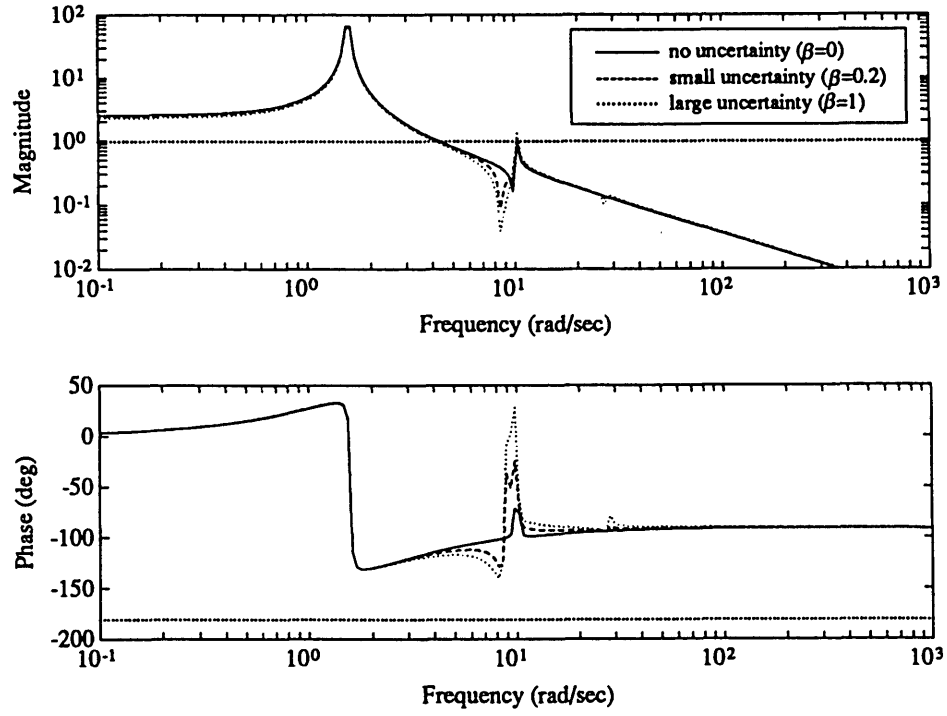

Figure 3.10(b). Loop transfer functions $g_{yu}K$ for the three SWLQG compensators above. The loop crossover is 4 rad/sec.

Figure 3.11 shows a comparison of a pole zero inversion and notch filter. The notch filter is given by

$$\frac{s^2 + 2\zeta_o \omega s + \omega^2}{s^2 + 2\alpha\zeta_o \omega s + \omega^2} \tag{3.23}$$

Note that the *width* of the bucket in the magnitude plot of the notch filter controlled by the choice of ζ_o, while the *depth* of the notch is a function of α. The parameters for the notch filter are chosen such that the depth of the magnitude bucket of the notch filter is the same as that of the pole zero inversion, and the width is wider, to accommodate increased uncertainty in the open loop pole frequency. In examining the phase plot, the absence of the lightly damped pole used to invert an open loop zero creates a smaller phase drop in the compensator phase. Instead of -150° of phase drop, which could de-stabilize the system if there are modelling errors, the notch filter phase drop is only -50°. The zero inversion of an open loop pole is

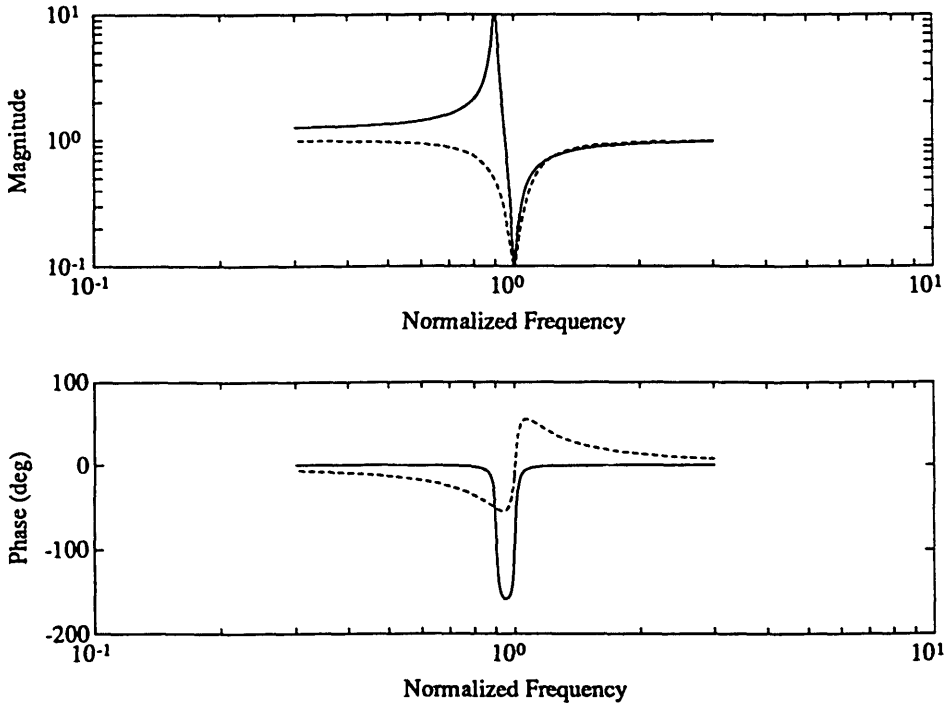

Figure 3.11. A notch filter (ω=1, ζ_o=0.2, α=10) and pole zero inversion.

preserved in the notch filter, without the large phase drop. Although the choice of ζ_o will affect the phase drop of the notch filter, the phase drop of the notch filter will never be as large as that of the pole zero inversion.

Notice also in Figure 3.10(a) the drop in gain of the compensators at low frequency, as the uncertainty in the 10 rad/sec mode is increased. This also occurs in the notch filter, pole zero inversion comparison in Figure 3.11. In return for increased robustness in the compensator by damping the lightly damped poles, the low frequency compensator gain decreases, as does the closed loop performance improvement. This is a tradeoff between performance improvement and compensator robustness.

Figure 3.12(a) shows three SWLQG compensators for de-sensitizing the same mode as in Figure 3.10(a), at 10 rad/sec, but the crossover of the loop transfer function is now 15 rad/sec. Therefore, the mode lies in Region 2 as in Figure 3.3, or in the crossover region, but before the loop crossover. Instead of adding damping to the compensator poles first, as it did in Figure 3.10(a), the SWLQG compensator damps both the poles and zeros, and moves them together, thus creating a pole zero cancellation. Therefore, for uncertain modes in Region 2, the SWLQG compensators essentially use no compensation for the structural modes, just as in the high gain LQG asymptote in Equation 3.19 for modes in Region 1. Notice also that the low frequency gain of the compensator again decreases with increased uncertainty in the 10 rad/sec mode. The SWLQG compensator is giving away a small amount of closed loop performance improvement, in return for a more robust compensator, as in Figure 3.10(a).

Truncation of Compensator States

In addition to lack of robustness, another weakness of LQG compensators is in the large dimension. If there are compensator dynamics that are not important to

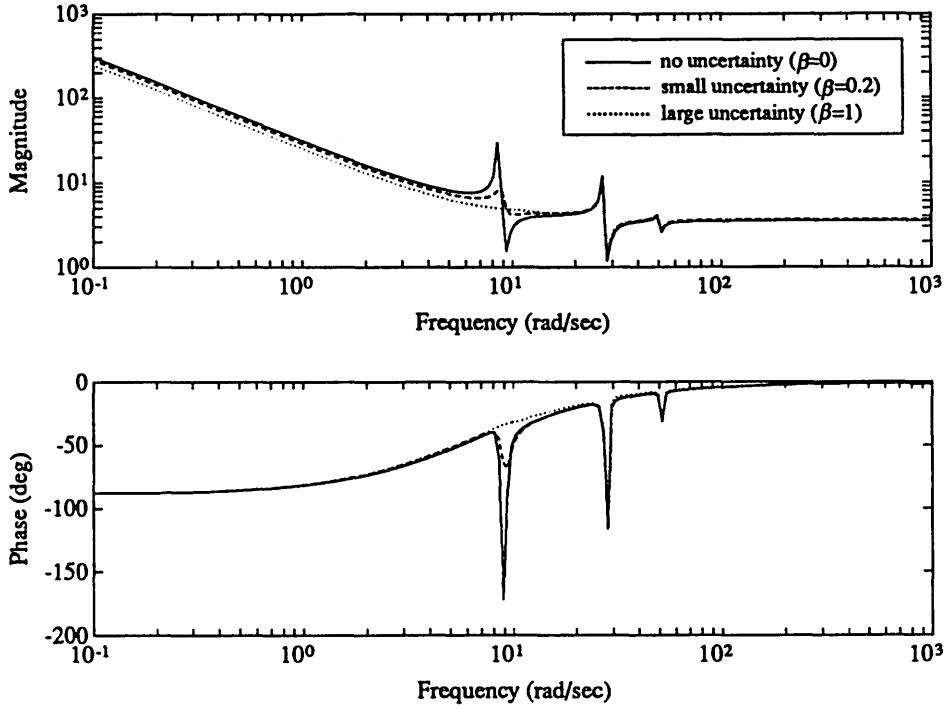

Figure 3.12(a). SWLQG compensators for Typical Section 1A for three different uncertainties in the mode at 10 rad/sec (Region 3).

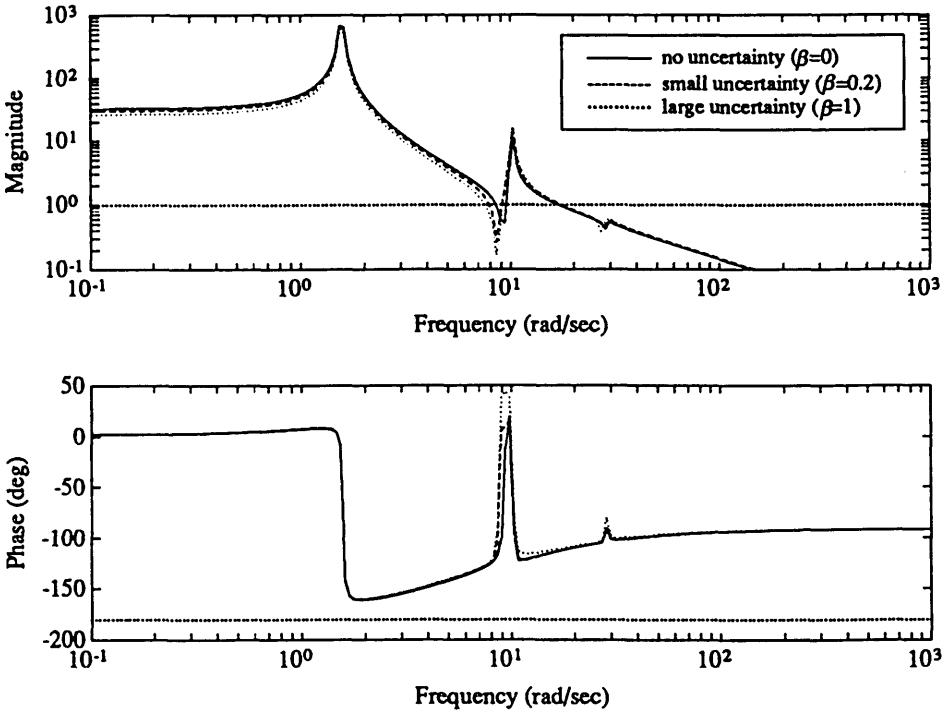

Figure 3.12(b). Loop transfer functions $g_{yu}K$ for the three SWLQG compensators above. The loop crossover is 15 rad/sec.

the stability and performance goals of the controller design, then they considered superfluous and may be truncated. For this topology, the locations of the compensator pole zero inversions, in relation to the regions in Figure 3.3 will yield the importance, and possible truncation of compensator states. The compensator dynamics in Region 1, according to Equation 3.19, are pole zero cancellations. These dynamics, therefore, can be truncated from the compensator. For the compensator dynamics in Region 2, from the SWLQG compensators in Figure 3.12(a), the pole zero inversions often are removed in the robustification process, and therefore can be truncated from the compensator.

Compensator dynamics in Region 3 are addressed by the SWLQG compensators in Figure 3.12(a). For these dynamics, the pole zero inversions often became notch filters. Therefore, these dynamics are not truncated. Compensator dynamics in Region 4 are given by the low gain, LQG asymptote in Equation 3.17, or the inversion of the input to output transfer function g_{yu}. In examining an example of these dynamics, in Figure 3.5(a) and (b), the LQG compensator contains pole zero inversions of the modes at 28 and 51 rad/sec. These dynamics lie in Region 4, well after the loop crossover at 4 rad/sec. If these dynamics are truncated, the performance and stability of the closed loop system would not be altered. Therefore, compensator dynamics in Region 4 are truncated.

The decision of where the division between Regions 3 and 4 in Figure 3.3 is very important. According to the previous discussion, it means the difference between truncating or not truncating modes in a compensator. Modes in Region 3 have loop gains above -3 dB, while those in Region 4 do not. Checking the closed loop stability, therefore, is very important when designing the compensator.

Summary

The optimal LQG compensator for topologies such as those given in Section

3.2 was presented in the previous section. The LQG compensator is a blending of the high gain LQG asymptote (Equation 3.19) and the low gain LQG asymptote (Equation 3.17), with the division between the two approximately the crossover frequency of the loop transfer function $g_{yu}K$. The high gain asymptote is a high gain controller, with the temporal relationship between the performance and output. The low gain asymptote is a rate feedback controller, inverting the input output transfer function at high frequency. The LQR weighting, ρ, changes the bandwidth of the system, and therefore the mixture of the high and low gain LQG asymptotes, as was shown in Figure 3.6(a). Also, as the sensor noise in the system increases, or as the Kalman Filter weighting μ increased, the high gain integral control used at low frequency becomes high gain lag control. And the rolloff of the compensator and loop transfer function is made steeper, by using a high frequency, heavily damped pole pair in Region 4. These were both shown in Figure 3.7(a) and (b).

In Region 1, open loop modes are not inverted, and the compensator uses pole zero cancellations. These modes are therefore, able to be truncated from the compensator. The LQG compensator, far outside the bandwidth in Region 4, inverts the dynamics in the disturbance to output transfer function g_{yw}, or the input output transfer function g_{yu} in this case. Because these compensator dynamics do not affect the closed loop performance or stability, they are able to be truncated. For modes within the crossover region, or in Regions 2 and 3, the LQG compensator exactly inverts the open loop zero with compensator poles, but do not exactly invert the open loop poles with compensator zeros. The SWLQG compensator robustifies modes in Region 2 by creating compensator pole zero cancellations, as shown in Figure 3.10(a). These compensator dynamics, therefore, can be truncated. And when the SWLQG compensator robustifies modes in Region 3, the compensator creates dynamics similar to notch filters, as shown in Figure 3.12(a).

The benefits of the optimal LQG compensator, along with the robustification

and truncation of superfluous states, are used to make a low order, robust compensator called a Neo-Classical compensator.

3.4 Neo-Classical Control

In this section, the analysis of compensator design from the previous section are interpreted to create a set of rules to design low order, robust compensators for the topology given in Section 3.2, or Topology I. These rules are used by convolving each step into the compensator, until a low order, robust compensator is returned at the completion of the design rule. Neo-Classical Design Rule 1 for analogous performance and output, and analogous disturbance and input, and collocated, dual, and complementary extreme, input and output topology is shown below.

Neo-Classical Design Rule 1

For analogous performance and output, *and* analogous disturbance and input, *and* collocated, dual, and complementary extreme input and output:

A. **Design a low frequency controller for Regions 1 and 2, i.e.**

$$K = k_0 \phi_{zy}$$

where k_0 is a gain used to set the bandwidth of the system subsequently, and ϕ_{zy} is the temporal relationship between the performance z and the output y.

B. **Select a bandwidth. Design the high frequency controller for Regions 3 and 4 such that the convolution of A and B yields a rate feedback compensator at high frequency. Adjust k_0 such that the crossover of the loop transfer function is equal to the choice of bandwidth. Insure that placement of these dynamics is made such that the phase margin at the loop crossover is approximately 30°-60°.**

C. **Add higher frequency rolloff dynamics, if necessary.**

D. **Examine the loop transfer function, $g_{yu}K$, consisting of the open loop system, g_{yu}, and the compensator designed from rules 1A-C. Notch filter all modes in Region 3, which may affect the closed loop stability of the system. If necessary, iterate to B if the phase margin is not in the 30°-60° range.**

The Neo-Classical compensator is a compilation of the previous results from the optimal compensation analysis, for topologies which fall into the Topology I category. In Design Rule 1A, a low frequency controller is created for Region 1, which resembles the high gain LQG asymptote given in Equation 3.19. It is a high gain controller, with the temporal relationship $\phi_{zy}(s)$.

$$K = k_0 \phi_{zy} \tag{3.24}$$

where the gain k_0 will be used to set the bandwidth after Design Rule 1B is completed.

Design Rule 1B states that first, a bandwidth is chosen. Then, a high frequency controller is designed. The LQG compensator, according to the low gain LQG asymptote in Equation 3.17, is a rate feedback controller, with the inversion of the disturbance to output transfer function, or input to output transfer function in this case, at high frequency, except for the dominant mode. The inversion of the dynamics of g_{yu} in Region 4 were shown to be superfluous, and compensation for modes in Region 3 is addressed in Design Rule 1D. Therefore, only a rate feedback controller is designed for high frequency in Design Rule 1B, with no extra compensator dynamics. The dynamics of this controller are convolved with the controller designed in Design Rule 1A (Equation 3.24), to yield a high frequency rate feedback compensator. For instance, if the temporal relationship ϕ_{zy} is an integrator, as in Typical Sections 1A and 1B, then the low frequency controller would be integral control, or position feedback. In order to design a high frequency rate feedback controller, a zero is added at an intermediate frequency, creating proportional control of the output, or rate feedback. In the example, the placement of the zero is made such that the phase margin of the loop transfer function is between 30° and 60°. This is how all dynamics are placed, as stated in the Design Rule 1B. The design constant k_0 is then adjusted, such that the crossover of the loop

transfer function is equal to the choice of the bandwidth.

Following Design Rule 1C, a high frequency rolloff is designed, consisting of two heavily damped poles, or one real pole. This rolloff is used for noise attenuation, and the rolloff of high frequency dynamics, and should only be used if necessary. The rolloff of the open loop transfer function may be sufficiently steep, such that no rolloff in the compensator is needed.

Design Rule 1D states that the loop transfer function, made up of the open loop transfer function g_{yu}, and the compensator designed from Design Rules 1A-C, is examined. Modes from Region 3, which have a loop gain above -3 dB are examined for possible closed loop stability problems. Those modes which present questionable closed loop stability are gain stabilized by using notch filters. The notch filter is used, as a result of the robust compensation techniques of the SWLQG compensators for modes in Region 3, as shown in Figure 3.12(a).

As an example, a Neo-Classical compensator is designed for Typical Section 1A, shown in Figure 3.1(a). The open loop transfer function g_{yu} is shown in Figure 3.13. This is dual to the LQG design in Figure 3.5(a)-(c). As shown in Design Rule 1A, a low frequency controller is constructed from the high gain LQG asymptote, or

$$K = k_0 \phi_{zy} = k_0 \frac{1}{s} \tag{3.25}$$

The value for the gain k_0 is adjusted when Design Rule 1B is complete.

The bandwidth chosen is the same as the bandwidth of the LQG compensator in Figure 3.5(b), or 4 rad/sec. Design Rule 1B states that a controller is designed such that its convolution with the controller from 1A yields a high frequency rate feedback controller. For this case, integral control (position feedback) is the low frequency controller, as shown in Equation 3.25. Therefore, a zero is convolved into the compensator to make the high frequency controller a proportional controller, or

rate feedback. This zero is placed at 1.8 rad/sec, such that the phase margin of the loop transfer function at the 4 rad/sec crossover is approximately 60°.

Design Rule 1C states that a rolloff controller is added, if necessary. A one pole rolloff is added, with a corner frequency of 100 rad/sec. Finally, the gain k_o is adjusted, such that the loop crossover of the compensator designed from 1A-C and the open loop system g_{yu}, is 4 rad/sec.

Design Rule 2D states that the loop transfer function from the compensator created from Design Rules 1A-C and the open loop transfer function g_{yu} is examined. Figure 3.14(a) shows the compensator designed from Design Rules 1A-C, and the corresponding loop transfer function is shown in Figure 3.14(b). Notice that the loop gain for the mode at 10 rad/sec is above -3 dB. This mode is stable for this particular system, but in a system with phase delays, its stability might be questionable because of a small phase margin. Therefore, this mode is notch filtered. A notch

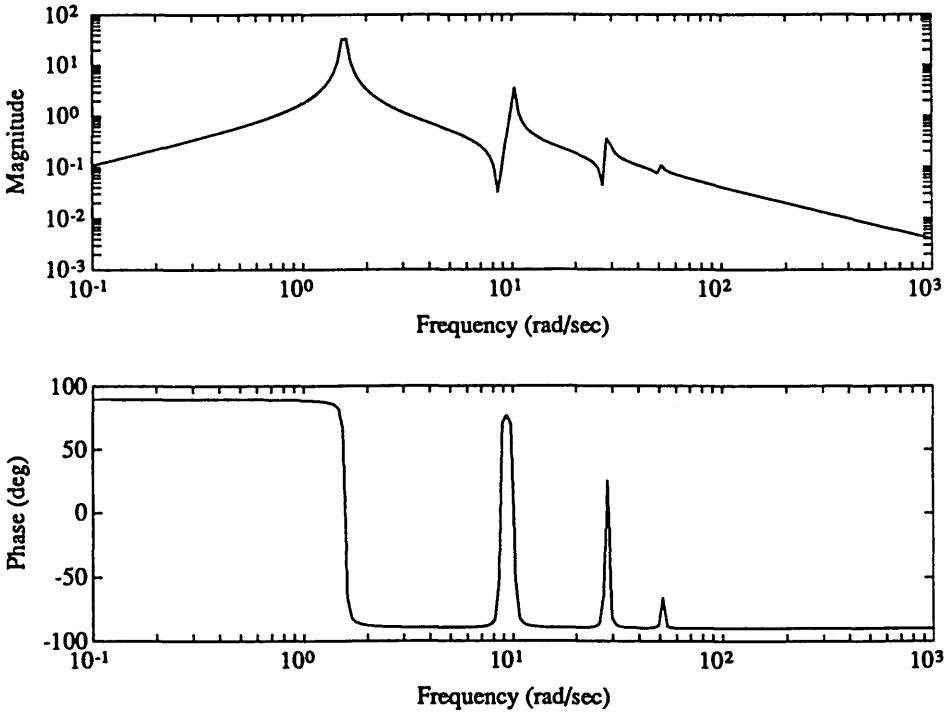

Figure 3.13. Open loop input output transfer function g_{yu} for Typical Section 1A.

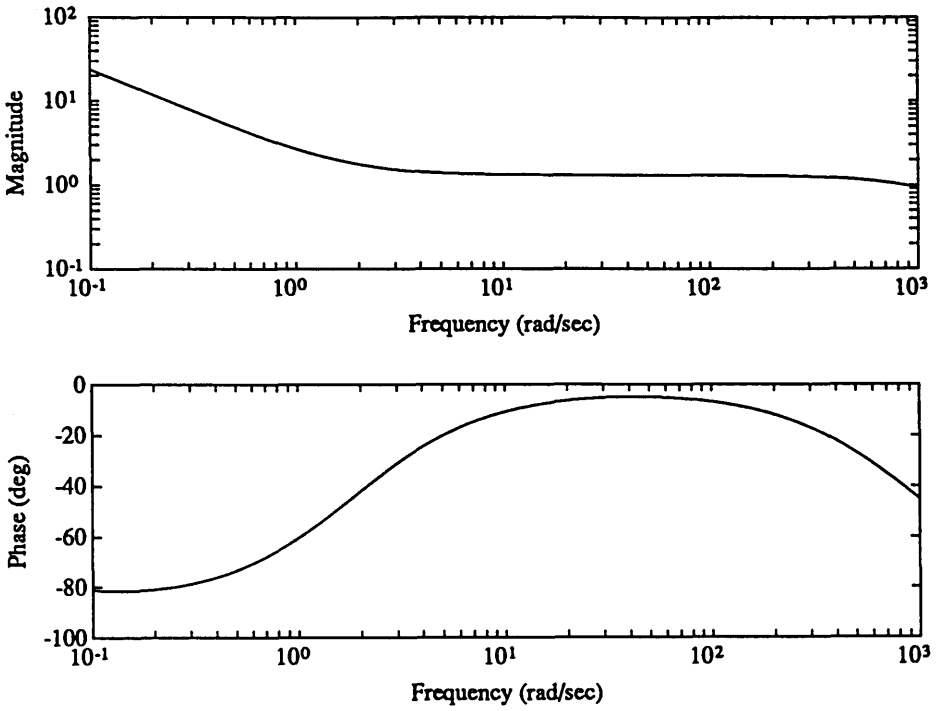

Figure 3.14(a). Proportional-integral (PI) controller (ω_z=-1.8 rad/sec) with a one pole rolloff (ω_p=-100 rad/sec) for Typical Section 1A.

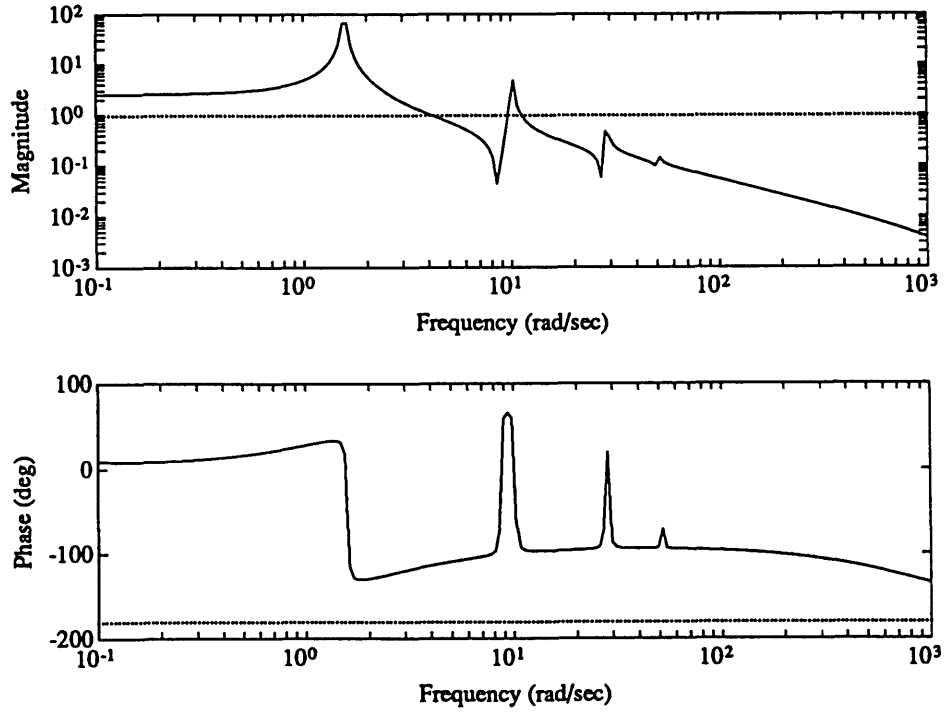

Figure 3.14(b). Loop transfer function $g_{yu}K$ consisting of the PI controller and rolloff and the open loop transfer function.

filter, as in Equation 3.23, is constructed for this example with the following characteristics: ω=10, α=10, ζ_o=0.02.

Notice the modes above 10 rad/sec. These modes fall into Region 4, from Figure 3.3, and therefore are not compensated, as stated in Design Rule 1B.

Figure 3.15(a) shows the resulting 4 state Neo-Classical compensator, plotted with the 8 state LQG compensator from Figure 3.5(a), designed for Typical Section 1A. The corresponding loop and closed loop transfer functions are shown in Figures 3.15(b) and (c). Notice the low frequency gain of the two compensators is identical. This is a result of both compensators having a system bandwidth of 4 rad/sec, and using a low frequency integral control. Both the Neo-Classical and LQG compensators gain stabilize the open loop pole at 10.1 rad/sec with a compensator zero inversion. However, the Neo-Classical compensator has no compensator pole, as an inversion of the of the open loop zero at 8.6 rad/sec. The high frequency pole zero inversions in the Neo-Classical compensator at 28 and 51 rad/sec are not present in the LQG compensator. Also at high frequency, the gain of the compensator is greater than that of the LQG compensator. This is the result of using the more robust notch filters, rather than pole zero inversions.

In comparing the loop transfer functions of the Neo-Classical compensator with and without the notch filter in Figures 3.15(b) and 3.14(b) respectively, the mode at 10.1 rad/sec is gain stabilized. Also notice that the phase at crossover is 50°, within the 30°-60° range. Figure 3.12(c) shows the open and closed loop disturbance to performance transfer functions. The performance improvement of the Neo-Classical design is the same as the LQG design, 27.7 dB. The Neo-Classical compensator has 4 states, compared to the 8 state LQG compensator. The robustness of the Neo-Classical compensator is better, from not using lightly damped compensator poles at 8.6, 27, and 51 rad/sec to cancel open loop zeros.

Figure 3.16 shows the open loop input output transfer function g_{yu}, for

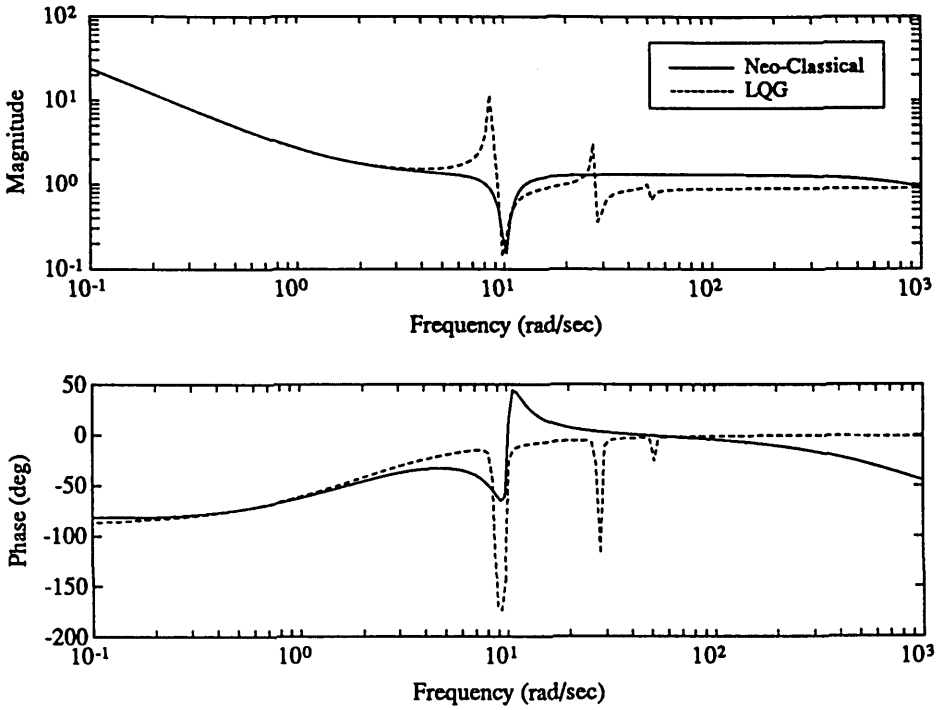

Figure 3.15(a). 4 state Neo-Classical compensator K and the LQG compensator (ρ=1E-1, μ=1E-8) for Typical Section 1A.

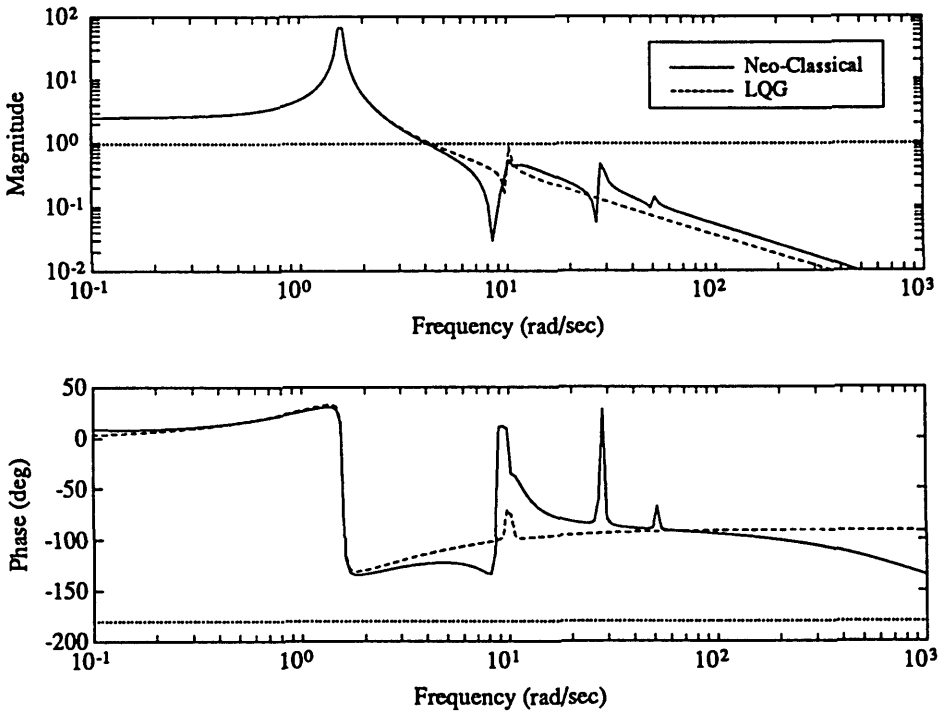

Figure 3.15(b). Loop transfer functions $g_{yu}K$ consisting of the compensators in Figure 3.15(a) and the open loop transfer function.

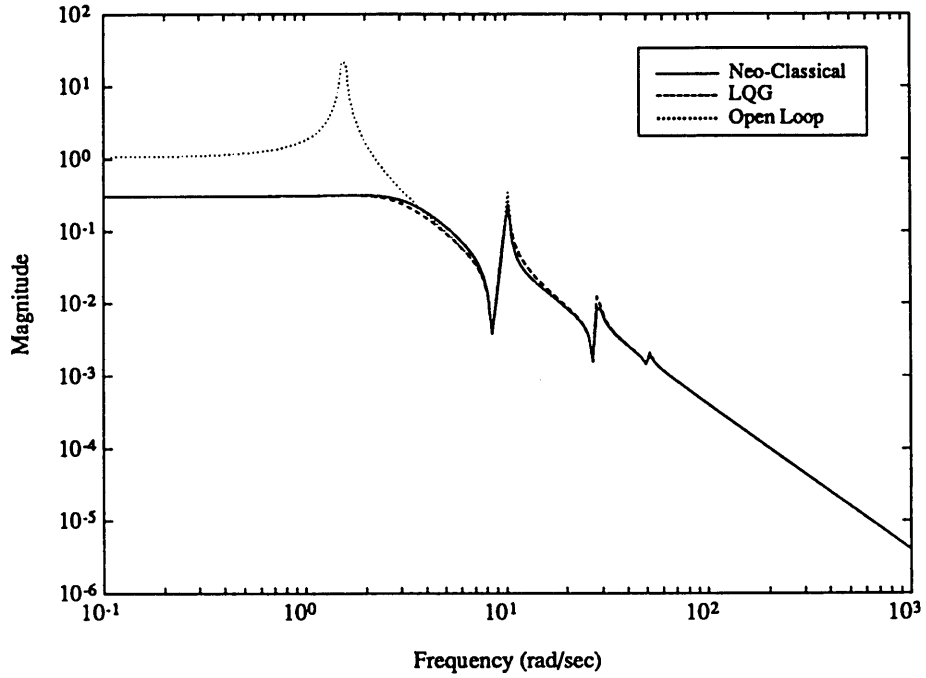

Figure 3.15(c). Open and closed loop disturbance to performance transfer functions for Typical Section 1A. Performance improvement with both the Neo-Classical and LQG compensators is 27.7 dB.

Typical Section 1B in Figure 3.1(b). In order to design a Neo-Classical compensator for this typical section, Design Rule 1 is again used. This design is dual to the LQG design in Figures 3.9(a) and (b). Using Design Rule 1A, the low frequency controller again is high gain integral control, as in Equation 3.25. The gain constant k_o is set when Design Rule 1B is completed.

Using design Rule 1B, a bandwidth of 15 rad/sec is selected, identical to that of the LQG compensator in Figure 3.9(b). The high frequency rate feedback controller is created by placing a zero in the compensator. The zero frequency is set at -2.5 rad/sec, such that the phase margin at the 15 rad/sec crossover is approximately 60°. The gain constant k_o is set such that the bandwidth of the system is 15 rad/sec.

A one pole rolloff filter is added to the compensator, following Design Rule

1C. The pole frequency is set at 100 rad/sec.

Design Rule 1D states that the loop transfer function of the compensator designed with Design Rules 1A-C, and the open loop transfer function g_{yu}, is examined. The modes at 28 and 51 rad/sec create a loop gain greater than -3 dB, therefore these modes are gain stabilized with two notch filter with the following characteristics: (ω=28, α=10, ζ_o=0.02) (ω=51, α=20, ζ_o=0.02).

Figure 3.17(a) shows the resulting 6 state Neo-Classical and 8 state LQG compensators (Figure 3.9(a)) for Typical Section 1B, shown in Figure 3.1(b). Notice how the two compensators are again very similar at low frequency. The LQG lightly damped compensator poles or open loop zero inversions are not used in the Neo-Classical compensator, and the compensator zeros or open loop pole inversions are very similar for modes at 28 and 51 rad/sec. The high frequency gain of the Neo-Classical compensator again is higher than that of the LQG compensator, due to the

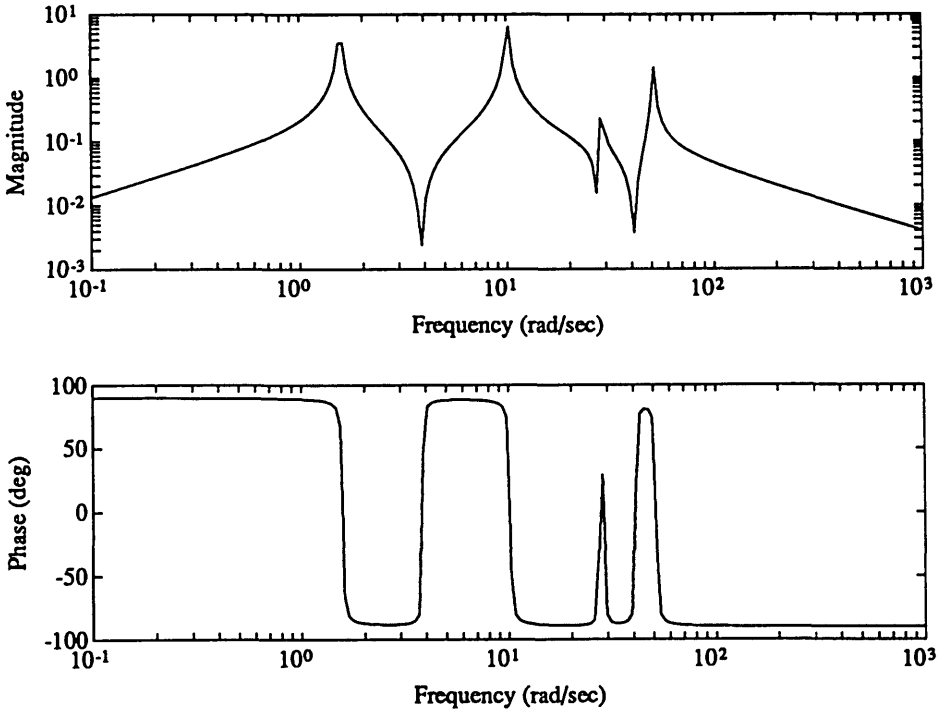

Figure 3.16. Open loop input output transfer function g_{yu} for Typical Section 1B.

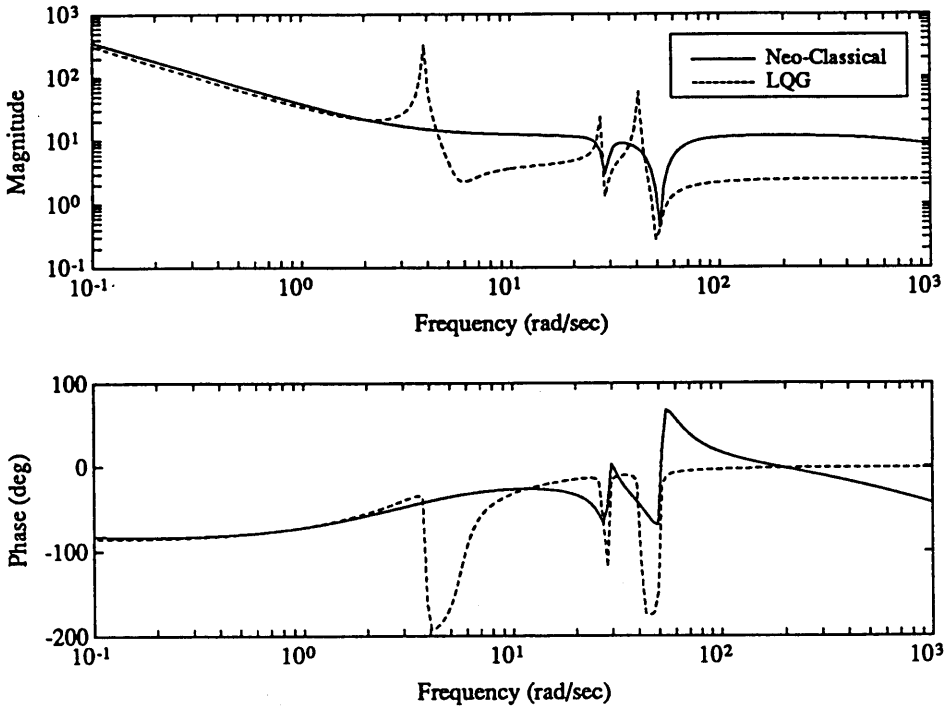

Figure 3.17(a). 6 state Neo-Classical compensator K and the LQG compensator (ρ=1E-2, μ=1E-8) for Typical Section 1B.

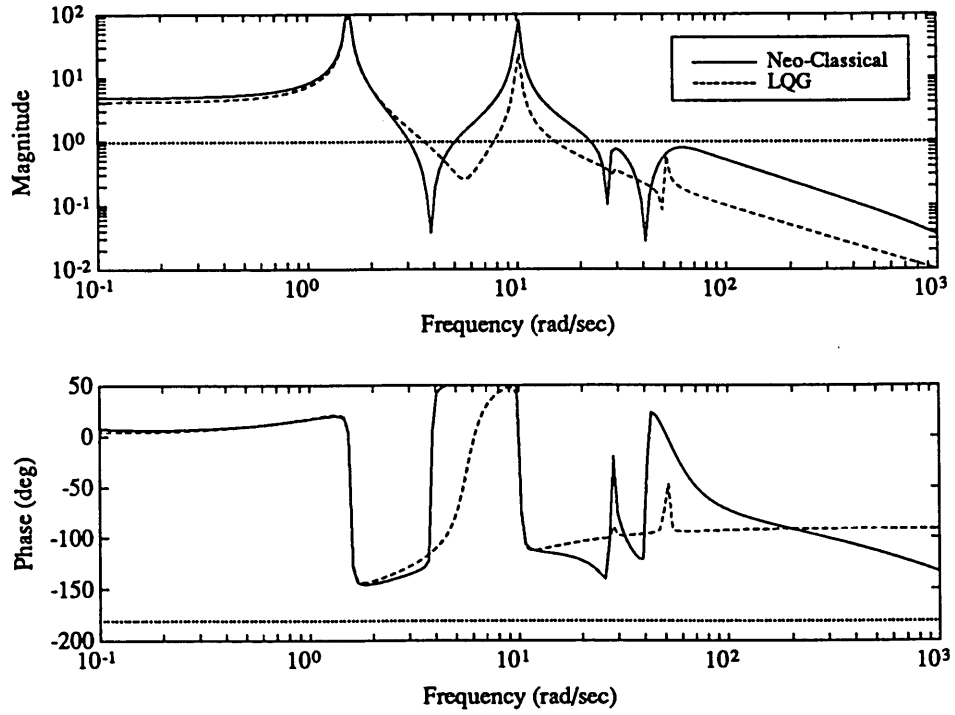

Figure 3.17(b). Loop transfer functions $g_{yu}K$ consisting of the compensators in Figure 3.17(a) and the open loop transfer function.

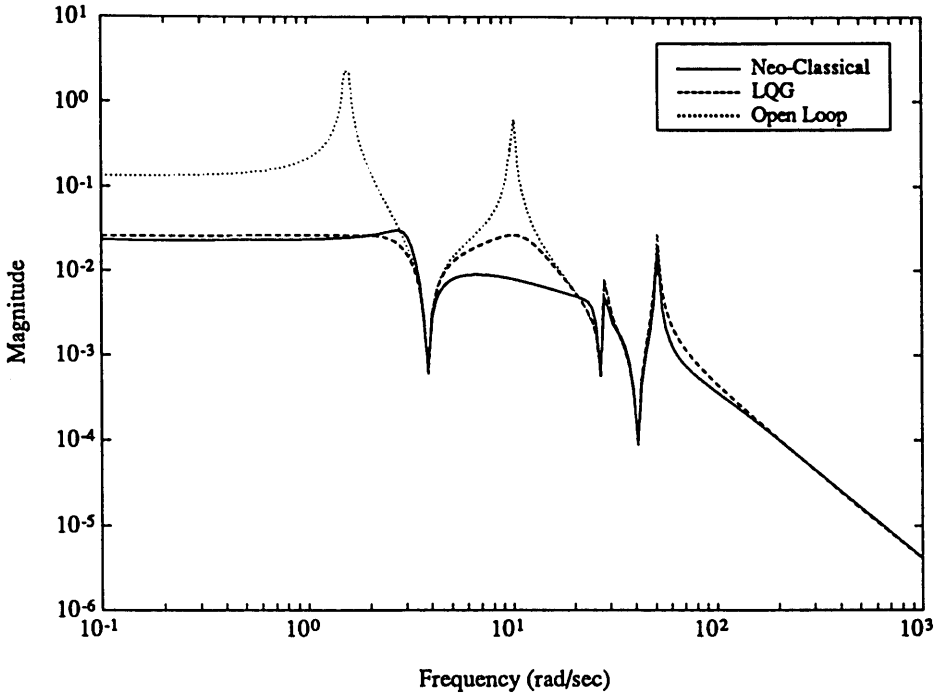

Figure 3.17(c). Open and closed loop disturbance to performance transfer functions for Typical Section 1B. Performance improvement with both the Neo-Classical and LQG compensators is 31.1 dB.

use of notch filters.

Figure 3.17(b) shows the loop transfer function for the Neo-Classical compensator and LQG compensators. Notice how the modes at 28 and 51 rad/sec are gain stabilized by both compensators, but the Neo-Classical compensator does not compensate the modes at 1.6 and 10.1 rad/sec because they lie within the bandwidth.

Figure 3.17(c) shows the open and closed loop disturbance to performance transfer functions, for both the Neo-Classical and LQG compensators for Typical Section 1B in Figure 3.1(b). The closed loop performance improvement from both designs is 31.1 dB. The Neo-Classical compensator has 6 states, compared to the 8 state LQG compensator. The robustness of the Neo-Classical compensator is better,

as a result of not using lightly damped compensator poles at 9, 27, and 36 rad/sec to cancel open loop zeros.

3.5 Experimental Implementation

Optimal and Neo-Classical compensators such as those designed in Sections 3.2 and 3.3 were designed and implemented experimentally on the Middeck Active Control Experiment (MACE). A few different techniques such as LQG, truncated LQG, and SWLQG were used to design modern controllers, while the design rules for Neo-Classical control presented in Section 3.3 were used to design Neo-Classical controllers.

The first topology for which controllers were designed and run was MACE 1A, a pointing loop around the payload z-axis, shown in Figure 3.18. The performance metric z is the z-axis integrated rate gyro in the payload. The metric is bandlimited, from 0.5-50 Hz. The output y is also the z-axis rate gyro in the

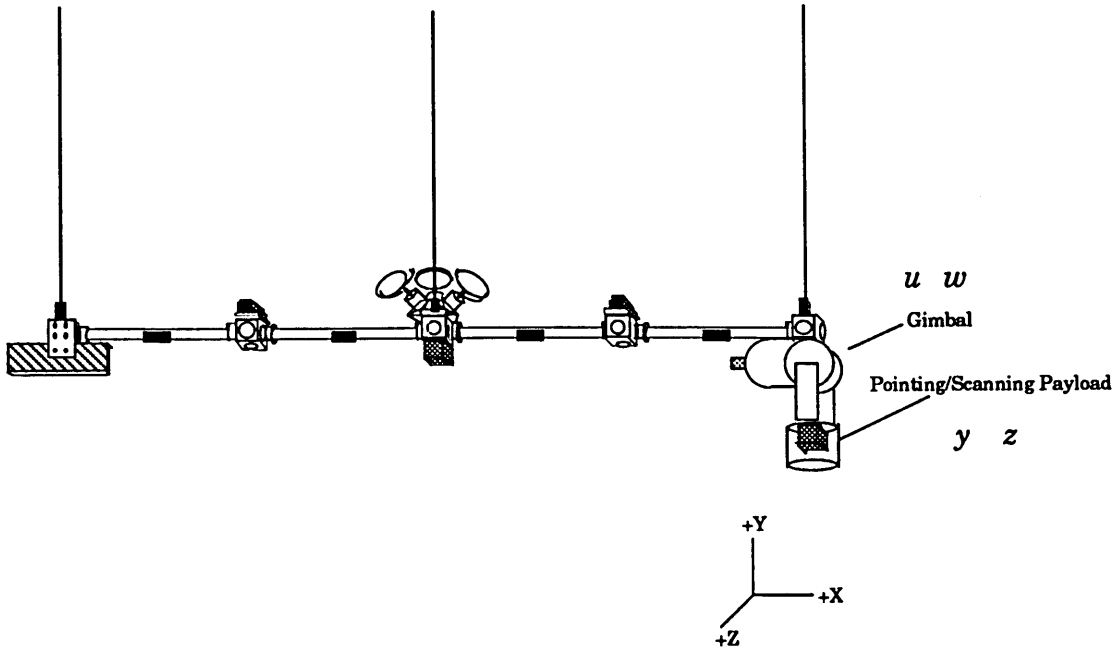

Figure 3.18. MACE 1A: The topology for the payload pointing loop.

payload. The disturbance w and the output u are the z-axis relative torque of the gimbal. Because the input is a relative torque between the payload and the end of the bus, and the output is the inertial rotational velocity of the payload, the loop is collocated but not dual. Fleming (1990) showed that a collocated sensor actuator pair, which are not dual, but preserve the alternating pole zero pattern, can be treated as dual. Such sensor actuator pairs are called pseudo-dual.

For this topology, the performance z is the time integration of the output y, giving the following relationship between the two

$$z = \phi_{zy} y = \frac{1}{s} y \tag{3.26}$$

The disturbance w and the input u are identical.

$$w = u \tag{3.27}$$

Therefore, this topology falls into the Topology I category

The experimental measurement of the input output transfer function, g_{yu}, is shown in Figure 3.19. Notice how the phase reflects the alternating pole zero pattern, but it also shows a large phase delay in the loop. If there was no phase delay in the system, the phase at 20 Hz would be -90°. However, the rate gyro, Bessel filter, and AC-100 add a time delay which makes the phase -180° at 20 Hz. The finite element model, which was used for the control designs, was a 40 state model, with 2 states for the integrated rate gyro, 3 states for the rate gyro dynamics, and 4 states for the PADE approximation of the time delay in the control loop, and 31 states for the structural modes.

Figure 3.20(a) shows a model based 23 state compensator, which was truncated from a 40 state LQG compensator, designed from the 40 state model. The

truncation was based upon a Hankel Singular Value analysis [Pro-Matlab (1992)] and only affected modes in the compensator above 100 Hz, which were not important in the experiment. Thus, for the purposes of this experiment, the 40 state and 23 state LQG compensators were equivalent.

The LQG compensator used integral control (position feedback) at low frequency, similar to the high gain LQG asymptote given in Equation 3.20. The integral control changes to proportional control (rate feedback) with the use of a zero at 8 Hz, creating a PI controller similar to the previous LQG compensators. The LQG compensator also used pole zero inversions of the modes at 6.8, 9.4, 14, 36, and 88 Hz. This is consistent with the low gain LQG asymptote (Equation 3.17), which inverts the input output transfer function, g_{yu} at high frequencies, except for the dominant mode.

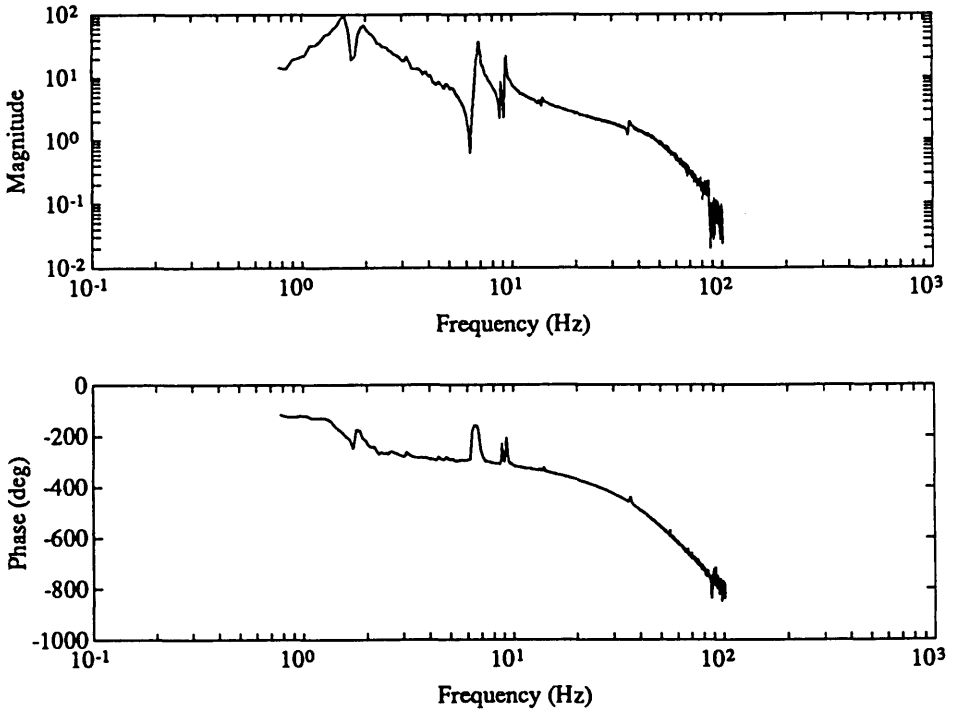

Figure 3.19. Measurement of the open loop input output transfer function g_{yu} from z-axis gimbal to z-axis payload rate gyro, for MACE 1A.

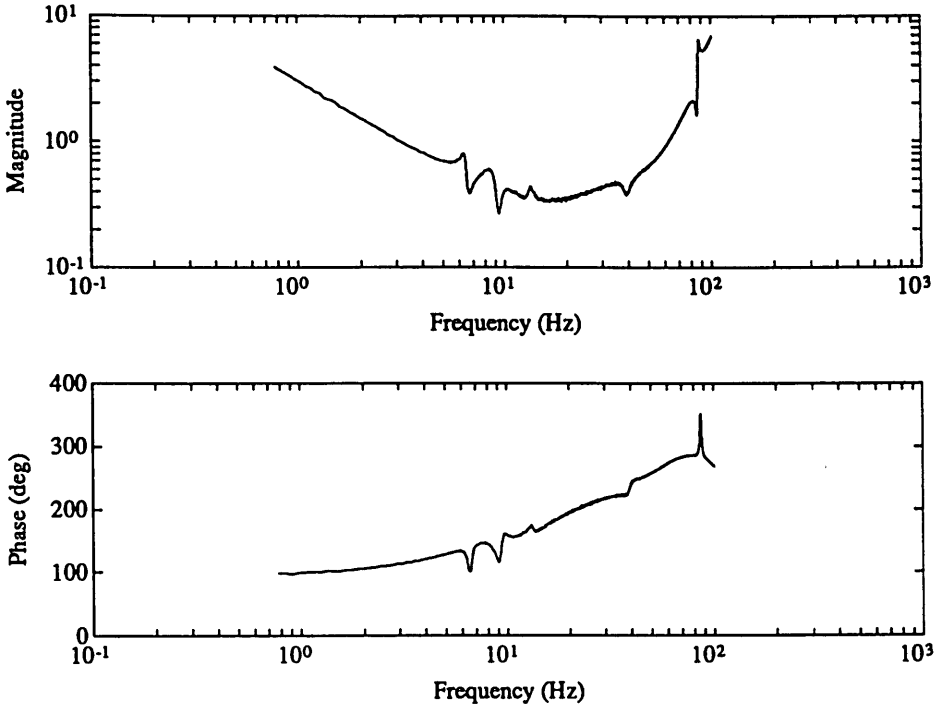

Figure 3.20(a). Model based 23 state LQG compensator K designed for MACE 1A.

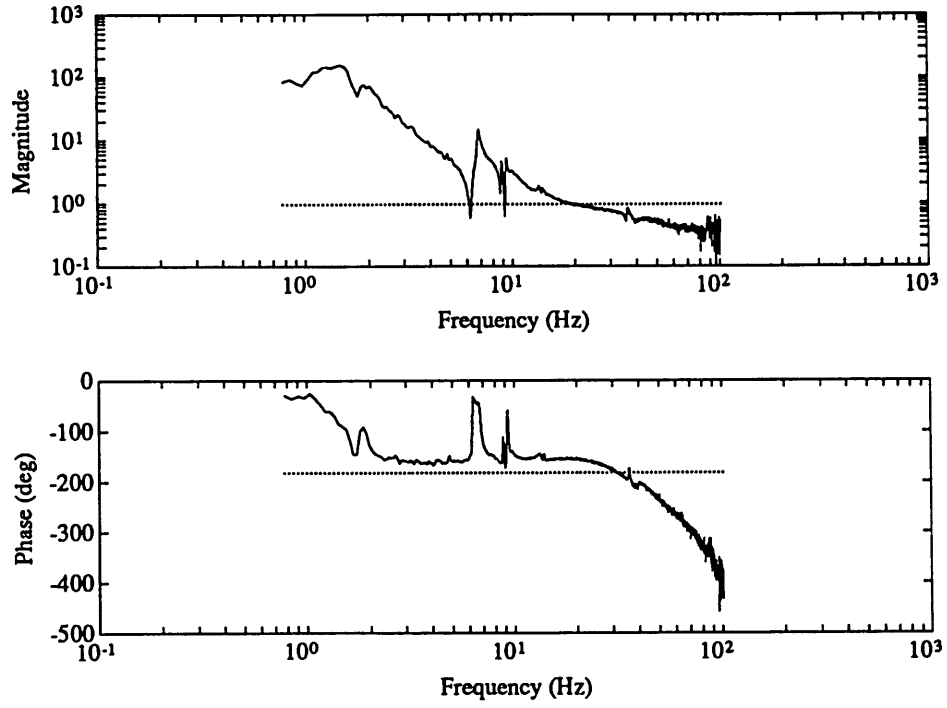

Figure 3.20(b). Measurement of the loop transfer function $g_{yu}K$ consisting of the LQG compensator and open loop transfer function.

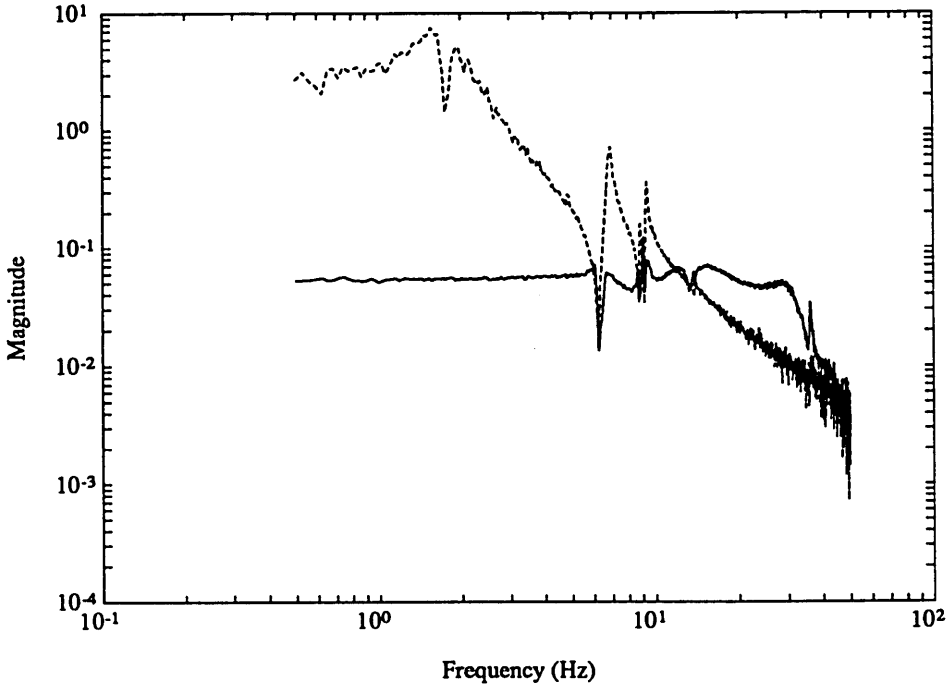

Figure 3.20(c). Measurement of the open and closed loop disturbance to performance transfer functions for MACE 1A. Performance improvement with the LQG compensator was 25.7 dB.

Figure 3.20(b) shows a measurement of the loop transfer function, $g_{yu}K$, consisting of the model based 23 state LQG compensator (Figure 3.20(a)), and the open loop transfer function (Figure 3.19). Notice how the compensator pole zero inversions of the modes at 6.8, 9.4, and 14 Hz were not exact, but the inversions of the modes at 36 and 88 Hz were approximately exact. This is agreeable with the previous analysis of LQG compensators, where modes that lie in Region 2 (6.8, 9.4, and 14 Hz) are not exactly inverted in an LQG compensator, while modes in Region 4 (36 and 88 Hz) are exactly inverted.

An aspect of the LQG compensator which was different from those designed in Section 3.3 can be seen at high frequency. There was high gain at high frequency, with commensurate phase lead added at loop crossover. Notice how the phase of the

compensator increases as the frequency increases. This was a result of the phase lead (and high frequency magnification) added by the LQG compensator. The large time delay is represented in the model using a fourth order PADE approximation, with dynamics that contain damped nonminimum phase zeros. The phase delay, therefore, limits the collocated dual properties of the control loop, and subsequently also limits the bandwidth and performance improvement for this topology. The LQG compensator constructed several lead filters in order to compensate for this phase lag, adding phase lead at crossover, at the expense of high frequency amplification. A discussion of this type of compensation is in Chapter 6, for noncollocated control with nonminimum phase zeros in the input output transfer function g_{yu}.

Figure 3.20(c) shows the measured open and closed loop disturbance to performance transfer functions for the model based 23 state LQG compensator MACE 1A. The performance improvement with this LQG design was 25.7 dB. Notice the closed loop transfer function did not roll off with the same slope as the open loop transfer function. This was a result of the large phase lag in the open loop transfer function, and the compensation technique of phase lead and high frequency amplification in the LQG controller. Further increase in the bandwidth of the LQG compensator, by decreasing the LQR weighting ρ, created closed loop stability problems at high frequency. As ρ decreased, in an attempt to increase performance improvement, the gain and bandwidth of the compensator increased, as did the phase lead and high frequency amplification. The loop transfer function, shown in Figure 3.20(b), began to contain additional high frequency loop crossovers from modes above 50 Hz, which de-stabilized the closed loop system.

Figure 3.21(a) shows a 13 state reduced order LQG compensator, truncated down from the same model based 23 state LQG compensator in Figure 3.20(a). Truncation lower than 13 states resulted in an unstable closed loop system. Notice that most of the pole zero inversions of the compensator were truncated (6.8, 9.4, 14,

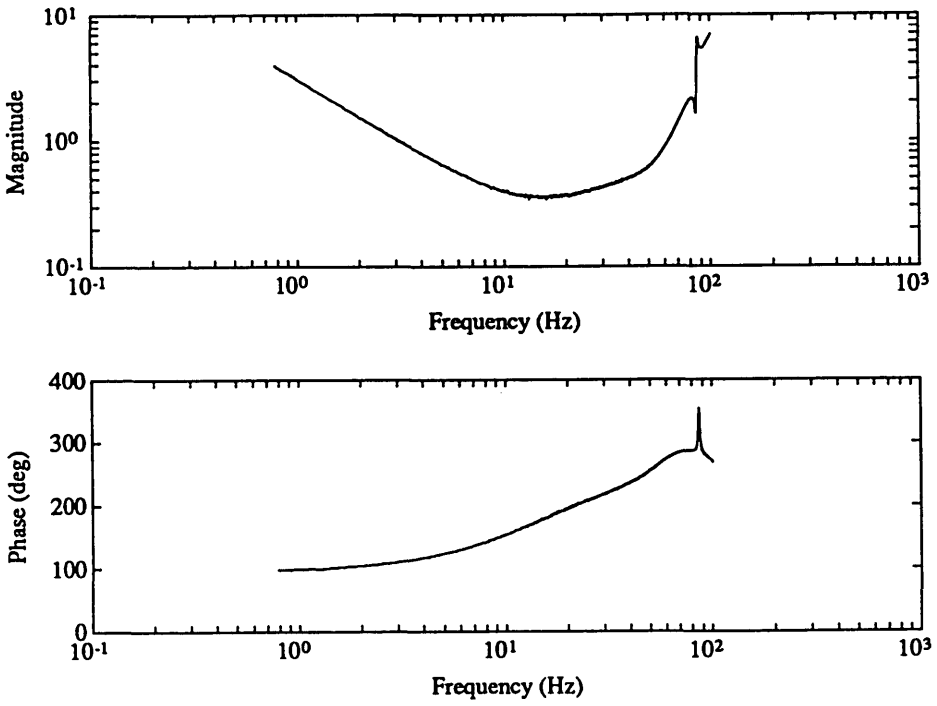

Figure 3.21(a). 13 state reduced order LQG compensator K (truncated from 23 states) for MACE 1A.

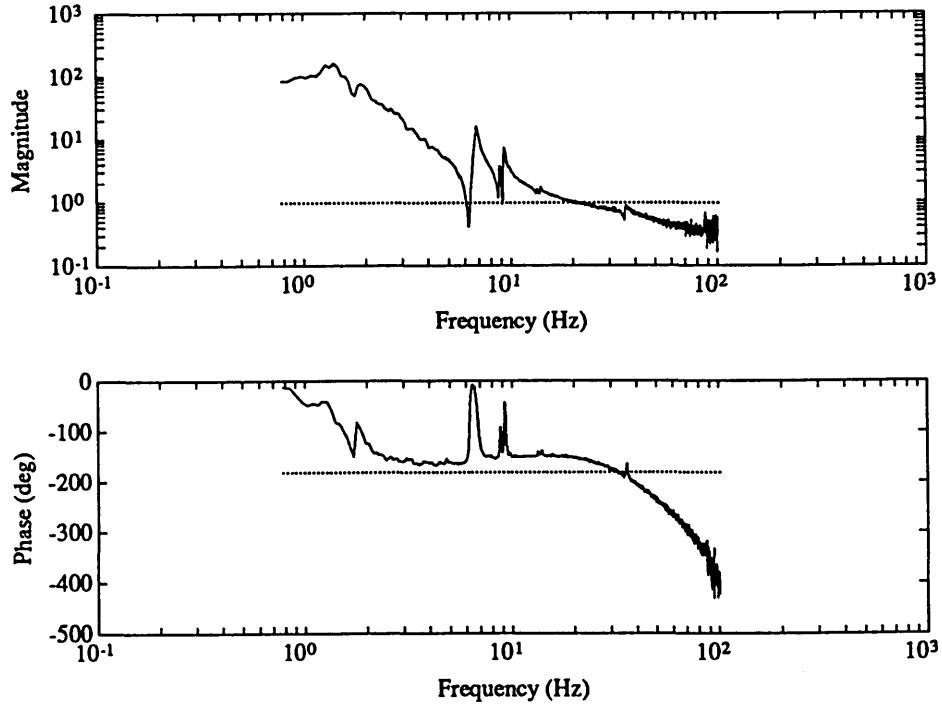

Figure 3.21(b). Measurement of the loop transfer function $g_{yu}K$ consisting of the truncated LQG compensator and the open loop transfer function.

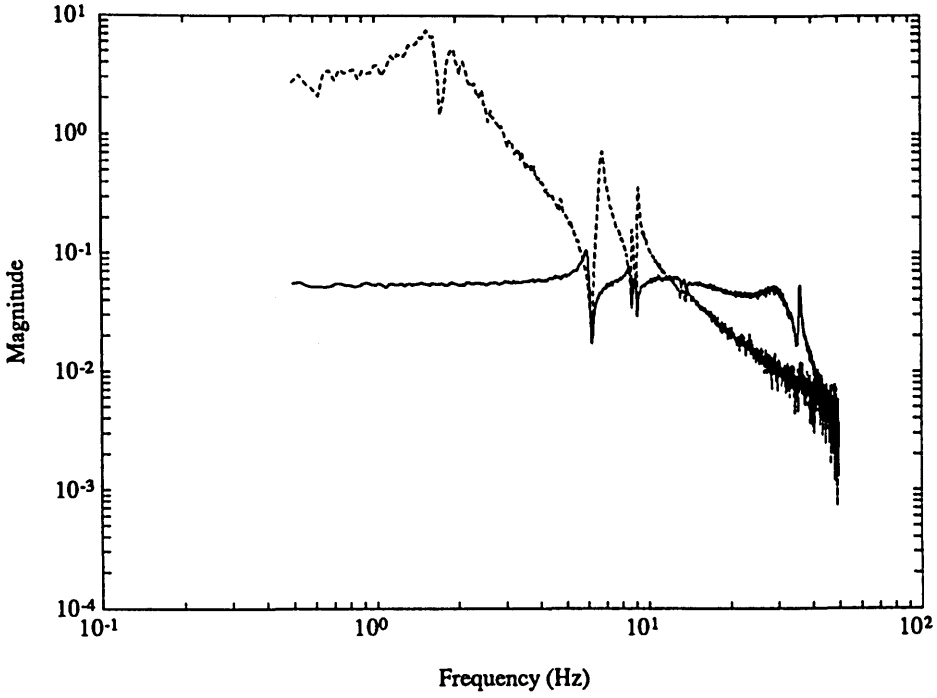

Figure 3.21(c). Measurement of the open and closed loop disturbance to performance transfer functions for MACE 1A. Performance improvement with the truncated LQG compensator was 25.8 dB.

and 36 Hz). All that remains is the PI controller with a zero at 8 Hz, and the lead filters which add phase lead at crossover and high frequency amplification, and a pole zero inversion at 88 Hz. The pole zero inversion at 88 Hz was not truncated, as it might have de-stabilized the closed loop system.

Figure 3.21(b) shows the measured loop transfer function, $g_{yu}K$, consisting of the 13 state truncated LQG compensator (Figure 3.21(a)), and the open loop transfer function (Figure 3.19). Notice the similarities to the loop transfer function from the 23 state LQG controller (Figure 3.20(b)). They are almost identical. Figure 3.21(c) shows the measured open and closed loop disturbance to performance transfer functions for the model based 13 state truncated LQG compensator MACE 1A. Notice that it is also almost identical to the closed loop system from the 23 state

LQG compensator (Figure 3.19(c)), as was the performance improvement of 25.8 dB. The truncation of the weak pole zero inversions at 6.8, 9.4, and 14 Hz (Region 2), and 36 Hz (Region 4) did not affect the stability or performance improvement of the closed loop system.

A Neo-Classical controller was designed for the MACE 1A topology, using the Neo-Classical Design Rule 1 presented in Section 3.3. Using Design Rule 1A, and the temporal relationship between z and y in Equation 3.24, the low frequency controller is integral control.

$$K = k_o \phi_{zy} = k_o \frac{1}{s} \tag{3.28}$$

For the experiment, a 2 state stabilized integrator was used, as stated in Table 2.4, to prevent integration of DC bias of the rate gyro. The design constant k_o was chosen upon the completion of Design Rule 1B.

Using Design Rule 1B, a bandwidth of 20 Hz was chosen, similar to that of the LQG compensators (Figures 3.20(b) and 3.21(b)). Then a high frequency controller was created by adding a compensator zero, thus creating PI controller. The zero frequency of the PI controller was set at 8 Hz. The zero was not able to be placed such that the phase at crossover is approximately 60°, as a result of the large phase delay. Its placement, therefore, was somewhat arbitrary, and could be moved after the construction of the lead filters.

Four lead filters, each with 2 damped poles and 2 damped zeros, were created in order to compensate for the large phase lag in the control loop, similar to the high frequency amplification and phase lead in the LQG compensator in Figure 3.21(a). The lead filters provided lead at crossover versus high frequency amplification. The gain k_o of the compensator was then adjusted to create a 20 Hz bandwidth.

Following Design Rule 1C, a rolloff was not added to the compensator

because the dynamics would add phase lag, and the rolloff from the open loop dynamics was steep enough after the 20 Hz crossover (Figure 3.19).

From Design Rule 1D, in examining the loop transfer function $g_{yu}K$ consisting of the controller designed from Design Rules 1A-C, and the open loop transfer function g_{yu} from Figure 3.19, the stability of the mode at 36 Hz was in question. Therefore a two pole notch filter (Equation 3.23) was constructed for the 36 Hz mode (ω=36Hz, α=10, ζ_o=0.02). The resulting 12 state Neo-Classical compensator designed for MACE 1A is shown in Figure 3.22(a).

Notice the similarities between the 12 state Neo-Classical compensator in Figure 3.22(a), and the 13 state truncated LQG compensator in Figure 3.21(a). The PI controller and lead filters are equivalent. The LQG controller added a one pole rolloff, which the Neo-Classical compensator did not. The truncated LQG compensator inverted the 88 Hz mode, while the Neo-Classical compensator notch filtered the 36 Hz mode.

Figure 3.22(b) shows the measured loop transfer function, $g_{yu}K$, made up of the 12 state Neo-Classical compensator (Figure 3.22(a)), and the open loop transfer function (Figure 3.19). Again notice the similarities to the loop transfer function from the 13 state truncated LQG compensator (Figure 3.21(b)). They are almost identical, except the loop gain of the Neo-Classical compensator rose above 0 dB at the 88 Hz mode. The stability of the mode at 88 Hz was in question because of the amplification from the lead filters. This was a result of a noisy measurement of the transfer function, however, and the mode was not actually unstable in closed loop.

Figure 3.22(c) shows the measured open and closed loop disturbance to performance transfer functions for the 12 state Neo-Classical compensator for MACE 1A. The performance improvement was 25.8 dB, identical to that from the 13 state truncated LQG compensator. Additional performance was again limited by the phase lag in the control loop. Additional phase lead, and subsequent high frequency

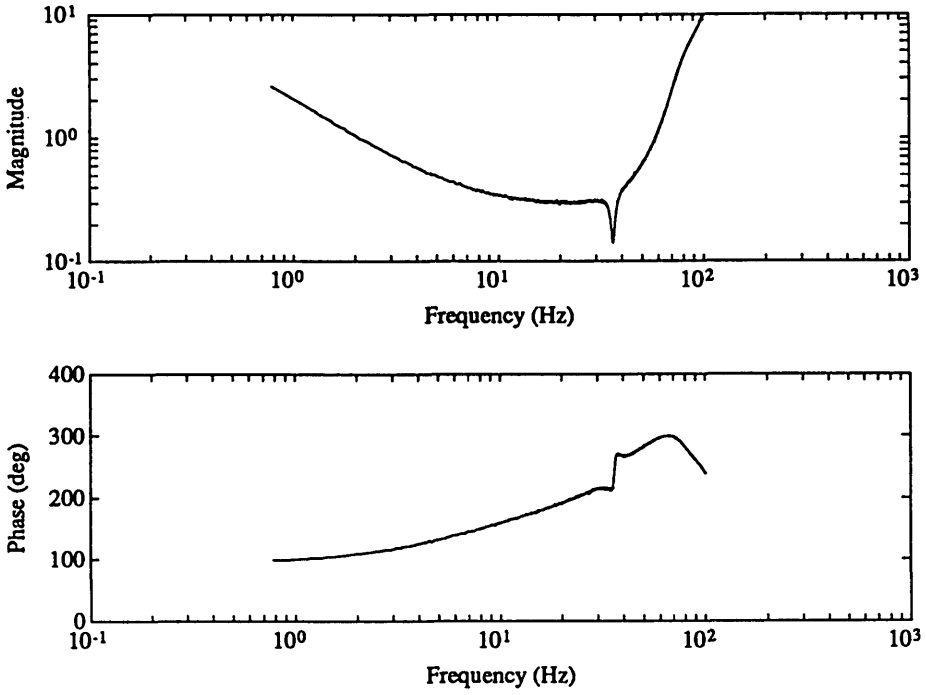

Figure 3.22(a). 12 state Neo-Classical compensator K for MACE 1A: 2 states for the stabilized integrator; 8 states for the lead filters; 2 states for the notch filters.

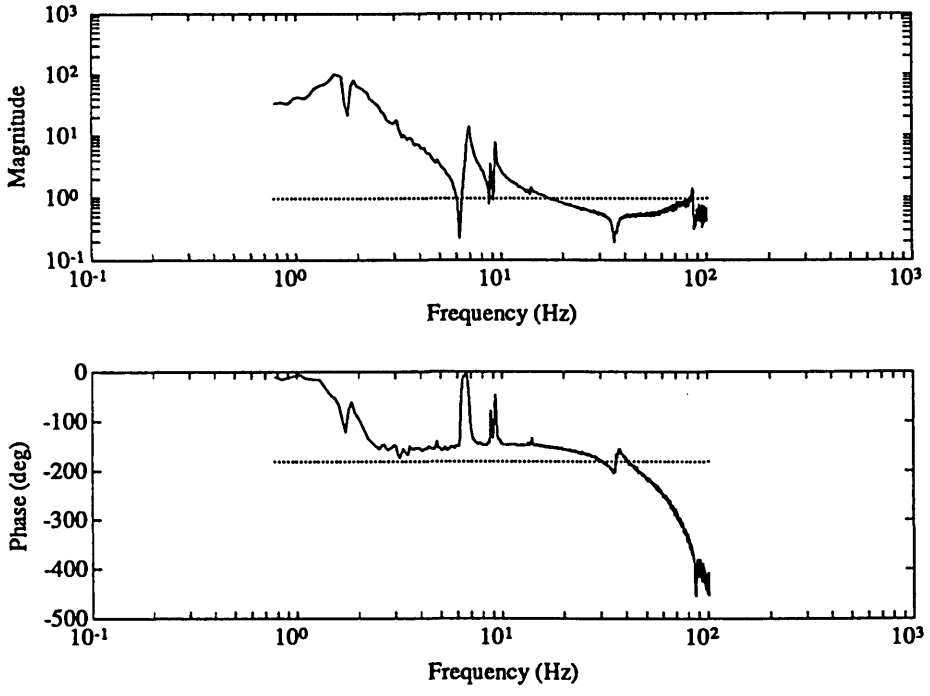

Figure 3.22(b). Measurement of the loop transfer function $g_{yu}K$ consisting of the Neo-Classical compensator and open loop transfer function.

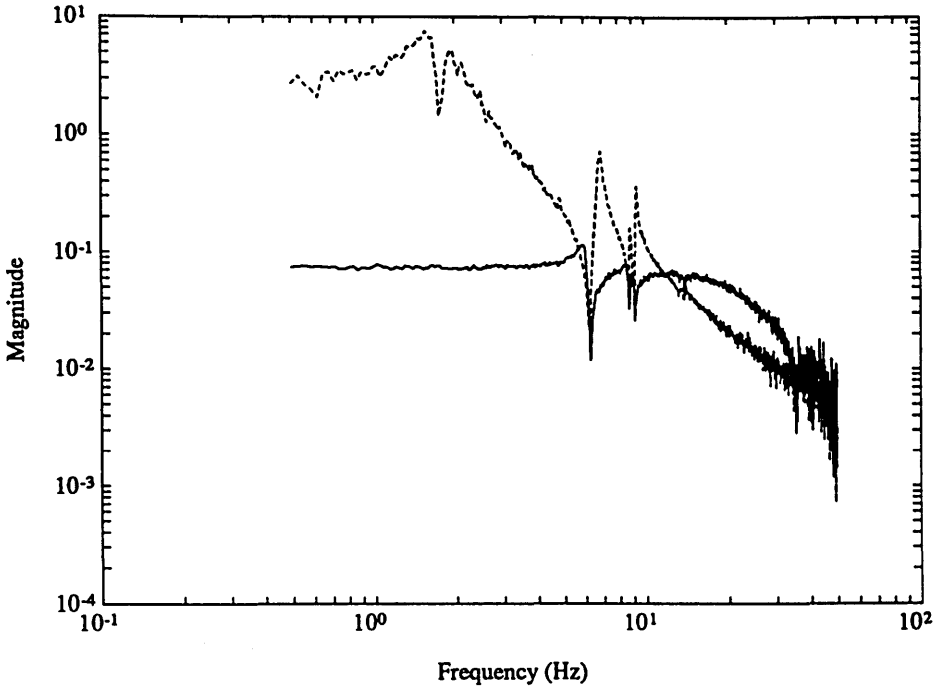

Figure 3.22(c). Measurement of the open and closed loop disturbance to performance transfer functions for MACE 1A. Performance improvement with the Neo-Classical compensator was 25.8 dB.

amplification from the lead filters would have de-stabilized the 88 Hz mode, along with other higher frequency modes.

Figure 3.23 shows MACE 1B, the topology for the bus vibration reduction loop. The performance metric z is the z-axis integrated inertial rate gyro of the bus. The metric is bandlimited, from 0.5-50 Hz. The output y is also the z-axis rate gyro of the bus. The disturbance w and the output u act identically the z-axis inertial torque of the torque wheels. The sensor actuator pair is collocated and dual, as the input is an inertial torque, and the output is an inertial rotational velocity, both acting at the center node. The pole zero pattern of the input output transfer function g_{yu}, therefore is alternating poles and zeros, as shown in Figure 3.24. Notice the large time delay in the loop is evident, similar to the input output transfer function for MACE 1A in Figure 3.19.

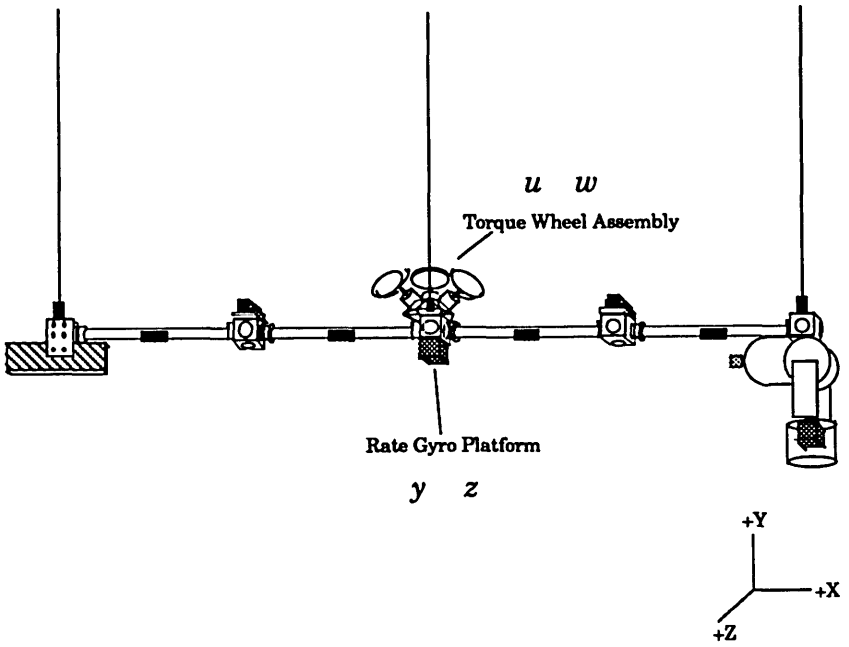

Figure 3.23. MACE 1B: The topology for the bus vibration reduction loop.

A Neo-Classical compensator was designed for the MACE 1B topology using Neo-Classical Design Rule 1. Notice that the topology is very similar to that of MACE 1A, the payload pointing topology, with the disturbance and input being identical

$$w = u \tag{3.29}$$

And the performance and output are related by the same temporal relationship, as in Equation 3.26

$$z = \phi_{zy} y = \frac{1}{s} y \tag{3.30}$$

Using Design Rule 1A, a low frequency controller was created, based upon the temporal relationship given in Equation 3.30.

$$K = k_0 \phi_{zy} = k_0 \frac{1}{s} \tag{3.31}$$

For this case, the low frequency controller was an integrator. The integrator for the experiment was a two pole, stabilized integrator (Table 2.4). The design constant k_o was chosen upon the completion of Design Rule 1B.

Following Design Rule 1B, the bandwidth chosen for this design was 20 Hz. Next, a high frequency controller was created by placing a zero in the compensator, at 8 Hz, in order to create a rate feedback compensator at high frequency. Thus, a PI controller is created. Four lead filters were also constructed, exactly as in the Neo-Classical compensator for MACE 1A (Figure 3.22(a)), in order to compensate for the large phase lag in the control loop. The design constant k_o was chosen to set the crossover of the loop transfer function to be 20 Hz.

From Design Rule 1C, no rolloff dynamics were added, as a result of the steep rolloff of the open loop transfer function in Figure 3.25.

Following Design Rule 1D, in plotting the loop transfer function $g_{yu}K$, consisting of the compensator designed with Design Rules 1A-C, and the open loop transfer function g_{yu} in Figure 3.24, the closed loop stability of the mode at 36 Hz was questionable. Therefore, a two pole notch filter (Equation 3.23) was constructed for the 36 Hz mode (ω=36Hz, α=20, ζ_o=0.02).

The resulting 12 state Neo-Classical compensator, designed for MACE 1B is shown in Figure 3.25(a). Notice the similarities to the Neo-Classical compensator for MACE 1A (Figure 3.22(a)). The only difference, in addition to the relative gain of the compensators, is the notch filter in Figure 3.25(a) (MACE 1A) is *deeper* than the notch filter in Figure 3.23(a) (MACE 1B). This is a result of the larger value of α (20 versus 10) in the notch filter construction.

Figure 3.25(b) shows the measured loop transfer function, $g_{yu}K$, consisting of the 12 state Neo-Classical compensator (Figure 3.25(a)), and the open loop transfer function (Figure 3.24). Notice how the 36 Hz mode was gain stabilized by the 36 Hz notch filter. Figure 3.25(c) shows the measured open and closed loop disturbance to

performance transfer functions for the 12 state Neo-Classical compensator for MACE 1B. The performance improvement with the Neo-Classical controller was 12.5 dB.

Many different optimal and robust controllers have been designed and implemented on this bus vibration reduction topology, MACE 1B. Grocott and Miller (1992) compared multimodel and LQG controllers, both designed with a model made from the identification of the open loop system. The best performance improvement was 9 dB for the 24 state LQG controller and 12 dB for the 24 state multimodel controller. How (1993) designed robust controllers using the Popov method, and the performance improvement was 11.5 dB for his 24 state compensators. And Grocott (1992) designed and implemented 24 state SWLQG controllers, with the best performance improvement being 12.8 dB. The Neo-Classical controller, with 12 states and 12.5 dB performance improvement, was of

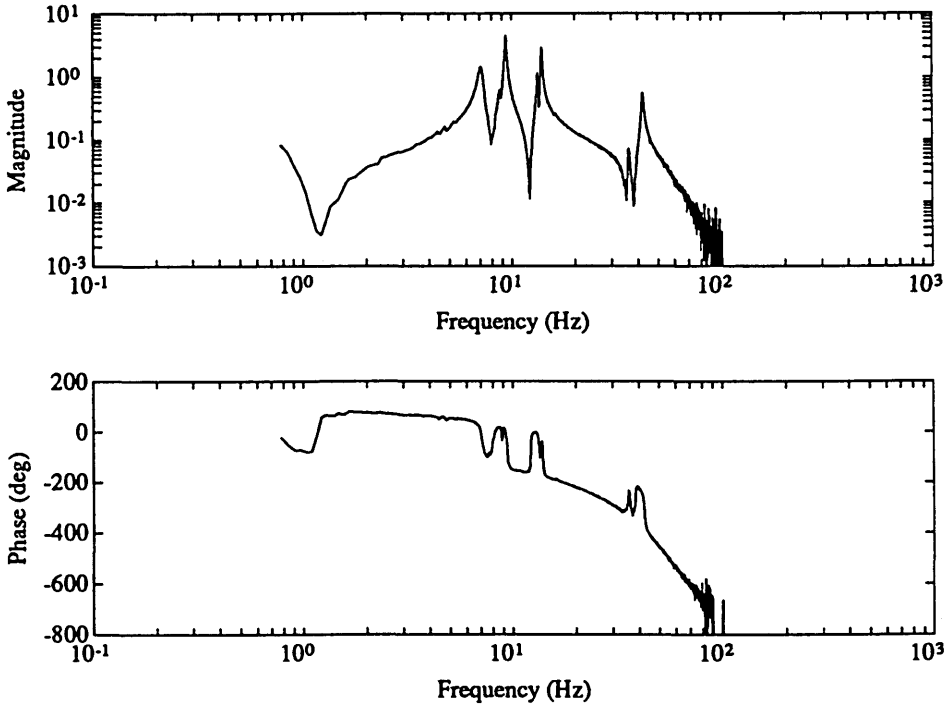

Figure 3.24. Measurement of the open loop input output transfer function g_{yu} from z-axis torque wheels to z-axis bus rate gyro for MACE 1B.

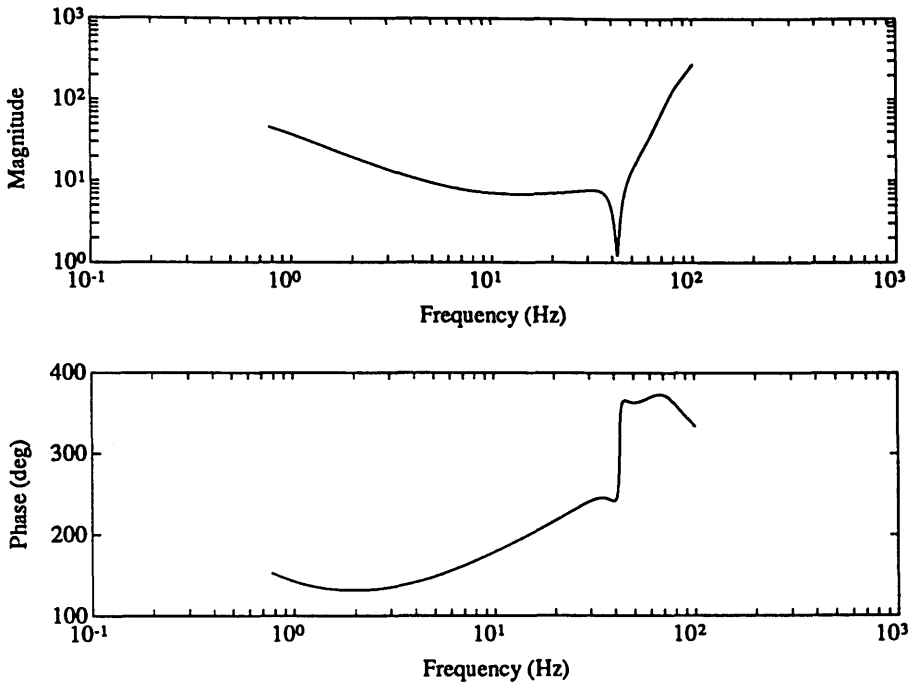

Figure 3.25(a). 12 state Neo-Classical compensator K for MACE 1B: 2 states for the stabilized integrator; 8 states for the lead filters; 2 states for the notch filter.

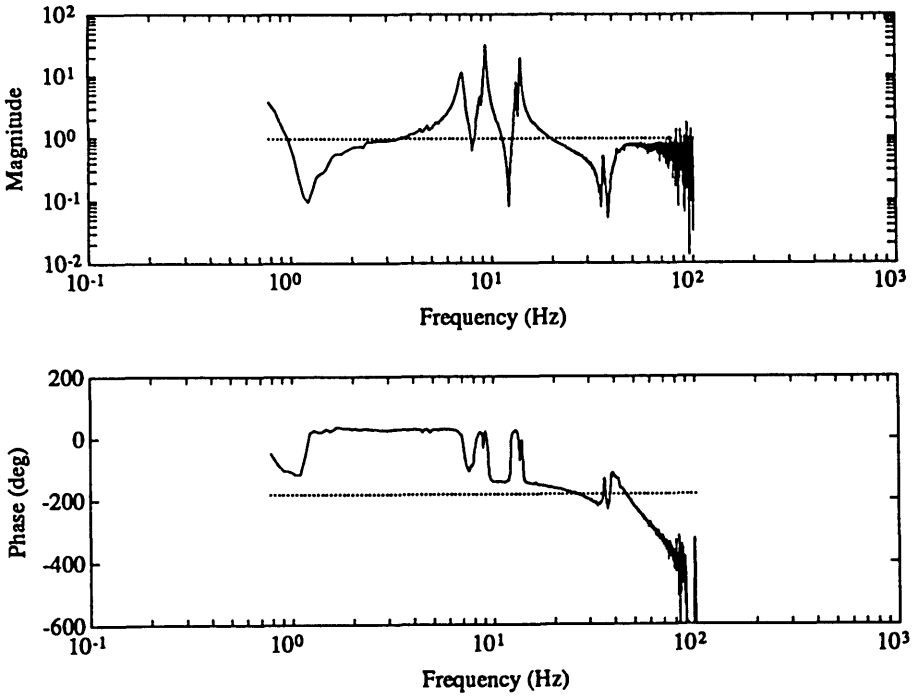

Figure 3.25(b). Measurement of the loop transfer function $g_{yu}K$ consisting of the Neo-Classical compensator and open loop transfer function.

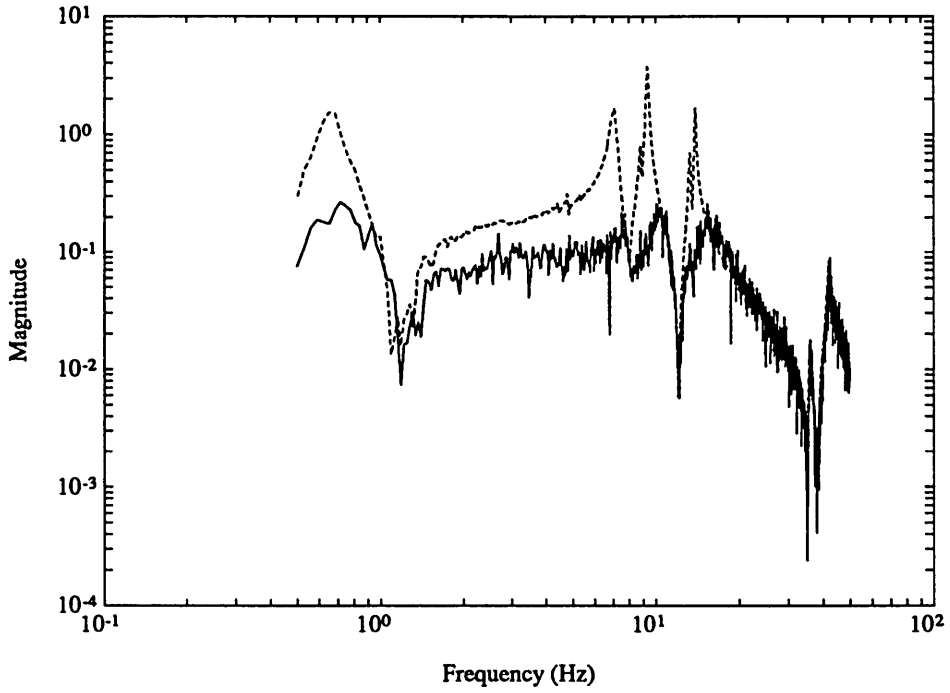

Figure 3.25(c). Measurement of the open and closed loop disturbance to performance transfer functions for MACE 1B. Performance improvement with the Neo-Classical compensator was 12 dB.

equal or lesser dimension and on the same order of performance improvement compared to other compensators, designed for their optimality and robustness characteristics.

Chapter 4

SISO Topology II: Analogous Performance & Output *or* Analogous Disturbance & Input

4.1 Introduction

This chapter examines the implications on the control design for Topology II, that is when the performance and output are analogs, *or* the disturbance and input are analogs, and the input output pair is collocated, dual, and complementary extreme. Two topologies of the typical section will first be presented. They are the same as in Topology I, but in one case, the performance is in a different spatial location of the structure, and in the other case, the disturbance is in a different spatial location of the structure. The LQG and SWLQG compensators will be examined, showing differences and similarities to the compensators designed for Topology I. The results will again be interpreted and presented in a design rule for Neo-Classical compensators. Finally, LQG, SWLQG, and Neo-Classical compensators were designed and implemented on the MACE test article, and the closed loop results will be shown.

4.2 Topologies Examined

Chapter 3 examined a simplified topology of the disturbance rejection control design problem, namely when the performance z and output y are analogs, *and* the disturbance w and input u are analogs. In this chapter, the control design will be examined where only one of these is true.

If the disturbance w and the input u are identical, such that

$$w(s) = u(s) \tag{4.1}$$

Then the general SISO disturbance rejection problem simplifies to

$$\begin{Bmatrix} z \\ y \end{Bmatrix} = \begin{bmatrix} g_{zw} & g_{zu} \\ g_{yu} & g_{yu} \end{bmatrix} \begin{Bmatrix} w \\ u \end{Bmatrix} = \begin{bmatrix} g_{zu} & g_{zu} \\ g_{yu} & g_{yu} \end{bmatrix}_{w=u} \begin{Bmatrix} w \\ u \end{Bmatrix} \tag{4.2}$$

This topology is called Topology IIA because the disturbance and input are analogous, but the performance and output are not. The following relationships occur between the transfer functions.

$$g_{yw} = g_{yu} \tag{4.3}$$

$$g_{zw} = g_{zu} \tag{4.4}$$

And the closed loop transfer function from disturbance to performance is

$$\frac{z}{w} = \frac{g_{zw}}{1 + g_{yu}K} = \left.\frac{g_{zu}}{1 + g_{yu}K}\right|_{w=u} \tag{4.5}$$

If the above transfer function is set equal to ε, and solved for the compensator K,

$$K = \frac{g_{zw} - \varepsilon}{\varepsilon g_{yu}} = \left.\frac{g_{zu} - \varepsilon}{\varepsilon g_{yu}}\right|_{w=u} \tag{4.6}$$

Good disturbance rejection is achieved as ε tends to zero, giving the disturbance to performance transfer function minimizing compensator

$$\lim_{\varepsilon \to 0} K = \frac{g_{zw}}{\varepsilon g_{yu}} = \frac{g_{zu}}{\varepsilon g_{yu}}\bigg|_{w=u} \tag{4.7}$$

In the control design process, again there are two important aspects. One is the minimization of the transfer function given in Equation 4.5. This can be accomplished by setting the magnitude of K to be large, or

$$\left|\frac{z}{w}\right| = \left|\frac{g_{zu}}{g_{yu}K}\right| \qquad \text{for} \qquad \left|g_{yu}K\right| \gg 1 \tag{4.8}$$

The second, and more important aspect of control design is the structure of the input output transfer function g_{yu}. As in Chapter 3, the collocated, dual, and complementary extreme actuator sensor pair will be examined, thus creating an alternating pole zero pattern in the g_{yu} transfer function.

Figure 4.1(a) shows an example of Topology IIA. The output y_1 is the vertical rate of the tip mass, and the performance z_2 is the vertical position of the third mass. The input u_1 and disturbance w_1 are the same, i.e. a vertical force on the tip mass. Notice that this topology is the same as that in Figure 3.1(a), except the performance z_3 is now on the third mass. Optimal compensation will examine the implications on the control design from Topology I when the performance is in a different spatial location.

Figure 4.2(a) shows the open loop disturbance to performance transfer function for Typical Section 2A (w_1 to z_3). There is a missing zero pair between the pole pairs at 1.6 and 10.1 rad/sec, and two real zeros at 14 rad/sec (nonminimum phase) and -14 rad/sec (minimum phase). Notice that the input output transfer function g_{yu}, is the same as that for Typical Section 1A, given in Figure 3.2(a).

This chapter will also examine the dual topology to that just discussed previously, i.e. when there is a relationship between the performance z and the output y, such that they are analogs.

$$z(s) = \phi_{zy}(s)y(s) \tag{4.9}$$

There is no explicit relationship between the disturbance w and input u, however. This topology is called Topology IIB because the performance and output are analogous, but the disturbance and input are not. Then the general SISO disturbance rejection problem simplifies to

$$\begin{Bmatrix} z \\ y \end{Bmatrix} = \begin{bmatrix} g_{zw} & g_{zu} \\ g_{yw} & g_{yu} \end{bmatrix} \begin{Bmatrix} w \\ u \end{Bmatrix} = \left[\begin{matrix} \phi_{zy}g_{yw} & \phi_{zy}g_{yu} \\ g_{yw} & g_{yu} \end{matrix} \right]_{z=\phi_{zy}y} \begin{Bmatrix} w \\ u \end{Bmatrix} \tag{4.10}$$

The following relationships occur between the transfer functions.

$$g_{zw} = \phi_{zy}g_{yw} \tag{4.11}$$

$$g_{zu} = \phi_{zy}g_{yu} \tag{4.12}$$

And the closed loop transfer function from disturbance to performance is

$$\frac{z}{w} = \frac{g_{zw}}{1 + g_{yu}K} = \left. \frac{\phi_{zy}g_{yw}}{1 + g_{yu}K} \right|_{z=\phi_{zy}y} \tag{4.13}$$

If the above transfer function is set equal to ε, and solved for the compensator K,

$$K = \frac{g_{zw} - \varepsilon}{\varepsilon g_{yu}} = \left. \frac{\phi_{zy}g_{yw} - \varepsilon}{\varepsilon g_{yu}} \right|_{z=\phi_{zy}y} \tag{4.14}$$

Good disturbance rejection is achieved as ε tends to zero, giving the disturbance to

performance transfer function minimizing compensator

$$\lim_{\varepsilon \to 0} K = \frac{g_{zw}}{\varepsilon g_{yu}} = \left. \frac{\phi_{zy} g_{yw}}{\varepsilon g_{yu}} \right|_{z=\phi_{zy} y} \tag{4.15}$$

Control design is a function of the pole zero structure of g_{yu}, and seeking to minimize the closed loop transfer function given in Equation 4.13. The input output pair is collocated, dual, and complementary extreme, resulting in an alternating pole zero pattern. Disturbance rejection, or minimization of the transfer function given in Equation 4.13 can be accomplished by setting the magnitude of K to be large, or

$$\left|\frac{z}{w}\right| = \left|\frac{\phi_{zy} g_{yw}}{g_{yu} K}\right| \qquad \text{for} \qquad |g_{yu} K| \gg 1 \tag{4.16}$$

Figure 4.1(a) shows an example of this type of topology with y_1 and u_1 collocated, dual, and complementary extreme, and z_1 and y_1 are analogs.

The output y_1, is the vertical rate of the tip mass, while the performance z_1 is the vertical position of the tip mass. The temporal relationship ϕ_{zy}, is then given by

$$z_1(s) = \frac{1}{s} y_1(s) \tag{4.17}$$

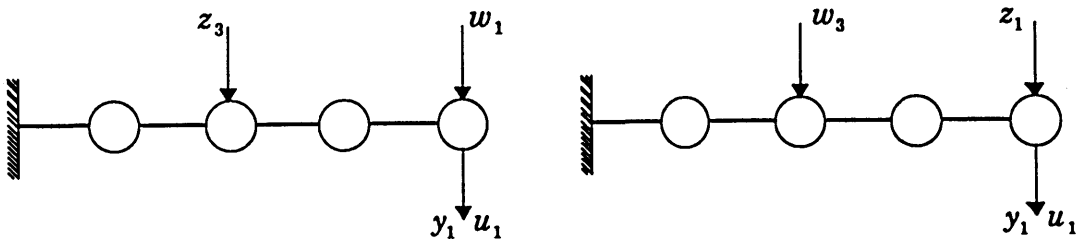

(a) Typical Section 2A (b) Typical Section 2B

Figure 4.1. Topology II: (a) Topology IIA - analogous disturbance and input (b) Topology IIB - analogous performance and output. Both with collocated, dual, *and* complementary extreme input and output.

$$\text{therefore,} \qquad \phi_{zy}(s) = \frac{1}{s} \tag{4.18}$$

Notice that this topology is the similar to that in Figure 3.1(a), except that the disturbance w_3 has moved to the third mass.

Figure 4.2(b) shows the open loop transfer function from disturbance to performance for Typical Section 2B (w_3 to z_1). The input output transfer function g_{yu}, is the same as that given in Figure 3.2(a).

In examining the disturbance to performance transfer function minimizing compensators in Equations 4.7 and 4.15, they are identical. Both are high gain compensators, with the filter g_{zw}/g_{yu}. This suggests that the compensation techniques for Topology IIA and IIB should be similar.

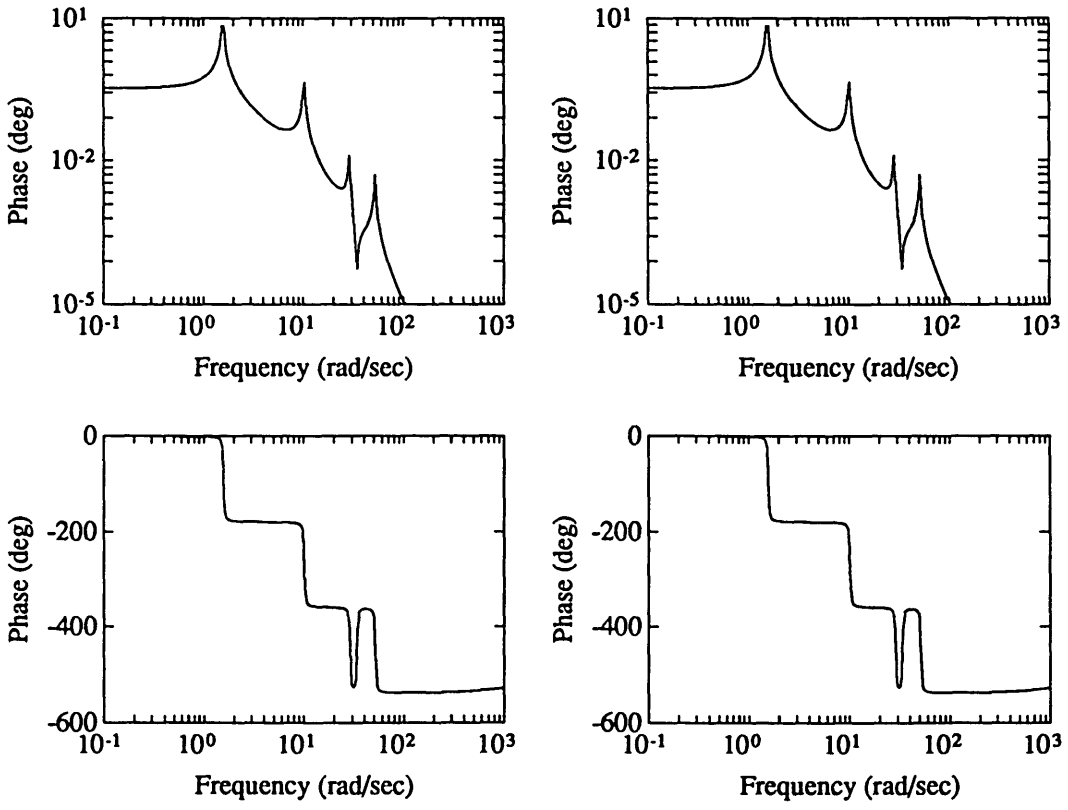

(a) g_{zw} for Typical Section 2A (b) g_{zw} for Typical Section 2A

Figure 4.2. Disturbance to performance transfer functions.

The filter dynamics g_{zw}/g_{yu} can be divided into two parts

$$\frac{g_{zw}}{g_{yu}} = \phi_o g_o \tag{4.19}$$

where ϕ_o is the temporal relationship between the performance and output, and g_o is a structural filter. Then the simplified disturbance to performance transfer function minimizing compensator for both Topology IIA and IIB is

$$\underset{\varepsilon \to 0}{LIM}\, K = \frac{g_{zw}}{\varepsilon g_{yu}} = \frac{1}{\varepsilon}\phi_o g_o \tag{4.20}$$

Notice that for Topology IIB, the structural filter g_o is g_{yw}/g_{yu} and the temporal relation ϕ_o is identically ϕ_{zy}. For Topology IIA, both the ϕ_o and g_o lie within the filter dynamics g_{zu}/g_{yu}.

For Typical Sections 2A and 2B, the input output transfer functions, g_{yu}, are the same, as are the disturbance to performance transfer functions, g_{zw}, shown in Figure 4.2. Therefore, the disturbance to performance transfer function minimizing compensators are identical for both Typical Section 2A and 2B.

In the previous chapter, certain issues were examined such as bandwidth, structural modes within four regions of the loop transfer function, dominant mode control, robust control, and truncation of the compensator. This chapter will build upon that analysis, by examining what happens to the optimal compensators designed for the topologies discussed in Chapter 3, if the disturbance or performance are at different spatial locations in the structure.

4.3 Optimal Compensation

In Chapter 3, optimal compensation techniques such as LQG revealed

distinct trends for topologies where the u and w are analogs, *and* y and z are analogs, *and* u and y were also collocated, dual, complementary extreme. This section will examine the changes in the optimal compensators if the performance and output are nonanalogous, or noncollocated in this case, or if the disturbance and input are nonanalogous, or noncollocated in this case. Once again, the LQG compensators will be compared to their asymptotes.

Asymptotic Properties of the LQG Compensator:

The LQG asymptote for low noise (i.e. the Kalman Filter weighting μ tends to zero) and expensive control (i.e. the LQR weighting ρ tends to infinity) was shown in Equation 2.30 to be

$$\underset{\substack{\mu\to 0\\ \rho\to\infty}}{LIM}\, K(s) = \frac{G\Phi B_w}{g_{yw}} = \frac{k_{LG}}{\sqrt{\rho}} \frac{s}{s^2 + 2\zeta_{dm}\omega_{dm}s + \omega_{dm}^2} \frac{1}{g_{yw}} \tag{4.21}$$

where ζ_{dm} and ω_{dm} are the damping ratio and frequency of the dominant mode, and k_{LG} is a scalar constant. For the Topology IIA, where the disturbance w and the input u are identical, the low gain LQG asymptote simplifies to

$$\underset{\substack{\mu\to 0\\ \rho\to\infty}}{LIM}\, K(s) = \frac{k_{LG}}{\sqrt{\rho}} \frac{s}{s^2 + 2\zeta_{dm}\omega_{dm}s + \omega_{dm}^2} \frac{1}{g_{yw}} = \frac{k_{LG}}{\sqrt{\rho}} \frac{s}{s^2 + 2\zeta_{dm}\omega_{dm}s + \omega_{dm}^2} \frac{1}{g_{yu}}\bigg|_{w=u} \tag{4.22}$$

Notice this low gain LQG asymptote is identical to that of Topology I, given in Equation 3.17. The poles of the low gain asymptote for Topology IIA are the zeros of the input output transfer function, g_{yu}, and the zeros are at the poles of the g_{yu} transfer function, except for the dominant poles.

For Topology IIB, the temporal relationship between z and y does not create the simplifications similar to Topology IIA, and therefore the low gain asymptote for Topology IIB is given by

$$\underset{\substack{\mu\to 0\\ \rho\to\infty}}{LIM}\, K(s) = \frac{G\Phi B_w}{g_{yw}} = \frac{k_{LG}}{\sqrt{\rho}} \frac{s}{s^2 + 2\zeta_{dm}\omega_{dm}s + \omega_{dm}^2} \frac{1}{g_{yw}} \tag{4.23}$$

The poles of the low gain asymptote for Topology IIB are the zeros of the disturbance output transfer function, g_{yw}, and the zeros are at the poles of the g_{yw} transfer function, except for the dominant poles.

The LQG asymptote for low noise (i.e. the Kalman Filter weighting μ tends to zero), cheap control (i.e. the LQR weighting ρ tends to zero), and μ less than ρ was shown in Equation 2.32 to be

$$\underset{\substack{\mu\to 0\\ \rho\to 0\\ \rho>\mu}}{LIM}\, K(s) = \pm\frac{1}{\sqrt{\rho}} \frac{g_{zw}}{g_{yw}} \tag{4.24}$$

For Topology IIA, the high gain LQG asymptote simplifies to

$$\underset{\substack{\mu\to 0\\ \rho\to 0\\ \rho>\mu}}{LIM}\, K(s) = \pm\frac{1}{\sqrt{\rho}} \frac{g_{zw}}{g_{yw}} = \pm\frac{1}{\sqrt{\rho}} \frac{g_{zu}}{g_{yu}}\bigg|_{w=u} \tag{4.25}$$

The poles of the high gain LQG asymptote are the zeros of the input output transfer function g_{yu}, identical to the poles of the low gain LQG asymptote for Topology IIA (Equation 4.22) and the zeros are the zeros of the input to disturbance transfer function g_{zu}. Notice that the high gain LQG asymptote is identical to the disturbance to performance transfer function minimizing compensator for Topology IIA given in Equation 4.7. This is the high gain asymptote for Typical Section 2A.

For Topology IIB, the high gain LQG asymptote simplifies to

$$\underset{\substack{\mu\to 0\\ \rho\to 0\\ \rho>\mu}}{LIM}\, K(s) = \pm\frac{1}{\sqrt{\rho}} \frac{g_{zw}}{g_{yw}} = \pm\frac{1}{\sqrt{\rho}} \frac{\phi_{zy} g_{yw}}{g_{yw}}\bigg|_{z=\phi_{xy}y} \tag{4.26}$$

assuming μ is smaller than ρ. Notice that this high gain asymptote is the same as that for Topology I given in Equation 3.19, except the compensator pole zero cancellations are the zeros of the disturbance to output transfer function, g_{yw}, not the input output transfer function, g_{yu}. In comparing Equation 4.26 with 4.15, the high gain LQG asymptote for Topology IIB does *not* match the disturbance to performance transfer function minimizing compensator, as the Topology IIA high gain asymptote did. Therefore, although the disturbance to performance transfer functions minimizing compensators are identical for Topologies IIA and IIB, the high gain LQG asymptotes are not.

For Typical Section IIB, given the temporal relationship between z and y in Equation 4.18, the high gain LQG asymptote is

$$\underset{\substack{\mu\to 0\\ \rho\to 0\\ \rho>\mu}}{LIM}\, K(s) = \pm\frac{1}{\sqrt{\rho}}\frac{\phi_{zy}g_{yw}}{g_{yw}} = \pm\frac{1}{s\sqrt{\rho}} \tag{4.27}$$

The high gain asymptote is an integrator, as it was for Typical Sections 1A and 1B.

The creation of the LQG asymptotes are dependent upon the disturbance to performance transfer function g_{yw} being minimum phase. In examining Typical Sections 2A and 2B in Figure 3.1, the g_{yw} transfer function for Typical Section 2A is collocated and dual, while it is noncollocated and dual for Typical Section 2B. The gzu transfer function is also assumed to be minimum phase in the high gain asymptote. With the assumption that μ is smaller than ρ, however, this assumption is not as stringent. Although the disturbance to performance transfer function for Typical Section 2B contains a nonminimum phase zero at 14 rad/sec and a missing pair of zeros between the pole pairs at 1.6 and 10.1 rad/sec, the low gain asymptote will still be used to show the implications of these pole zero patterns.

The LQG and SWLQG compensators will first be examined for the nonanalogous performance output pair, such as that in Typical Section 2A.

Typical Section Results for a Nonanalogous Performance/Output: LQG compensator

Figure 4.3 shows the open loop input output transfer function for Typical Section 2A given in Figure 4.1(a). Figure 4.4(a) shows a typical 8 state LQG compensator with a small value for the Kalman Filter weighting, (μ=1E-8), and an intermediate value for the LQR weighting (ρ=1E-2), and the low and high gain LQG asymptotes from Equations 4.22 and 4.25. Figure 4.4(b) shows the corresponding loop transfer function, $g_{yu}K$, consisting of the LQG compensator (Figure 4.4(a)), and the open loop transfer function (Figure 4.3). The bandwidth is approximately 6 rad/sec.

The LQG compensator uses integral control, or position feedback, at low frequency, matching the high gain LQG asymptote in Equation 4.25. Note in the filter g_{zu}/g_{yu} of the high gain LQG asymptote, the performance z is a position, and

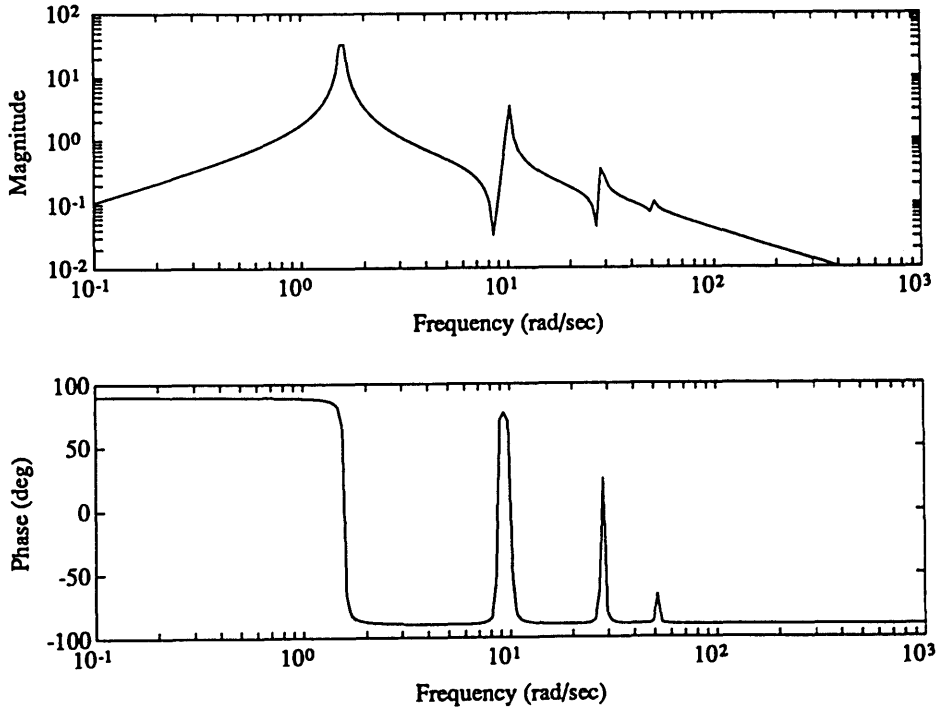

Figure 4.3. Open loop input output transfer function g_{yu} for Typical Section 2A.

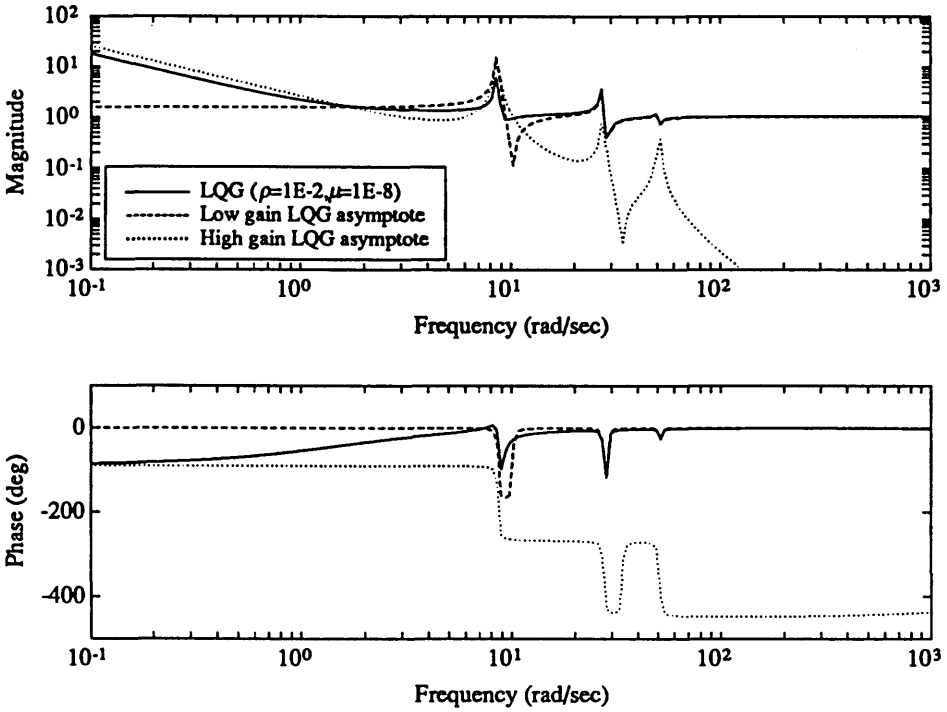

Figure 4.4(a). 8 state LQG compensator K (ρ=1E-2, μ=1E-8) for Typical Section 2A, and the low and high gain LQG asymptotes.

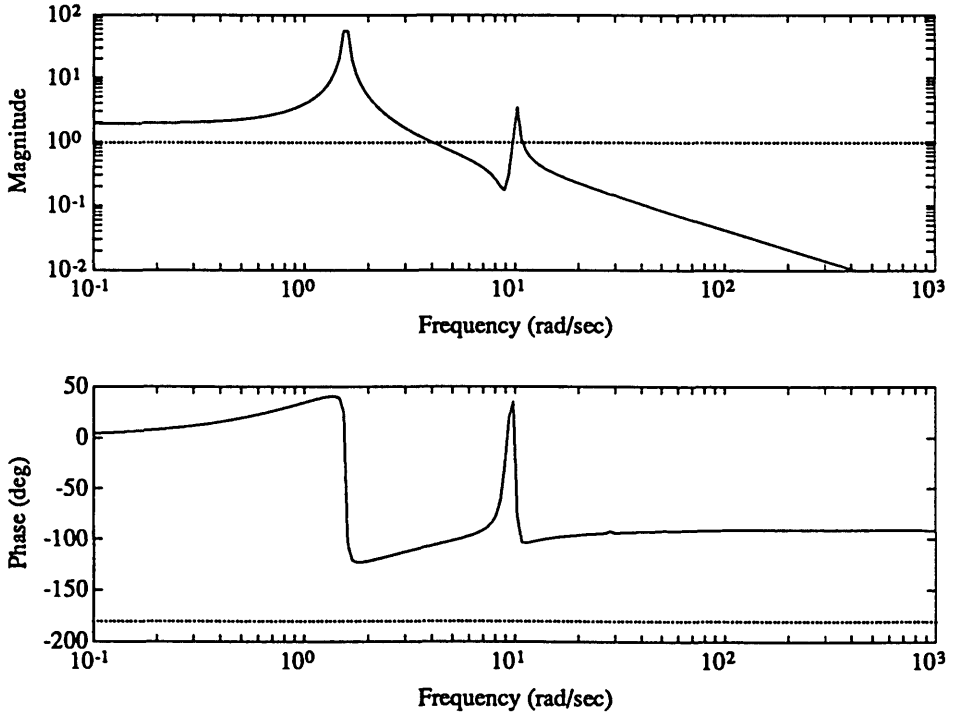

Figure 4.4(b). Loop transfer function $g_{yu}K$ consisting of the LQG compensator and the open loop transfer function.

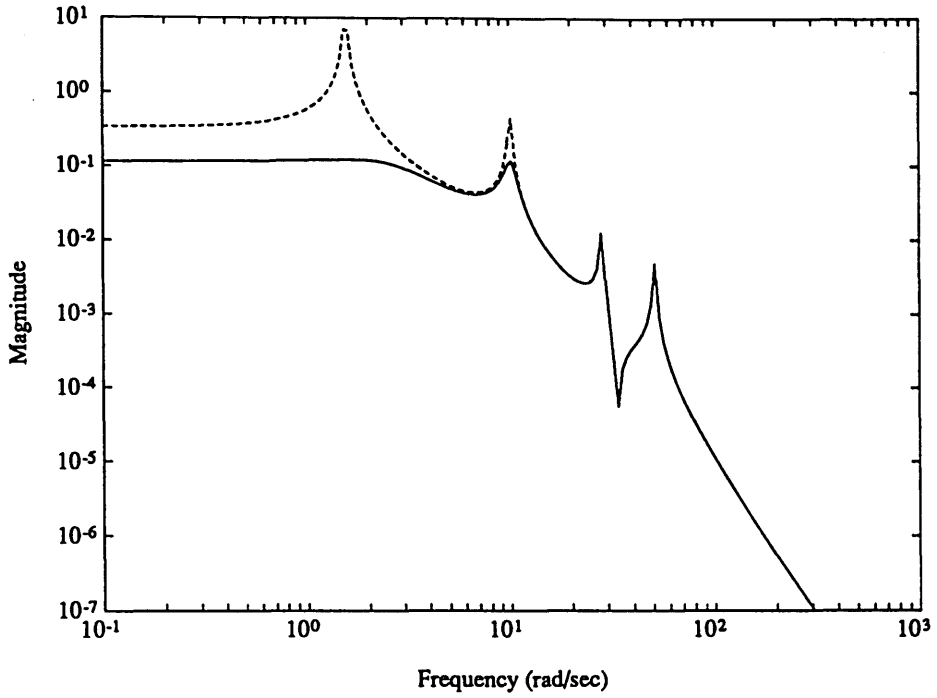

Figure 4.4(c). Open and closed loop disturbance to performance transfer functions for Typical Section 2A. Performance improvement with the LQG compensator is 26.8 dB.

the output y is a velocity. Thus the temporal relation ϕ_o is an integrator and at low frequency, the filter g_{zu}/g_{yu} is an integrator. At high frequency, the compensator inverts the g_{yu} transfer function, similar to the low gain rate feedback LQG asymptote in Equation 4.22. In order to do this, the LQG compensator uses a zero at 1.4 rad/sec, thus creating a PI controller.

Comparing this LQG compensator with LQG compensator in Figure 3.5(a), with a collocated performance z, at high frequency, in Region 4, the compensators are identical, inverting the g_{yu} transfer function. At low frequency, in Region 1, both compensators uses integral control by placing a zero in the crossover region. Therefore, both compensators use PI controllers. The only difference between the two is the LQG compensator for Typical Section 2A (Figure 4.4(a)) does not contain a lightly damped zero at 10.1 rad/sec open loop pole, as the compensator does for

Typical Section 1A (Figure 3.5(a)). This is a result of the Region 1 compensator dynamics, i.e. the high gain LQG asymptote, for Typical Section IIA includes not only the temporal relation between z and y, ϕ_o, but also the structural filter g_o. Because this mode is in the crossover region, or Region 3, it is in a transition from the low gain asymptote with a lightly damped zero at 10.1 rad/sec, to the high gain LQG asymptote, with no zero pair. This will be seen more easily as the bandwidth is increased.

In Figure 4.4(b) notice that the high frequency open loop dynamics are inverted by the compensator. But the mode at 10.1 rad/sec creates an additional loop crossover. This is a result of the more heavily damped compensator zero in Figure 4.4(a). Figure 4.3(c) shows the open loop and closed loop disturbance to performance transfer functions. The performance improvement with the LQG compensator is 26.8 dB.

Figure 4.5(a) shows LQG compensators for three values of the LQR weighting ρ, with the Kalman Filter weighting held constant (μ=1E-8). Figure 4.5(b) shows the corresponding loop transfer functions. As ρ is decreased, the gain of the compensator increases, and the magnitude of the compensator begins to resemble the high gain LQG asymptote shown in Figure 4.4(a). Notice that the poles do not change as a function of ρ, and the compensator does not become unstable or nonminimum phase. If the LQG compensator identically matched that of the high gain LQG asymptote, it would be unstable or nonminimum phase. Therefore, only the magnitude matches the asymptote. The poles of the compensator do not change because they are the zeros of the input output transfer function, g_{yu}, in both the low and high gain asymptotes in Equations 4.22 and 4.25. This is also a result of the transfer function g_{yw} being alternating poles and zeros. This leads to the generalization for Topology IIA that only stable minimum phase dynamics from the structural filter g_o should be added in Regions 1 and 2.

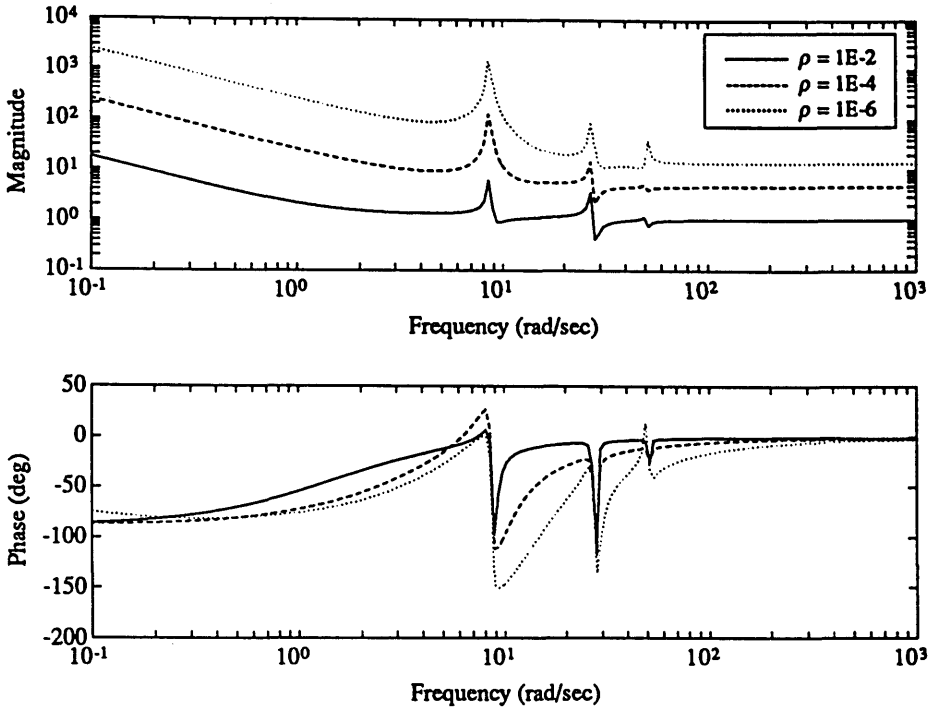

Figure 4.5(a). LQG compensators for Typical Section 2A for three values of ρ. μ=1E-8.

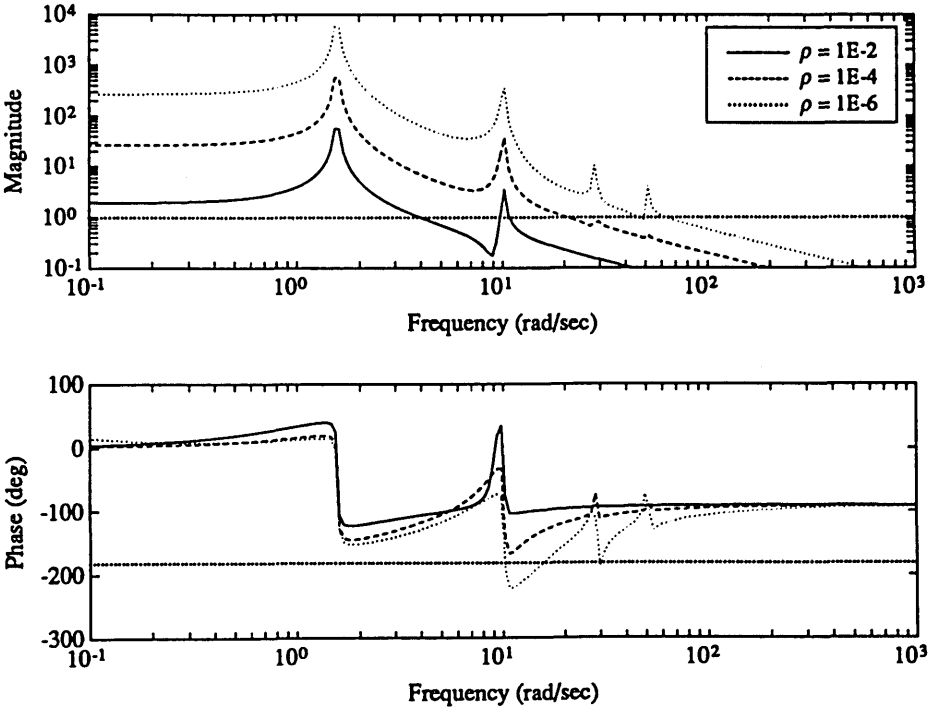

Figure 4.5(b). Loop transfer functions corresponding to the three LQG compensators in Figure 4.5(a).

The magnitude of the LQG compensators resembles the high gain LQG asymptote, which is also the disturbance to performance transfer function minimizing compensator, in Region 1. In Region 4, the LQG compensator inverts the input output transfer function, g_{yu}, except for the dominant mode, as the LQG compensators did for Topology I. The LQG compensator for Regions 2 and 3, or the crossover region, is again in transition between the low and high gain LQG asymptotes. In Figure 4.5(b), for the lowest bandwidth compensator, ρ=1E-2, the bandwidth is approximately 6 rad/sec. The compensator does not place a zero at the open loop poles at 10.1 rad/sec because it is so close to Region 2, where the transition to the high gain LQG asymptote dominates. In the intermediate bandwidth case, ρ=1E-4, the bandwidth is approximately 20 rad/sec. Notice how the LQG compensator inverts the mode at 28 rad/sec, which is in Region 3. This inversion of the modes in Region 3 is the prevalent case. Therefore, the LQG compensator for modes in Regions 3 and 4 are essentially the same for Topology I and IIA.

Typical Section Results for a Nonanalogous Performance/Output: SWLQG compensator

Because the LQG controller compensates modes within Region 3 for Topology IIA similar to those for Topology I, the SWLQG compensators are essentially the same. If modes in Region 3 of the SWLQG compensator are de-sensitized, the SWLQG compensator creates a notch filter, as they did for Topology I, shown in Figure 3.10(b).

For modes within Region 2, where the transition to the high gain LQG asymptote begins, the results are also very similar to those for Topology I. The LQG compensators, as the bandwidth increased, begin to drop the phase of the loop transfer function below 180° before loop crossover (Regions 1 and 2), as shown in Figure 4.5(a) and (b). Figure 4.6(a) shows an LQG compensator (β=0), and an SWLQG compensator with a slight sensitivity added to the mode at 28 rad/sec

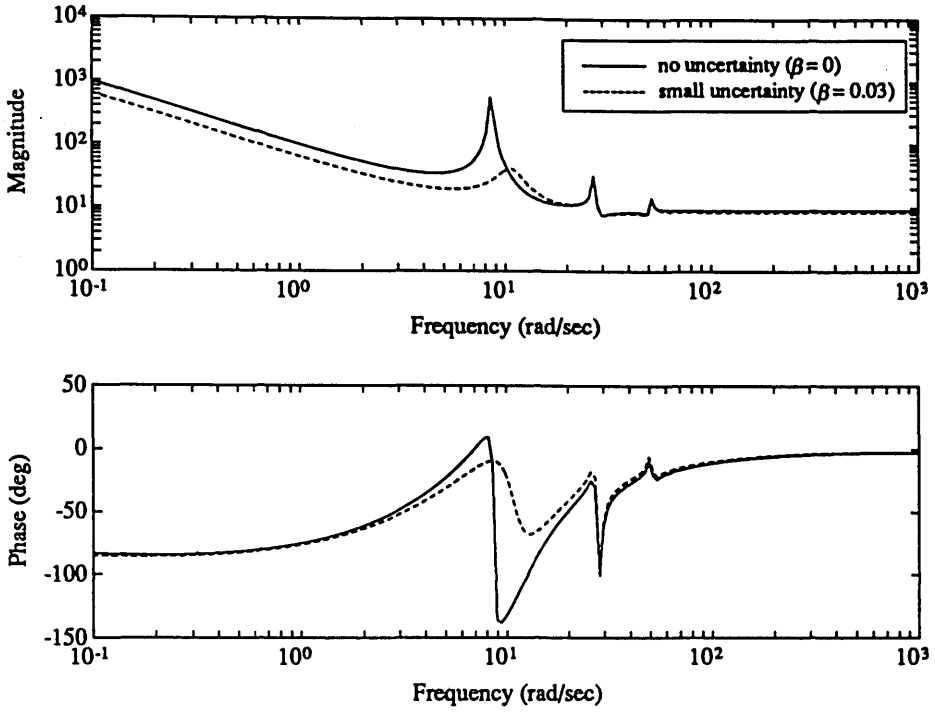

Figure 4.6(a). LQG (ρ=1E-5, μ=1E-8) and SWLQG (de-sensitizing the 10.1 rad/sec mode) compensators for Typical Section 2A.

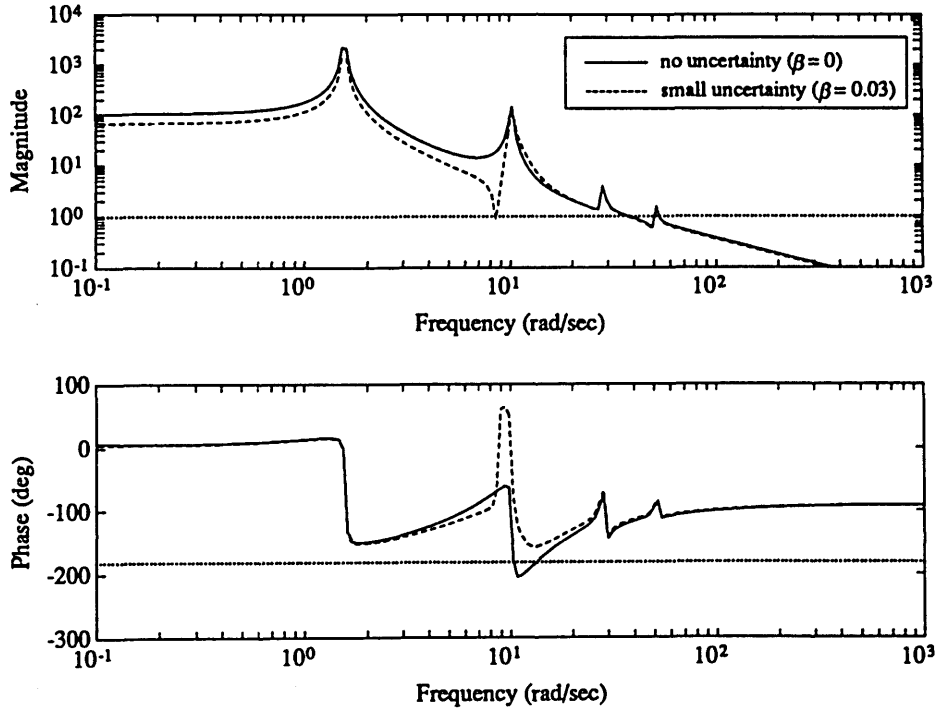

Figure 4.6(b). Loop transfer functions for the LQG and SWLQG compensators in Figure 4.6(a).

(β=0.03). Figure 4.6(b) shows the corresponding loop transfer functions. The bandwidth for both compensators is approximately 35 rad/sec. The SWLQG compensator immediately damped the compensator pole. This leads to the generalization for Topology IIA that not only should only stable, minimum phase dynamics from the structural filter g_o be added to Regions 1 and 2, but also the additions are not very robust, and therefore should be checked for closed loop stability.

Typical Section Results for a Nonanalogous Disturbance/Input; LQG compensator

The low and high gain LQG asymptotes for Topology IIB are given in Equations 4.23 and 4.26. Specifically for Typical Section 2B, the low and high gain asymptotes are given in Equations 4.23 and 4.27. Remember, however, that these asymptotes are dependent upon the disturbance to performance transfer function being minimum phase, which it is not for Typical Section 2B.

Figure 4.7 shows the open loop transfer function g_{yu} for Typical Section 2B, given in Figure 4.1(b). Figure 4.8(a) shows a typical 8 state LQG compensator and the low and high gain asymptotes given in Equations 4.23 and 4.27. The corresponding loop transfer function consisting of the LQG compensator (Figure 4.8(a)) and the open loop system (Figure 4.7) is shown in Figure 4.8(b). The LQG compensator has a small value for the Kalman Filter weighting (μ=1E-8), and an intermediate value for the LQR weighting (ρ=1E-1).

The LQG compensator resembles the high gain LQG asymptote (Equation 4.27), an integrator, or position feedback, at low frequency. The magnitude of dynamics from 10 to 100 rad/sec match the low gain LQG asymptote of Equation 4.23, by inverting the g_{yw} transfer function. At higher frequencies, however, the compensator rolls off instead of matching the low gain LQG asymptote. If the value

of the Kalman Filter weighting μ is made smaller than 1E-8, then the magnitude of the LQG compensator would match the low gain asymptote at higher frequencies as well.

The compensator contains a PI controller, as in the previous topology, with a zero at 1.4 rad/sec. The zero is used as a transition from the low frequency integral, or position feedback (high gain asymptote), to the high frequency proportional, or rate feedback (low gain asymptote). Therefore, in this analysis, the magnitude of the compensator is consistent with the low and high gain LQG asymptotes in Equations 4.23 and 4.27. In examining the phase of the compensator, however, it is unstable at 34 rad/sec.

Figure 4.8(b) shows the loop transfer function $g_{yu}K$ for the LQG compensator. The loop crossover is approximately 4 rad/sec, but there are additional loop crossovers at 28 and 200 rad/sec. These are a result of the compensator attempting

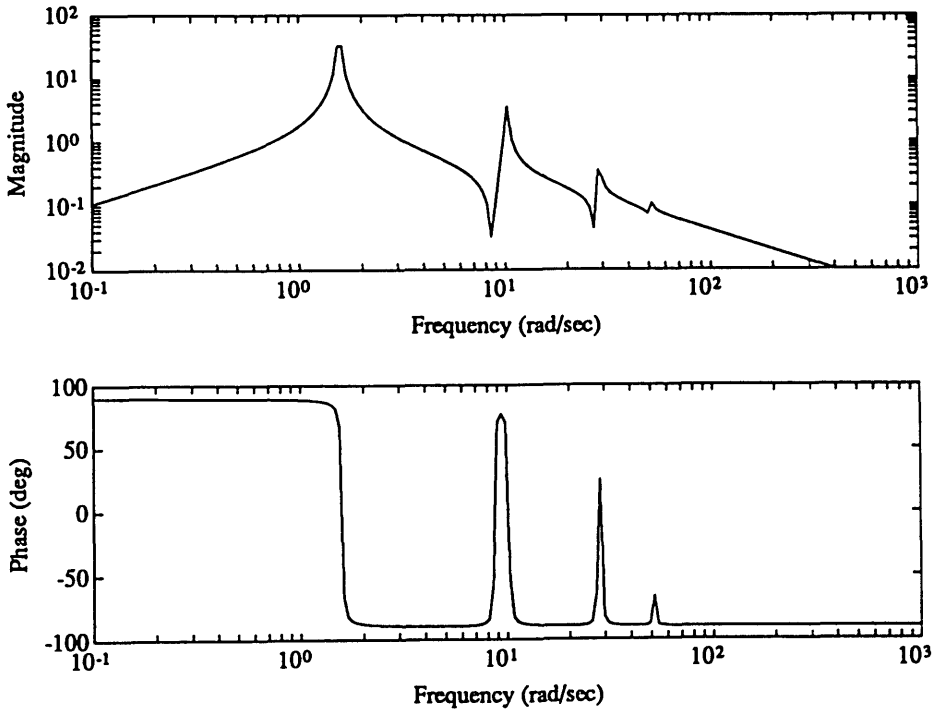

Figure 4.7. Open loop input output transfer function g_{yu} for Typical Section 2B.

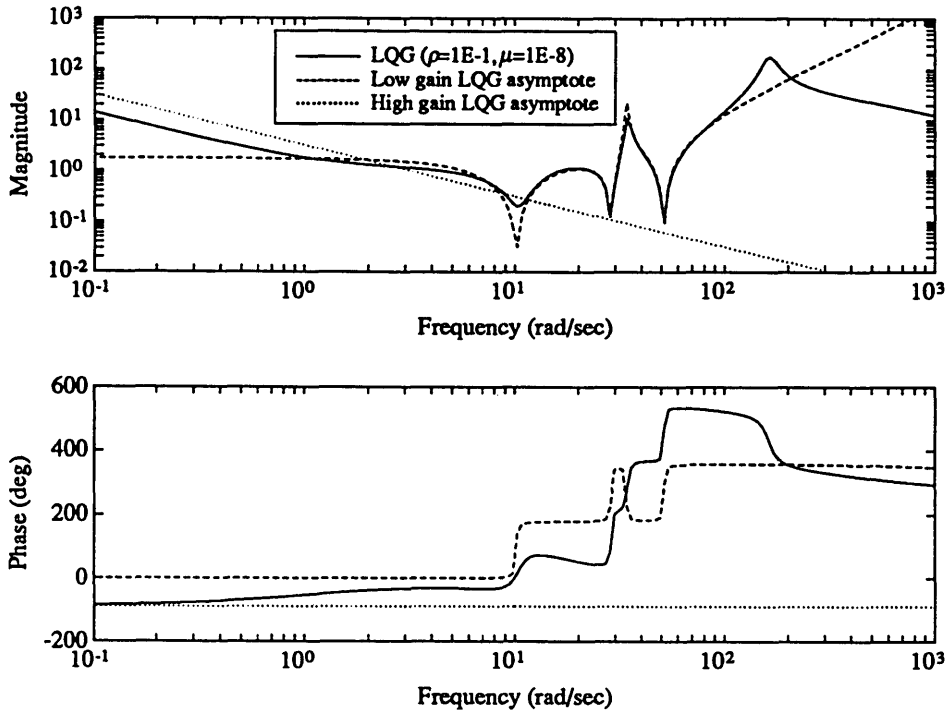

Figure 4.8(a) 8 state LQG compensator K (ρ=1E-1, μ=1E-8) for Typical Section 2B, and the low and high gain LQG asymptotes.

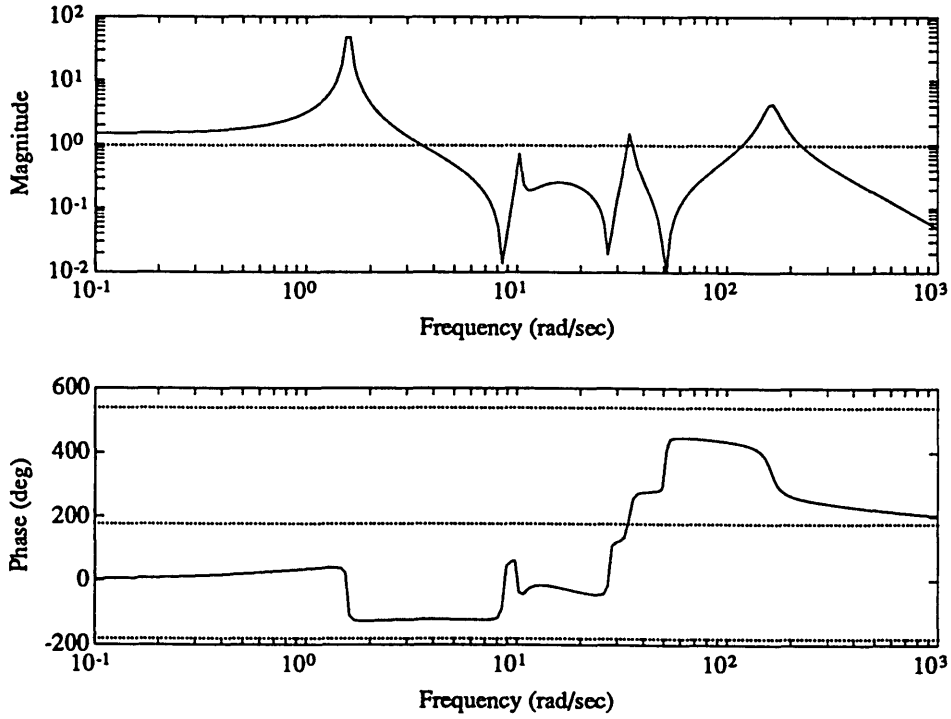

Figure 4.8(b) Loop transfer function $g_{yu}K$ consisting of the LQG compensator and the open loop transfer function.

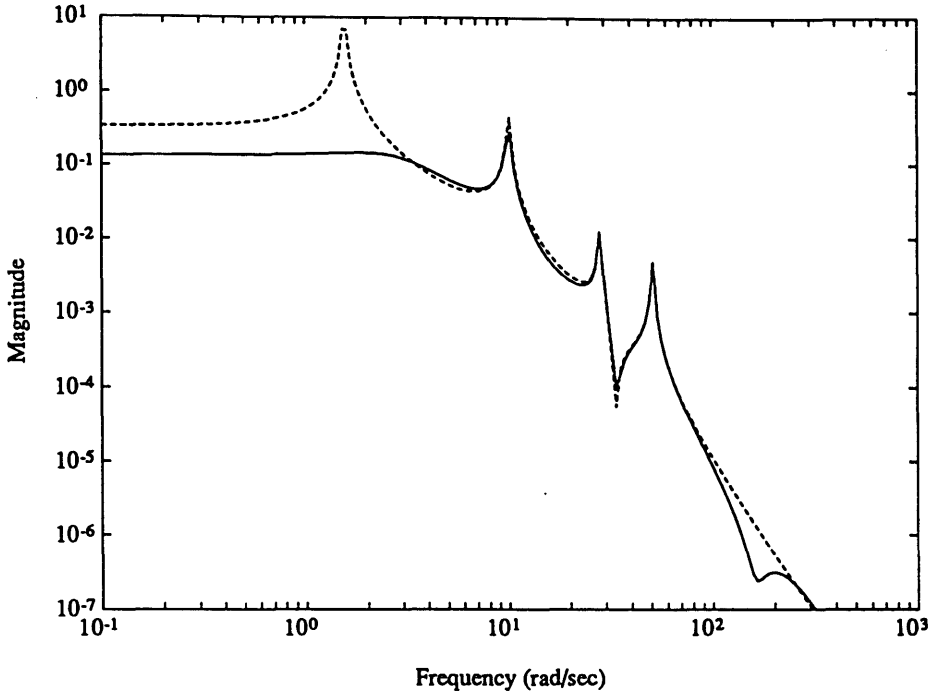

Figure 4.8(c). Open and closed loop disturbance to performance transfer functions for Typical Section 2B. Performance improvement with the LQG compensator is 24.7 dB.

to match the dynamics low gain LQG asymptote. Notice how the magnitude of the low gain asymptote at high frequency increases (Figure 4.8(a)), instead of being constant, is it was for both Typical Section 1A (Figure 3.5(a)) and 2A (Figure 4.4(a)). This is a result of the noncollocated disturbance output pair in Typical Section 2B. Figure 4.3(c) shows the open loop and closed loop disturbance to performance transfer functions. The performance improvement for this compensator is 24.7 dB.

Figure 4.9(a) shows LQG compensators for three values of the LQR weighting ρ, with the Kalman Filter weighting μ remaining constant (μ=1E-8). As ρ decreases, the gain of the compensator increases, additional unstable poles occur at 120 rad/sec, and for the smallest ρ case, a nonminimum phase zero pair occurs at 32 rad/sec. The compensator resembles the high gain LQG asymptote, an integrator, in Regions 1 and 2 for all cases. However, the compensators are unstable and

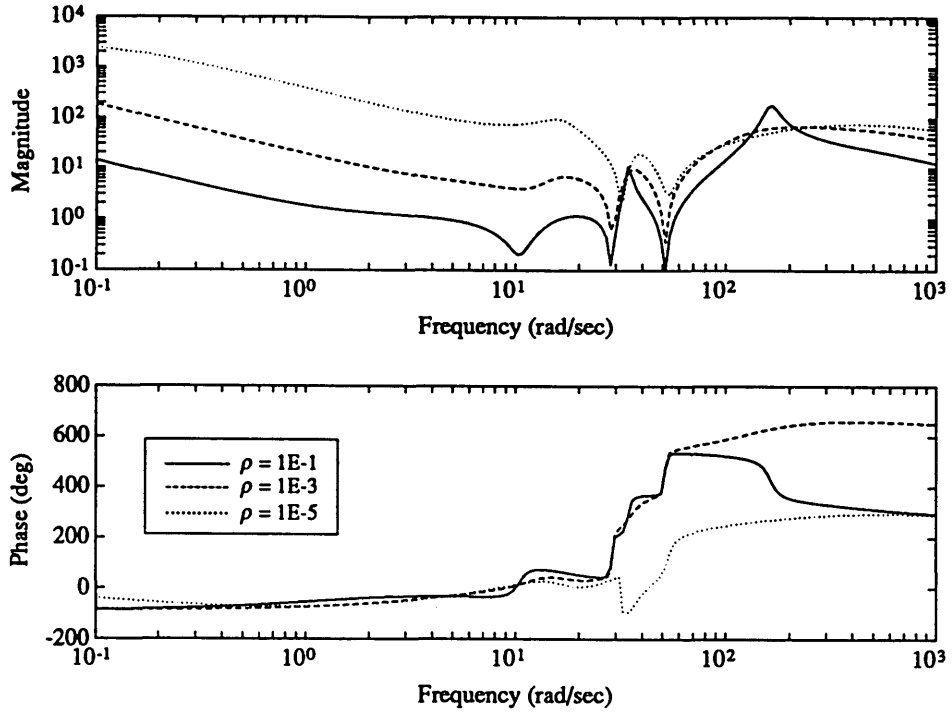

Figure 4.9(a). LQG compensators for Typical Section 2B for three values of ρ. μ=1E-8.

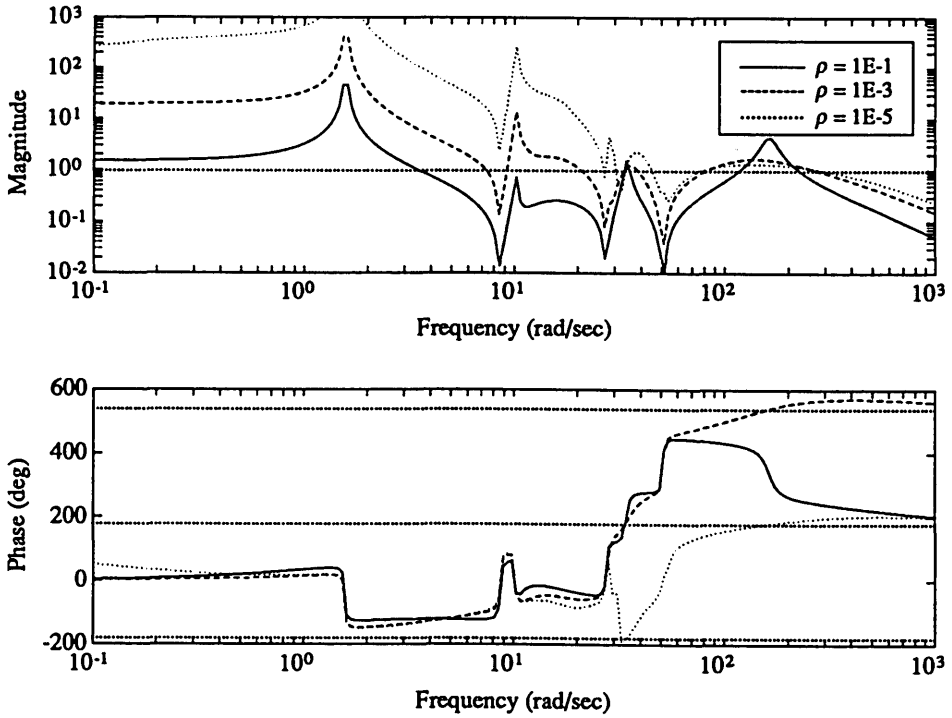

Figure 4.9(b). Loop transfer functions corresponding to the three LQG compensators in Figure 4.9(a).

nonminimum phase for each case. This is a result of the pole zero pattern of the disturbance to output transfer function. In examining Equation 4.27, the compensator attempts to invert g_{yw}, but cannot because it contains a nonminimum phase zero. Figure 4.9(b) shows the corresponding loop transfer functions for the three LQG compensators. As ρ decreases, additional high frequency loop crossovers occur.

For most cases of Typical Section 2B, the LQG compensators are unstable and/or nonminimum phase. For Typical Section 2A, the compensators are stable and minimum phase. The disturbance to performance transfer function minimizing compensator is identical to the high gain LQG asymptote for Typical Section 2A, and the asymptote is valid because g_{yw} is minimum phase. The transfer function minimizing compensator for Typical Section 2B, which is identical to that of Typical Section 2A, does not match the high gain LQG asymptote, and the asymptote is not valid because g_{yw} is nonminimum phase. Therefore, it would be insightful to compare an LQG compensator and the transfer function minimizing compensator for Typical Section 2B.

Figure 4.10 shows a low noise, cheap control LQG compensator (ρ=1E-5, μ=1E-8), and the disturbance to performance transfer function minimizing compensator for Typical Section 2B, given in Equation 4.15. The bandwidth with this compensator is 35 rad/sec. Notice the magnitude of the compensator matches that of the transfer function minimizing compensator in Regions 1 and 2, except for the high frequency poles at 8.3 rad/sec. In fact, for most systems, it is observed that the magnitude of the LQG compensator matches that of the transfer function minimizing compensator, usually better than the high gain LQG asymptote. This will be seen in the closed loop tests on the MACE test article in Section 4.5.

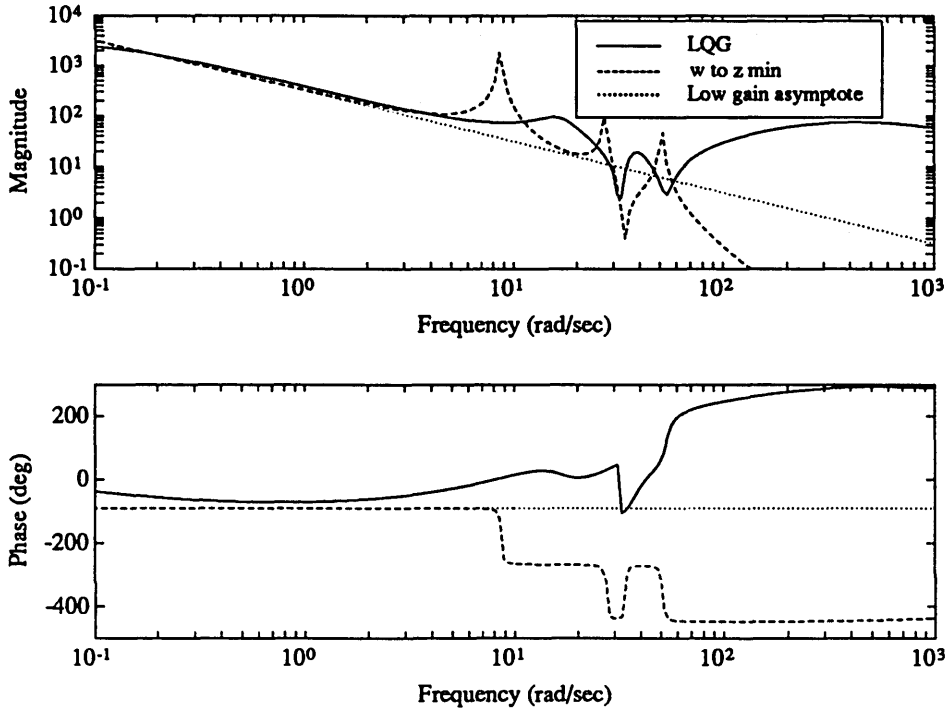

Figure 4.10. LQG compensator (ρ=1E-5, μ=1E-8) , the high gain LQG asymptote, and the disturbance to performance transfer function minimizing compensator (Equation 4.15) for Typical Section 2B.

Typical Section Results for a Nonanalogous Disturbance/Input; SWLQG compensator

Figures 4.9(a) shows how the LQG compensator is unstable and/or nonminimum phase for many different combinations of the Kalman Filter and LQR weightings. Although unstable compensators are capable of being implemented, they are not robust. The SWLQG compensator adds robustness in this case by removing the unstable poles or nonminimum phase zeros. Figure 4.11(a) shows two compensators. The first is the LQG compensator shown in Figure 4.8(a) with an unstable mode at 30 rad/sec. The second is a SWLQG compensator with the mode at 28 rad/sec slightly de-sensitized (β=0.2). The de-sensitization stabilizes the LQG compensator. Figure 4.11(b) shows the loop transfer function for both the LQG and

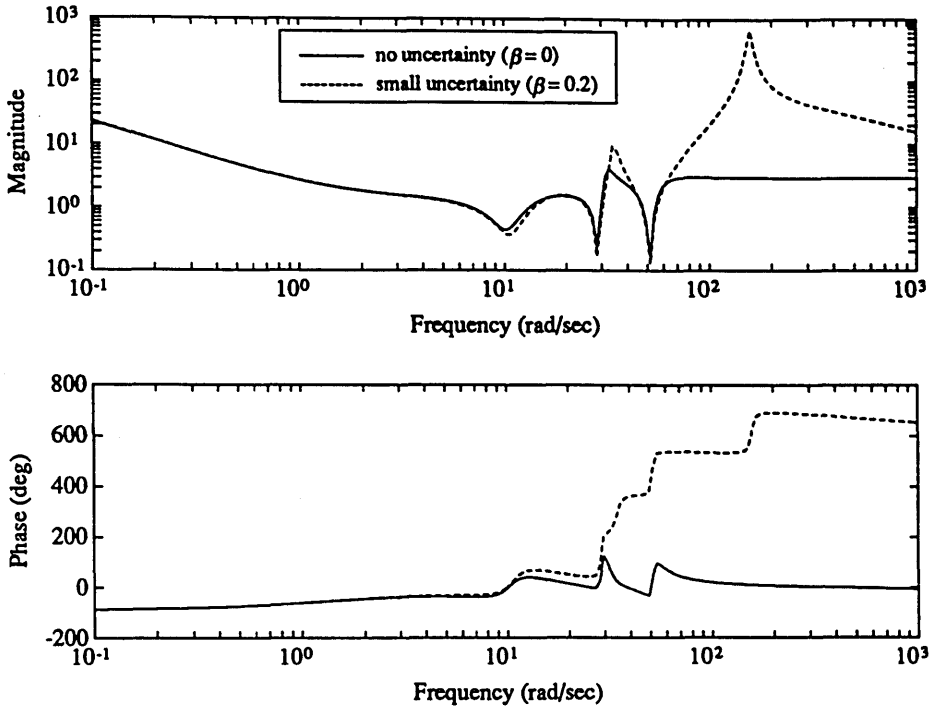

Figure 4.11(a). LQG (ρ=0.1, μ=1E-8) and SWLQG (de-sensitizing the 28 rad/sec mode) compensators for Typical Section 2B.

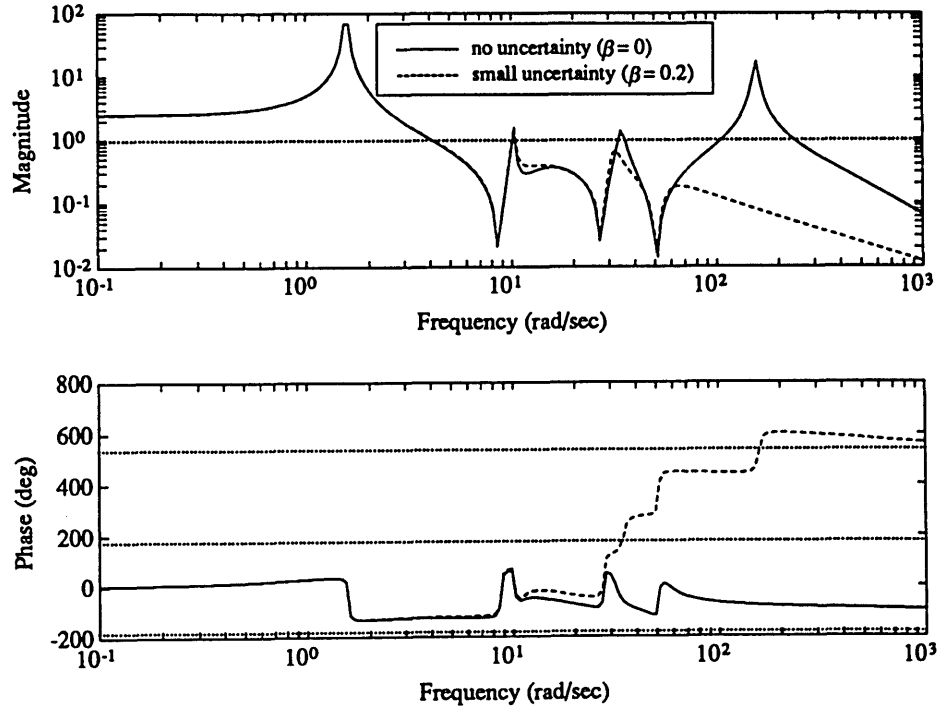

Figure 4.11(b). Loop transfer functions for the LQG and SWLQG compensators in Figure 4.9(a).

SWLQG compensators. Notice how the mode at 30 rad/sec is phase stabilized by the SWLQG compensator, and the high frequency magnitude of the compensator drops such that there are no loop crossover except for that at 4 rad/sec.

Summary

The LQG compensators developed for Topology IIA are quite similar to those developed for Typical Section 1A Topology I. The compensators are stable and minimum phase, and the asymptotes are valid, since the disturbance to performance transfer functions for each are minimum phase. In Region 4, both compensators matched the low gain LQG asymptote, which is identical for the two cases: an inversion of the input output transfer function, g_{yu}, except for the dominant mode. The SWLQG compensators designed for both Topologies I and IIA create notch filters in Region 3. The primary difference in the compensators lies in compensating the modes in Regions 1 and 2.

The Region 1 compensators for both Topology I and IIA are dominated by the high gain LQG asymptote, which is identically the disturbance to performance transfer function minimizing compensator for each. For Topology I, it is a high gain compensator, with the temporal relationship between the performance and output, ϕ_{zy}. For Topology IIA, it is a high gain compensator, with the filter g_{zu}/g_{yu}. For Topology IIA, the temporal relationship between z and y is embedded in the filter. If the filter is split into two parts, as stated earlier,

$$\frac{g_{zu}}{g_{yu}} = \phi_o g_o \tag{4.28}$$

where ϕ_o is the temporal relationship between z and y, and g_o is a structural filter. Therefore, the only difference between the compensators designed for Topology I and

IIA is the structural filter, g_o, which is the structural dynamics in the transfer function in the plant from the output to performance.

For Topology IIA, the SWLQG compensators show the additional dynamics added in Region 1 and 2 to replicate the structural filter g_o, are not very robust.

For Topology IIB, where the disturbance and input are analogous, but the performance and output are not, the results are not as easy to interpret. The asymptotes of the LQG compensator are not applicable because of the nonminimum phase zeros in the disturbance to output transfer function g_{yw}. The compensators are unstable and/or nonminimum phase for many combinations of Kalman Filter and LQR weightings. Unstable and nonminimum phase compensators, although theoretically correct, are shown to be nonrobust by the SWLQG compensators.

The magnitude of the compensators for Topology IIB seems to match that of the disturbance to performance transfer function minimizing compensator. This statement, which was not shown explicitly in the example with Typical Section 2B, will be shown more thoroughly in the MACE experiment in Section 4.5.

Therefore, the magnitude of the compensators for Topologies IIA and IIB in Regions 1 and 2 matched that of the disturbance to performance transfer function minimizing compensator, which, according to Equations 4.7 and 4.15, are identical for both topologies. It must follow, therefore, in order to design a low order, robust Neo-Classical compensator for Topology II, Topology IIA should be used as the template. For both Topologies IIA and IIB, the filter dynamics can be split into the temporal relationship between z and y, and the structural filter g_o.

$$\frac{g_{zw}}{g_{yu}} = \phi_o g_o \tag{4.29}$$

This leads to a generalized statement for Neo-Classical design for all topologies that fall into the Topology II category.

For Typical Section 2A and 2B, the function of the LQG compensators for varying values of the Kalman Filter weighting μ was examined. Similar results to the compensators designed for Typical Section 1A are seen (Figure 3.7(a) and (b)). These include the PI controller becoming a lag controller, and the high frequency rolloff becoming steeper, and at a lower frequency.

4.4 Neo-Classical Control

This section presents the Neo-Classical design rules for topologies as in Topology II, comprised of Topology IIA (analogous performance/output) and Topology IIB (analogous disturbance/input). The optimal compensators are shown to be similar to those designed for Topology I, and the design rules are also be similar. The design rule for analogous disturbance and input, or analogous performance and output, with the input and output being collocated, dual, and complementary extreme on the following page.

Neo-Classical Design Rule 2A states that the filter, g_{zw}/g_{yu}, is examined first, and split into two parts: the temporal relationship between z and y, ϕ_o and the structural filter g_o. The temporal relationship, although is usually simple to estimate for the case of a collocated performance/output pair, can usually be estimated for the general case by comparing the output and performance. For instance, in Typical Section 2A, since the performance z is the position on the third mass, and the output y was rate, the temporal relationship ϕ_o is an integration.

After the filter dynamics have been split, Neo-Classical Design Rules 2B-D are identical to Neo-Classical Design Rules 1A-D. This shows the similarities between the control designs of Topologies I and II.

Neo-Classical Design Rule 1E states that stable, minimum phase dynamics are added to the compensator in Regions 1 and 2, replicating the structural filter, g_o.

Neo-Classical Design Rule 2

For analogous performance and output, *or* analogous disturbance and input, *and* collocated, dual, and complementary extreme input and output:

A. **Examine the filter dynamics g_{zw}/g_{yu}. Split the filter into two parts, the temporal relationship between the performance z and the output y, ϕ_o, and the structural filter g_o.**

$$\frac{g_{zw}}{g_{yu}} = \phi_o g_o$$

B. **Design a low frequency controller for Regions 1 and 2, i.e.**

$$K = k_o \phi_{zy}$$

where k_o is a gain used to set the bandwidth of the system subsequently.

B. **Select a bandwidth. Design the high frequency controller for Regions 3 and 4 such that the convolution of A and B yields a rate feedback compensator at high frequency. Adjust k_o such that the crossover of the loop transfer function is equal to the choice of bandwidth. Insure that placement of these dynamics is made such that the phase margin at the loop crossover is approximately 30°-60°.**

C. **Add higher frequency rolloff dynamics, if necessary.**

D. **Examine the loop transfer function, $g_{yu}K$, consisting of the open loop system, g_{yu}, and the compensator designed from rules 1A-C. Notch filter all modes in Region 3, which may affect the closed loop stability of the system. If necessary, iterate to B if the phase margin is not in the 30°-60° range.**

F. **Add stable, minimum phase dynamics in Regions 1 and 2, replicating the magnitude of g_o, without jeopardizing the closed loop stability of the system.**

The magnitude of the compensators designed for both Topology IIA and IIB matched that of the magnitude of the disturbance to performance transfer function minimizing compensator, g_{zw}/g_{yu}, at low frequency, i.e. Regions 1 and 2. For those designed for Topology IIA, the compensators are stable and minimum phase. Therefore, only stable, minimum phase dynamics are added to the compensator. The designer, however, must be also be careful not to jeopardize the closed loop stability of the system by adding the structural filter to Regions 1 and 2. As shown

in Figure 4.5(a) and (b), adding dynamics to the high gain compensator at low frequency creates possible loss closed loop robustness.

As an example, a Neo-Classical control design is made for Typical Section 2A using Neo-Classical Design Rule 2. Design Rule 2A states that the filter g_{zw}/g_{yu} is split into two parts: the temporal relationship between z and y, ϕ_o and the structural dynamics g_o.

$$\frac{g_{zw}}{g_{yu}} = \phi_o g_o \tag{4.30}$$

For Typical Section 2A, the performance z is the integration of the output y. Therefore ϕ_o is an integration

$$\phi_o = \frac{1}{s} \tag{4.31}$$

and the structural filter g_o is given by

$$g_o = \frac{g_{zw}}{g_{yu}} s \tag{4.32}$$

Figure 4.12 shows the filter dynamics g_{zw}/g_{yu}, the temporal relationship ϕ_o, and structural filter g_o for Typical Section 2A. Note that these are identical to those for Typical Section 2B.

Design Rule 2B states the low frequency controller is designed as the temporal relationship ϕ_o, and a gain k_o. For Typical Section 2A, this is a high gain integrator, or position feedback. The design constant k_o is chosen to set the bandwidth when Design Rule 2C is completed.

Design Rule 2C states a bandwidth is selected. For this design, approximately 6 rad/sec bandwidth is chosen, similar to the LQG design in Figure 4.4(a). Then, a high frequency controller is designed to add rate feedback. For this

case, convolving a zero into the compensator creates a high frequency rate feedback controller, or proportional feedback. The zero is set at 1.8 rad/sec, creating a phase margin at crossover of approximately 60°. The design constant k_0 is then adjusted, to set the 6 rad/sec bandwidth.

Using Design Rule 2D, one rolloff pole is added, at 100 rad/sec.

The next step, in accordance with Design Rule 2E, is to examine the loop transfer function made up of the controller created from Design Rules 2A-D, and the open loop transfer function, g_{yu}. The mode at 10 rad/sec has a loop gain greater than one. Therefore it falls into Region 3, and should be notch filtered. The notch filter constructed, using Equation 3.231, has the following characteristics: (ω=10.1, α=10, ζ_0=0.02).

Design Rule 2F states that the structural filter dynamics g_0, are added to the compensator in Regions 1 and 2, without jeopardizing the closed loop stability. In examining g_0 in Figure 4.12 for Typical Section 2A, there are no structural dynamics within the 6 rad/sec bandwidth. Therefore, no additional dynamics will be convolved into the Neo-Classical compensator, and the design is complete. The resulting 4 state Neo-Classical compensator is shown in Figure 4.14(a), along with the 8 state LQG design from Figure 4.4(a), for Typical Section 2A. The open loop input output transfer function is shown in Figure 4.13.

Both the LQG and Neo-Classical compensator use integral (position) feedback at low frequency, and rate (proportional) feedback at high frequency. The Neo-Classical compensator does not add the pole zero inversions at 28 and 51 rad/sec as they do not affect the closed loop stability or performance. Notice the compensator dynamics around 10 rad/sec. The Neo-Classical compensator places a notch filter to gain stabilize the open loop pole at 10 rad/sec. The LQG compensator contains a heavily damped zero pair at 9.5 rad/sec. This is a result of the compensator dynamics being in the crossover region, and not necessarily in similar to the low

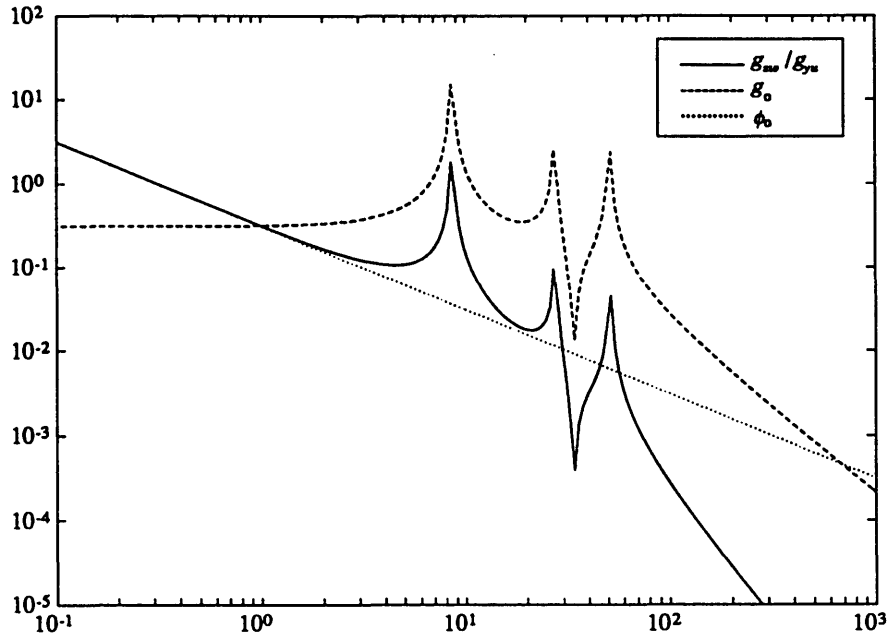

Figure 4.12. Filter dynamics g_{zw}/g_{zw} for both Typical Section 2A and 2B, and the division into the temporal relationship and structural filter.

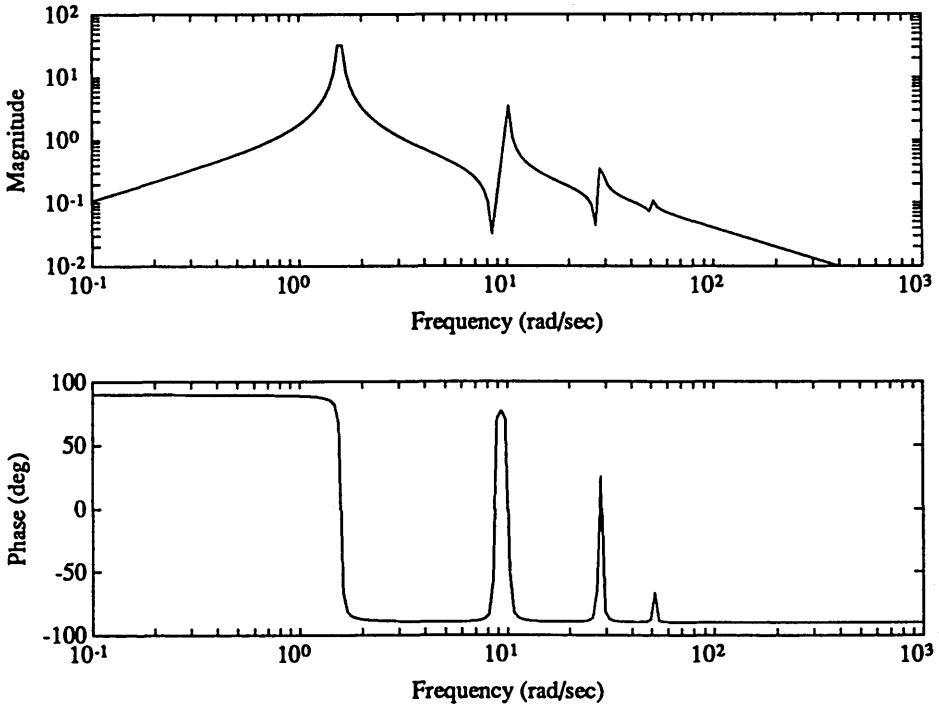

Figure 4.13. Open loop input output transfer function g_{yu} for Typical Section 1A.

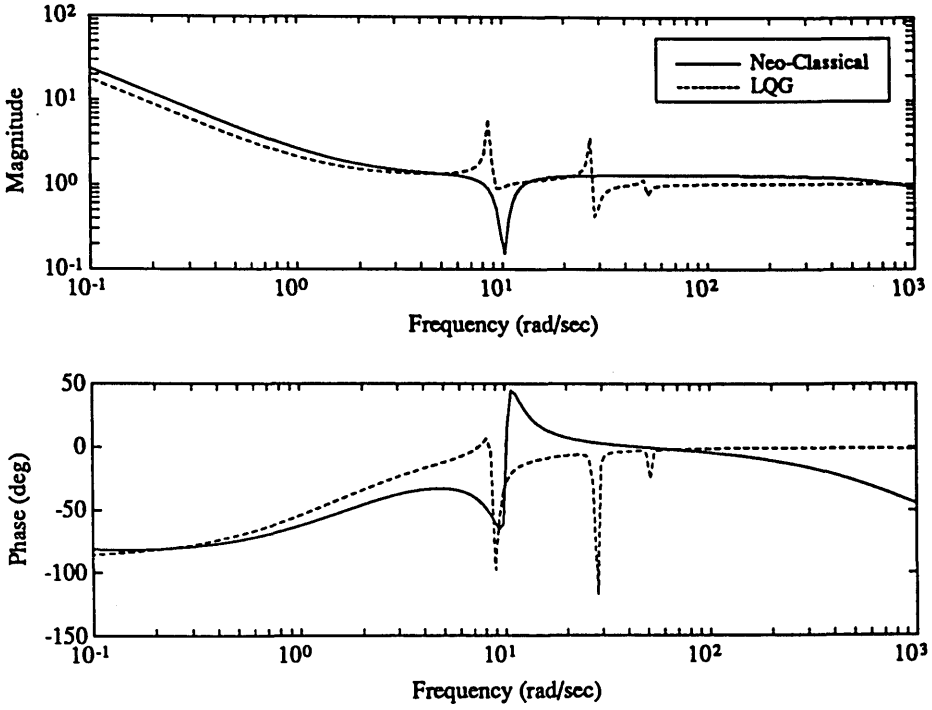

Figure 4.14(a) 4 state Neo-Classical compensator K and the LQG compensator (ρ=1E-2, μ=1E-8) for Typical Section 2A.

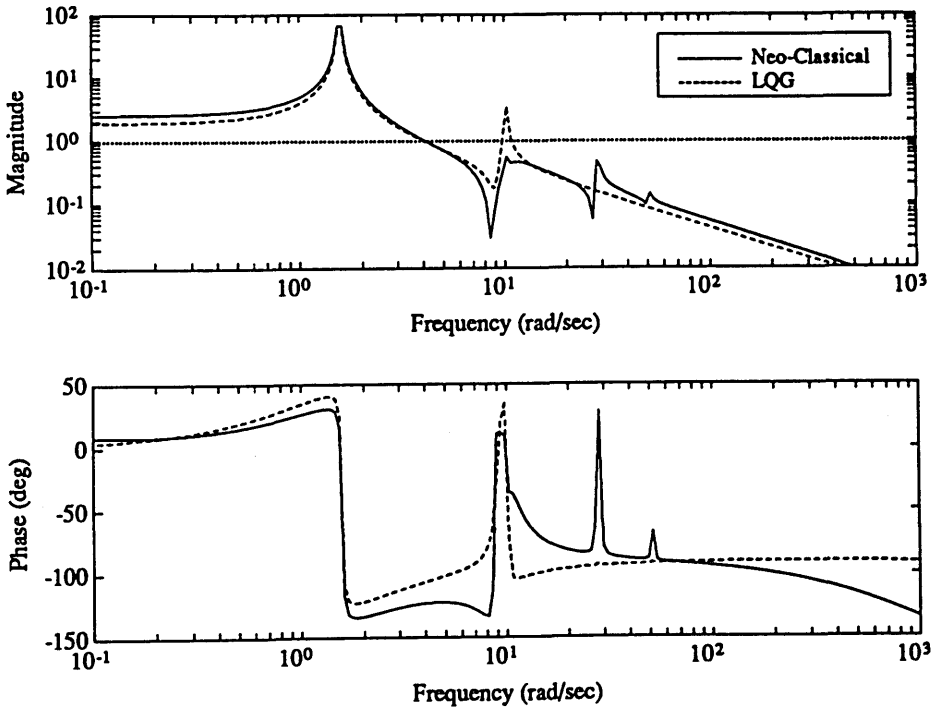

Figure 4.14(b) Loop transfer functions $g_{yu}K$ consisting of the compensators in Figure 4.14(a) and the open loop transfer function.

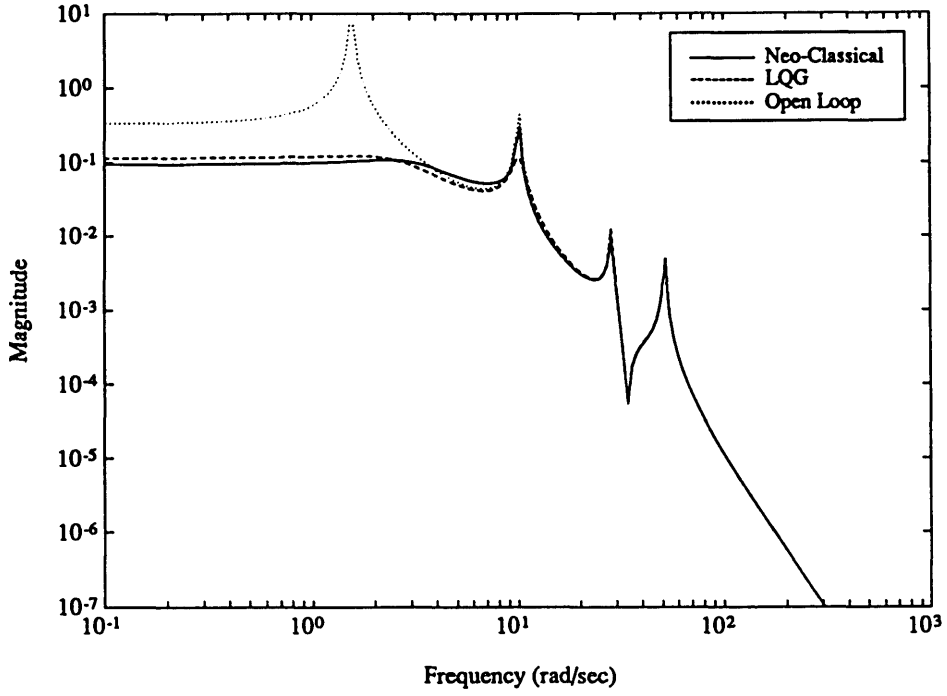

Figure 4.14(c). Open and closed loop disturbance to performance transfer functions for Typical Section 2A. Performance improvement with both the Neo-Classical and LQG compensators is 27.1 dB.

gain (lightly damped zero pair at 10 rad/sec) and high gain (no zero pair) asymptotes of LQG, as seen in Figure 4.4(a). Note that the Neo-Classical compensator is designed assuming that the mode at 10 rad/sec might be closed loop unstable because of possible unmodeled phase lag in the loop, and therefore notch filtered. The LQG compensator has no knowledge of a phase lag.

Figure 4.14(b) shows the loop transfer function for the LQG compensator in Figure 4.14(a), and the open loop system in Figure 4.13. Notice how the mode at 10 rad/sec is gain stabilized by the Neo-Classical design, but is not gain stabilized by the LQG design. This is a result of the notch filter present in the Neo-Classical compensator, but not in the LQG compensator.

Figure 4.14(c) shows the open and closed loop transfer functions with the

Neo-Classical and LQG designs in Figure 4.14(a). The performance improvement for both designs is 26.8 dB. The Neo-Classical compensator contains 4 states, compared to the 8 state LQG compensator. The Neo-Classical compensator is also more robust, as a result of gain stabilizing the loop gain in Figure 4.14(b), and not inverting the open loop zeros at 27.4 and 51.1 rad/sec.

Notice that the Neo-Classical compensator for this design is identical to the Neo-Classical design for Typical Section 1A in Figure 3.5(a). This follows from the fact that the filter dynamics g_{zw}/g_{yu} for Typical Section 2A and Typical Section 1A are identical below the 6 rad/sec crossover, i.e. an integrator with no structural modes.

Notice also that if a Neo-Classical control design is designed for Typical Section 2B, the same compensator as in Figure 4.14(a) would be created. This is a result of the filter dynamics g_{zw}/g_{yu} being identical for both typical sections.

Although this was a very simple example because there were no filter dynamics within the bandwidth of the system, in the more complex systems, such as those of the MACE test article, the design of the filter dynamics will be very important to the compensator design, and eventual performance improvement.

4.5 Experimental Implementation

Optimal LQG, SWLQG, and Neo-Classical compensators were designed and implemented experimentally on the MACE test article for a topology consistent with Topology II. Figure 4.15 shows an example of this topology on the MACE test article, MACE 2. In the MACE 2 topology, the output y is the z-axis rate gyro in the payload, while the performance z is the integrated z-axis payload rate gyro. The disturbance w is a z-axis inertial torque about the center of the bus, created by the torque wheels. This topology is the same as the payload pointing loop topology of

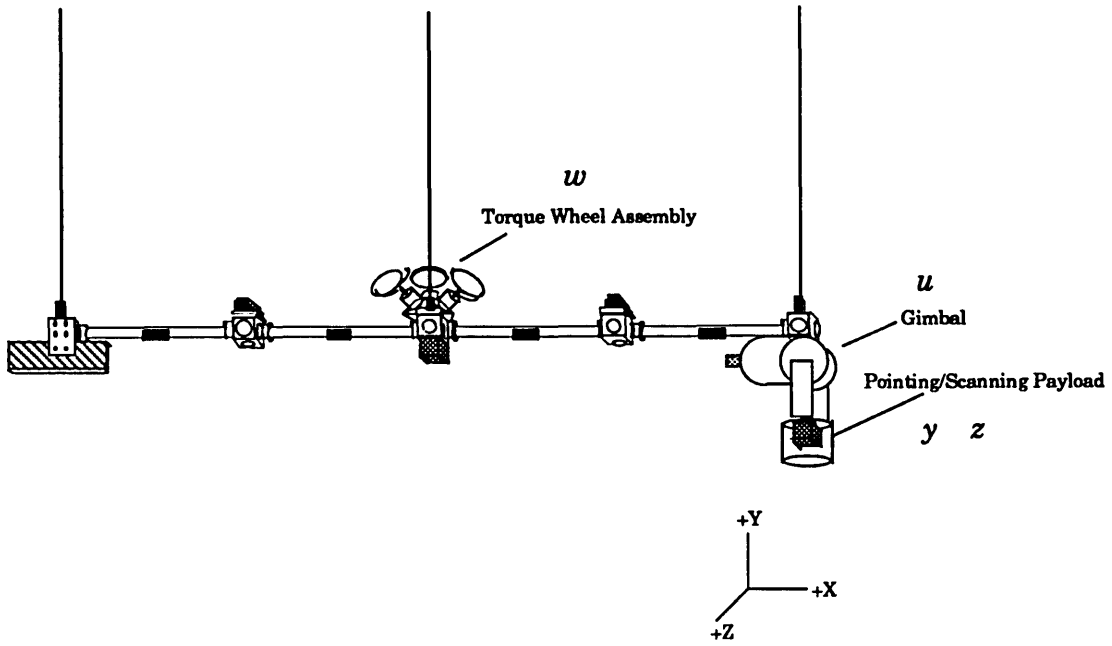

Figure 4.15. MACE 2: The topology of the payload pointing loop with the z-axis torque wheels as the disturbance.

MACE 1A, shown in Figure 3.18, except that the disturbance is the torque wheels, not at the gimbal. Because the performance and output are analogous, and the disturbance and input are not, this topology falls into the Topology IIB category. The implications are that the disturbance to output transfer function does not contain alternating poles and zeros, and therefore, the construction of the optimal compensators such as LQG may have difficulties.

Figure 4.16 shows the measured open loop disturbance to performance transfer function g_{zw}. Notice that this is s times the disturbance to output transfer function, g_{yw}, which is important in the construction of the LQG compensator, as shown in the LQG asymptotes in Equations 4.23 and 4.26. In this transfer function, there is are nonminimum phase zeros at 1.8, 14, and 35 Hz, and a pair of missing zeros between the poles at 6.8 and 8.8 Hz. The large phase delay of the loop also evident.

Figure 4.17 shows the measured open loop input output transfer function, g_{yu},

for MACE 2. Figure 4.18(a) shows the model based 24 state LQG compensator designed for MACE 2. This compensator contains a PI controller with a zero of 3 Hz. There are two lightly damped pole pairs at 6 and 9.4 Hz, and a nonminimum phase lightly damped zero pair at 14 Hz. The LQG compensator also constructs several lead filters in order to add lead at crossover, versus high frequency amplification.

For MACE 2, the high gain asymptote for Topology IIB in Equation 4.26 is

$$\underset{\substack{\mu\to 0\\ \rho\to 0\\ \rho>\mu}}{LIM}\, K(s) = \pm\frac{1}{\sqrt{\rho}}\frac{\phi_{zy} g_{yw}}{g_{yw}} = \pm\frac{1}{s\sqrt{\rho}} \tag{4.33}$$

as a result of the performance z being the integration of the output y. Therefore, in Regions 1 and 2, the LQG compensator should resemble an integrator, and in examining Figure 4.18(a), it does not. The asymptotes for this design, because g_{yw} contains nonminimum phase zeros, are not valid. The magnitude of the LQG compensator in Regions 1 and 2, however, matches that of the disturbance to performance transfer function minimizing compensator shown in Figure 4.19. Notice the LQG compensator contains two lightly damped pole pairs at 6 and 9.4 Hz, matching the transfer function minimizing compensator.

Figure 4.18(b) shows the measurement of the loop transfer function consisting of the open loop input output transfer function (Figure 4.17), and the 24 state model based LQG compensator (Figure 4.18(a)). Notice how the phase of the loop transfer function drops quickly at 14 Hz as a result of the nonminimum phase zero pair. The gain and phase margins at this point are very small, and the robustness of this compensator to changes in the plant was questionable. The magnitude of the loop transfer function also rises above 0 dB at 36 and 70 Hz. This was a result of the attempt of the compensator to invert the open loop disturbance to output transfer function g_{yw}, except for the dominant mode, similar to the low frequency LQG asymptote in Equation 4.23. It is similar to the LQG compensator

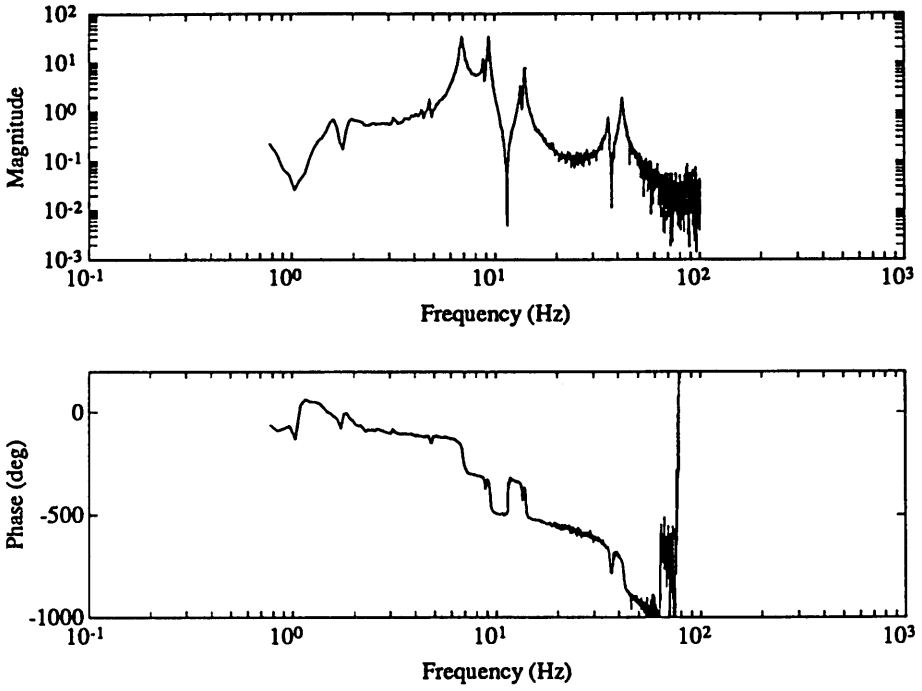

Figure 4.16. Measurement of the disturbance to performance open loop transfer function g_{zw} from z-axis torque wheels to the integrated z-axis payload rate gyro, for MACE 2.

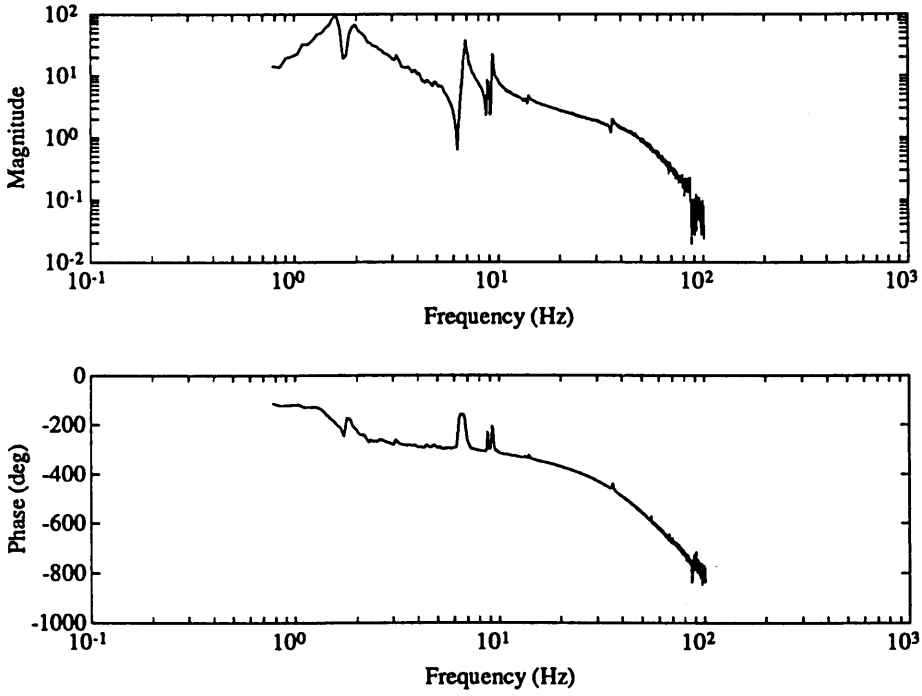

Figure 4.17. Measurement of the open loop input output transfer function g_{yu} from z-axis gimbal to z-axis payload rate gyro, for MACE 2.

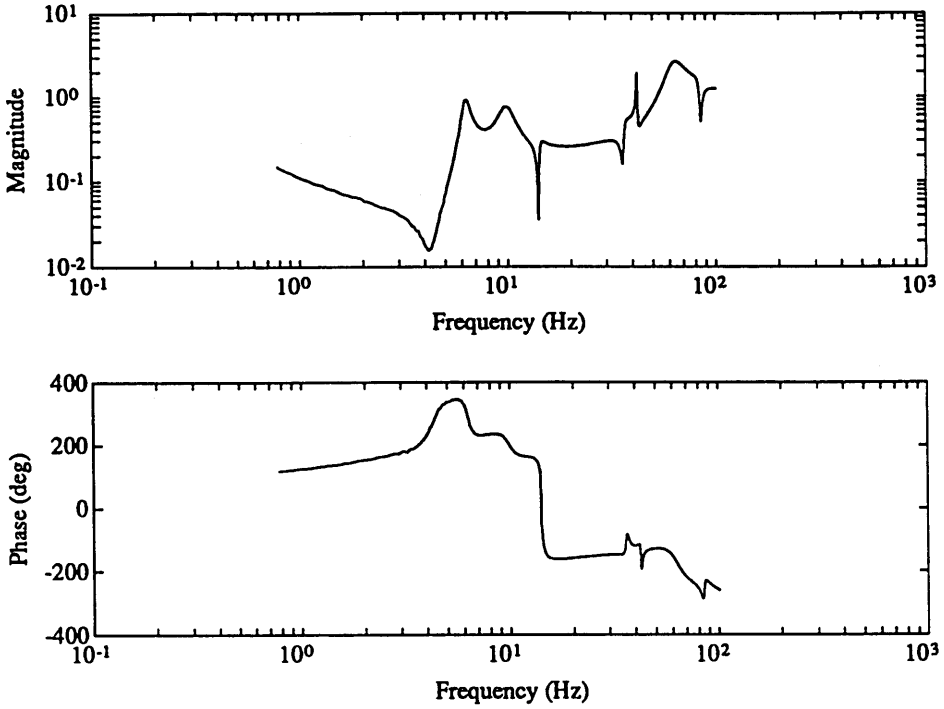

Figure 4.18(a). Model based 24 state LQG compensator K designed for MACE 2.

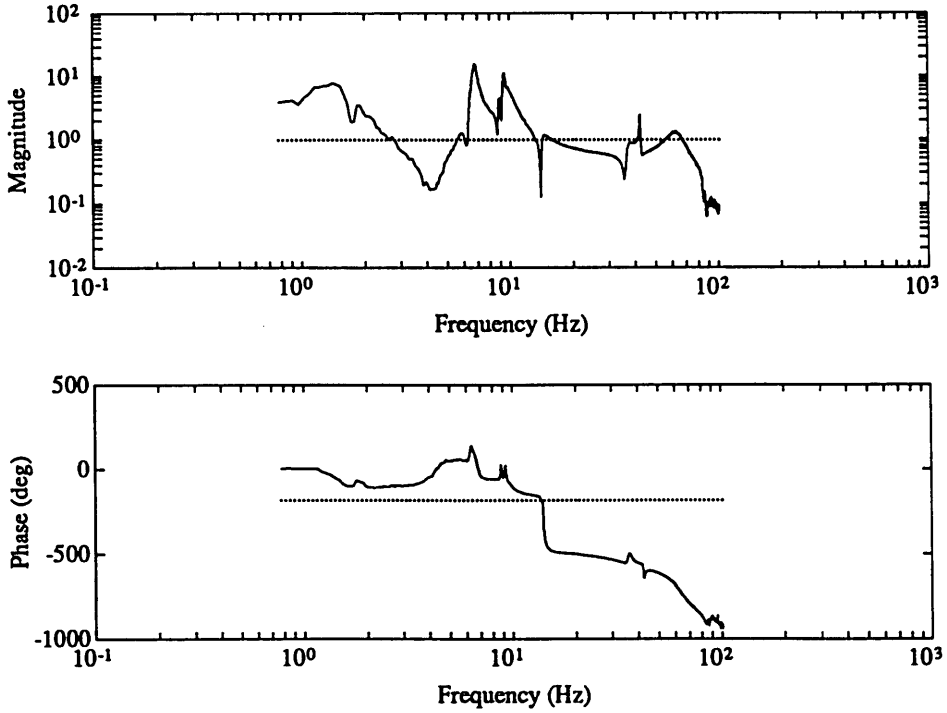

Figure 4.18(b). Measurement of the loop transfer function $g_{yu}K$ consisting of the LQG compensator and open loop transfer function.

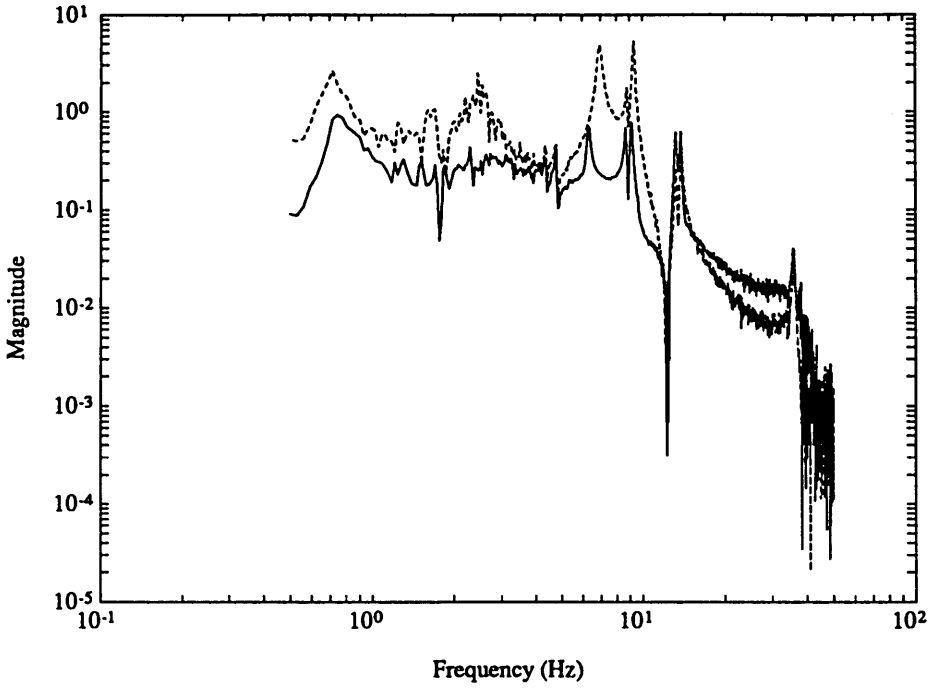

Figure 4.18(c). Measurement of the open and closed loop disturbance to performance transfer functions for MACE 2. Performance improvement with the 24 state LQG compensator was 12 dB.

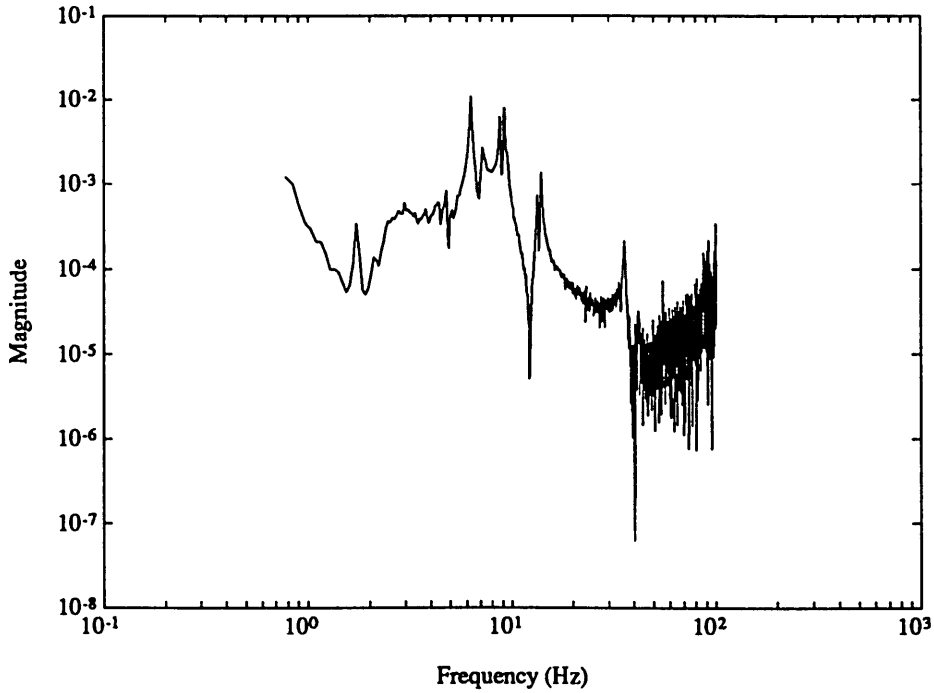

Figure 4.19. Measurement of the disturbance to performance transfer function minimizing compensator for MACE 2.

designed for Typical Section 2B in Figure 4.8(a) and (b), where additional loop crossovers occurred at frequencies above the bandwidth. The SWLQG compensator showed these additional loop crossovers are nonrobust for Topology IIB compensators. The bandwidth is approximately 17 Hz.

Figure 4.18(c) shows the measurement of the open and closed loop disturbance to performance transfer functions for the model based 24 state LQG compensator for MACE 2. Notice that because of model errors, the open loop peaks at 6.8 and 9.4 Hz could not be exactly reduced. There was marginal low frequency closed loop performance improvement. At high frequency, amplification can be seen as a result of the lead filters in the LQG compensator. The performance improvement of this design was 11.6 dB.

Further performance improvement was hindered by the high frequency amplification in the LQG compensator (Figure 4.18(a)). As the LQR weighting ρ was reduced, the amplification in the compensator increased, driving the modes at 36 and 70 Hz unstable. Also, further truncation of the compensator resulted in an unstable closed loop system.

Figure 4.20(a) shows the measurement of a model based 24 state SWLQG compensator, designed MACE 2. This compensator was de-sensitized to frequency changes in the modes at 14, 36, 88 Hz. Comparing the LQG compensator (Figure 4.18(a) and the SWLQG compensator (Figure 4.20(a)), the nonminimum phase lightly damped zeros at 14 Hz were immediately made minimum phase, indicating the low robustness of the lightly damped nonminimum phase zeros. The compensator gain was also reduced by a small amount.

Figure 4.20(b) shows the measurement of the loop transfer function consisting of the model based 24 state SWLQG compensator (Figure 4.20(a)), and the open loop transfer function g_{yu}, in Figure 4.19. Comparison of Figures 4.18(b) and 4.20(b) shows how the mode at 14 Hz was phase stabilized SWLQG

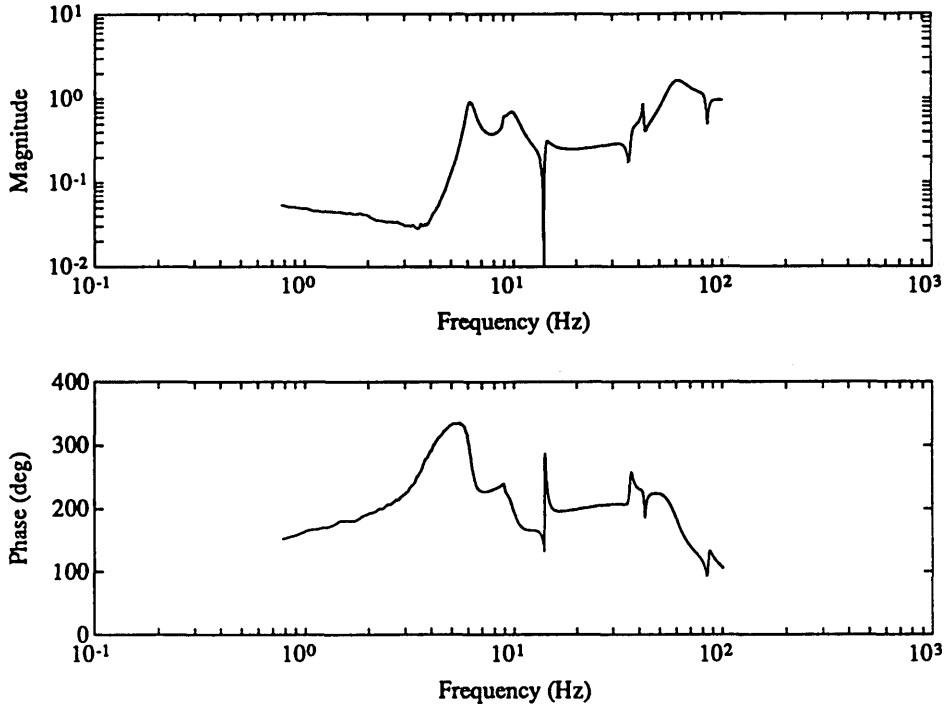

Figure 4.20(a). Model based 24 state SWLQG compensator K designed for MACE 2.

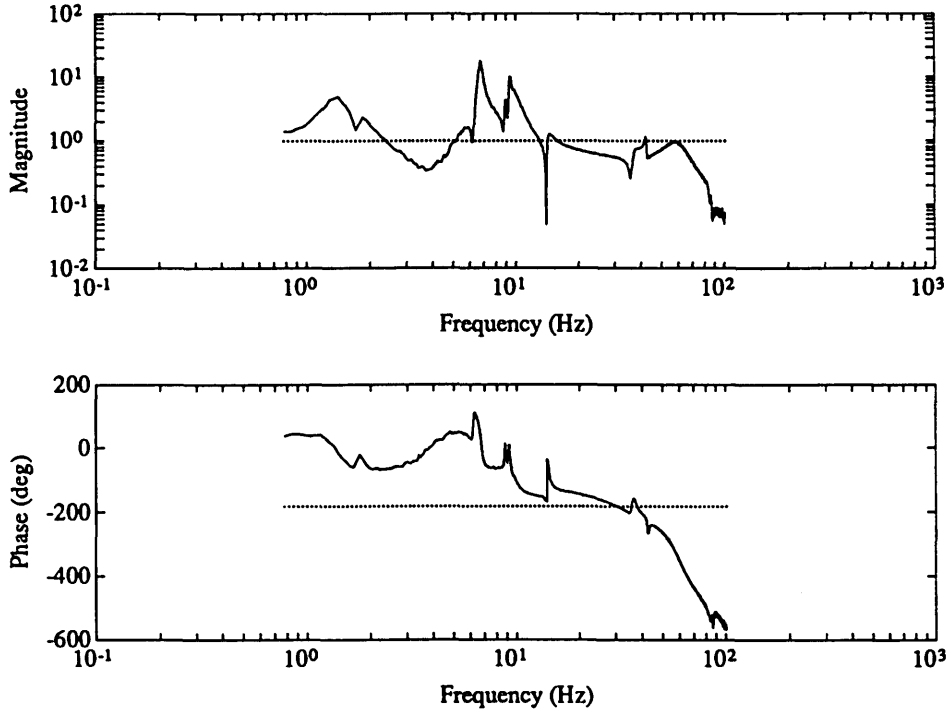

Figure 4.20(b). Measurement of the loop transfer function $g_{yu}K$ consisting of the SWLQG compensator and open loop transfer function.

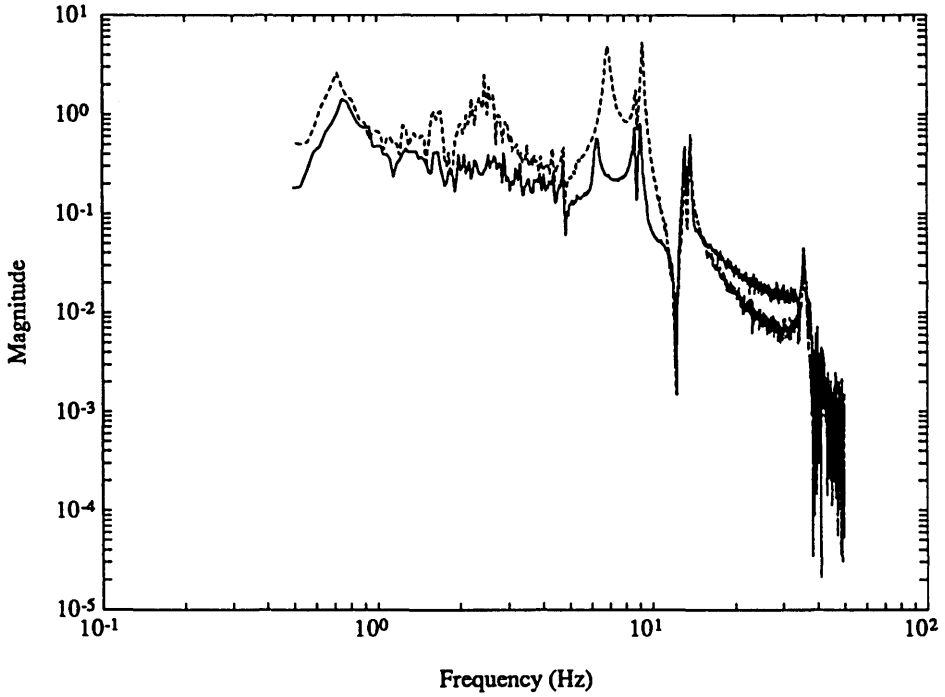

Figure 4.20(c). Measurement of the open and closed loop disturbance to performance transfer functions for MACE 2. Performance improvement with SWLQG compensator was 11.6 dB.

compensator, such that the phase of the loop transfer function does not cross -180° until 30 Hz. This is a result of the SWLQG compensator using a minimum phase zero pair at 14 Hz. Also, the magnitude of the compensator at 36 and 70 Hz is smaller, such that there are no loop crossovers, similar to the SWLQG compensators designed for Typical Section 2B in Figure 4.11(a) and (b). The de-sensitization attempts to gain stabilize these modes.

Figure 4.20(c) shows the measurement of the open and closed loop disturbance to performance transfer functions with the SWLQG compensator for MACE 2. The performance improvement was 11.6 dB, 0.4 dB smaller than that of the LQG compensator. The tradeoff for robustness in the SWLQG compensator, caused a decrease in the performance improvement, as can be expected.

Next, a Neo-Classical compensator was designed for MACE 2. Since the

performance and output are analogous, but the disturbance and input are not, Neo-Classical Design Rule 2 is used.

Following Design Rule 2A, the filter dynamics g_{zw}/g_{yu} were split into two parts, a temporal relationship between z and y, and the structural filter. The measurement of the filter dynamics is shown in Figure 4.21. Knowing that the performance is the integration of the output, the temporal relationship ϕ_o is

$$\phi_o = \frac{1}{s} \tag{4.34}$$

The structural dynamics g_o are then given by

$$g_o = \frac{g_{zw}}{g_{yu}} s \tag{4.35}$$

Using Design Rule 2B, a low frequency, high gain controller was designed, with the temporal relationship ϕ_o and a gain k_o. For this case, the low frequency controller was a high gain integrator, or position feedback. The design constant k_o is set upon the completion of Design Rule 2C.

Following Design Rule 2C, a bandwidth of 20 Hz was chosen, similar to the payload pointing loop topology MACE 1A in Chapter 3. Next, a high frequency controller was chosen such that its convolution with the low frequency controller from 2B yielded rate feedback at high frequency. For this case, the low frequency integral control (position feedback) is changed to proportional control (rate feedback) at high frequency by adding a compensator zero. The zero frequency is chosen to be 8 Hz. Four lead filters, each with two poles and two zeros, were also constructed, identical to those designed for the Neo-Classical compensators designed previously (Figures 3.22(a) and 3.25(a)). The lead filters add phase lead at crossover, with the tradeoff of high frequency amplification, similar to the LQG compensators. Finally, the design constant k_o was chosen to set the loop gain crossover at 20 Hz.

Using Design Rule 2D, there were no rolloff dynamics added to the design, as a result of the open loop transfer function g_{yu} rolling off substantially (Figure 4.17).

Design Rule 2E states that the loop transfer function made up of the controller designed from Design Rules 2A-D, and the open loop transfer function g_{yu} in Figure 4.17 is examined. The mode at 36 Hz was gain stabilized, as a result of its loop gain being greater than -3 dB, and posing closed loop stability problems. A second order notch filter was constructed (ω=36 Hz, α=10, ζ_o=0.02) and added to the compensator.

Design Rule 2F states that dynamics from the structural filter g_o in Equation 4.35 resulting from the splitting of the filter dynamics g_{zw}/g_{yu} in Figure 4.21, is convolved into the compensator, without jeopardizing the closed loop stability of the system. In examining the filter dynamics, the resonances stand out at 6.0 and 9.4 Hz. For this reason, two lightly damped poles were added to the compensator at

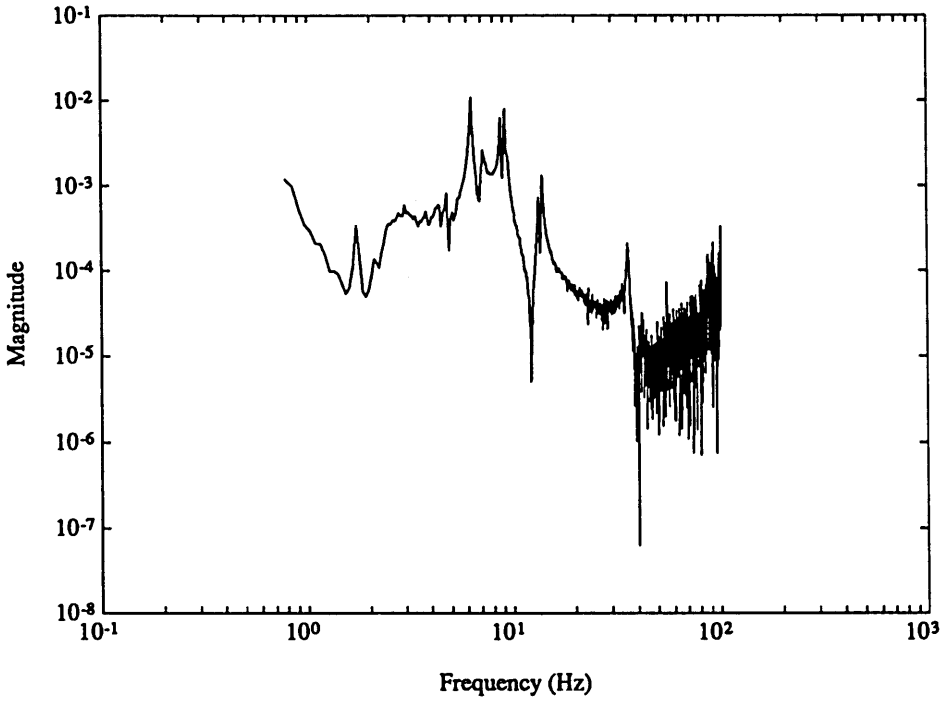

Figure 4.21. Measurement of the filter dynamics g_{zw}/g_{yu} for MACE 2.

these frequencies. In order to stabilize the closed loop system, two zero pairs were also added, at 6.0 and 10.4 Hz. Thus, 4 states were added to the Neo-Classical design. The resulting 16 state Neo-Classical design is shown in Figure 4.22(a).

Comparing the Neo-Classical compensator (Figure 4.22(a)) and the SWLQG compensator in Figure 4.20(a), in Regions 1 and 2, they both contain PI controllers, but the Neo-Classical design has a faster zero pole (ω_z=-8 Hz versus ω_z=-1 Hz), thus creating integral control over a larger frequency range. They both contain the resonances replicating in the filter g_{zw}/g_{yu} at 6.0 and 9.4 Hz. And the SWLQG compensator notches the 14 Hz mode, while the Neo-Classical compensator notches the 36 Hz mode. Also, both compensators contain the lead filters, adding phase lead at crossover and high frequency amplification.

Figure 4.22(b) shows the measurement of loop transfer function, consisting of the 16 state Neo-Classical compensator (Figure 4.22(a)), and the open loop input output transfer function g_{yu} (Figure 4.17). Notice the loop crossover is 20 Hz, the same as the Neo-Classical design shown design for MACE 1A in Figure 3.22(b). Also notice that the bandwidth is larger than that of the LQG (Figure 4.18(b)) and SWLQG (Figure 4.20(b)) designs (20 Hz versus 14 Hz). This was a result of the magnitude of the LQG and SWLQG compensator inverting the higher frequency dynamics in the g_{yw} transfer function, except for the dominant mode, as in the low gain LQG asymptote (Equation 4.23). Additional loop crossovers at higher frequencies (36 and 88 Hz), thus creating closed loop stability problems and limited performance improvement for the optimal controllers.

Figure 4.22(c) shows the measurement of the open and closed loop disturbance to performance transfer functions for the 16 state Neo-Classical design for MACE 2. This design created a low frequency performance improvement from the PI controller, while adding magnitude reduction of the peaks at 6.8 and 9.4 Hz. The peaks could not be reduced exactly because of modeling errors, and closed loop

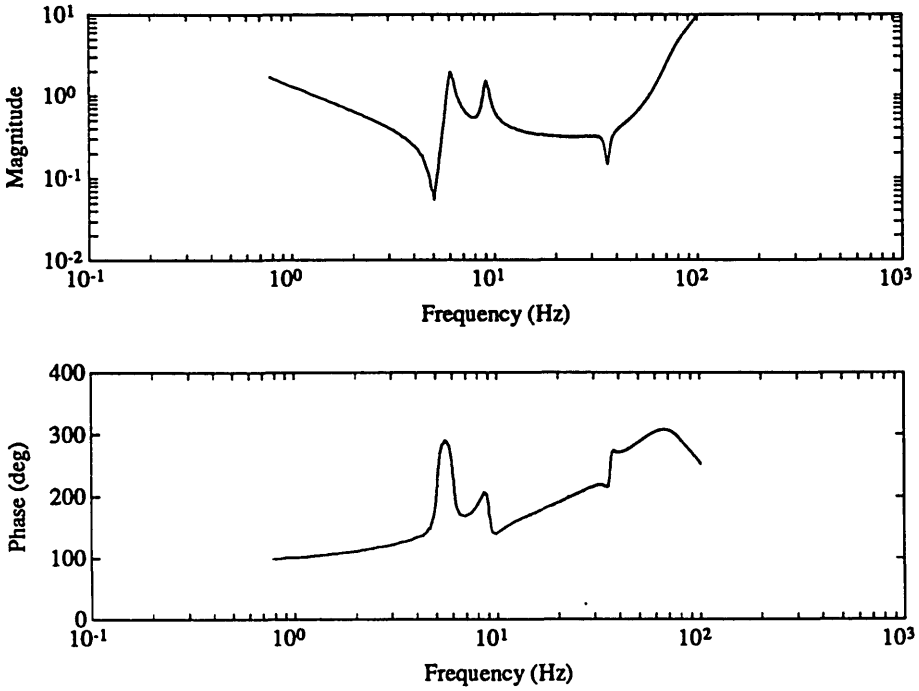

Figure 4.22(a). 16 state Neo-Classical compensator K designed for MACE 2: 2 states for the stabilized integrator; 8 states for the lead filters; 2 states for the notch filters; 4 states for the structural filter.

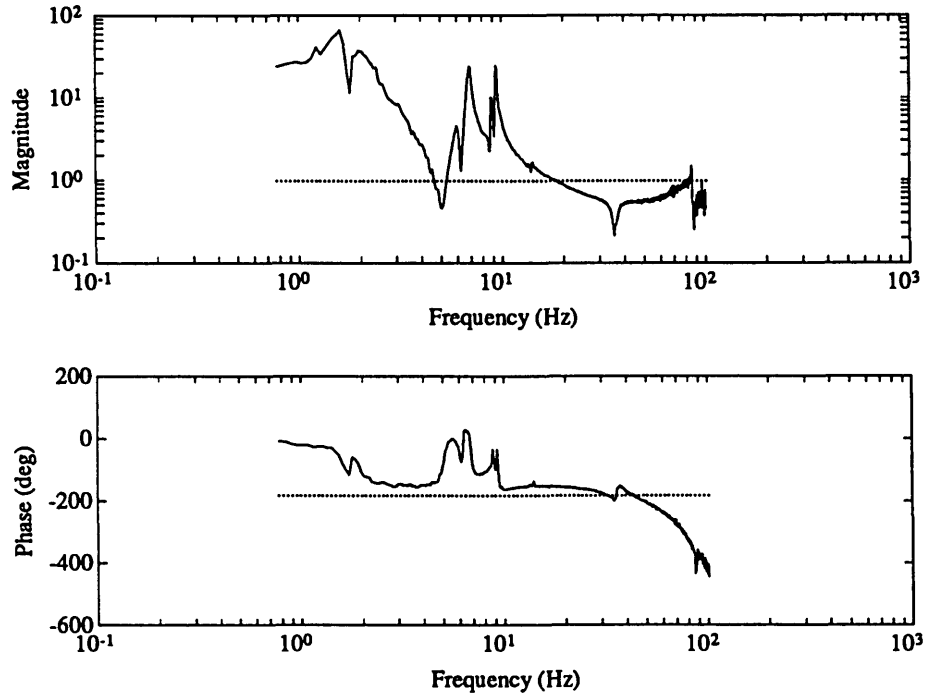

Figure 4.22(b). Measurement of the loop transfer function $g_{yu}K$ consisting of the Neo-Classical compensator and open loop transfer function.

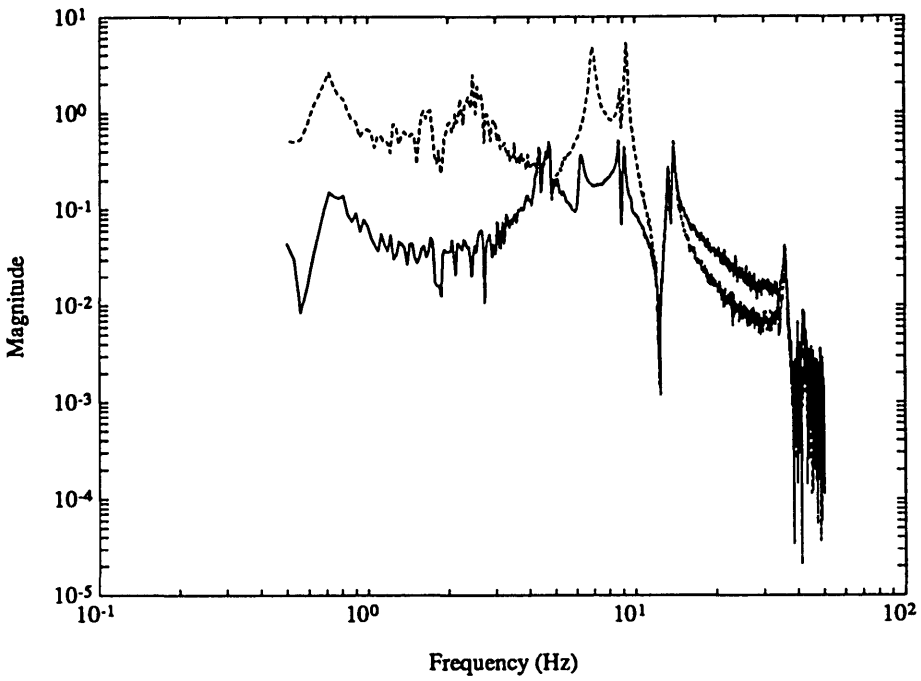

Figure 4.22(c). Measurement of the open and closed loop disturbance to performance transfer functions for MACE 2. Performance improvement with the Neo-Classical compensator was 15.9 dB.

stability concerns with adding the exact filter dynamics (Design Rule 2F). The performance improvement of this design was 15.9 dB, better than both the LQG (12 dB) and SWLQG (11.6 dB) designs. This is a result of the higher frequency zero in the PI controller, thus yielding a higher gain and a larger frequency range of integral control in the Neo-Classical design, and the higher loop crossover. The Neo-Classical design was also 16 states, compared to the 24 states for the LQG and SWLQG designs. This shows that Neo-Classical control design is a viable design technique for low order, robust compensators for topologies with a nonanalogous disturbance or performance.

Chapter 5

SISO Topology III: Nonanalogous Performance & Output *and* Nonanalogous Disturbance & Input

5.1 Introduction

This chapter examines the implications on the control design when simplifications such as those in Topologies I and II cannot be made, i.e. the general SISO disturbance rejection problem with a nonanalogous performance and output, and nonanalogous disturbance and input. The input output pair is collocated, dual, and complementary extreme, similar to the first two topologies. A test will be developed which can be used to evaluate the effectiveness of input output pairs in minimizing the disturbance to performance transfer function. Optimal compensation techniques will be examined, with the results summarized in Neo-Classical Design Rule 3. Finally, compensators designed and implemented on the MACE test article will be presented.

5.2 Topologies Examined

Topologies I and II are simplifications of the general disturbance rejection problem given by

$$\begin{Bmatrix} z \\ y \end{Bmatrix} = \begin{bmatrix} g_{zw} & g_{zu} \\ g_{yw} & g_{yu} \end{bmatrix} \begin{Bmatrix} w \\ u \end{Bmatrix} \tag{5.1}$$

These simplifications include the disturbance and input being analogous, or performance and output being analogous. The topologies in this chapter, called Topology III, contain nonanalogous performance and output, and nonanalogous disturbance and input, and therefore, the general system in Equation 5.1 is used.

The closed loop disturbance to performance transfer function of the general disturbance rejection problem is

$$\frac{z}{w} = \frac{g_{zw} + \left(g_{zw}g_{yu} - g_{zu}g_{yw}\right)K}{1 + g_{yu}K} \tag{5.2}$$

The input output pair is collocated, dual, and complementary extreme. Therefore, the input output transfer function, g_{yu}, which is important in the closed loop stability of the system, contains a pattern of alternating poles and zeros.

In the previous topologies, disturbance rejection could be accomplished by using a high gain compensator. For this topology, however, setting the magnitude of K to be large yields

$$\left|\frac{z}{w}\right| = \left|\frac{g_{zw}g_{yu} - g_{zu}g_{yw}}{g_{yu}}\right| \qquad \text{for} \qquad \left|g_{yu}K\right| \gg 1 \tag{5.3}$$

The magnitude of the disturbance to performance transfer function does not tend to zero as the magnitude of K increases, as it did for the previous topologies: Equation

3.9 (Top. I); Equation 4.8 (Top. IIA); Equation 4.16 (Top. IIB). For the general disturbance rejection problem, there is an extra term in the numerator of the closed loop disturbance to performance transfer function, resulting in a nonzero transfer function when the magnitude of K is large.

This leads to a test for actuator sensor pairs in determining the effectiveness in reducing the disturbance to performance transfer function, using a high gain compensator. The sensor actuator pair can be chosen such that

$$\left|\frac{g_{zw}g_{yu} - g_{zu}g_{yw}}{g_{yu}}\right| \ll |g_{zw}| \tag{5.4}$$

This result simply states that in order to loop shape, i.e. use a high gain compensator, the magnitude of the disturbance to performance closed loop transfer function must be less than the magnitude of the open loop w to z transfer function. If this is satisfied, then the pair is a good choice for disturbance rejection. Of course, the compensator will also have to take the pole zero structure of g_{yu} into account.

If the input output pair satisfies this test, then the closed loop transfer function simplifies to

$$\frac{z}{w} = \frac{g_{zw}}{1 + g_{yu}K} \tag{5.5}$$

If the above transfer function is set equal to ε, and solved for the compensator K,

$$K = \frac{g_{zw} - \varepsilon}{\varepsilon g_{yu}} \tag{5.6}$$

Good disturbance rejection is achieved as ε tends to zero, giving the disturbance to performance transfer function minimizing compensator

$$\lim_{\varepsilon \to 0} K = \frac{g_{zw}}{\varepsilon g_{yu}} \tag{5.7}$$

This compensator (Equation 5.7) and closed loop system (Equation 5.5) are identical to those for Topologies IIA (Equations 4.7 and 4.5) and IIB (Equations 4.15 and 4.13).

Setting the magnitude of K to be large for disturbance rejection, the closed loop disturbance to performance transfer function simplifies to

$$\left|\frac{z}{w}\right| = \left|\frac{g_{zw}}{g_{yu}K}\right| \qquad \text{for} \qquad \left|g_{yu}K\right| \gg 1 \tag{5.8}$$

For the general closed loop disturbance to performance transfer function given in Equation 5.2, when the test given in Equation 5.4 is not satisfied, the alternative to a high gain compensator is to derive the dynamic compensator that drives the numerator of the closed loop disturbance to performance transfer function (Equation 5.2) to zero. Setting the closed loop transfer function from w to z equal to ε

$$\frac{z}{w} = \frac{g_{zw} + \left(g_{zw}g_{yu} - g_{zu}g_{yw}\right)K}{1 + g_{yu}K} = \varepsilon \tag{5.9}$$

And solving for the compensator K yields

$$K = \frac{g_{zw} - \varepsilon}{\varepsilon g_{yu} - \left(g_{zw}g_{yu} - g_{zu}g_{yw}\right)} \tag{5.10}$$

Good disturbance rejection is achieved as ε tends to zero, giving the disturbance to performance transfer function minimizing compensator for the general SISO case

$$\lim_{\varepsilon \to 0} K = \frac{-g_{zw}}{g_{zw}g_{yu} - g_{zu}g_{yw}} \tag{5.11}$$

The resulting compensator is not a high gain controller, as in Equation 5.7. Instead, it is a constant gain controller which inverts the second term in the numerator of Equation 5.9, and cancels the first. Although, in principle, this accomplishes the disturbance rejection goal, it would be very difficult to implement due to practical robustness concerns.

Figure 5.1 shows an example of Topology III. In Typical Section 3, the performance z_3 is the vertical position of the third mass, and the disturbance w_3 is a vertical force, also on the third mass. The output y_1 is the vertical velocity of the tip mass, and the input u_1 in the vertical force on the tip mass. Notice that the input output pair is collocated, dual, and complementary extreme, similar to those in the previous topologies.

Figure 5.2 shows the pertinent transfer functions for Typical Section 3. Notice that g_{yu} and g_{zw} have alternating poles and zeros, but g_{yw} and g_{zu} do not. The transfer functions g_{yw} and g_{zu} both have a pair of missing zeros between the pole pairs at 1.6 and 10.1 rad/sec, and minimum phase (-14 rad/sec) and nonminimum phase (14 rad/sec) zeros.

Figure 5.3 shows a magnitude plot of the sensor actuator test given in Equation 5.4 for Typical Section 3. Notice that the test is satisfied for low frequency, up to 3 rad/sec. A high gain compensator, therefore, can be used for this sensor

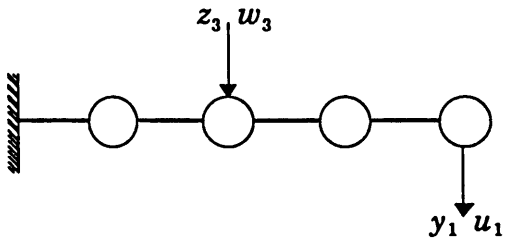

Typical Section 3

Figure 5.1. Topology III: Nonanalogous performance and output, and nonanalogous disturbance and input, with a collocated, dual, and complementary extreme input and output.

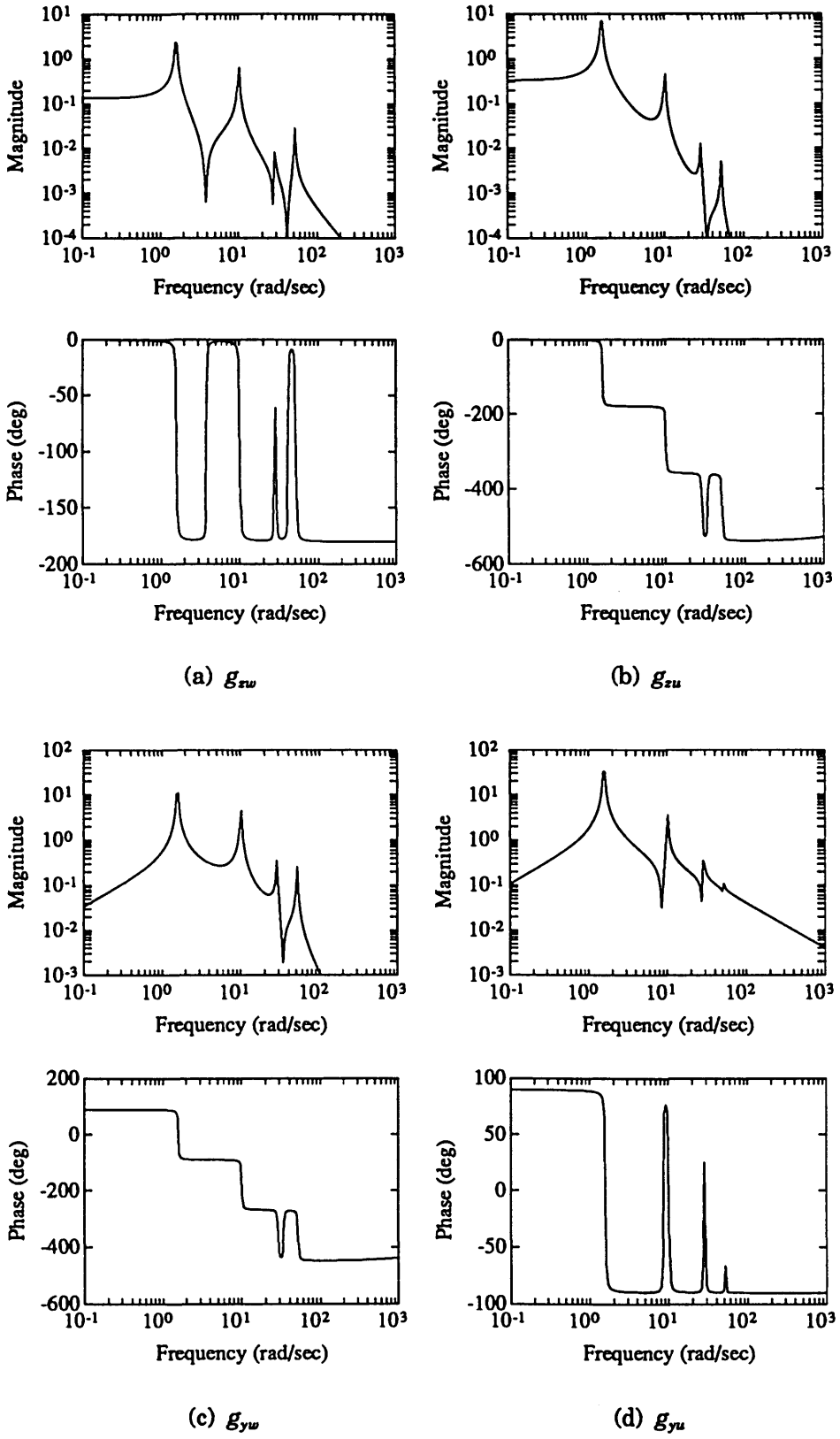

Figure 5.2. Open loop transfer functions for Typical Section 3.

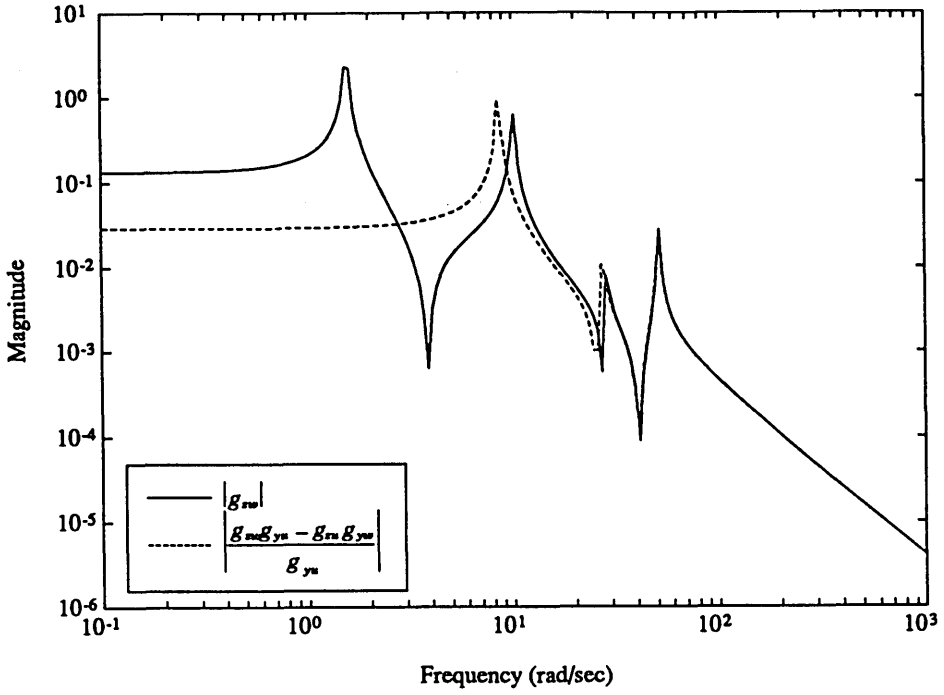

Figure 5.3. Test for Typical Section 3 showing the ability of the input output pair to loop shape, i.e. use a high gain compensator.

actuator pair, if the disturbance rejection performance metric is in a frequency range less than 3 rad/sec. For higher frequency disturbance rejection, this input output pair is not a good choice for loop shaping.

5.3 Optimal Compensation

In Chapters 3 and 4, optimal compensation techniques such as LQG revealed distinct trends for simplified topologies where the disturbance w and input u were analogous, and/or the performance z and output y were analogous. This chapter examines topologies where w and u, and z and y are not analogous.

Asymptotic Properties of the LQG Compensator

The LQG asymptote for low noise (i.e. the Kalman Filter weighting μ tends to zero), and expensive control (i.e. the LQR weighting ρ tends to infinity), is a rate feedback compensator, inverting the g_{yw} transfer function, except for the dominant mode

$$\underset{\substack{\mu\to 0\\ \rho\to\infty}}{LIM}\, K(s) = \frac{G\Phi B_w}{g_{yw}} = \frac{k_{LG}}{\sqrt{\rho}} \frac{s}{s^2 + 2\zeta_{dm}\omega_{dm}s + \omega_{dm}^2} \frac{1}{g_{yw}} \tag{5.12}$$

Since there are no simplifications for Topology III, this is the low gain LQG asymptote for all LQG compensators, including Typical Section 3.

The LQG asymptote, for low noise (i.e. the Kalman Filter weighting μ tends to zero), and cheap control (i.e. the LQR weighting ρ tends to infinity), and μ being smaller than ρ,

$$\underset{\substack{\mu\to 0\\ \rho\to 0\\ \rho>\mu}}{LIM}\, K(s) = \pm\frac{1}{\sqrt{\rho}} \frac{g_{zw}}{g_{yw}} \tag{5.13}$$

This is the high gain LQG asymptote for all LQG compensators in Topology III, including Typical Section 3.

The creation of the LQG asymptotes are dependent upon the disturbance to output transfer function g_{yw} being minimum phase. The high gain LQG asymptote is also dependent upon the gzu transfer function being minimum phase, but this is not as stringent because of the assumption that μ is less than ρ. In examining Figure 5.2(c), the g_{yw} transfer function for Typical Section 3 contains a nonminimum phase zero at 14 rad/sec and a missing pair of zeros between the pole pairs at 1.6 and 10.1 rad/sec. Although the asymptotes are not valid, they will still be used to show the implications of these pole zero patterns on the LQG compensator.

Typical Section Results: LQG compensator

Figure 5.5(a) shows an 8 state LQG compensator and the low gain and high gain LQG asymptotes given in Equations 5.12 and 5.13 for Typical Section 3. The open loop input output transfer function g_{yu} is shown in Figure 5.4. The Kalman Filter weighting μ is small (μ=1E-8) and the LQR weighting is an intermediate value (ρ=1E-2). Notice how the magnitude of the compensator approximately matches that of the low gain LQG asymptote from 25 to 150 rad/sec. At approximately 150 rad/sec, the compensator rolls off. If the Kalman Filter weighting μ is made smaller, the magnitudes would match at high frequency.

At low frequency, the LQG compensator matches the high gain LQG asymptote (Equation 5.13) by creating integral control, or position feedback. But the high gain LQG asymptote also predicts a lightly damped zero pair at 4 rad/sec,

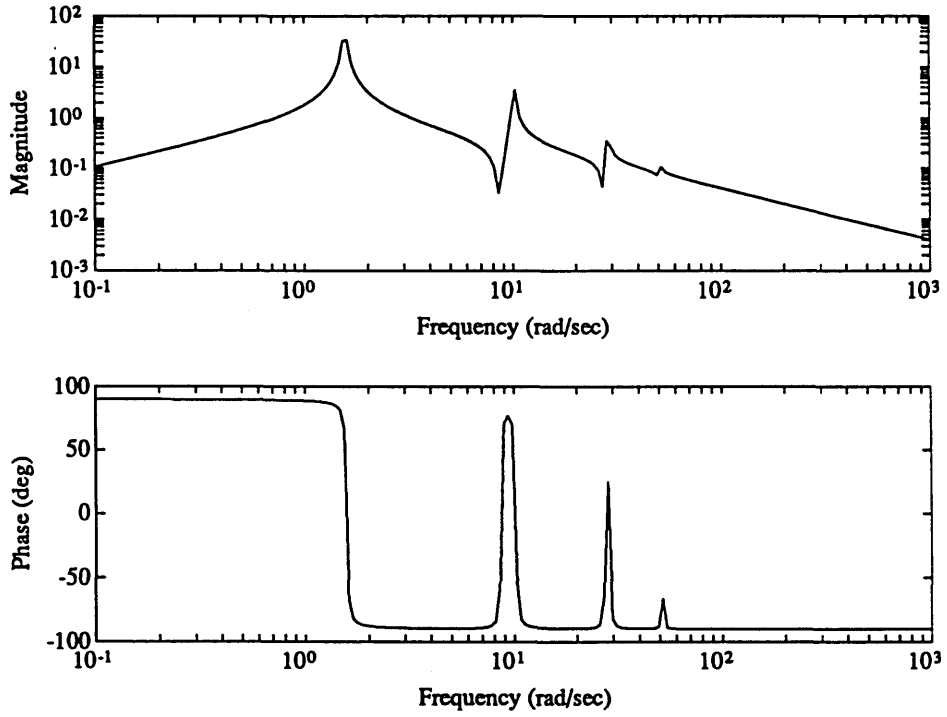

Figure 5.4. Open loop input output transfer function g_{yu} for Typical Section 3.

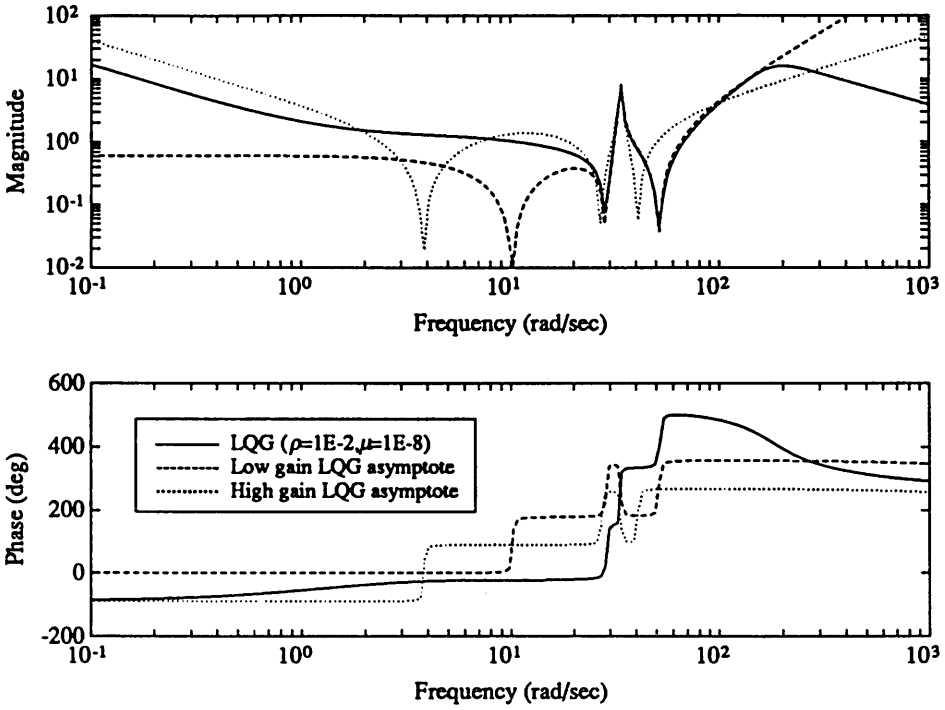

Figure 5.5(a). 8 state LQG compensator K (ρ=1E-2, μ=1E-8) for Typical Section 3, and the low and high gain LQG asymptotes.

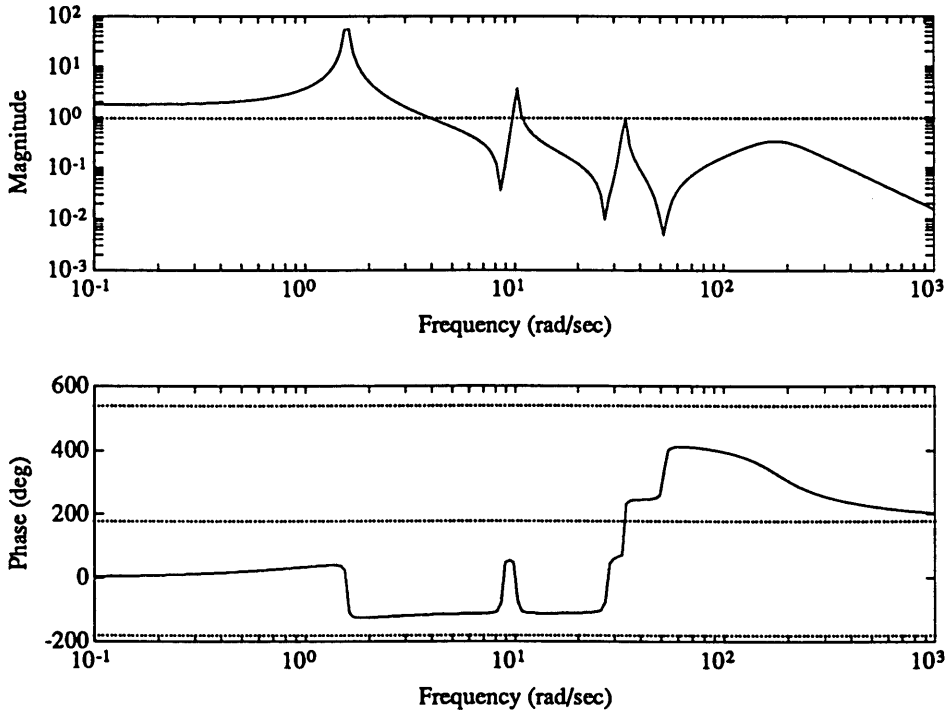

Figure 5.5(b). Loop transfer function $g_{yu}K$ consisting of the LQG compensator and the open loop transfer function.

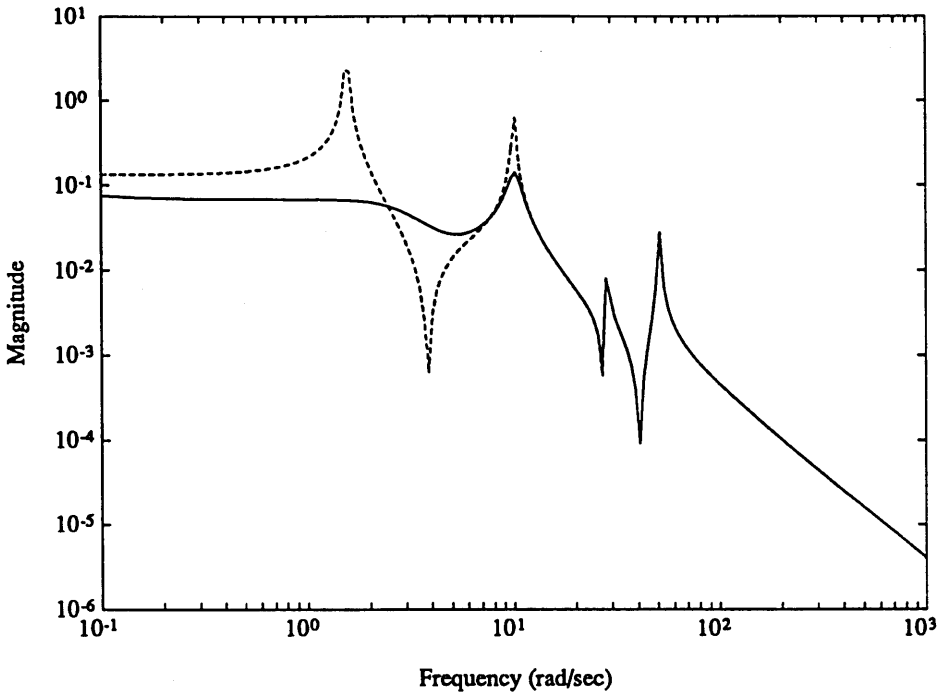

Figure 5.5(c). Open and closed loop disturbance to performance transfer functions for Typical Section 3. Performance improvement with the LQG compensator is 21.5 dB.

which does not occur in the LQG compensator. The LQG compensator again contains a PI controller, with a zero at 1.3 rad/sec, used to change the integral (position) control at low frequency to proportional control (rate) control at high frequency.

Notice also that the LQG compensator contains an unstable pole pair at 34 rad/sec. This is a result of the pole zero pattern of g_{yw} not being alternating poles and zeros. It is similar to the LQG compensator designed for Typical Section 2B (Figure 4.8(a)), also with an unstable pole at 34 rad/sec. Note that the disturbance and output are identical for Typical Section 2B (Figure 4.1(b)) and Typical Section 3 (Figure 5.1), as are the g_{yw} transfer function (nonminimum phase zero at 14 rad/sec).

Figure 5.5(b) shows the loop transfer function $g_{yu}K$ for the LQG compensator, and the open loop transfer function in Figure 5.4. The loop crossover is 4 rad/sec,

with another loop crossover as a result of the mode at 10 rad/sec. Notice how the unstable pole pair at 34 rad/sec causes the phase of the loop transfer function to rise above 180°.

Figure 5.5(c) shows the open and closed loop transfer function disturbance to performance transfer functions for the LQG compensator. The magnitude is reduced at low frequency, up to 2 rad/sec, as is the mode at 10 rad/sec. The performance improvement is 21.5 dB.

Figure 5.6(a) shows LQG compensators for three values of the LQR weighting ρ, with the Kalman Filter weighting being a constant (μ=1E-8). Figure 5.6(b) shows the corresponding loop transfer functions for the three LQG compensators. The magnitude of the compensator does not increase at low frequency proportional to $1/\sqrt{\rho}$, as predicted by the high gain LQG asymptote in Equation 5.13. The LQG compensator is unstable, but minimum phase for the largest ρ case, stable and minimum phase for the intermediate ρ case, and unstable and nonminimum phase for the smallest case of ρ. In examining the loop transfer functions, as ρ is decreased, the magnitude of the loop transfer function becomes approximately one at high frequency.

Figures 5.4 and 5.5 show how the LQG compensator is unstable and for many different choices of the Kalman Filter and LQR weightings for Typical Section 3. These are a result of the pole zero structure of g_{yw} containing a nonminimum phase zero and missing zero pair, instead of alternating poles and zeros. As stated previously, these types of compensation techniques, although needed for certain control designs, are not robust in the control of structures.

Because of the pole zero structure of g_{yw}, there are limitations in the control design. LQG does not create high gain compensators such as those used in the previous topologies. Examining Figure 5.6(a), as ρ decreases, the magnitude of the compensator seems to approach a limit. For Typical Section IIB, where the

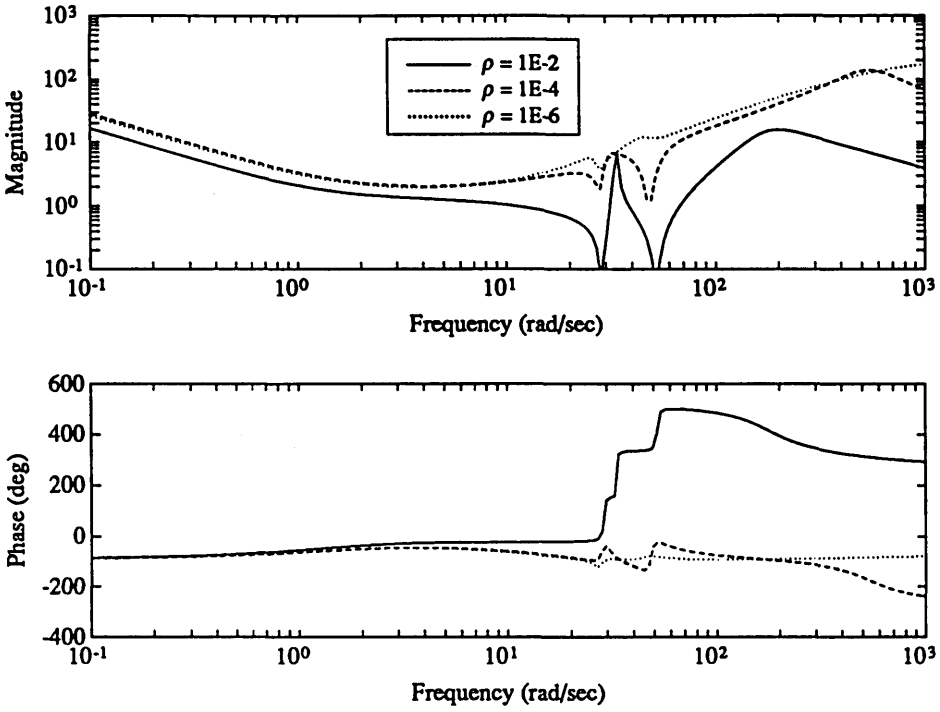

Figure 5.6(a). LQG compensators Typical Section 3 for three values of ρ. μ=1E-8.

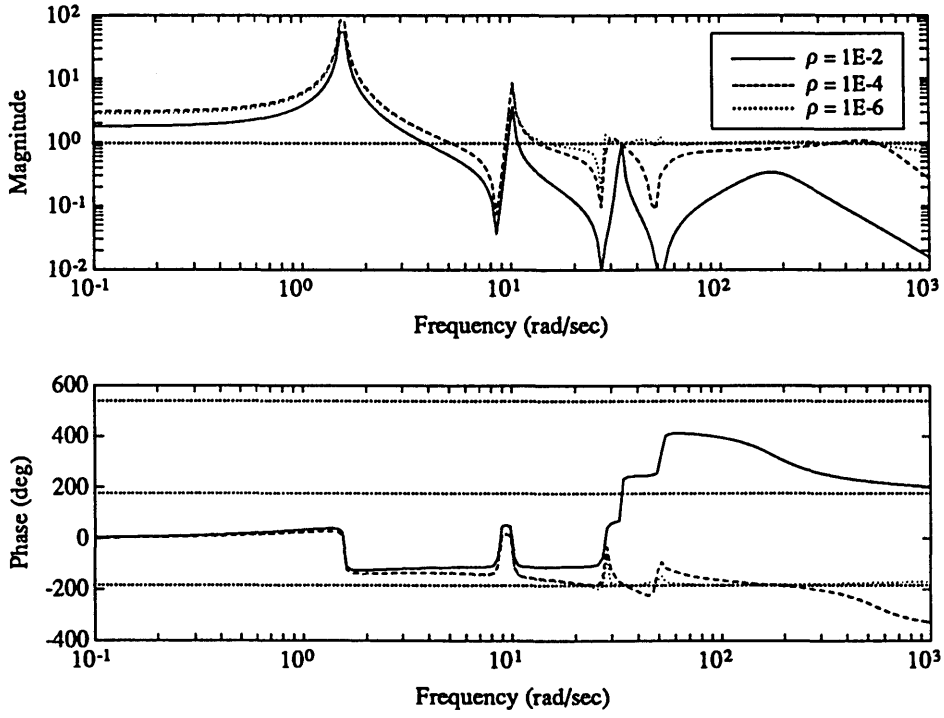

Figure 5.6(b). Loop transfer functions corresponding to the three LQG compensators in Figure 5.6(a).

asymptotes were not valid because of the g_{yw} transfer function, the LQG compensator was compared to the disturbance to performance transfer function minimizing compensator. For Topology III, when the actuator sensor test from Equation 5.4 is not satisfied, the disturbance to performance transfer function minimizing compensator is given by Equation 5.11.

Figure 5.7(a) shows the LQG compensator with smallest value for ρ, from Figure 5.6(a) (ρ=1E-6, μ=1E-8), plotted with the disturbance to performance transfer function minimizing compensator shown in Equation 5.11, which creates a subtraction in the numerator of the disturbance to performance transfer function (Equation 5.2). Except for the pole pair at 4 rad/sec, these are very similar. These are not identical because of the nonminimum phase zeros in the g_{yw} and g_{zu} transfer functions. In cases where these zeros are not present, the low noise, cheap control LQG compensator creates an exact subtraction in the numerator of the closed loop disturbance to performance transfer function, thus matching the transfer function minimizing compensator in Equation 5.11. The compensator also has an unstable pole at 16 rad/sec, and two nonminimum phase zero pairs at 10 and 46 rad/sec.

Figure 5.8(b) shows the loop transfer function $g_{yu}K$ consisting of the LQG compensator and the open loop transfer function in Figure 5.4. The magnitude of the loop transfer function is approximately one, except for the lightly damped pole zero pairs. At low frequency, the magnitude is greater then one, indicating the use of a high gain compensator for loop shaping (Figure 5.3). If the transfer function minimizing compensator is exactly used, then the magnitude of the loop gain is identically one, but the closed loop system is unstable because of the pole zero structure of g_{yw}. Figure 5.8(c) shows the open and closed loop disturbance to performance transfer functions for the LQG compensator. At low frequency, the magnitude is reduced, as a result of the integral control of the LQG compensator, i.e. loop shaping. For the modes at higher frequency, the magnitude reduction is

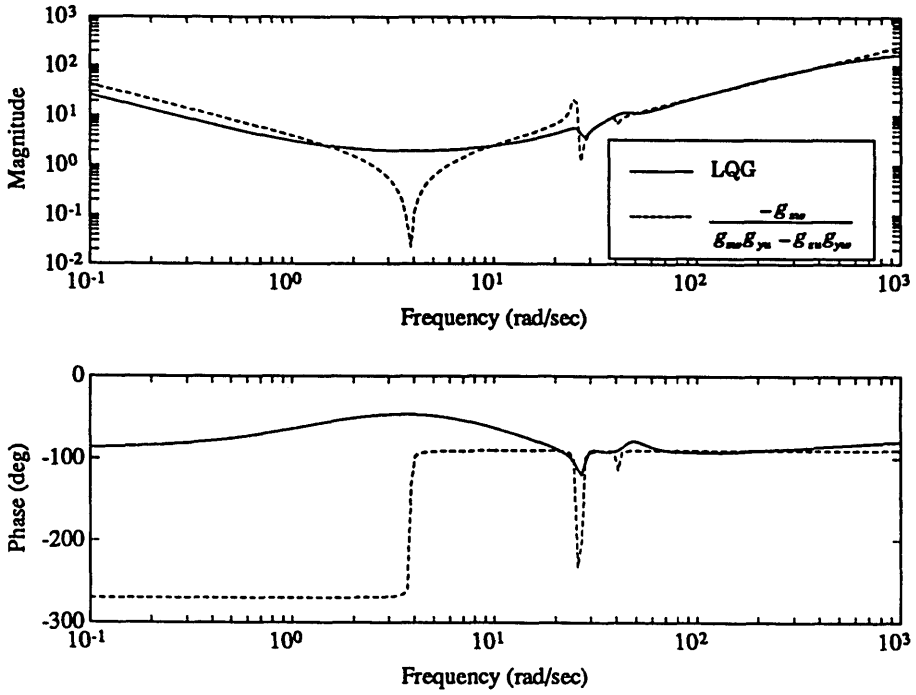

Figure 5.7(a). Low noise, cheap control LQG compensator (ρ=1E-6, μ=1E-8), and the disturbance to performance transfer function minimizing compensator for Typical Section 3.

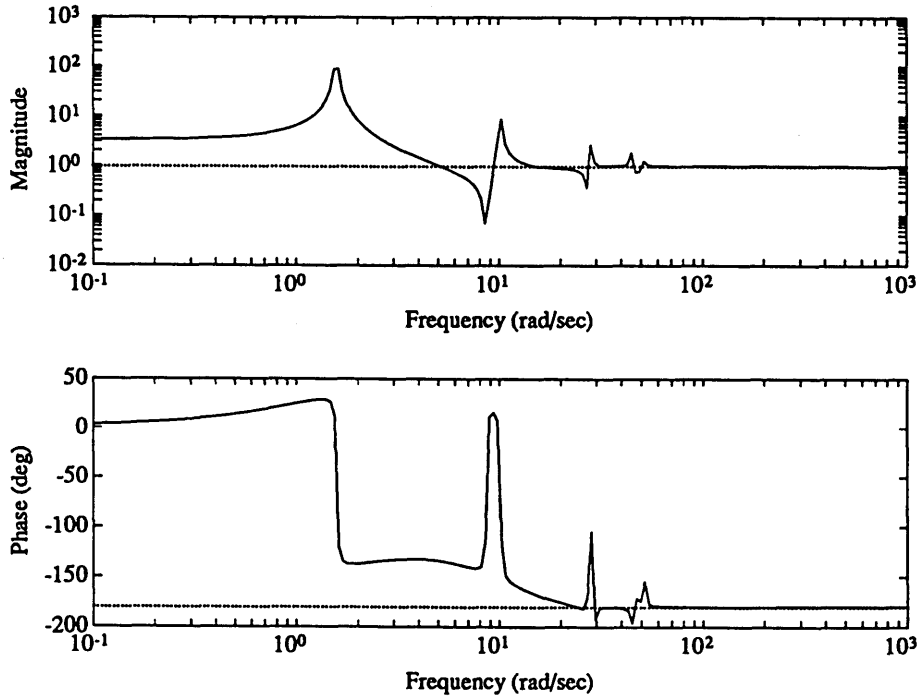

Figure 5.7(b). Loop transfer function $g_{yu}K$ consisting of the LQG compensator and the open loop transfer function.

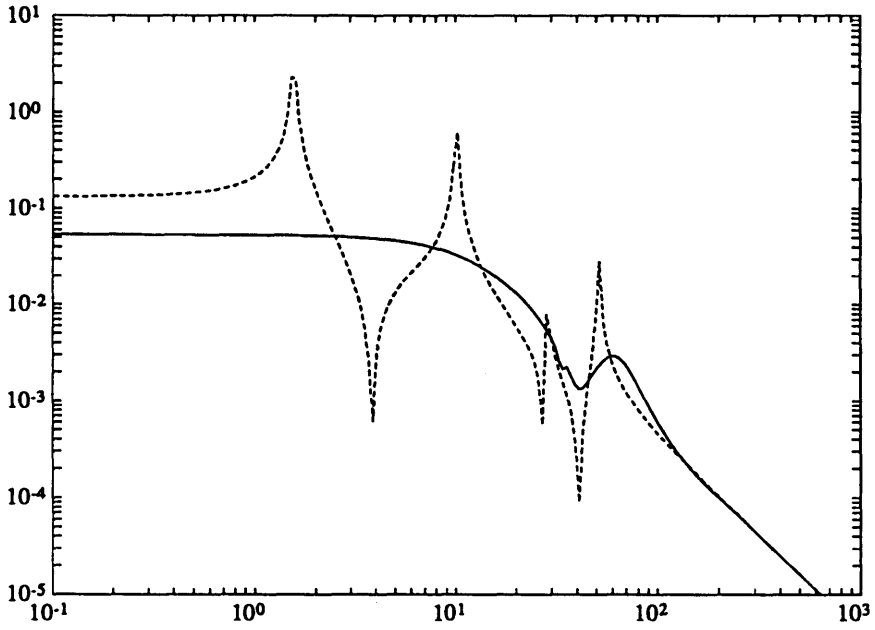

Figure 5.7(c). Open and closed loop disturbance to performance transfer functions for Typical Section 3. Performance improvement with the LQG compensator is 25.3 dB.

accomplished by *damping* the modes, consistent with the high frequency, low gain LQG asymptote.

The performance improvement with this compensator is 25.3 dB, only slightly larger than the 21.5 dB performance improvement from the LQG compensator with ρ=1E-2 in Figures 5.5(a)-(c). Although this compensator accomplishes the disturbance rejection goal theoretically, it is not a robust compensator from a practical viewpoint. Factors such as modeling errors and sensor noise make the compensator shown in Equation 5.11 infeasible experimentally.

Summary

A test is presented which examines the ability of the actuator sensor choice to minimize the disturbance to performance transfer function using a high gain

compensator. When this test is satisfied, the LQG compensator creates a high gain compensator. When this test is not satisfied, the LQG compensator creates a subtraction in the numerator of the closed loop disturbance to performance transfer function. This subtraction, although theoretically correct, is not a valid design because of robustness concerns such as modeling errors and sensor noise. What the compensator also does, in examining the closed loop transfer function, is to damp the higher frequency modes by using rate feedback, as in the low gain, LQG asymptote.

In most cases, the LQG compensators for this topology are unstable or nonminimum phase. And because of the pole zero pattern of g_{yw}, and the inability to loop shape using a high gain compensator (Equations 5.5-5.8), the performance improvement may be minimal, even for the cheap control, LQG compensators. In a larger, more complex structure, where the pole zero patterns of the g_{yw} transfer function may contain multiple missing zeros or nonminimum phase zero pairs, the LQG compensators are unstable or nonminimum phase for most choices of the LQR and Kalman Filter weightings. This places a fundamental limit on sensor actuator pair choices for the practical minimization of certain disturbance to performance transfer functions.

For Typical Section 3, the function of the LQG compensators for varying values of the Kalman Filter weighting μ was examined. Similar results to the compensators designed for Typical Section 1A are seen (Figure 3.7(a) and (b)). These include the PI controller becoming a lag controller, and the high frequency rolloff becoming steeper, and at a lower frequency.

5.4 Neo-Classical Control

This section presents Neo-Classical Design Rule 3 Topology III, i.e. with a nonanalogous disturbance and input, and nonanalogous performance and output,

and collocated, dual, and complementary extreme input output pair.

Neo-Classical Design Rule 2

For nonanalogous performance and output, *and* nonanalogous disturbance and input, *and* collocated, dual, and complementary extreme input and output:

A. **Test the input output pair for the ability to loop shape, i.e. use a high gain control.**

$$\left|\frac{g_{zw}g_{yu} - g_{zu}g_{yw}}{g_{yu}}\right| \ll |g_{zw}|$$

If the input output pair satisfies the test for all frequencies then proceed to Design Rule 2. If not, proceed to B.

B. **Examine the filter dynamics g_{zw}/g_{yu}. Split the filter into two parts, the temporal relationship between the performance z and the output y, ϕ_o, and the structural filter g_o.**

$$\frac{g_{zw}}{g_{yu}} = \phi_o g_o$$

C. **If the test in A is satisfied at low frequencies, then design a low frequency controller for Regions 1 and 2, i.e.**

$$K = k_o \phi_{zy}$$

where k_o is a gain used to set the bandwidth of the system subsequently. If the test in A is not satisfied at low frequency, then proceed to D and design a rate feedback controller for all frequencies.

D. **Select a bandwidth. Design the high frequency controller for Regions 3 and 4 such that the convolution of A and B yields a rate feedback compensator at high frequency. Adjust k_o such that the crossover of the loop transfer function is equal to the choice of bandwidth. Insure that placement of these dynamics is made such that the phase margin at the loop crossover is approximately 30°-60°.**

E. **Add higher frequency rolloff dynamics, if necessary.**

F. **Examine the loop transfer function, $g_{yu}K$, consisting of the open loop system, g_{yu}, and the compensator designed from rules 1A-E. Notch filter all modes in Region 3, which may affect the closed loop stability of the system. If necessary, iterate to D if the phase margin is not in the 30°-60° range.**

G. **Add stable minimum phase dynamics in Regions 1 and 2, replicating the magnitude of g_o, in the frequency range where the input output test is satisfied without jeopardizing the closed loop stability of the system.**

In Design Rule 3A, the input output pair is tested for the ability to loop shape, or use a high gain controller. If this test is satisfied over all frequencies, such that

$$\left|\frac{g_{zw}g_{yu} - g_{zu}g_{yw}}{g_{yu}}\right| \ll |g_{zw}| \tag{5.14}$$

then the closed loop transfer function (Equation 5.5), and disturbance to performance transfer function minimizing compensator (Equation 5.7), are identical to those for Topology IIA and IIB. Therefore, the Neo-Classical compensator is designed using the Neo-Classical Design Rule 2 presented for Topology II.

If the test in Equation 5.14 is not satisfied over all frequencies, the actuator sensor combination is not necessarily a poor choice. There can be frequency ranges, potentially as small as one mode, in which the test is satisfied and a high gain controller can be used. In a MIMO control design, for instance, a series of SISO controllers can be designed on collocated, dual, and complementary extreme input output pairs, such that each pair minimizes a certain frequency range of the disturbance to performance transfer function. The result is a closed loop system with good robustness and performance characteristics.

Design Rule 3B separates the filter g_{zw}/g_{yu} into two parts: the temporal relationship between z and y, ϕ_o and the structural filter g_o.

$$\frac{g_{zw}}{g_{yu}} = \phi_o g_o \tag{5.15}$$

In Design Rule 3C, if the test in 5.14 is satisfied at low frequency, then a low frequency controller is designed using ϕ_o, and a gain k_o.

$$K = k_o \phi_o \tag{5.16}$$

If the test in Equation 5.14 is not satisfied at low frequency, then the designer proceeds to 3D and designs a rate feedback controller for all frequencies. There are two occasions in which this would occur. If the test is satisfied at higher frequencies, a high gain compensator may be used in the frequency range where the test is satisfied. This high gain compensator, however, is added to the compensator in 3F. Therefore, the next step is to design a rate feedback controller for all frequencies in 3D.

If the test in Equation 5.14 is not satisfied for any frequency range, the LQG compensator attempts to create a subtraction in the numerator of the disturbance to performance transfer function, usually using unstable or nonminimum phase compensators. The best practical controller is a rate feedback controller, adding damping to the structural modes. Therefore, the next step is to design a rate feedback controller for all frequencies in 3D.

In Design Rule 3D, a selection of a bandwidth is made first. Then, if the test is satisfied at low frequency, and a high gain, low frequency controller was made in 3C (Equation 5.16), then dynamics are convolved into the compensator such that the high frequency controller is rate feedback. If this is not the case, then a rate feedback controller is created for all frequencies. The gain k_0 is then adjusted to set the bandwidth.

Design Rule 3E states that rolloff dynamics are added to the compensator, if necessary, such as one pole, or two heavily damped poles.

In Design Rule 3F, the loop transfer function consisting of the controller from 3A-E and the open loop system g_{yu} is examined. If any mode has a loop gain greater than -3 dB, and its closed loop stability appears in question, the mode is to be gain stabilized using a second order notch filter. Care should be taken in the examination, however. Some modes may have a loop gain greater than one, with large gain and phase margins. These modes are being damped by the rate feedback

of the compensator and should not be notch filtered.

In Design Rule 3G, the structural filter, g_o, the test from 3A, and bandwidth are compared. If there are structural resonances in the filter, within Regions 1 and 2 where disturbance rejection can be accomplished using a high gain controller, and in which the actuator sensor test in Equation 5.14 passes, then these dynamics are added to the compensator, without jeopardizing the closed loop stability of the system

In designing a Neo-Classical compensator for Typical Section 3, the first step is to apply the test in Design Rule 3A. Figure 5.8 shows this test for Typical Section 3. Notice that the test is satisfied up to 3 rad/sec, or in a low frequency region.

Using Design Rule 3B, the filter g_{zw}/g_{yu} is split into the temporal relationship between the performance z and output y, ϕ_o and the structural filter g_o. The performance z is a position, and the output y is a velocity. Therefore ϕ_o is an

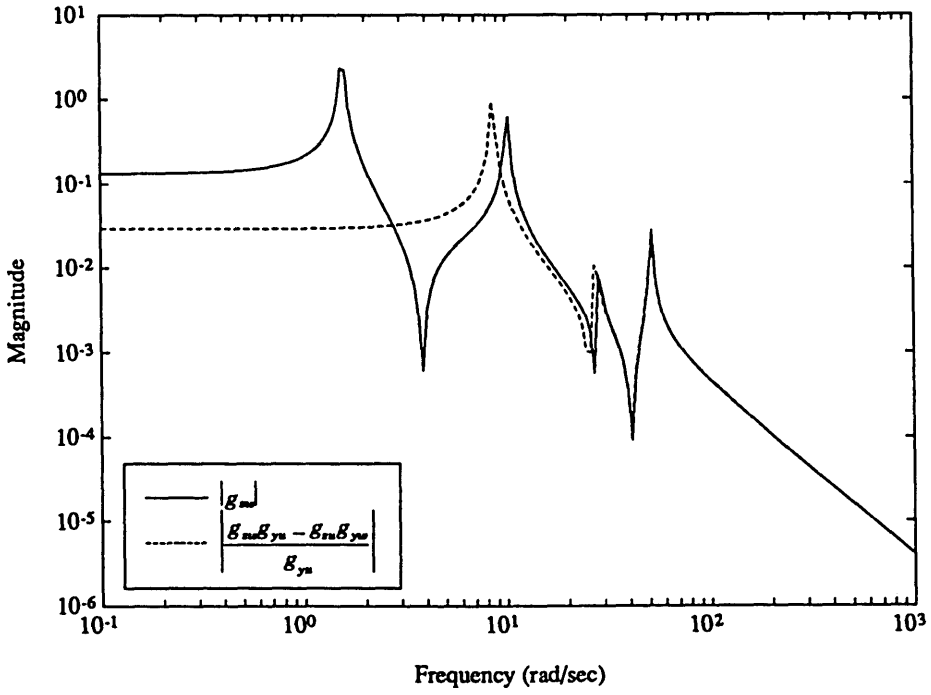

Figure 5.8. Test for Typical Section 3 showing the ability to loop shape using a high gain compensator.

integrator

$$\phi_o = \frac{1}{s} \tag{5.17}$$

and the structural filter g_o is given by

$$g_o = \frac{g_{zw}}{g_{yu}} s \tag{5.18}$$

These are shown in Figure 5.9.

Design Rule 3C is used to design a low frequency controller. Since the test in Figure 5.8 is satisfied at low frequency, the low frequency controller is given by a gain k_o times the temporal relationship between z and y in Equation 5.18.

$$K = k_o \frac{1}{s} \tag{5.19}$$

The gain k_o is set upon the completion of Design Rule 3D.

Following Design Rule 3D, a 10 rad/sec bandwidth is chosen. A zero is convolved into the compensator, in order to create a PI controller, and subsequent rate feedback at high frequency. The zero is placed at 3.5 rad/sec, such that the phase margin at crossover is approximately 60°. The gain k_o is then adjusted in order to approximate the 10 rad/sec bandwidth.

A one pole rolloff is added to the compensator at 100 rad/sec, following Design Rule 3E.

Using Design Rule 3F, examining the loop transfer function consisting of the controller designed from 3A-E, and the open loop system g_{yu} in Figure 5.10, there are no modes above 10 rad/sec which need gain stabilized.

Following Design Rule 3G, filter dynamics from g_o are to be added to Regions

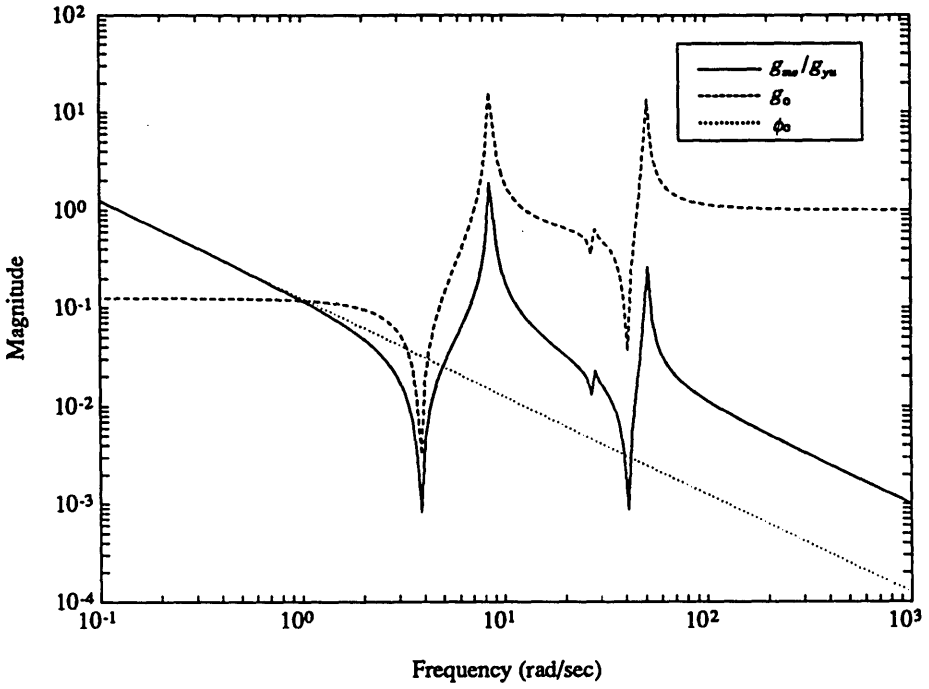

Figure 5.9. Filter dynamics g_{zw}/g_{yu} for Typical Section 3, and the division into the temporal relationship between z and y, and the structural filter.

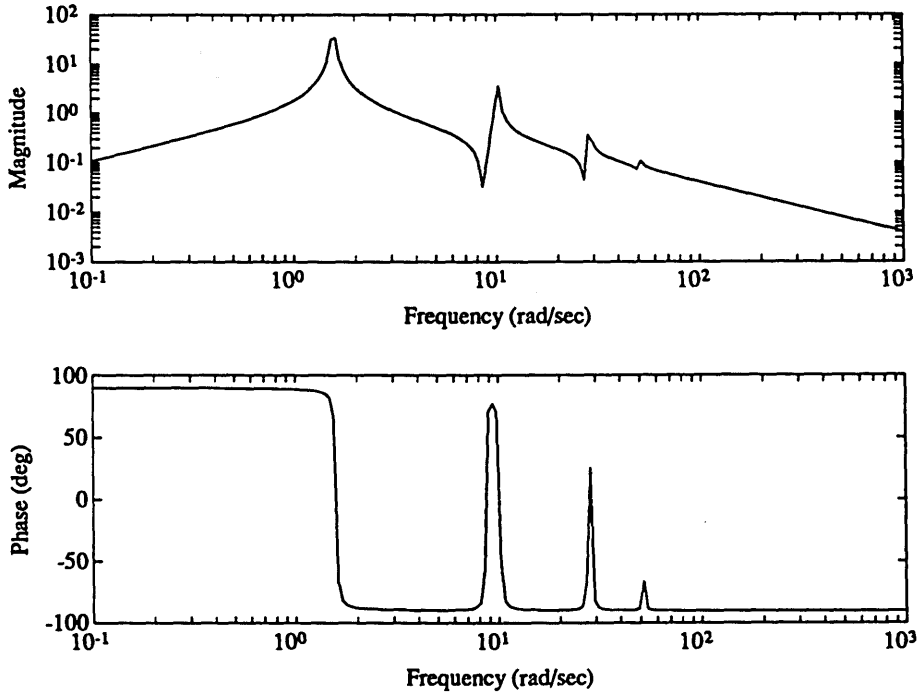

Figure 5.10. Open loop input output transfer function g_{yu} for Typical Section 3.

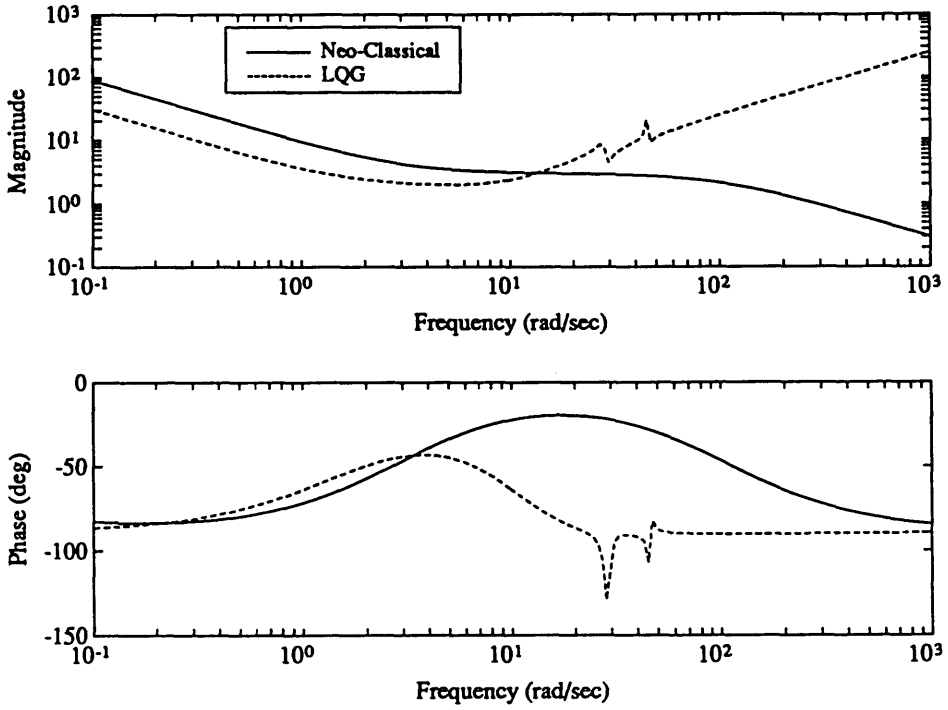

Figure 5.11(a). 2 state Neo-Classical and 8 state LQG compensator (ρ=1E-6, μ=1E-8) designed for Typical Section 3.

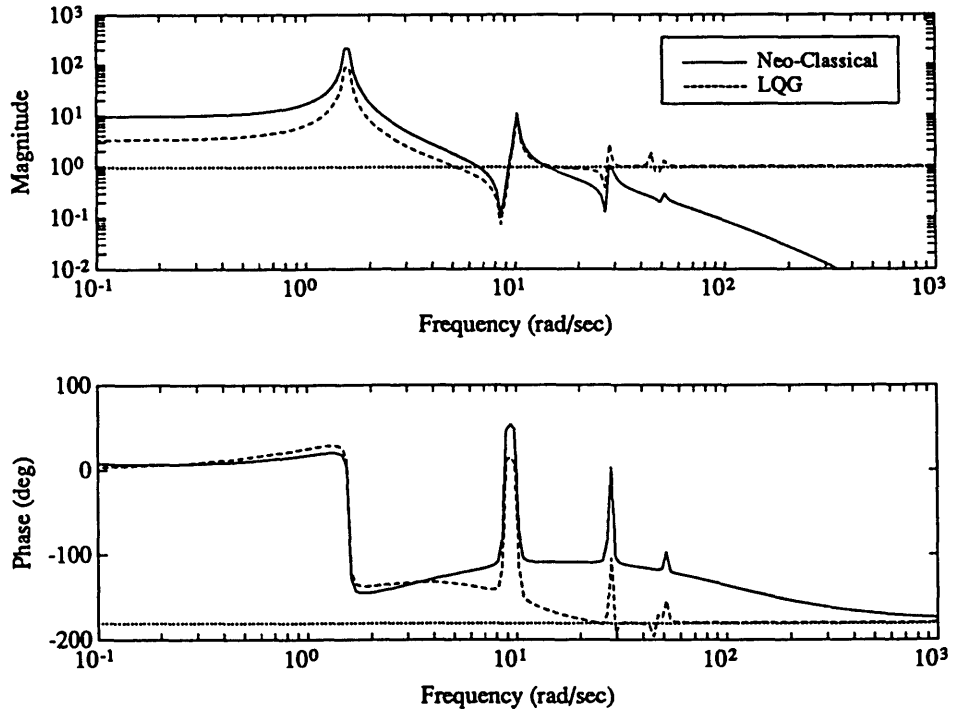

Figure 5.11(b). Loop transfer functions $g_{yu}K$ consisting of the compensators in Figure 5.10(a) and the open loop transfer function.

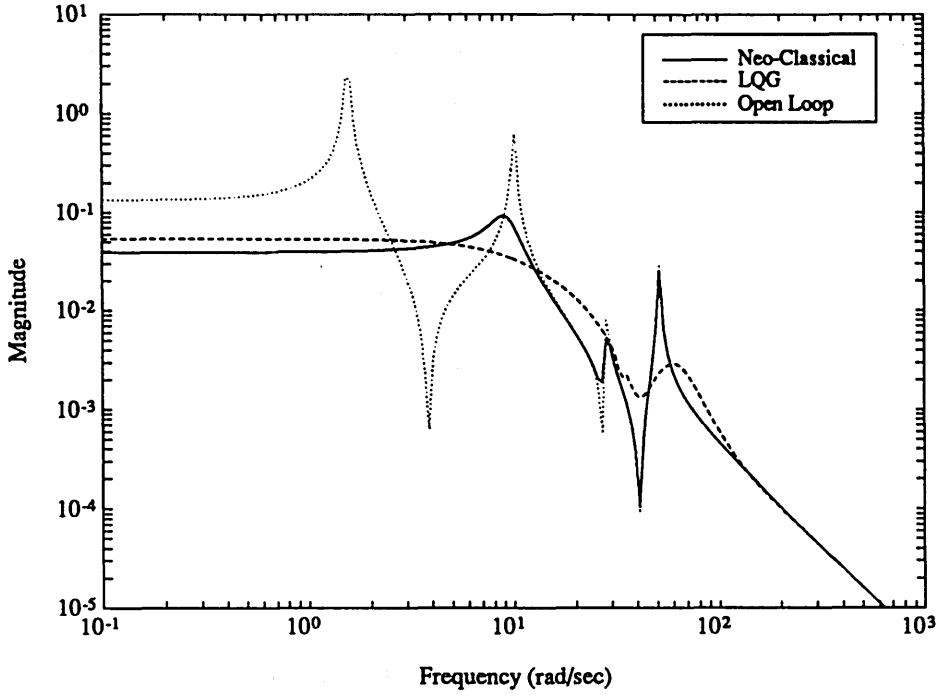

Figure 5.11(c). Open and closed loop disturbance to performance transfer functions for Typical Section 3. Performance improvement with the Neo-Classical compensator is 24 dB and the LQG compensators is 25.3 dB.

1 and 2, where the test from 3A is satisfied. Figure 5.8 shows this test is satisfied up to 3 rad/sec. In examining the structural filter g_o in Figure 5.9, notice that there are no structural dynamics in this range. Therefore, no additional compensator dynamics are added.

The resulting 2 state Neo-Classical compensator designed for Typical Section 3 is shown in Figure 5.11(a). The Neo-Classical compensator is plotted with the low noise, cheap control LQG compensator from Figure 5.7(a). Notice how both compensators use integral control (position feedback) up to 3 rad/sec, corresponding to where the test in 3A is satisfied (Figure 5.8), and proportional control (rate feedback) up to 3 rad/sec.

Figure 5.11(b) shows the loop transfer functions $g_{yu}K$, consisting of the

compensators in Figure 5.11(a), and the open loop transfer function g_{yu} in Figure 5.10. The bandwidth of the Neo-Classical design is approximately 10 rad/sec.

The open and closed loop disturbance to performance transfer functions of the Neo-Classical and LQG compensators are shown in Figure 5.11(c). The closed loop performance improvement for the 2 state, stable minimum phase Neo-Classical design is 24 dB, only slightly lower than that of the low noise, cheap control LQG compensator (25.3 dB). The LQG compensator also has 8 states, and in unstable and nonminimum phase.

5.5 Experimental Implementation

Optimal LQG, SWLQG, and Neo-Classical compensators were designed and implemented experimentally on the MACE test article for a topology consistent with Topology III, i.e. nonanalogous performance and output, and nonanalogous disturbance and input. Figure 5.12 shows the MACE 3 topology. The output y is the z-axis rate gyro of the bus, while the performance z is the integrated z-axis payload rate gyro. The input u is a z-axis inertial torque about the center of the bus, created by the torque wheels, and the disturbance w is the relative torque of the z-axis gimbal. Since the performance and output are not analogous, and the disturbance and input are not analogous, and the actuator sensor pair are collocated, dual, and complementary extreme, this topology falls into the Topology III category.

Notice that the disturbance and output are noncollocated. Therefore, the disturbance to output transfer function does not contain alternating poles and zeros. There are nonminimum phase zeros at 1.8 and 35 Hz. Therefore, the asymptotes of the LQG compensator again may not apply. The performance and input are also noncollocated.

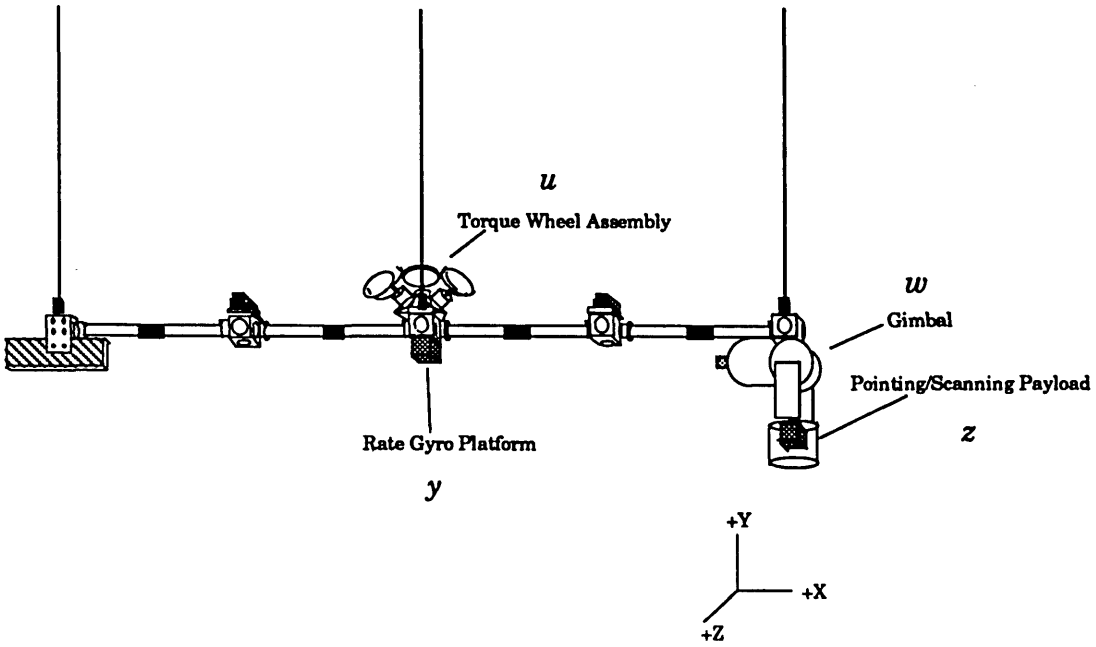

Figure 5.12. MACE 3: Topology for the payload pointing loop with the bus loop used as the sensor actuator pair.

Figure 5.13 shows a measurement of the open loop input output transfer function g_{yu} for MACE 3. Figure 5.14 shows a model based 24 state LQG compensator MACE 3. In an attempt to create a stable compensator, both the Kalman Filter and LQR weightings were made large. As a result of the nonminimum phase zeros in the g_{yw} transfer function. However, a stable compensator was never obtained. The 24 state LQG compensator contained unstable pole pairs at 11.0, 18.4, and 27.6 Hz, and a nonminimum phase zero at 1.9 Hz and nonminimum phase zero pair at 6.6 Hz. The theoretical performance of this design, evaluated on the model was 0 dB. Varying the LQR and Kalman Filter weightings only modified to the unstable and nonminimum phase dynamics in the compensator. The LQG compensator was unstable and nonminimum phase for all combinations of LQR and Kalman Filter weightings which would create a closed loop system with any performance improvement. This compensator was not implemented.

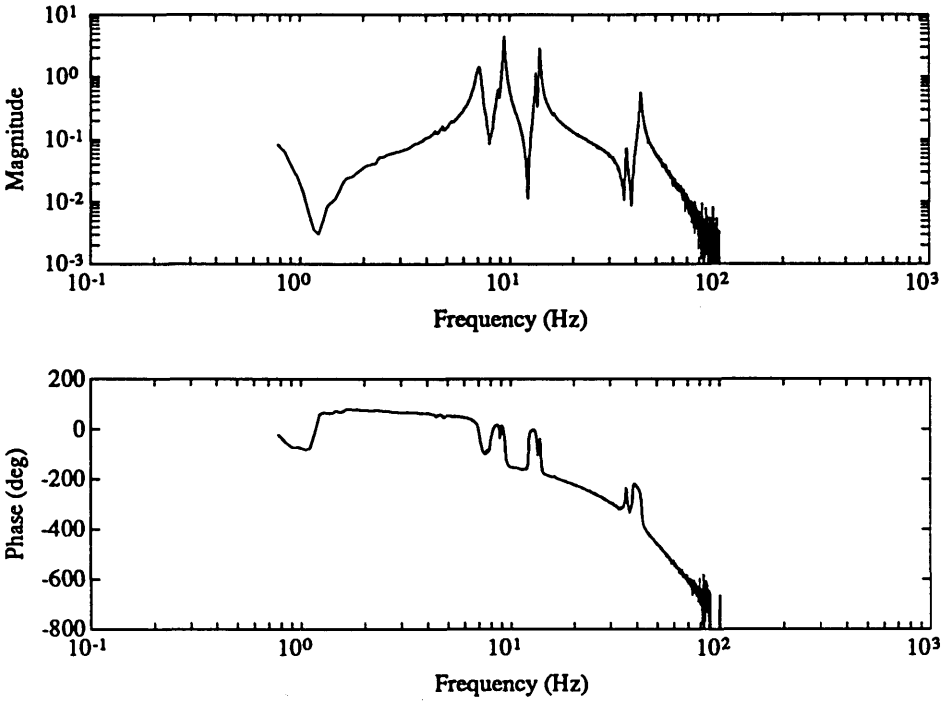

Figure 5.13. Measurement of the open loop input output transfer function g_{yu} for MACE 3.

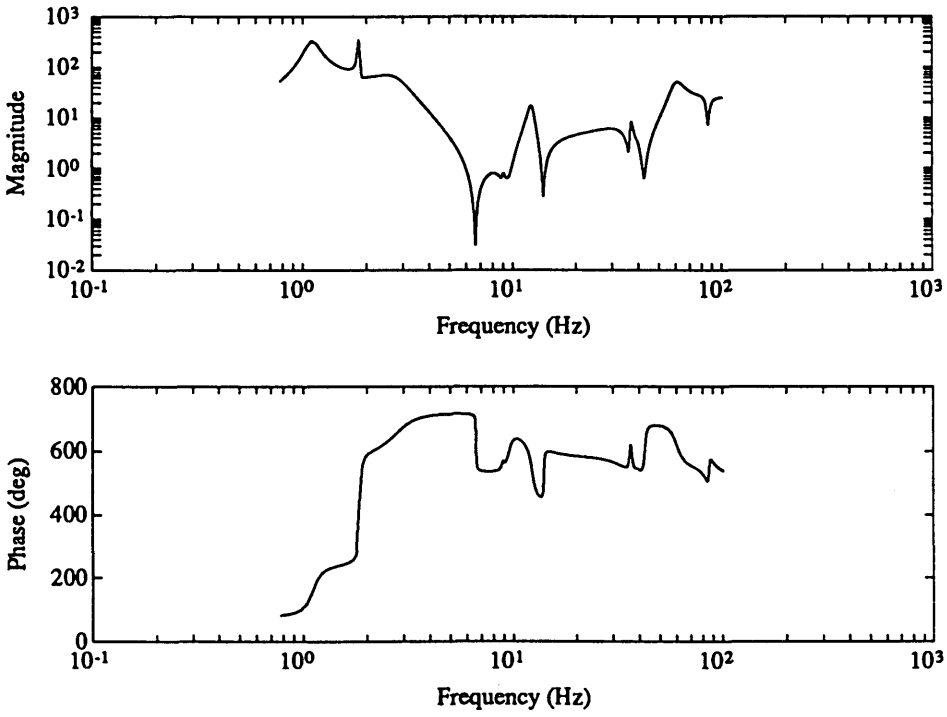

Figure 5.14. Model based 23 state LQG compensator designed for MACE 3.

Figure 5.15(a) shows a model based 24 state SWLQG compensator with the modes at 1.2, 6.8, 9.4, 14, and 36 Hz sensitized. This resulted in a stable, minimum phase compensator, which created a performance improvement of 0.5 dB when evaluated on the model. Figure 5.15(b) shows the measurement of the loop transfer function consisting of the SWLQG compensator and the open loop system in Figure 5.13. In examining this transfer function, the gain and phase margins at 1.0 and 14 Hz are very small. This is exemplified in the closed loop system, which was found to be experimentally unstable for this compensator. No amount of sensitization of the modes at these frequencies yielded a compensator with a stable closed loop system. And even with the loop closed, the closed loop performance improvement would have been small, as shown by the 0.5 dB theoretical performance improvement.

The LQG and SWLQG compensators in Figures 5.14 and 5.15(a) contain complex dynamics such as unstable poles and nonminimum phase zeros, and the closed loop systems are unstable experimentally and yield only marginal performance improvement on the design model. Practical optimal compensation of this topology failed. A Neo-Classical compensator was designed next.

Using Design Rule 3A, Figure 5.16 shows the test for the actuator sensor pair,

$$|g_{zw}| \qquad \text{versus} \qquad \left|\frac{g_{zw}g_{yu} - g_{zu}g_{yw}}{g_{yu}}\right|$$

for MACE 3.

Notice how the test is satisfied for the peaks at 6.8 and 9.4 Hz, but it is not satisfied in any other frequency range. If a high gain compensator were used, the closed loop transfer function would result in an additional peak at 8 Hz, thus nullifying the performance improvement. Therefore, there is no frequency range in which disturbance rejection can be accomplished by using a high gain compensator.

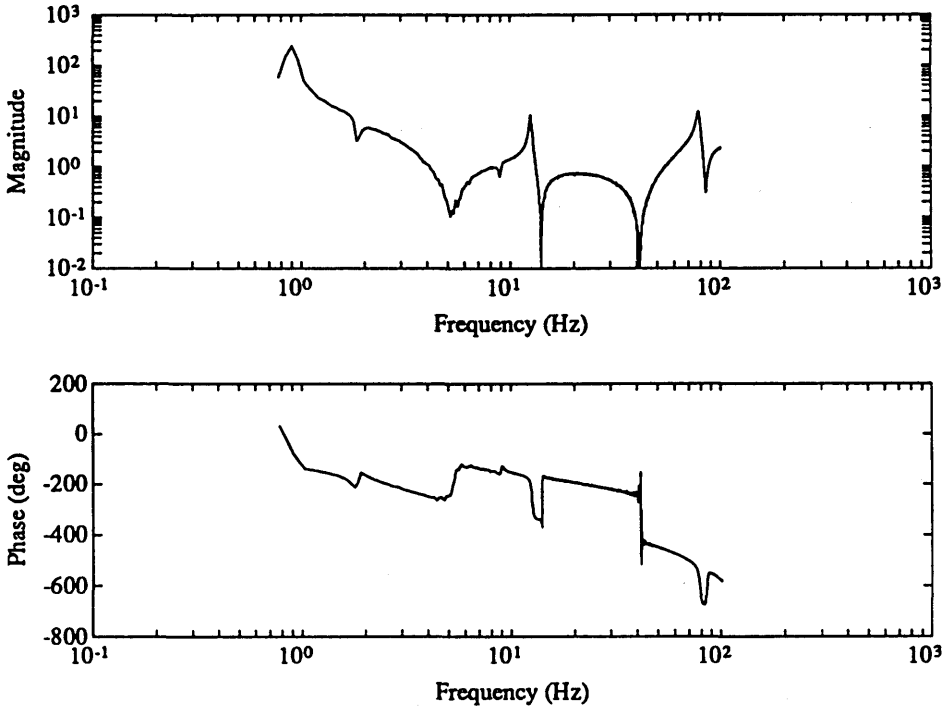

Figure 5.15(a). Model based 23 state SWLQG compensator designed for MACE 3.

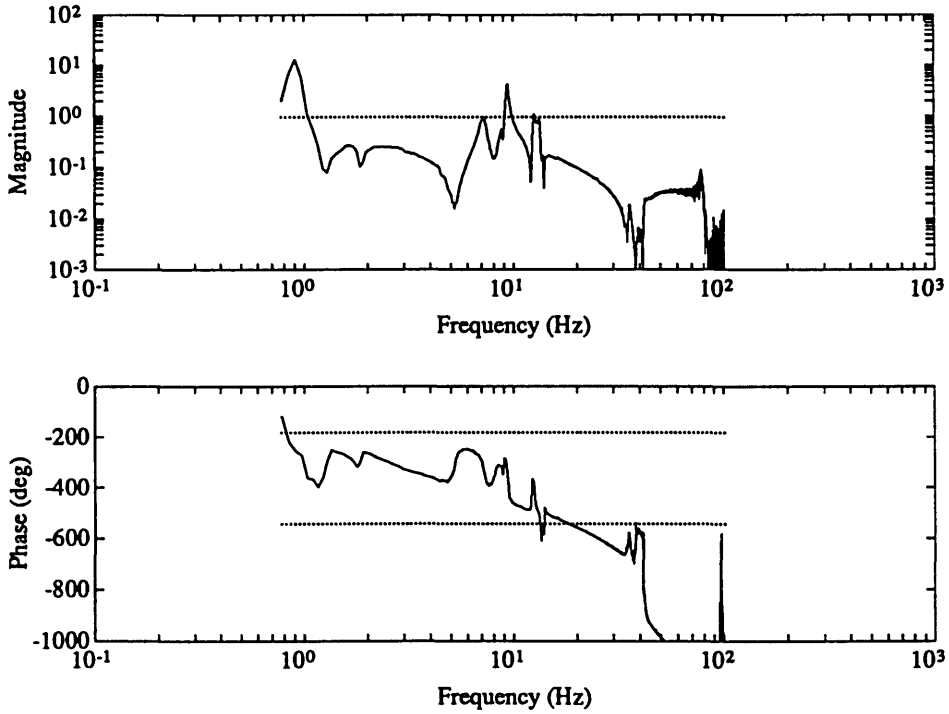

Figure 5.15(b). Measurement of the loop transfer function $g_{yu}K$ consisting of the SWLQG compensator and open loop transfer function.

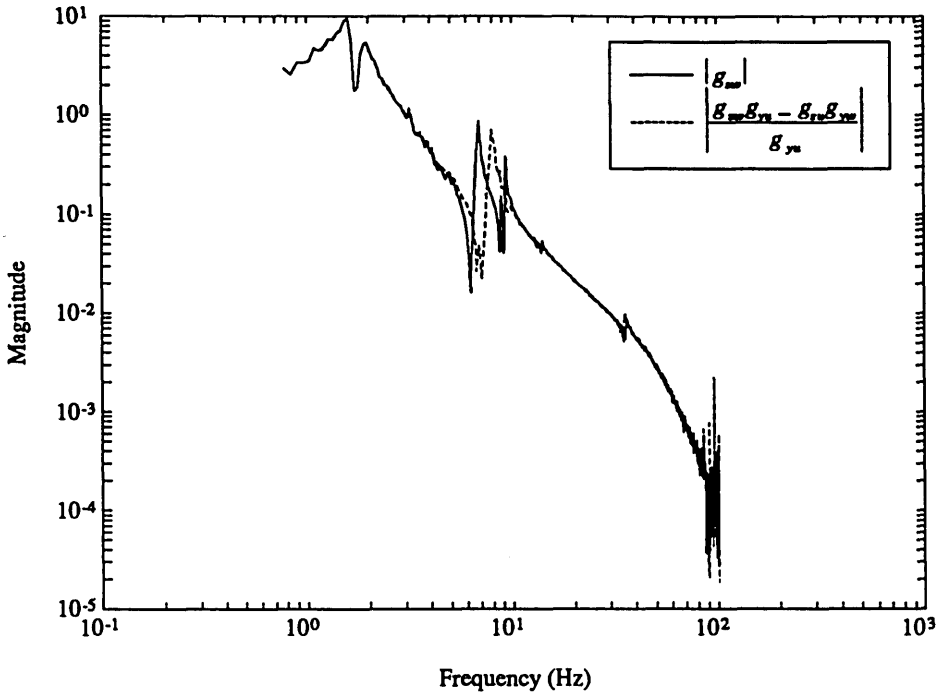

Figure 5.16. Measurement of the actuator sensor test from Design Rule 3A for the ability to loop shape.

Using Design Rule 3B, the filter g_{zw}/g_{yu} was split into the temporal relationship ϕ_o, and the structural filter g_o.

Following Design Rule 3C, since the test in 3A was not satisfied for any frequency range, the Neo-Classical compensator designed was a rate feedback controller at all frequencies.

Using Design Rule 3D, a bandwidth of approximately 30-35 Hz was chosen, in order to damp the modes at 6.8, 9.4, and 14 Hz. A constant controller, using rate feedback of the output y was then designed. In order to avoid integration of DC bias in the rate gyro, a two pole high pass filter was used in the control loop, with a corner frequency of 0.03 Hz (Table 2.4). Because of the phase lag of the system, a two pole lead filter was also designed and convolved into the compensator to add lead at the target frequency range between 5 and 15 Hz. The gain of the

compensator, k_o, was then adjusted in order to maximize the damping in the modes between 5 and 15 Hz. A 35 Hz loop crossover was then created.

Using Design Rule 3E, one rolloff pole was added, at 100 Hz, as a result of possible closed loop stability concerns with higher frequency modes.

Design Rule 3F states that the loop transfer function made up of the controller designed in rules 3A-D, and the open loop transfer function g_{yu} in Figure 5.17, is examined. The mode at 36 Hz had a loop gain greater than -3 dB, with a negative phase margin. It was therefore notch filtered (ω=36 Hz, α=10, ζ_o=0.02).

According to Design Rule 3G, the test from 3A, the structural filter g_o, and the bandwidth are compared. Because there was no frequency range where the test in 3A was passed (Figure 5.16), no additional dynamics were added to the compensator.

The resulting 7 state Neo-Classical compensator for MACE 3 is shown in

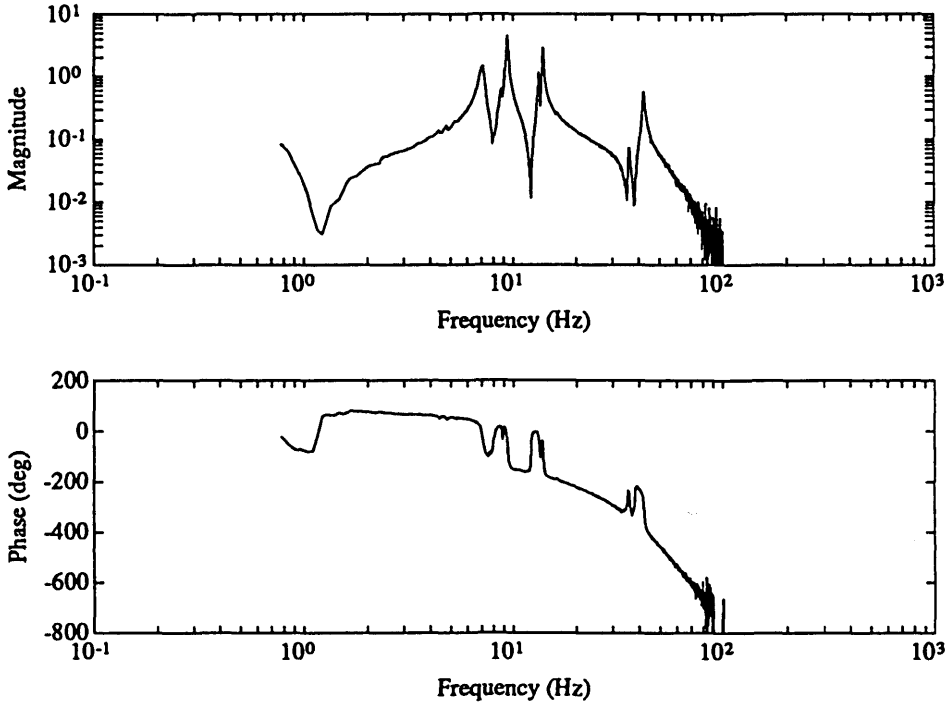

Figure 5.17. Measurement of the open loop input output transfer function g_{yu} for MACE 3.

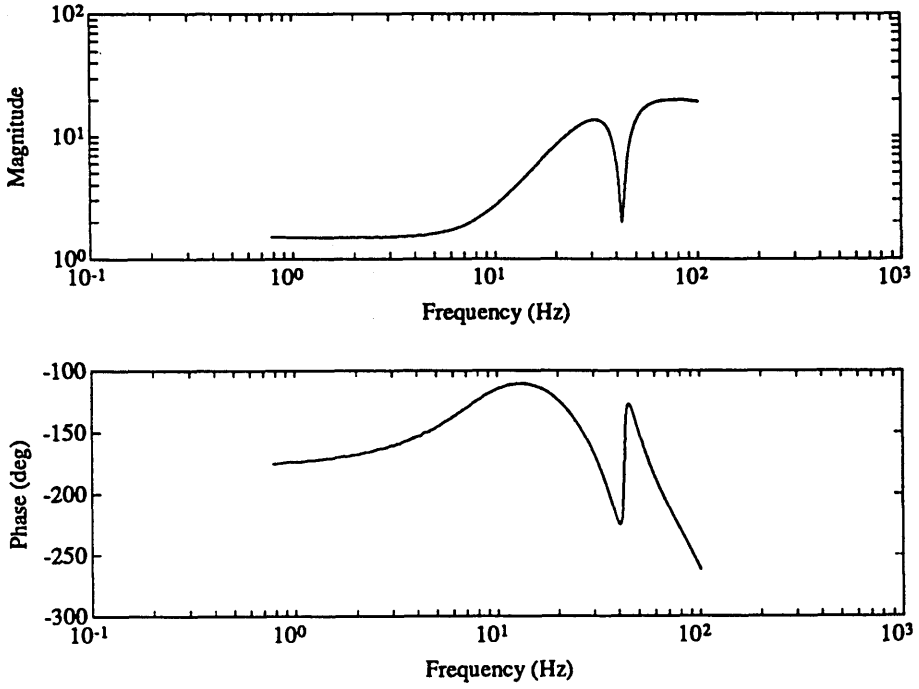

Figure 5.18(a). 7 state Neo-Classical compensator K for MACE 3: 2 states for the high pass filter; 2 states for a lead filter; 2 states for the 36 Hz notch filter; 1 state for the 100 Hz rolloff.

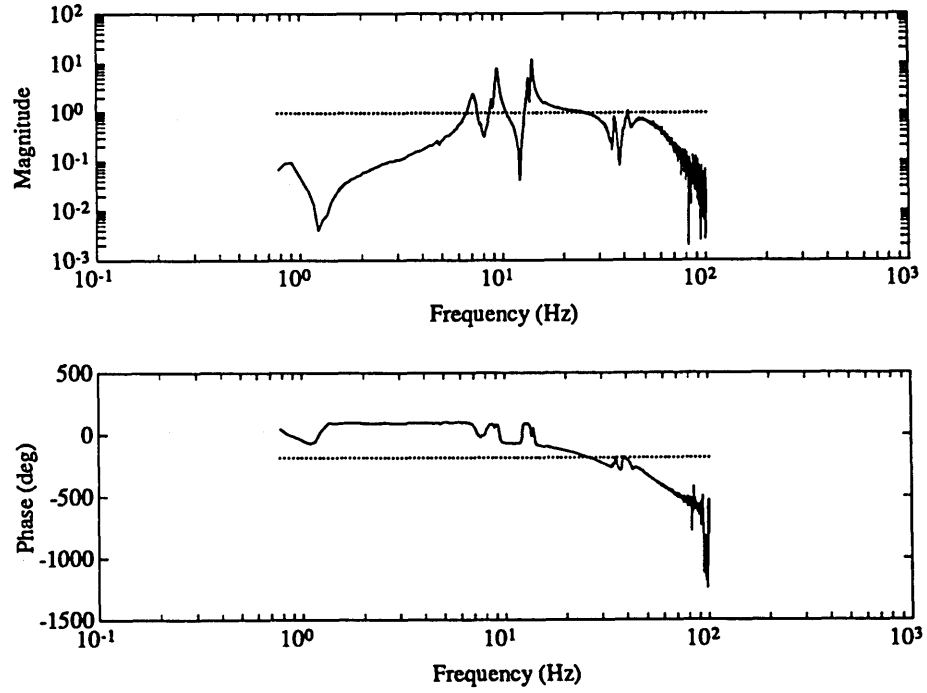

Figure 5.18(b). Measurement of the loop transfer function $g_{yu}K$ consisting of the 7 state Neo-Classical compensator and open loop transfer function.

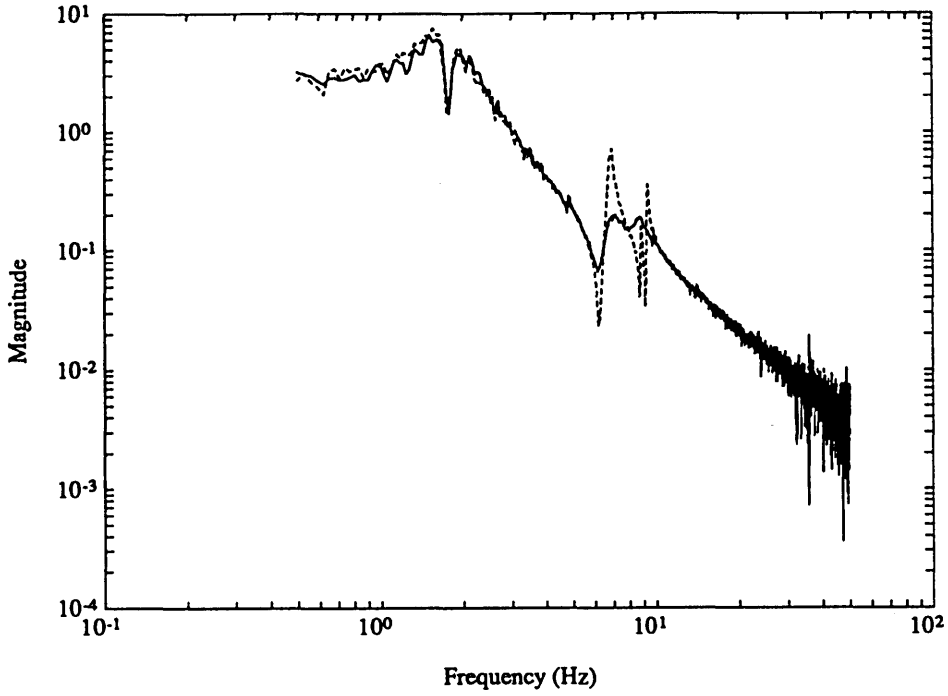

Figure 5.18(c). Measurement of the open and closed loop disturbance to performance transfer functions MACE 3. Performance improvement with the Neo-Classical compensator was 0.5 dB.

Figure 5.18(a). Figure 5.18(b) shows the measurement of the loop transfer function consisting of the Neo-Classical compensator, and the open loop system in Figure 5.17. The crossover is approximately 35 Hz. Notice how the three modes at 6.8, 9.4, and 14 Hz all have loop gain greater than 0 dB, thus being controlled (added damping).

Figure 5.18(c) shows the measurement of the open and closed loop transfer functions for the Neo-Classical compensator, impinged on MACE 3. The modes at 6.8, 9.4, and 14 Hz are all damped substantially from open loop. For instance, evaluating the closed loop system on the model yielded an increase in the damping in the mode at 6.8 Hz from 1.7% to 10%. The performance improvement was 0.5 dB wit the Neo-Classical compensator. Although the closed loop performance

improvement was small, the benefit of using this sensor actuator pair was not performance improvement, but added robustness by damping the modes at 6.8, 9.4, and 14 Hz, which could be used to robustify the subsequent control loops in a MIMO problem.

Chapter 6

Noncollocated Sensor Actuator Pairs

6.1 Introduction

This chapter will examine the implications on Neo-Classical control design with noncollocated sensor actuator pairs. In the examinations of the previous topologies, the assumption of collocated, dual, and complementary extreme sensor actuator pairs is made consistently. The resulting compensator design is therefore simplified as a result of the alternating pole zero pattern of the input output transfer function. In Section 2.6, the pole zero patterns of noncollocated input output pairs were discussed. This chapter examines how these patterns impact the control design. First, two topologies will be introduced, similar to the previous topologies, but using noncollocated input output pairs. LQG compensators will then be considered and compared with the previously designed optimal compensators. The changes and effects on the control design will be summarized in another Neo-Classical design rule. Finally, the closed loop results of a compensator designed using the rule, and implemented on the MACE test article will be shown.

6.2 Topologies Examined

In Section 2.6, the benefits of using collocated, dual, and complementary extreme input output pairs were presented, i.e. alternating poles and zeros. The critical input output transfer function, g_{yu}, is simplified by the alternating pole zero patterns, thus making the control design easier. However, in the controlled structures technology, with multiple inputs, outputs, performances, and disturbances, the use of noncollocated control is a common practice.

As input output pairs become noncollocated on a structure, the zero pairs increase in frequency. Pole zero cancellations then occur, and eventually, the zeros move higher in frequency, thus creating a pair of *missing* zeros between two pole pairs. In certain structures, noncollocation can create real nonminimum phase zeros. If the noncollocation distance is increased further, the zeros will decrease from infinity in pairs, one being minimum phase and the other nonminimum phase. Examples of zero movement are shown in Figure 2.6, and explained fully by Fleming (1990).

Figure 6.1(a) shows Typical Section 4A, in which the performance z_1 is the vertical position of the tip mass, and the output y_1 is the vertical velocity of the tip mass. The disturbance w_2 and input u_2 are equivalent, as a vertical force on the second mass. Because the performance and output are analogs, *and* the disturbance

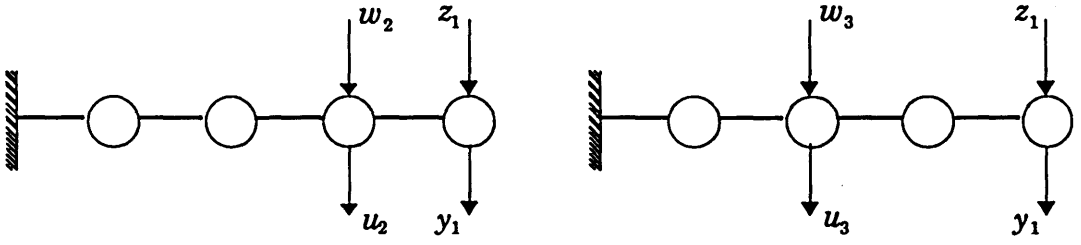

Typical Section 4A Typical Section 4B

Figure 6.1. Noncollocated input output pairs.

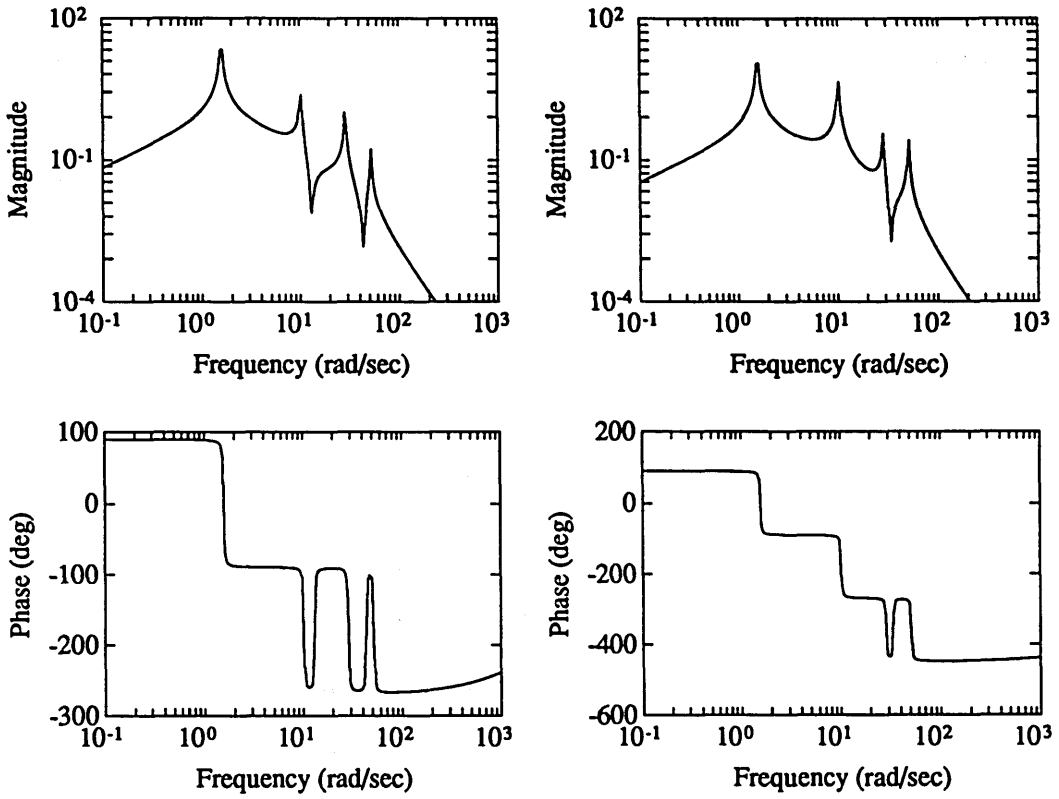

$g_{yu} = \frac{y_1}{u_2}$ for Typical Section 4A

$g_{yu} = \frac{y_1}{u_3}$ for Typical Section 4B

Figure 6.2. Open loop input output transfer functions.

and input are analogs, this topology falls in the Topology I category, with a noncollocated input output pair, u_2 and y_1.

Figure 6.1(b) shows Typical Section 4B, which also falls into the Topology I category. The performance z_1 is the vertical position of the tip mass, and the output y_1 is the vertical velocity of the tip mass, as in Typical Section 4A. The disturbance w_3 and input u_3, however, are equivalent vertical forces on the third mass. The noncollocated input output pair in Typical Section 4B is u_3 and y_1.

Figure 6.2(a) shows the input output transfer function for the pair y_1 and u_2. There is a missing zero pair between the first two pole pairs at 1.6 and 10.1 rad/sec. Figure 6.2(b) shows the input output transfer function for the pair y_1 and u_3. Again

there is a missing zero pair again between the first two pole pairs, and there is a nonminimum phase and minimum phase zero at 14 rad/sec. These two input output pairs will help to show the important issues concerning noncollocated control, i.e. missing zero pairs, and nonminimum phase zeros in the input output transfer function.

6.3 Optimal Compensation

Asymptotic Properties of the LQG Compensator

Typical Section 4A, because the output and performance are analogous, *and* the input and disturbance are analogous, falls into the Topology I category. For the low gain, expensive control problem, which was used to show similarities to the high frequency LQG compensator, the asymptotic limit was shown in Equation 3.17 to be

$$\underset{\substack{\mu\to 0\\ \rho\to\infty}}{LIM}\, K(s) = \frac{k_{LG}}{\sqrt{\rho}} \frac{s}{s^2 + 2\zeta_{dm}\omega_{dm}s + \omega_{dm}^2} \frac{1}{g_{yw}} = \frac{k_{LG}}{\sqrt{\rho}} \frac{s}{s^2 + 2\zeta_{dm}\omega_{dm}s + \omega_{dm}^2} \frac{1}{g_{yu}}\Bigg|_{\substack{z=\phi_{zy}y\\ w=u}} \tag{6.1}$$

where ζ_{dm} and ω_{dm} are the damping ratio and frequency of the dominant mode, and k_{LG} is a scalar constant. The compensator is a low gain inversion of the disturbance to output transfer function, g_{yw}, except for the dominant mode. The transfer function, g_{yw}, is also the input output transfer function, g_{yu}, for this topology.

For Topology I, the high gain LQG asymptote was shown in Equation 3.19 to be

$$\underset{\substack{\mu\to 0\\ \rho\to 0\\ \rho>\mu}}{LIM}\, K(s) = \pm\frac{1}{\sqrt{\rho}} \frac{g_{zw}}{g_{yw}} = \pm\frac{\phi_{zy}}{\sqrt{\rho}} \frac{g_{yu}}{g_{yu}}\Bigg|_{\substack{z=\phi_{zy}y\\ w=u}} \tag{6.2}$$

The high gain LQG asymptote is a high gain compensator, with the temporal relationship between z and y. The compensator poles and zeros are identically the

zeros of the input output transfer function, g_{yu}.

Given that the performance is the integration of the output, as in Typical Section 4A and 4B,

$$\phi_{zy}(s) = \frac{1}{s} \tag{6.3}$$

The high gain LQG asymptote becomes

$$\underset{\substack{\mu \to 0 \\ \rho \to 0 \\ \rho > 0}}{LIM} K(s) = \pm \frac{1}{s\sqrt{\rho}} \frac{g_{yu}}{g_{yu}} = \pm \frac{1}{s\sqrt{\rho}} \tag{6.4}$$

The high gain asymptote is a high gain integrator, or position feedback.

Both the low and high gain LQG asymptotes in Equations 6.1 and 6.2 are dependent upon the fact that the pole zero structure of g_{yw} is minimum phase, as noted previously. For Topology I, g_{yw} is identical to g_{yu}. In fact, for Typical Section 4A, where u_2 and w_2 are used, g_{yu} contains a missing zero pair. For Typical Section 4B, where u_3 and w_3 are used, g_{yu} contains a missing zero pair, and nonminimum phase zero. The high gain LQG asymptote is also dependent upon the g_{zu} transfer function being minimum phase. But this requirement is not as rigorous because μ is smaller than ρ.

Even though they are not expected to rigorously hold, the low and high gain LQG asymptotes will be compared to typical LQG compensators in order to identify the affects from the missing zeros or nonminimum phase zeros in the open loop input output transfer functions for the noncollocated input output pairs. The LQG compensators will also be compared to those designed for Typical Section 1A, where g_{yu} contains alternating poles and zeros.

Typical Section Results: Missing Zeros in g_{yu}
LQG compensator

Figure 6.4 shows an 8 state LQG compensator, designed for Typical Section 4A, plotted with the low and high gain LQG asymptotes of Equations 6.1 and 6.4. Figure 6.3 shows the open loop input output transfer function, g_{yu}. For this case, g_{yw} contains a missing zero pair between the pole pairs at 1.6 and 10.1 rad/sec, but no nonminimum phase zeros. The Kalman Filter weighting is a small value (μ=1E-8), and the LQR weighting ρ is an intermediate value (ρ=1E-1). At low frequency, the LQG compensator matches the integral control (position feedback) of the high gain asymptote (Equation 6.4). At high frequency, up to 300 rad/sec, the compensator matches the low gain asymptote (Equation 6.1). At 300 rad/sec, however, the LQG compensator rolls off, compared to the low gain LQG asymptote. If the Kalman Filter weighting is made smaller, the dynamics of the LQG compensator identically matches that of the low gain asymptote, since there are no nonminimum phase zeros in g_{yw}. However, in comparing the 300 rad/sec rolloff in this compensator to the LQG compensator for Typical Section 1A in Figure 3.5(a), where g_{yu} contains alternating poles and zeros, the rolloff of that compensator is greater than 1000 rad/sec. This indicates the rate of convergence of the low gain asymptote is dependent upon the pole zero pattern of g_{yu}. Specifically, the convergence is *faster* if g_{yu} contains alternating poles and zeros, and slower if g_{yu} contains a missing zero pair between two pole pairs.

Figure 6.5(a) shows LQG compensators for Typical Section 4A, for three values of the LQR weighting ρ, while holding the Kalman Filter weighting constant (μ=1E-8). These plots are complementary to those Figure 3.6(a) and (b), with collocated input output pairs. At low frequency, the compensator is a high gain integrator, and is proportional to $1/\sqrt{\rho}$, as suggested in Equation 6.4. At high frequency, magnitude of each compensator rolls off at approximately 300 rad/sec, as

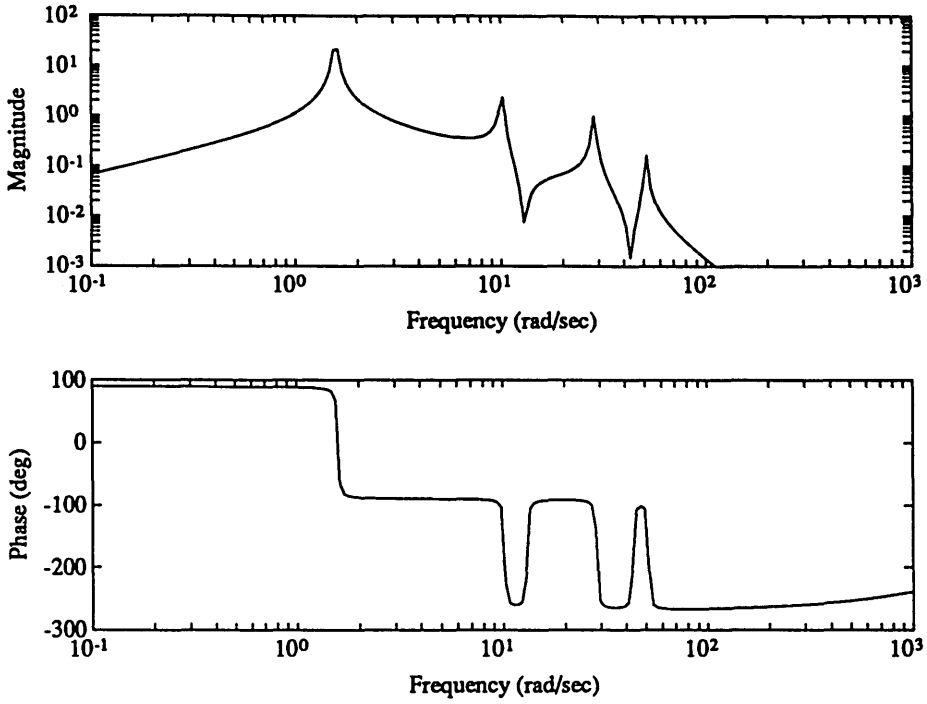

Figure 6.3. Open loop input output transfer function g_{yu} for Typical Section 4A.

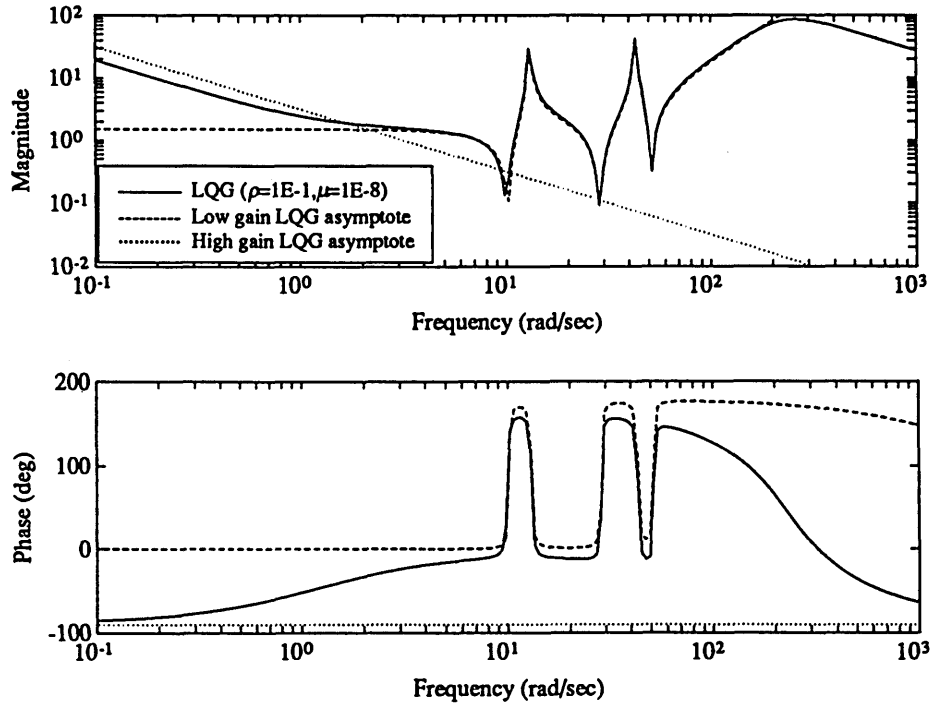

Figure 6.4. 8 state LQG compensator K (ρ=1E-1, μ=1E-8) for Typical Section 4A, and the low and high gain LQG asymptotes.

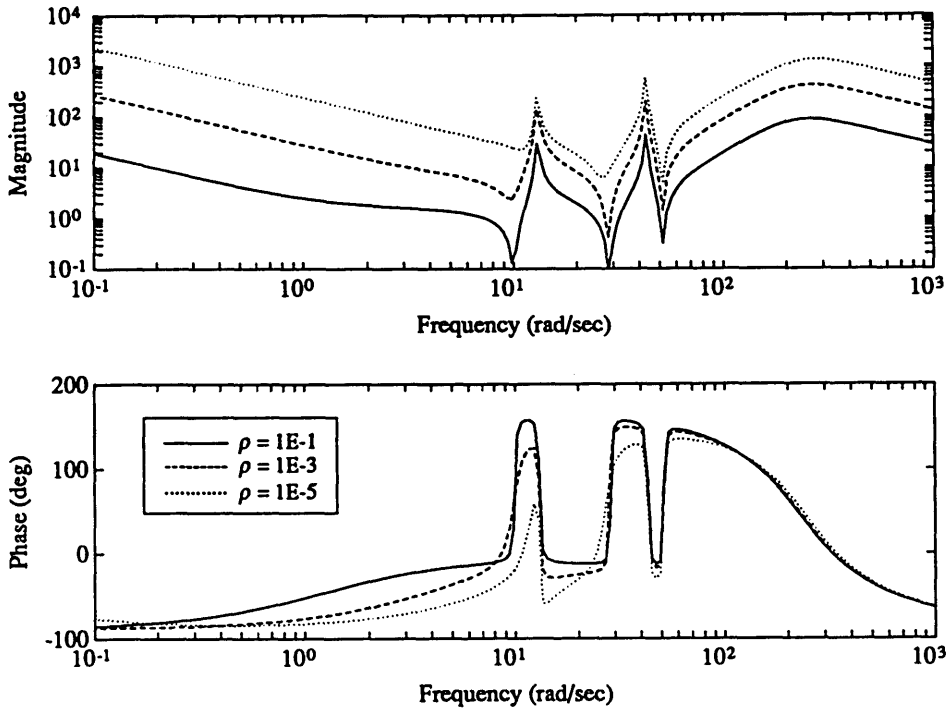

Figure 6.5(a). LQG compensators for Typical Section 4A for three values of ρ. μ=1E-8.

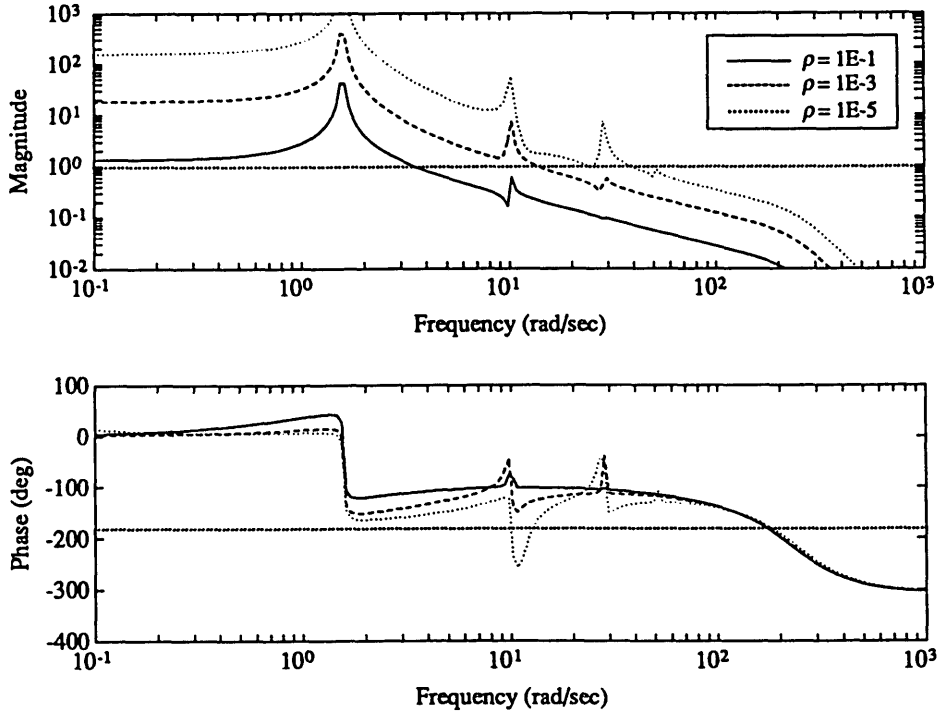

Figure 6.5(b). Loop transfer functions corresponding to the three LQG compensators in Figure 6.5(a).

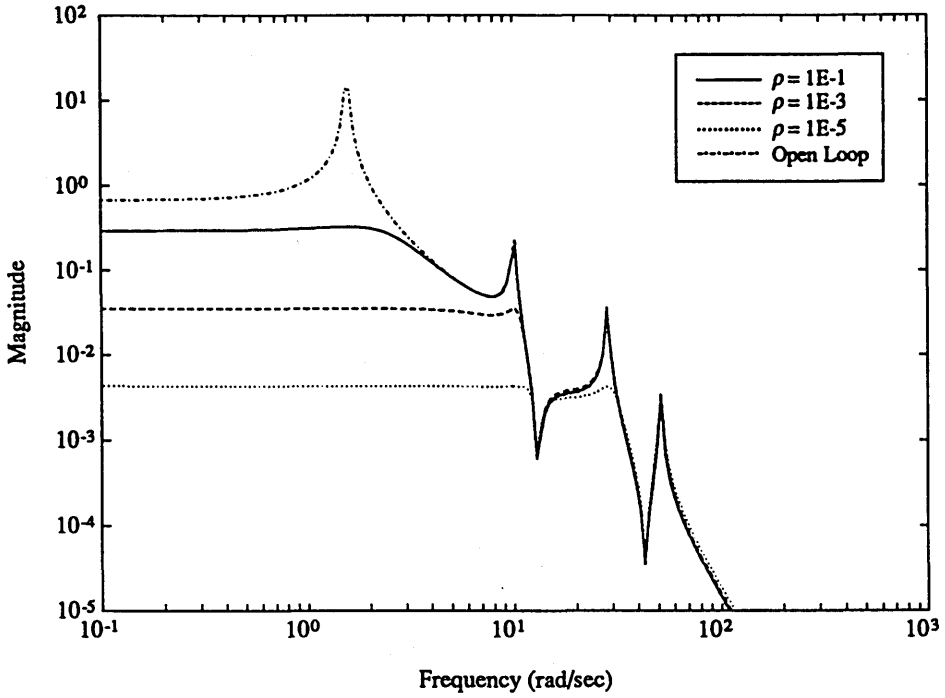

Figure 6.5(c). Open and closed loop disturbance to performance transfer functions corresponding to the three LQG compensators in Figure 6.5(a).

a result of the missing zero pair in the g_{yu} transfer function. At intermediate frequencies, the g_{yu} transfer function is inverted by each compensator, except for the dominant mode, as in the low gain asymptote.

The corresponding loop transfer functions, $g_{yu}K$, made up of the three compensators (Figure 6.5(a)), and the open loop system (Figure 6.3), are shown in Figure 6.5(b). Comparing the phase of the loop transfer functions with open loop phase shown in Figure 6.3 for the large and intermediate values of ρ, the phase does not drop below 180°. For the largest value of ρ, the LQG compensator places a lightly damped zero pair at approximately 9 rad/sec, thus making the noncollocated input output transfer function resemble a collocated transfer function, i.e. alternating poles and zeros. As ρ decreases, the bandwidth increases, and the zero pair at 9 rad/sec increases in frequency and becomes more damped in order to add

phase to the loop crossover region. For the smallest value of ρ, the phase of the loop transfer function drops below 180°, with the loop gain greater than one, indicating conditioned stability. This is similar to the conditioned stability of the LQG compensator for the small ρ case in Figure 4.6(a) and (b) for Typical Section 2A. The SWLQG compensator immediately brought the phase of the loop transfer function above 180°, thus indicating the low robustness of this LQG compensator.

The corresponding closed loop disturbance to performance transfer functions for the three LQG compensators (Figure 6.5(a)), impinged on Typical Section 4A, are shown in Figure 6.5(c). Notice how the magnitude of the closed loop transfer function decreases proportionally to $\sqrt{\rho}$ at low frequency.

Typical Section Results: Nonminimum Phase Zeros in g_{yu} LQG compensator

Figure 6.7 shows an LQG compensator designed for the topology in Typical Section 4B, and the low and high gain LQG asymptotes from Equations 6.1 and 6.4. Figure 6.6 shows the open loop input output transfer function g_{yu}, for Typical Section 4B. For this case g_{yu} contains a missing zero pair between the pole pairs at 1.6 and 10.1 rad/sec, and a nonminimum phase zero at 14 rad/sec. The Kalman Filter weighting is small (μ=1E-8), and the LQR weighting is an intermediate value (ρ=1E-1). At low frequency, the compensator matches the high gain LQG asymptote only below 0.1 rad/sec. At intermediate frequencies, the magnitude of the LQG compensator matches that of the low gain LQG asymptote, however, the phase does not. At high frequency, the magnitude of the compensator again rolls off at 300 rad/sec, well below that of the Typical Section 1A compensators (Figure 3.5(a)).

Figure 6.8(a) shows LQG compensators for Typical Section 4B for three values of ρ, with μ remaining constant (μ=1E-8). As ρ is decreased, at low frequencies, the compensator resembles an integrator, although it does not increase

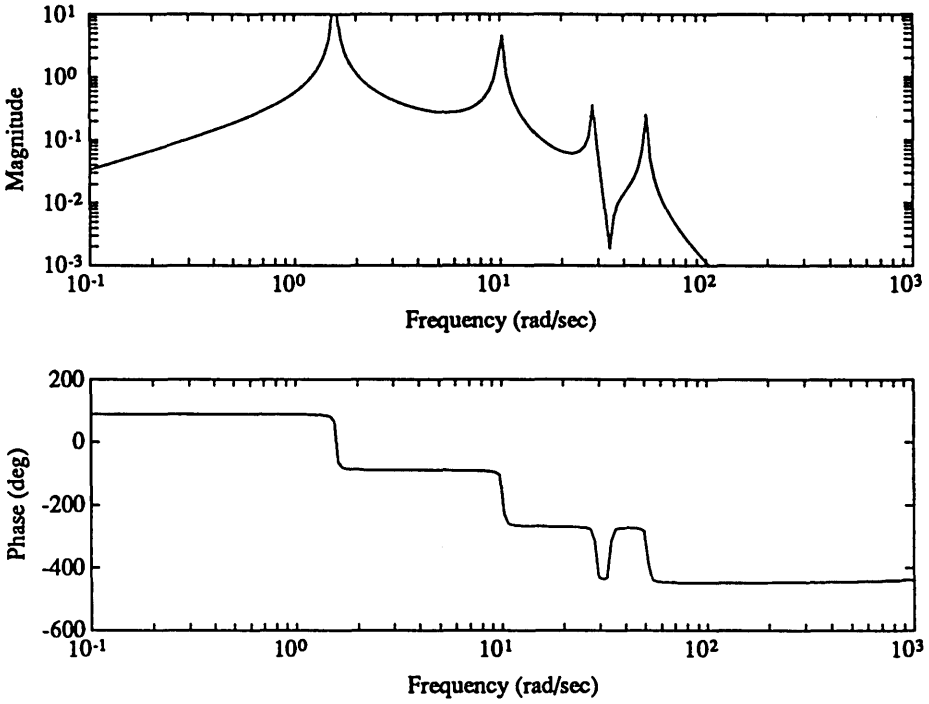

Figure 6.6. Open loop input output transfer function g_{yu} for Typical Section 4B.

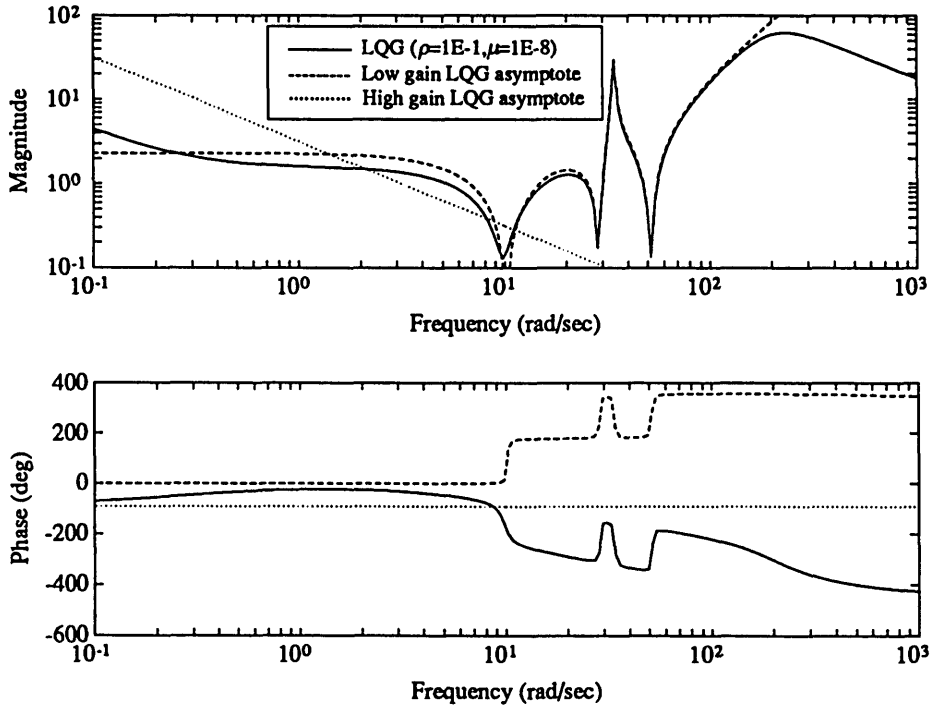

Figure 6.7. 8 state LQG compensator K (ρ=1E-1, μ=1E-8) for Typical Section 4B and the low and high gain LQG asymptotes.

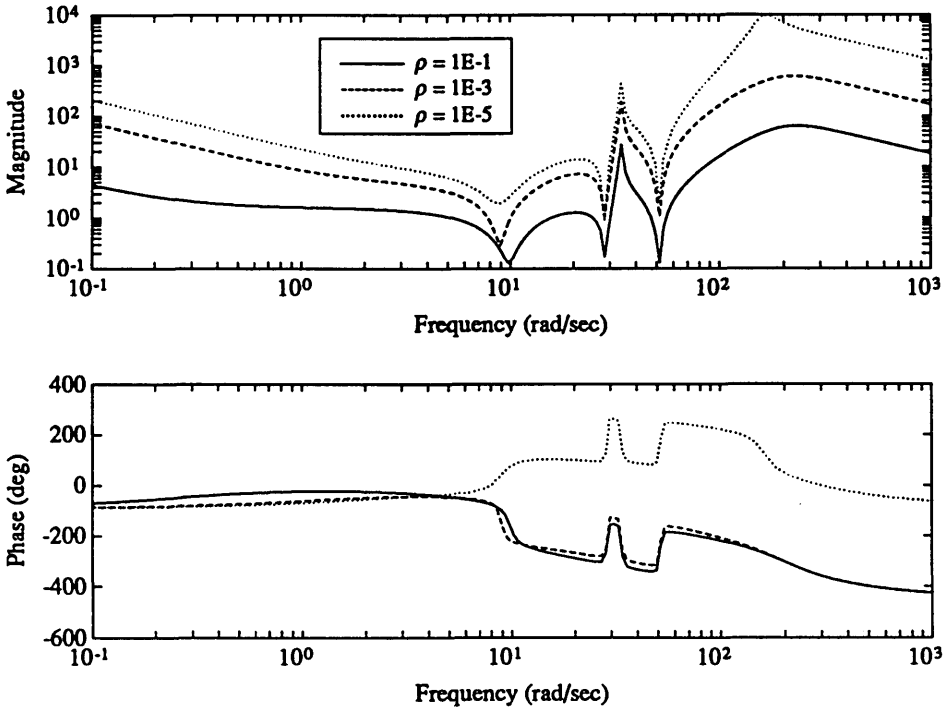

Figure 6.8(a). LQG compensators for Typical Section 4B for three values of ρ. μ=1E-8.

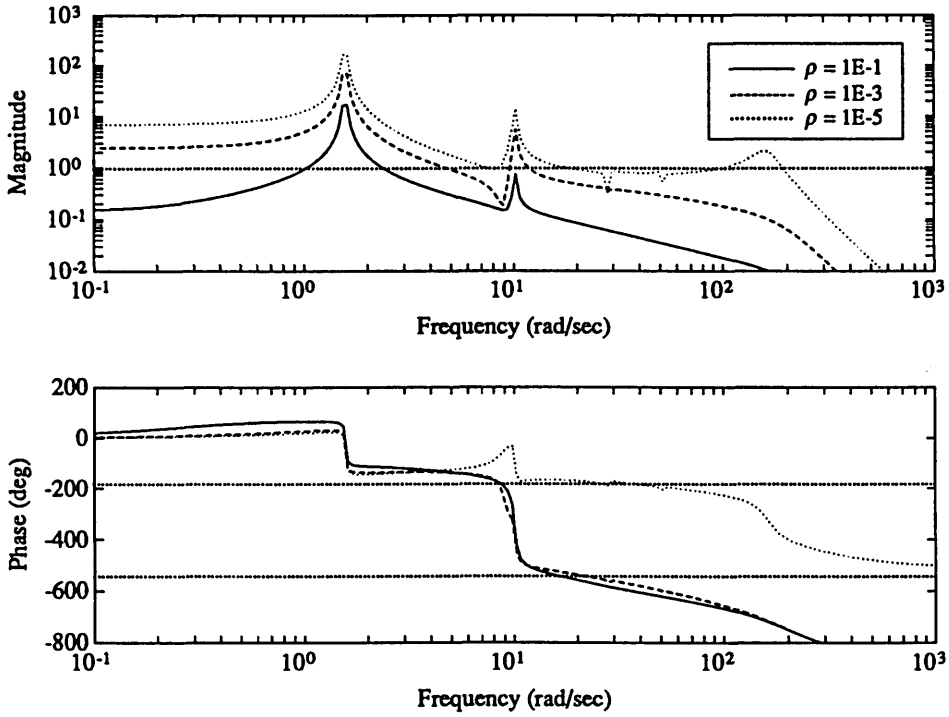

Figure 6.8(b). Loop transfer functions corresponding to the three LQG compensators in Figure 6.8(a).

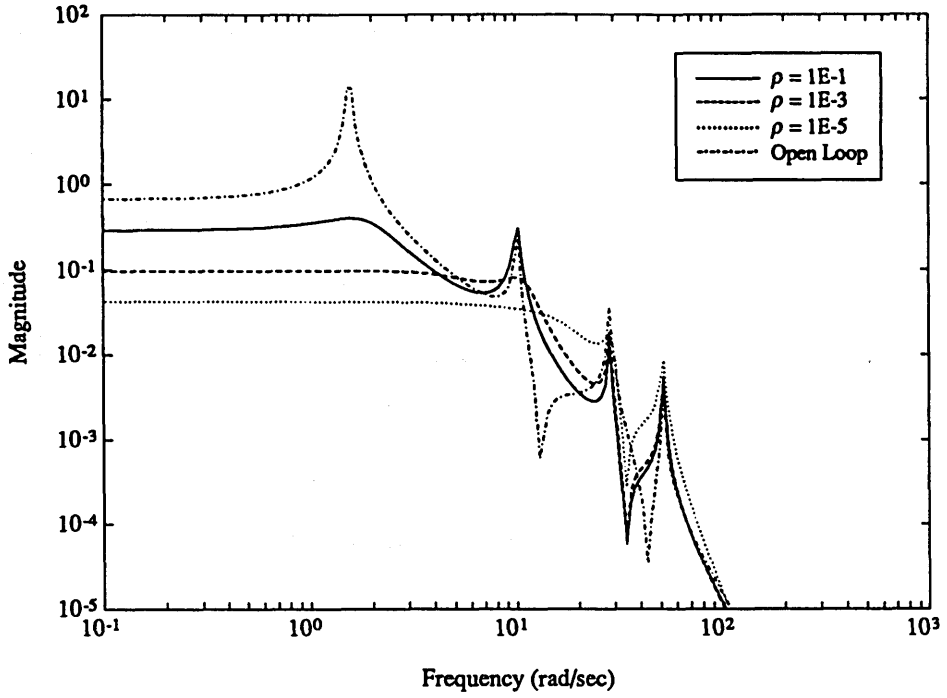

Figure 6.8(c). Open and closed loop disturbance to performance transfer functions corresponding to the three LQG compensators in Figure 6.8(a).

in magnitude proportional to $1/\sqrt{\rho}$, as suggested in Equation 6.4, and as it does for Typical Section 1A (Figure 3.6(a)) and Typical Section 4A (Figure 6.5(a)). At high frequency, the gain of the compensator increases as ρ decreases, and it continues to roll off between 200 and 300 rad/sec. For the large and intermediate cases of ρ, the compensator zero pair at approximately 10 rad/sec is nonminimum phase. For the smallest case of ρ, the zero pair becomes minimum phase.

The effects of this zero pair can be seen more easily in the loop transfer functions in Figure 6.8(b), consisting of the three LQG compensators (Figure 6.8(a)), and the open loop system (Figure 6.6). The nonminimum phase zero pair at 10 rad/sec in the compensator is used to reduce the phase by 180°, making the phase of the loop transfer function drop to the next phase *band*. This has the affect of adding phase margin at crossover by being able to shape the phase, and requires that the

magnitude of the loop transfer function be below 0 dB, at the point where the phase drops below -180° near 9 rad/sec. As ρ is decreased, and the crossover frequency increases, and the zero pair becomes minimum phase, because the compensator cannot shape the magnitude of the loop transfer function such that it drops below 0 dB near 9 rad/sec, as in the previous cases. The compensator, uses a high frequency amplification, while adding phase lead at the crossover frequency, instead of a nonminimum phase zero pair, in order to compensate for the phase loss due to the open loop nonminimum phase zero. The amplification is similar to those which occurred in the LQG compensators designed for the MACE test article for Topology I: LQG compensator for MACE 1A shown in Figure 3.20(a). The phase lag in the actuator sensor transfer function from the experiment is similar to the phase delay from the nonminimum phase zero, as shown in the nonminimum phase PADE approximation (Table 2.4) of the time delay.

The corresponding closed loop disturbance to performance transfer functions for the three LQG compensators (Figure 6.8(a)), impinged on Typical Section 4B, are shown in Figure 6.8(c). In comparing these transfer functions, with those from Figure 6.5(c), the closed loop magnitude is not reduced $\sqrt{\rho}$ because of the open loop nonminimum phase zero. In particular, virtually no control is exerted near 14 rad/sec, the frequency of the nonminimum phase zero. Notice above this frequency, the closed loop magnitude is pushed up. The lowest ρ case contains a crossover of approximately 14 rad/sec, and is near the limit on performance improvement for this topology. Therefore, the performance improvement of systems with open loop nonminimum phase zeros is limited.

For Typical Sections 4A and 4B, the compensators resulting from varying the Kalman Filter weighting were also examined. Similar results to the compensators designed in Typical Section 1A are seen (Figure 3.7(a) and (b)). These included the PI controller becoming a lag controller, and the high frequency rolloff becoming

steeper, and at a lower frequency.

Summary

If the input output transfer function, g_{yu}, has a missing zero pair, the compensator places a zero pair between the two pole pairs, and designs a compensator similar to those for Topology I, i.e. integral control (position feedback) at low frequencies and proportional control (rate feedback) and inversion of the input output transfer function, except for the dominant mode, at high frequencies. However, the practical performance improvement, is limited by the missing zero pair because the LQG compensator drops the phase of the loop transfer function below 180°, while the loop gain is greater than 0 dB, thus creating robustness concerns.

If the input output transfer function is nonminimum phase, the results are not as clear. For a crossover frequency far below the nonminimum phase frequency, the compensator is similar to those described previously. Occasionally, nonminimum phase zero pairs and unstable pole pairs are used to shape the phase of the loop transfer function, adding damping to the modes at crossover. However, as more performance is required, the control authority, of the compensator, and closed loop performance improvement, is limited by the nonminimum phase zero. The compensator gain does not increase at low frequency, and high frequency amplification occurs, in return for adding phase lead at crossover to compensate for the open loop nonminimum phase zero.

A similar analysis was performed for those typical sections which correspond to Topologies IIA, IIB, and Topology III, with noncollocated input output pairs. The results were quite similar. For missing zero pairs, the LQG compensator places a zero pair in the open loop transfer function, in order to create an alternating pole zero pattern in the g_{yu} transfer function, and then designs the compensators similar to those with collocated input output pairs. For noncollocated input output pairs

with nonminimum phase zeros, the performance improvement of these topologies is again limited. An example of a noncollocated input output pair which falls into the Topology IIB category is shown as an experiment in Section 6.4.

6.4 Neo-Classical Control

This section presents the Neo-Classical design rule for noncollocated input output pairs. The previous section showed the implications of noncollocated input output pairs on the control designs for Topology I. However, as was pointed out, the results are similar for Topologies II and III. Therefore, Neo-Classical Design Rule 4, for general SISO noncollocated input output pairs, is stated on the following page.

Design Rule 4A states that the pole zero pattern of the input output transfer function is checked first for three types of pole zero patterns: alternating poles and zeros; poles and missing zeros; poles and nonminimum phase zeros. These pole zero patterns encompass all of the pole zero patterns associated with collocated and noncollocated input output pairs.

Design Rule 4B states that if there are nonminimum phase zeros throughout the frequency range of the performance metric, then the selected sensor actuator pair is not to be used. For instance, if the performance metric is between 0-50 rad/sec, and if there are nonminimum phase zeros at 5 and 35 rad/sec, then the input output pair is not wise choice in the control design. Not only would optimal compensators give a nonrobust unstable and/or nonminimum phase compensator, but the pair would also only produce minimal performance improvement.

Design Rule 4C examines the case when there is a nonminimum phase zero at high frequency, compared to the frequency range of the performance metric. In this case, the compensator is designed using Neo-Classical Design Rules 1-3, with the bandwidth set by the frequency of the nonminimum phase zero. This is similar

Neo-Classical Design Rule 4

For noncollocated input output pairs

A. Examine the input output transfer function for three types of pole zero patterns:
alternating poles and zeros
poles and missing zeros
poles and nonminimum phase zeros

B. If there is a nonminimum phase zero in the frequency range of the performance, such that there would be no net performance improvement, then this sensor actuator pair is not to be used in the control design.

C. If there is a nonminimum phase zero at high frequency, then design the compensator using Neo-Classical Design Rules 1-3, with the bandwidth of the compensator being limited by the frequency of the nonminimum phase zero.

D. If there is a nonminimum phase zero at low frequency, then design the low and high frequency compensator such that the loop gain is greater than 0 dB in the frequency range of alternating poles and zeros, i.e. above the nonminimum phase zero. Then continue with Neo-Classical Design Rules 1-3.

E. If there is a frequency range with alternating poles and zeros, and a missing zero pair, which corresponds to the performance frequency range, add the zero pair as part of the compensator, with a higher frequency damped pole pair, to construct a frequency range with alternating poles and zeros. Then proceed with Neo-Classical Design Rules 1-3, being careful to check the loop transfer function for closed loop stability.

to the LQG compensators in Figure 6.8(a) and (b), where the bandwidth is limited by the 14 rad/sec nonminimum phase zero. For instance, if the performance metric is between 0-50 rad/sec, and if there was a nonminimum phase zero at 50 rad/sec, then compensators can be designed with lower bandwidths, usually up to 20-30 rad/sec in this case. Also, a nonminimum phase zero may add phase lag in the open loop transfer function. Phase lead could be added into the compensator by using lead filters, with a high frequency amplification as a tradeoff.

Design Rule 4D examines the case where there is a nonminimum phase zero

at low frequency. In this case, the low frequency, high gain LQG asymptote is not valid, as a result of the nonminimum phase zero. The LQG compensators for this case are difficult to interpret. Therefore, the insight of the control designer must be used in this case. A controller is designed such that the loop gain is greater than 0 dB within the frequency range of the alternating poles and zeros. For instance, if the performance metric is between 0-50 rad/sec, and if there is a nonminimum phase zero at 1 rad/sec, then a low frequency controller is designed which allows the magnitude of the loop transfer function to be greater than 0 dB at frequencies above the 1 rad/sec nonminimum phase zero, i.e. a region of alternating poles and zeros. Disturbance rejection can be achieved, therefore, at frequencies greater than the frequency of the nonminimum phase zero. Then the remainder of the Neo-Classical Design Rules 1-3 can be used. An example of the use of Design Rule 4D is shown as an experiment in Section 6.5.

According to Design Rule 4E, if there is a missing zero pair in the pole zero pattern of g_{yu}, then the compensation technique is to use a zero pair, to create an alternating pole zero pattern, as the LQG compensators do in Figure 6.5(a). A higher frequency pole pair is also added. The damping of the pole pair is dependent upon the required phase at crossover, and amplification at high frequency by the compensator. Care must be taken in the placement of the lightly damped zero pair, however. It must be placed between the two pole pairs. If modeling errors lead to this not being true, closed loop instabilities could result.

Design Rule 4A is used to design a Neo-Classical compensator for Typical Section 4A, where the input output pair u_2 y_1 is noncollocated. For this pair, in examining the open loop transfer function, g_{yu}, Figure 6.2(a), there are no nonminimum phase zeros in the g_{yu} transfer function, but there is a missing zero pair between the poles at 1.6 and 10.1 rad/sec. Therefore, Design Rule 4E is used, where a compensator zero pair is placed between the two pole pairs in the open loop

transfer function, to create a region of alternating poles and zeros. A higher frequency pole pair is also added, to insure rolloff of the compensator.

Figure 6.9 shows the open loop transfer function, g_{yu}, and the open loop transfer function convolved with a lightly damped (ζ_z=1%) zero pair added at 9 rad/sec, and a heavily damped pole pair at a higher frequency, 30 rad/sec (ζ_p=40%). Notice the alternating pole zero pattern at low frequency, up to 20 rad/sec, with a slight phase delay. The damped pole pairs act as a phase delay. This transfer function is now used as the open loop transfer function g_{yu}, and Design Rule 1 is used, since the topology falls into the Topology I category: the performance and output are analogs, *and* the disturbance and input are analogs.

Using Design Rule 1A, a low frequency controller is designed, consisting of the temporal relationship ϕ_{zy}, which is an integrator, since z_1 is the integration of y_1.

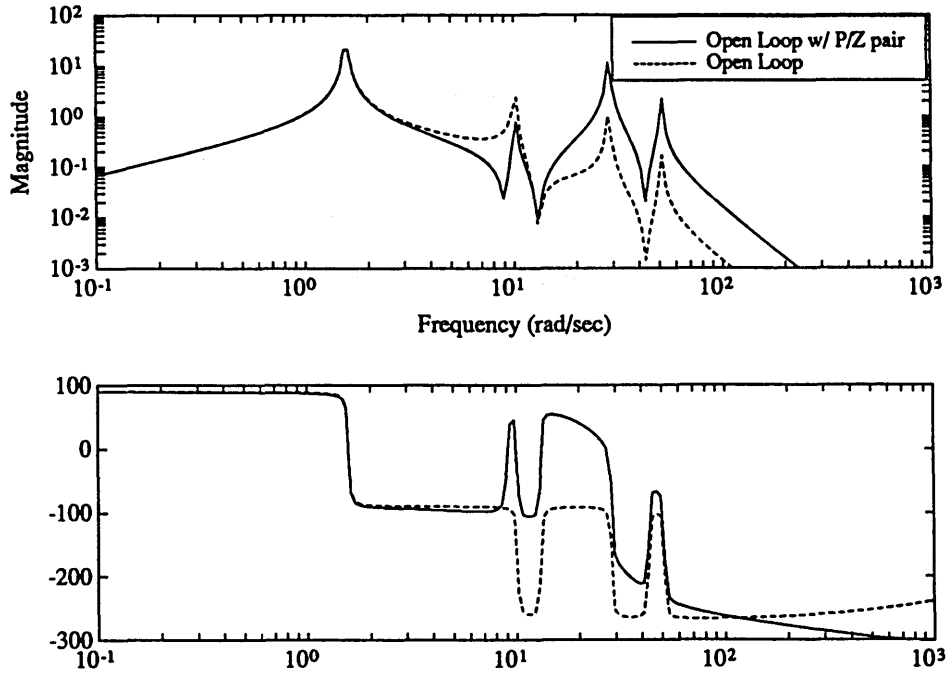

Figure 6.9. Open loop transfer function for Typical Section 4A, from u_2 to y_1, convolved with a zero pair (ω_z=10 rad/sec, ζ_z=1%) and pole pair (ω_p=30 rad/sec, ζ_p=40%).

Using Design Rule 1B, a closed loop bandwidth is chosen to be 3 rad/sec, similar to that of the LQG compensator for the large ρ case in Figure 6.5(a) and (b). Then, a zero is convolved into the compensator, in order to achieve rate feedback at high frequency. The zero frequency is chosen to be 1.5 rad/sec, in order that the phase margin at loop crossover is approximately 60°. The gain of the compensator is then adjusted such that the loop crossover is approximately 3 rad/sec.

Using Design Rule 1C, no high frequency rolloff dynamics are added, because they added phase to the crossover frequency, and there are no problems with sensor noise.

Following Design Rule 1D, the loop transfer function consisting of the open loop system in Figure 6.9, and the compensator designed from Design Rules 4E and 1A-C is examined. The modes at 28 and 51 rad/sec pose closed loop stability problems, and are therefore notch filtered. Figure 6.10(a) shows the resulting 6 state Neo-Classical compensator designed for the topology in Typical Section 4A, using w_2 and u_2 as the disturbance and input.

The 6 state Neo-Classical compensator is plotted with an 8 state LQG compensator for the large ρ case in Figure 6.5(a) for comparison. Both compensators use PI controllers, invert the open loop poles at 28 and 51 rad/sec, and contain a zero pair below the open loop pole pair at 10.1 rad/sec to create a pseudo open loop alternating pole zero pattern. The Neo-Classical compensator uses a 9 rad/sec zero pair, while the LQG compensator uses a 9.7 rad/sec zero pair. The Neo-Classical compensator, however, does not invert the open loop zeros at 14 and 42 rad/sec. This results in the phase of the compensator at 3 rad/sec being smaller than that of the LQG compensator. The Neo-Classical compensator trades phase at crossover for robustness by not inverting the open loop zeros.

Figure 6.10(b) shows the loop transfer functions, consisting of the open loop system in Figure 6.9, and the compensators from Figure 6.10(a). The loop crossover

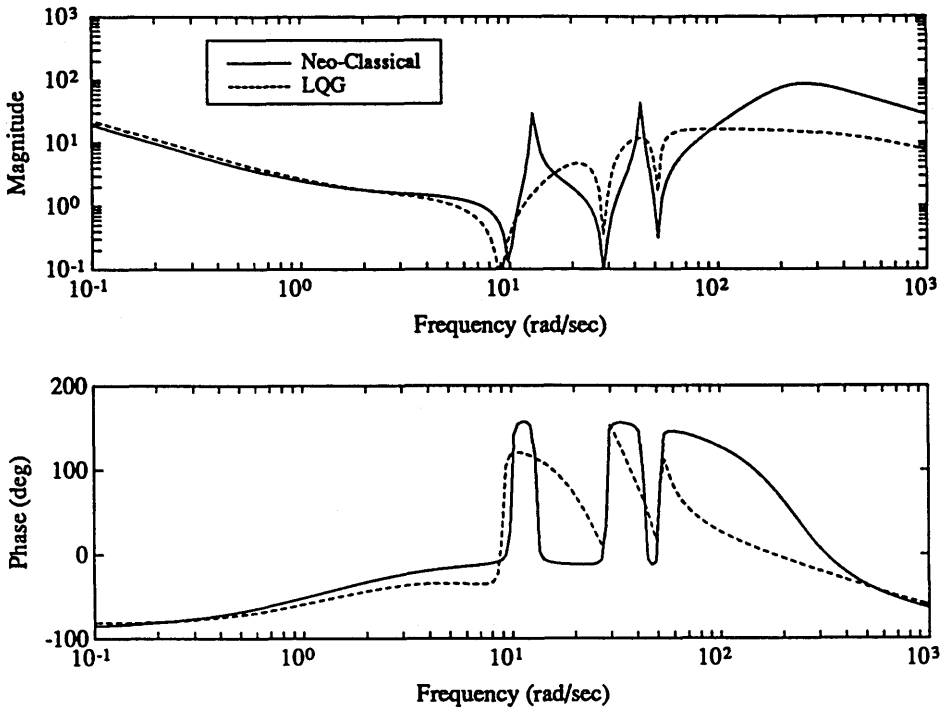

Figure 6.10(a). 6 state Neo-Classical compensator, and 8 state LQG (ρ=1E-1, μ=1E-8) compensator for Typical Section 4A.

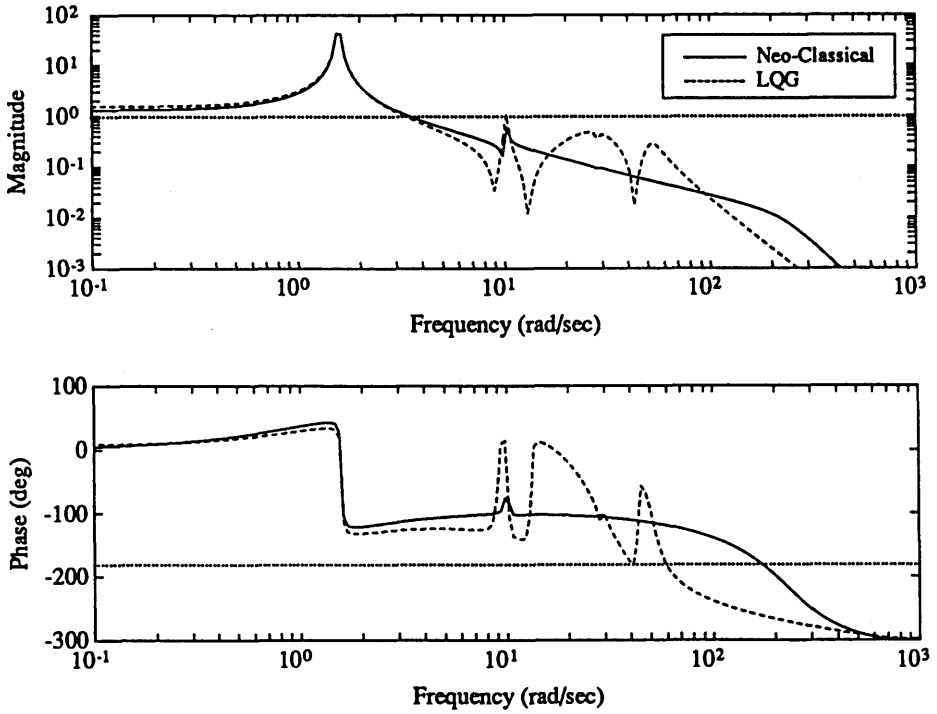

Figure 6.10(b). Loop transfer functions $g_{yu}K$ consisting of the compensators in Figure 6.10(a) and the open loop transfer function.

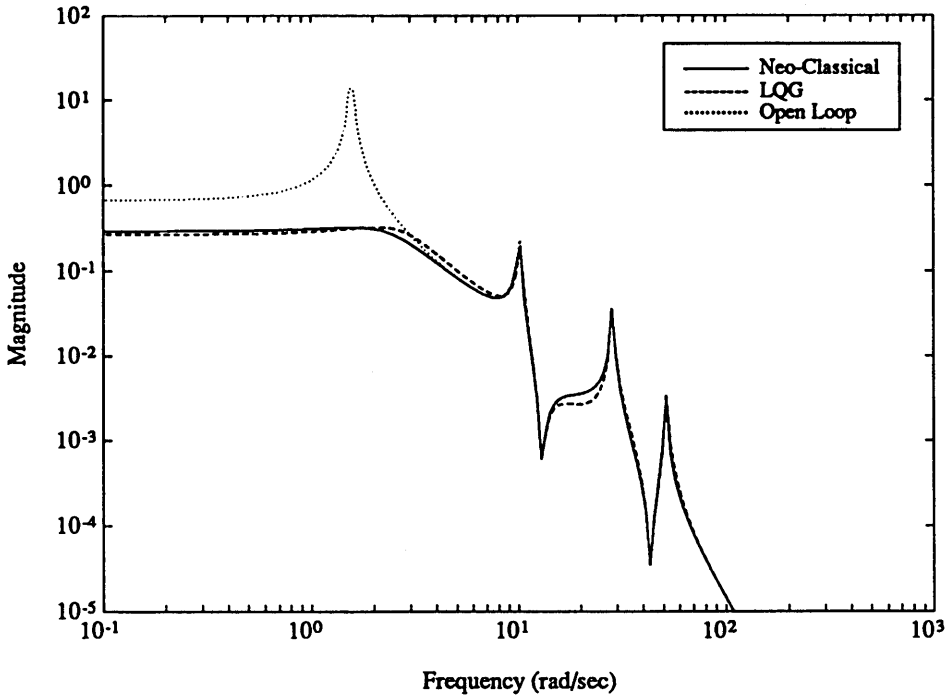

Figure 6.10(c). Open and closed loop disturbance to performance transfer functions for Typical Section 4. Performance improvement with both the Neo-Classical and LQG compensators is 24.0 dB.

is designed for approximately 3 rad/sec. Notice how the phase margin at crossover is larger for the LQG compensator. This is a result of not using the nonrobust lightly damped pole pairs. Figure 6.10(c) shows the open and closed loop disturbance to performance transfer functions for the two compensators in Figure 6.10(a), impinged on Typical Section 4A. The performance improvement for both designs is 24.0 dB.

6.5 Experimental Implementation

Noncollocated actuator sensor pair pose an interesting practical challenge for the control designer. Not only must the actuator sensor pair be able to pass the loop shaping test in Design Rule 3A, as shown in Chapter 5, but it also must contain a

frequency range where the input output transfer function resembles a collocated, or slightly noncollocated pair, i.e. alternating poles and zeros or nearly alternating poles and zeros.

In search of a noncollocated input output topology on the MACE test article, the pointing payload loop topology of MACE 1A was first examined, as shown in Figure 3.18, but using the output as the y-axis acceleration the node next to the gimbal (Figure 2.7). Design Rule 4A was used, because of the noncollocated sensor actuator pair. In examining the input output transfer function, nonminimum phase zeros were discovered at 1, 14, and 30 Hz. The performance metric was the integrated payload rate gyro, bandlimited from 0.5-50 Hz. This actuator sensor pair, as a result of the nonminimum phase zeros, was not a good choice for the control design, according to Design Rule 4B.

Next, the bus loop was examined, again using the y-axis acceleration on the same node. This topology is show in Figure 6.11 as MACE 4. The input u and the

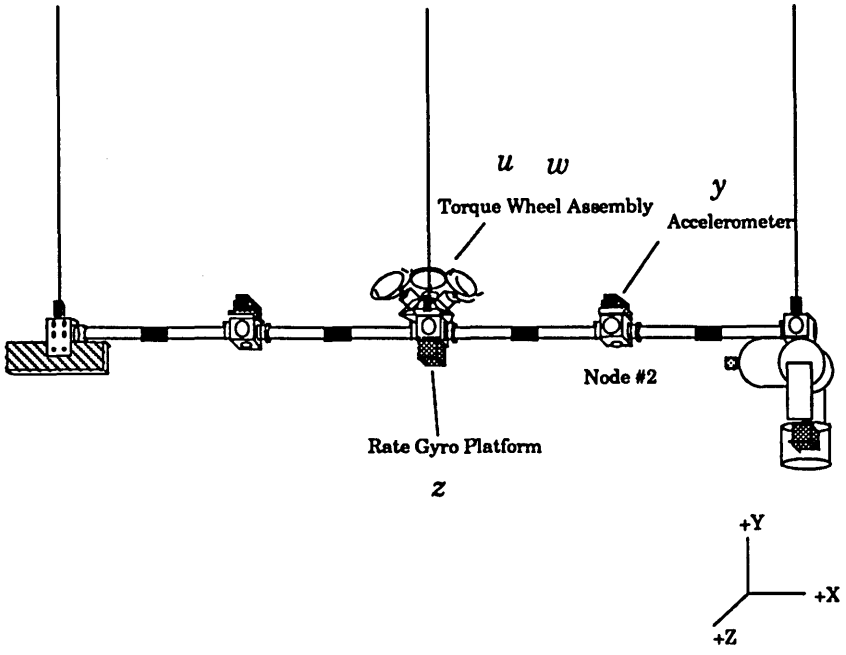

Figure 6.11. MACE 4: Topology for bus vibration reduction loop with the noncollocated accelerometer as the output.

disturbance w are the z-axis inertial torque produced by a rotation of the torque wheels at the center of the bus. The output y is the linear y-axis acceleration at node 2, and the performance z is the integrated rate gyro, at the center of the test article. The performance metric is bandlimited from 0.5-50 Hz.

Using Design Rule 4A, the open loop transfer function, g_{yu} was examined. Figure 6.12 shows the open loop transfer function from the z-axis torque wheels, to the y-axis acceleration. In this transfer function, there was a nonminimum phase zero at 0.8 Hz, and another at 60 Hz. Therefore, both Design Rule 4C and 4D were used. The bandwidth is limited by the open loop 60 Hz nonminimum phase zero to approximately 30-40 Hz. Design Rule 4D then was used. Control at low frequency was limited by the nonminimum phase zero at 0.8 Hz. In examining the pole zero pattern, however, from 2-30 Hz, it contains alternating poles and zeros. This is the

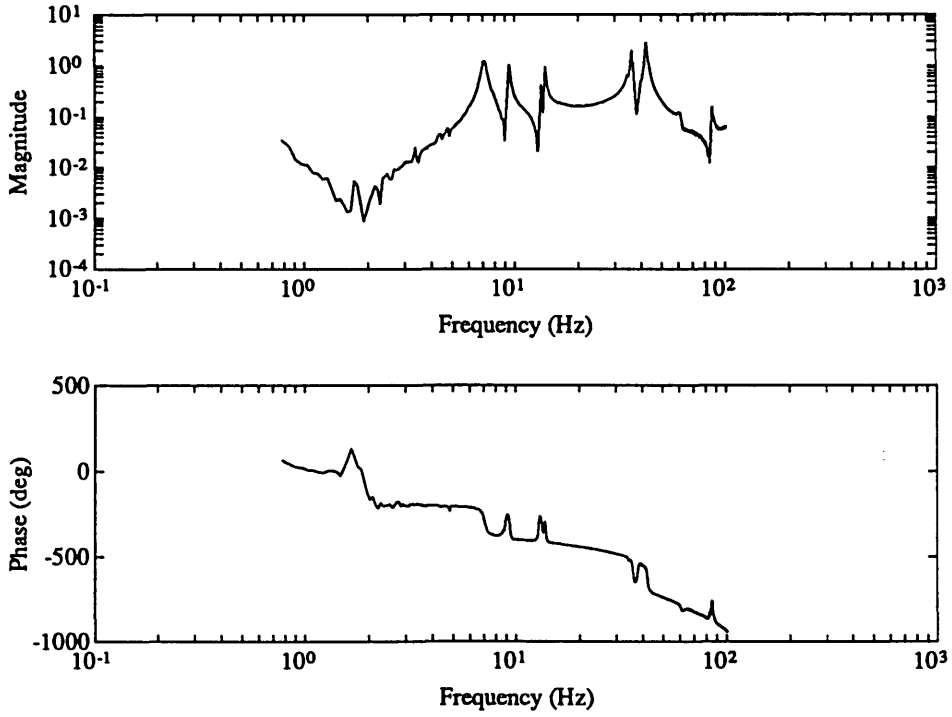

Figure 6.12. Measurement of the open loop input output transfer function g_{yu} from z-axis torque wheels to y-axis linear acceleration for MACE 4.

frequency range used in the control design.

Since the disturbance w and input u are analogous, and the performance z and the output y are not analogous, this topology falls into the Topology II category, (Topology IIB to be specific) and Design Rule 2 was used. Using Design Rule 2A, the filter dynamics, g_{zw}/g_{yu} were divided into the temporal relationship between z and y, and the structural filter g_o. Because the output is acceleration, and the performance is position, ϕ_o is a double integrator

$$\phi_o = \frac{1}{s^2} \tag{6.5}$$

And the structural filter g_o is given by

$$g_o = \frac{g_{zw}}{g_{yu}} s^2 \tag{6.6}$$

Using Design Rule 2B, a low frequency controller is designed, corresponding to a high gain controller, with the temporal relationship given in Equation 6.5. The low gain controller is a double integrator, or position feedback. Another low frequency controller must be used, however, due to the nonminimum phase zero at 0.8 Hz. Therefore, a controller was designed using rate feedback at all frequencies, or integral control.

Also, Because of the nonminimum phase zero at 0.8 Hz, the integral control, or rate feedback was only used at frequencies above 2 Hz. Therefore, instead of a pure integrator, a high pass integrator or lag filter was used, with a single pole at 2 Hz. A two pole, two zero lead filter was also added to the compensator to add phase lead at crossover. The gain of the compensator was then adjusted in order to create a loop crossover of approximately 20 Hz. This completed Design Rule 2C.

Following Design Rule 2D, a two pole rolloff filter was added (ω=100 Hz), as a result of possible closed loop stability problems with modes above 100 Hz.

Following Design Rule 2E, the loop transfer function consisting of the open loop system in Figure 6.11, and the compensator constructed from Design Rules 4D and 2A-D was examined. The modes at 36 and 42 Hz posed closed loop stability problems, and therefore needed gain stabilized. Two notch filters with nominal frequencies at 36 and 42 Hz were then constructed and convolved into the compensator.

According to Neo-Classical Design Rule 2F, the filter dynamics were examined for possible additions to the compensator. Figure 6.13 shows the g_{zw}/g_{yu} filter dynamics for MACE 4. Notice the large peaks at 9.4 and 14 Hz. The largest peak at 9.4 Hz was added to the compensator, by designing an inverse notch filter (ω=9.4 Hz, ζ=0.2, α=0.1). The resulting 9 state Neo-Classical compensator, designed for MACE 4, is shown in Figure 6.14(a).

Figure 6.14(b) shows the measured loop transfer function, $g_{yu}K$, of the 9 state

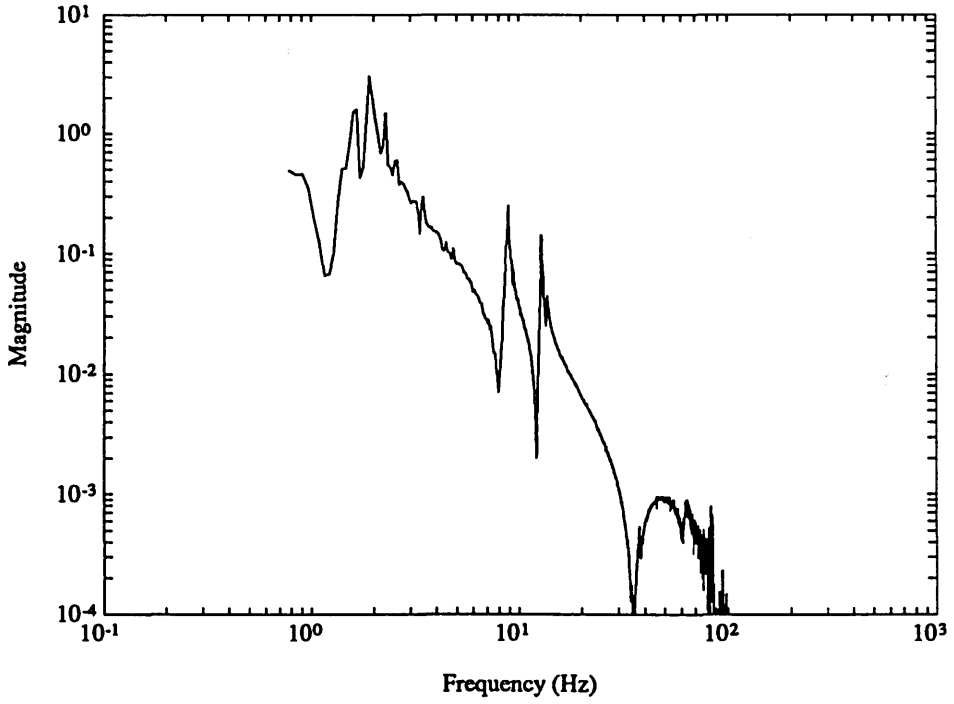

Figure 6.13. Measurement of the filter dynamics g_{zw}/g_{yu}, for MACE 4.

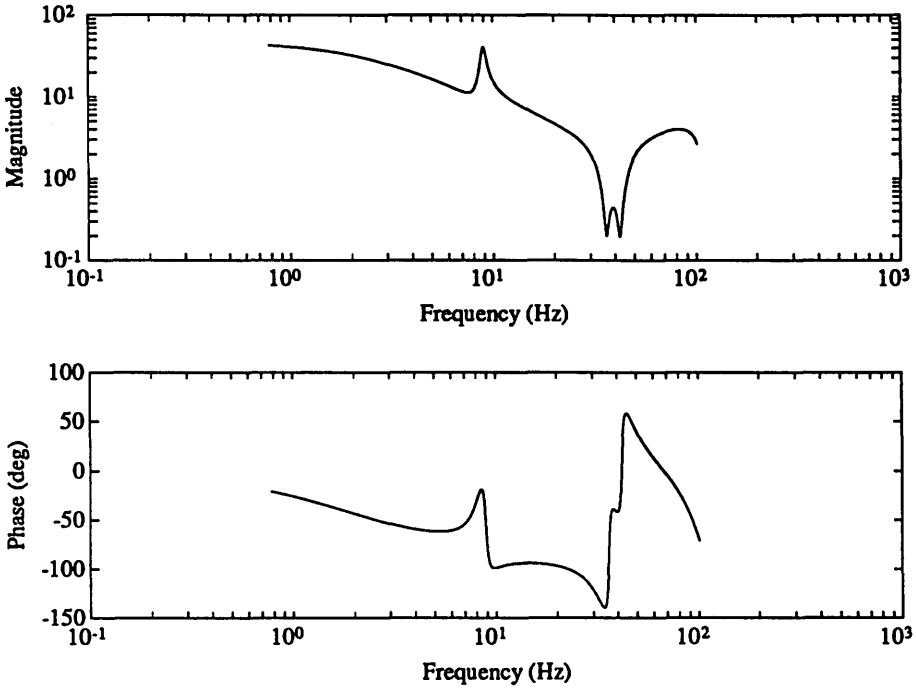

Figure 6.14(a). 9 state Neo-Classical compensator K for MACE 4: 2 states for the high pass filter; 4 states for the 36 and 42 Hz notch filters; 2 states for a filter dynamics; 1 state for the 100 Hz rolloff.

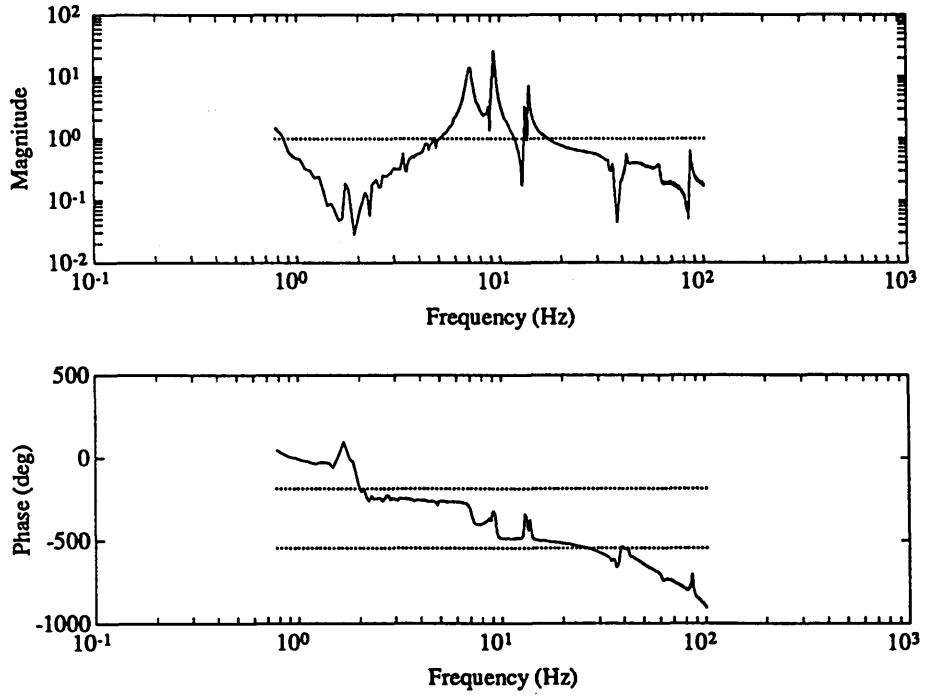

Figure 6.14(b). Measurement of the loop transfer function $g_{yu}K$ consisting of the 9 state Neo-Classical compensator and open loop transfer function.

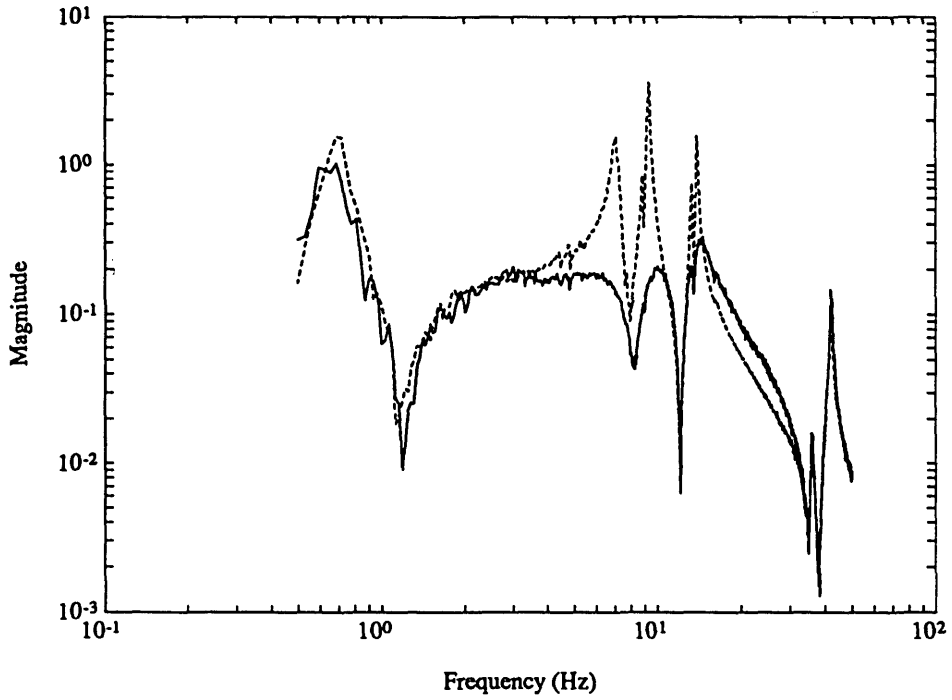

Figure 6.14(c). Measurement of the open and closed loop disturbance to performance transfer functions for MACE 4. Performance improvement with the 9 state Neo-Classical compensator was 9 dB.

Neo-Classical compensator (Figure 6.14(a)), and the open loop transfer function (Figure 6.12) for MACE 4. Notice how the modes within the 20 Hz bandwidth (Regions 1 and 2) at 6.8, 9.4, and 14 Hz all rise above the 0 dB line, and the modes above the bandwidth (Region 3) at 36 and 42 Hz are gain stabilized. The modes above 0 dB are being controlled. Figure 6.14(c) shows the measurement of the open and closed loop disturbance to performance transfer functions. The performance improvement was 9 dB. Notice how the compensator does not provide closed loop performance improvement below 2 Hz, as a result of the nonminimum phase zero and subsequent compensator design. But the reduction of the peaks at 6.8, 9.4, and 14 Hz was quite good, especially near 9.4 Hz, as a result of the added filter dynamics in the compensator.

Chapter 7

MIMO Control

7.1 Introduction

This chapter shows the adaptation of the SISO Neo-Classical Design rules presented previous chapters to the MIMO problem. These classical MIMO compensators include High Authority Control/Low Authority Control (HAC/LAC), and sequential loop closure. Two MIMO system will be examined on the MACE test article, each having two inputs, two outputs, one disturbance, and one performance. A summary of optimal LQG and SWLQG compensators for the MIMO problem will be made, followed by a discussion of the HAC/LAC and sequential loop closure methods. Finally, the experimental closed loop results for the MIMO controllers will be shown. The LQG and SWLQG compensators are also designed and implemented for comparison with the classical designs.

7.2 Optimal Compensation

Optimal LQG and SWLQG compensators are designed in the same manner for this MIMO input output system as in the SISO systems discussed in Section 2.3. The weighting matrices Q and W are identical to those in the previous compensators, defined by the performance and disturbance. These weighting matrices are given in Equations 2.9 and 2.12.

The weighting matrices R and V describe the influence of the inputs and outputs respectively in the LQR and Kalman Filter problems. It is assumed that these matrices are diagonal, as shown below

$$R = \rho R_o \tag{7.1}$$

$$V = \mu V_o \tag{7.2}$$

where R_o and V_o are diagonal, and ρ and μ are the positive scalar LQR and Kalman Filter weightings. The diagonal matrices are constructed using Bryson's Method [Bryson (1969)] for scaling in the LQG problem. For the R_o matrix, the diagonal entry is the inverse of the square of the corresponding maximum actuator input. The two actuators in this problem are the z-axis gimbal and z-axis torque wheels and the R_o matrix is

$$R_o = \begin{bmatrix} \dfrac{1}{(u_{gim})^2_{max}} & 0 \\ 0 & \dfrac{1}{(u_{tw})^2_{max}} \end{bmatrix} = \begin{bmatrix} \dfrac{1}{(0.658\text{Nm})^2} & 0 \\ 0 & \dfrac{1}{(0.087\text{Nm})^2} \end{bmatrix} \tag{7.3}$$

The V_o matrix is scaled in a similar manner, using the inverse of the square of the corresponding maximum sensor output. For the examples on the MACE test article, the two sensors are the rate gyros at the center of the bus, and in the payload.

Therefore, the scaling matrix V_o is diagonal.

$$V_o = \begin{bmatrix} \frac{1}{(y_{rg})^2_{max}} & 0 \\ 0 & \frac{1}{(y_{rg})^2_{max}} \end{bmatrix} = \begin{bmatrix} \frac{1}{\left(75\frac{deg}{sec}\right)^2} & 0 \\ 0 & \frac{1}{\left(75\frac{deg}{sec}\right)^2} \end{bmatrix} \tag{7.4}$$

The Kalman Filter weighting μ is usually smaller than the LQR weighting ρ, to ensure faster dynamics in the estimator. The LQR weighting is then varied to change the bandwidth of the closed loop system, thus changing the closed loop performance improvement.

The LQG compensator is given by

$$K(s) = G\left(sI - A + B_u G + HC_y\right)^{-1} H \tag{7.7}$$

where G is the 2×n LQR optimal LQR gain matrix, and H is the n×2 optimal Kalman Filter gain matrix, where n is the number of states.

7.3 Classical Compensation

There were two types of MIMO classical compensation implemented on the MACE test article. The first is a High Authority Control/Low Authority Control (HAC/LAC) compensator [Gupta *et al.* (1984)]. First a low authority controller, usually collocated velocity feedback, is closed on the structure. Active damping is added to critical modes, usually modes near the crossover region of a subsequent loop. By adding damping to these modes, not only will the model errors be smaller, especially in the phase, but the subsequent control design will be easier and more robust.

The second type of classical MIMO compensator designed for implementation is sequential loop closure [Maciejowski (1989)]. SISO compensators are designed one loop at a time, starting with the fastest or highest bandwidth loop. As one loop is closed, the subsequent loop of smaller bandwidth is designed around the new plant. These SISO compensators are designed using the Neo-Classical Design Rules presented previously.

7.4 Experimental Implementation

MIMO Payload Pointing Loop

Two topologies of the MACE test article will be examined, both with two inputs, two outputs, one performance and one disturbance. Figure 7.1 shows the first MIMO topology, MACE 5A. It is quite similar to MACE 1A, the payload pointing loop shown in Figure 3.15, since the disturbance and performance are the

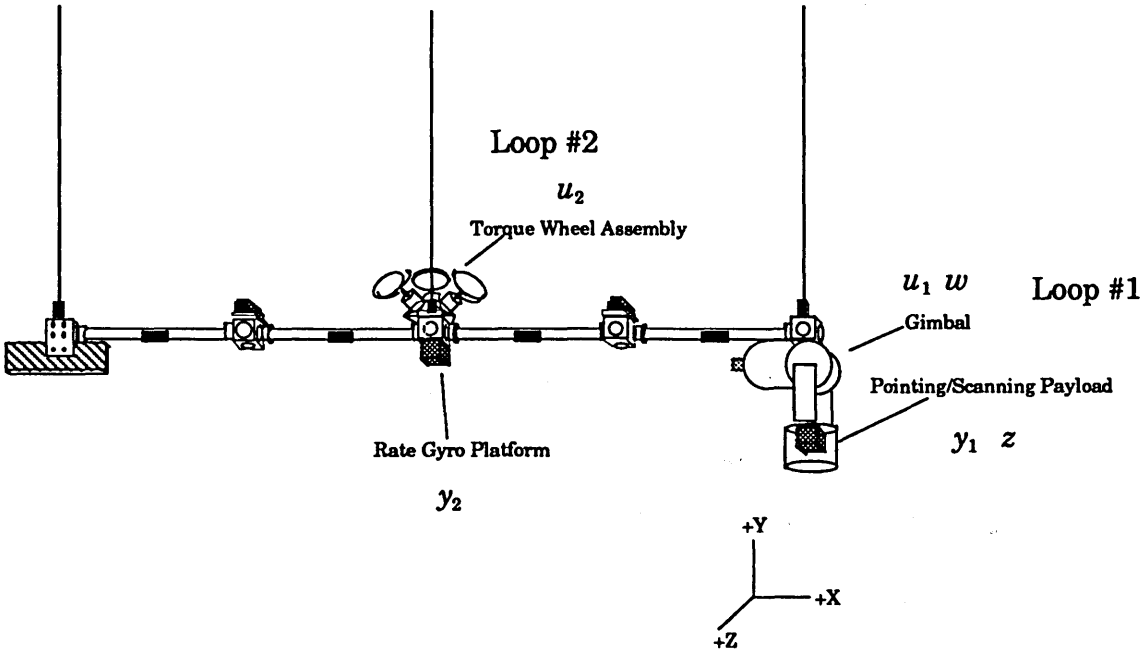

Figure 7.1. MACE 5A: Topology for the MIMO payload pointing loop.

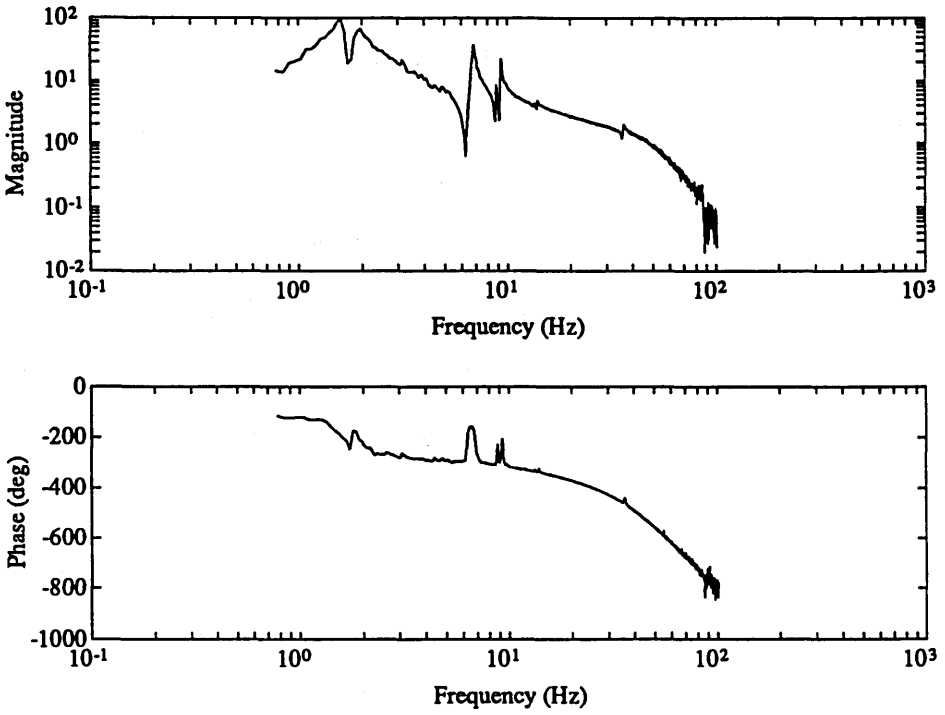

Figure 7.2. Measurement of the open loop input output transfer function for Loop #1: z-axis gimbal u_1, to z-axis payload rate gyro, y_1.

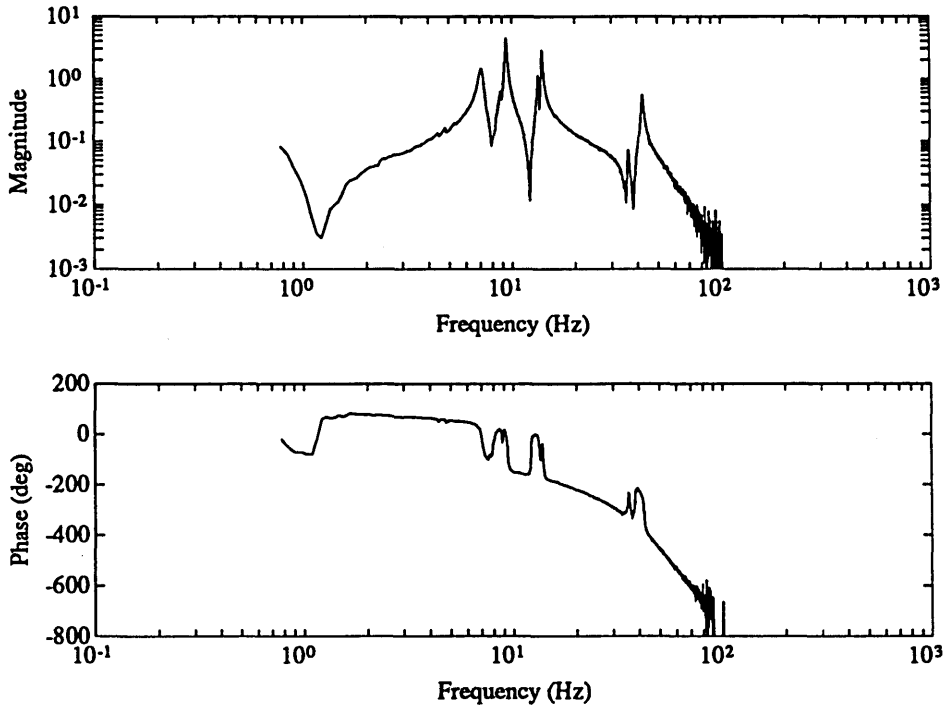

Figure 7.3. Measurement of the open loop input output transfer function for Loop #2: z axis torque wheels u_2, to z-axis bus rate gyro, y_2.

same. The disturbance w is the relative torque of the z-axis gimbal, and the performance metric z is the integrated payload rate gyro, or inertial payload angle, bandlimited from 0.5-50 Hz. The two inputs include the relative torque of the z-axis gimbal u_1, and inertial torque produced by the z-axis torque wheels u_2. The two outputs include the rate gyro in the payload y_1, and the rate gyro at the center of the bus y_2. Figure 7.2 shows the open loop transfer function g_{yu} from the z-axis gimbal, u_1, to the z-axis rate gyro in the payload, y_1, for Loop #1. Figure 7.3 shows the open loop transfer function g_{yu} from the z-axis torque wheels, u_2, to the bus rate gyro, y_2. for Loop #2.

The measurement of the open and closed loop disturbance to performance transfer functions for a model based 30 state two input two output LQG compensator are shown in Figure 7.4. This can be compared to the with the closed

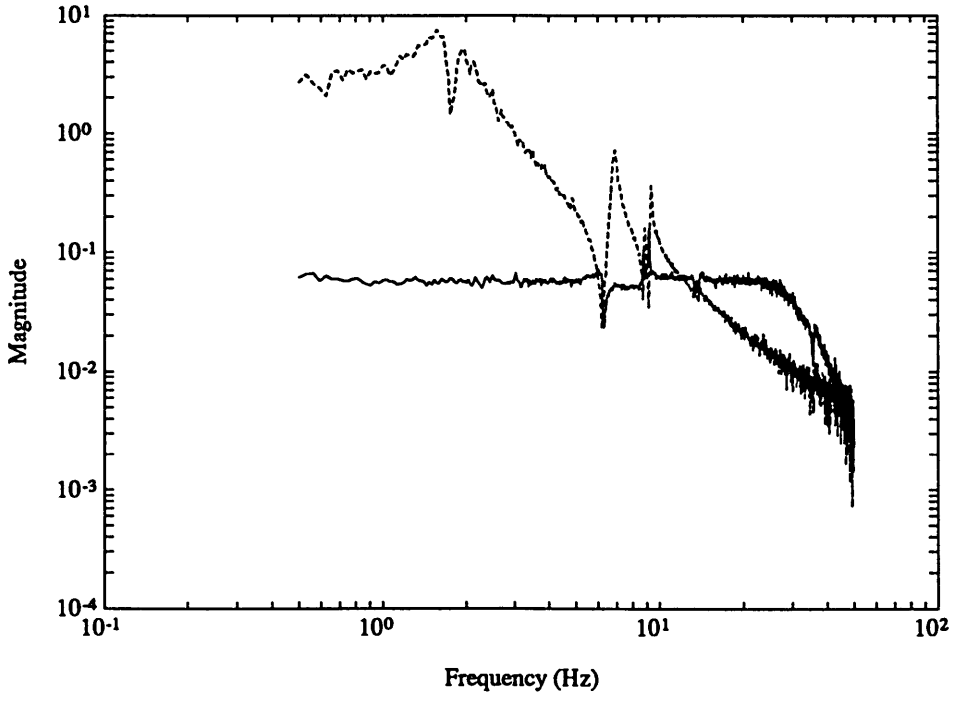

Figure 7.4. Measured open and closed loop disturbance to performance transfer functions with the model based 30 state MIMO LQG compensator for MACE 5A. Performance improvement was 25.4 dB.

loop system of the 23 state SISO LQG shown in Figure 3.20(c). They are quite similar, except the closed loop system with the MIMO LQG compensator is smoother in the region from 5 to 30 Hz. The SISO LQG compensator in Figure 3.20(a) contains weak pole zero inversions (Region 2) for the modes in this frequency range. Because the model is not exact in that region, and the inversions are not exact. The closed loop system is not smooth. The MIMO LQG closed loop, however, is much smoother. The MIMO LQG compensator does not use these pole zero inversions that the SISO LQG compensator does. The additional loops add damping and robustness to the closed loop system. The closed loop performance improvement, however, did not change (25.4 dB for MIMO LQG versus 25.7 dB for SISO LQG).

Figure 7.5 shows the measurement of the open and closed loop transfer function for a model based 30 state two input two output SWLQG compensator. The

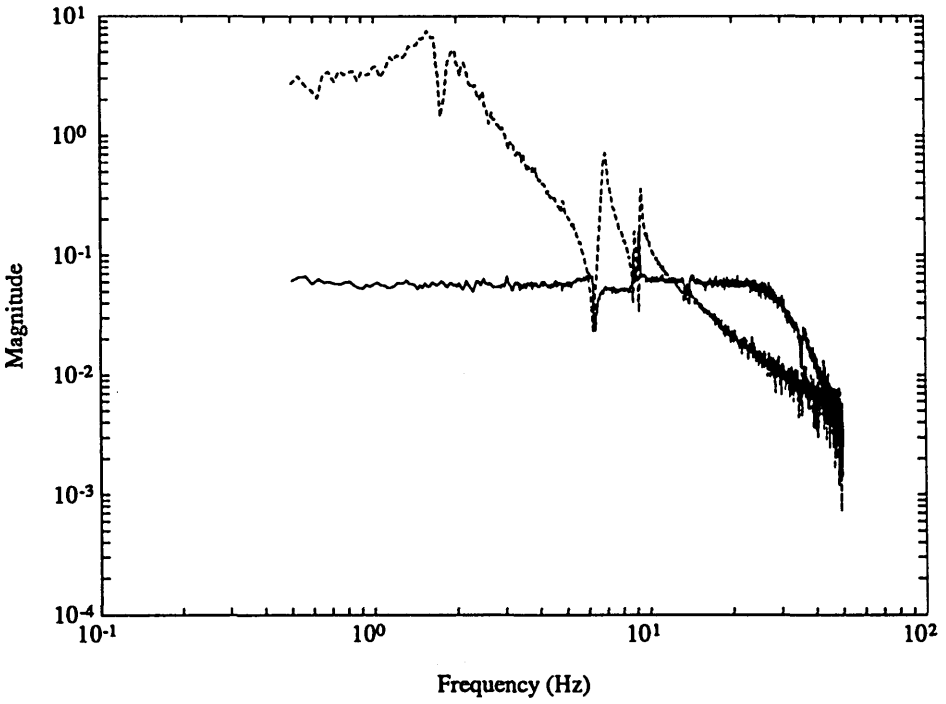

Figure 7.5. Measured open and closed loop disturbance to performance transfer functions with the model based 30 state MIMO SWLQG compensator for MACE 5A. Performance improvement was 25.3 dB.

modes at 6.8, 8.8, 9.4, and 14 Hz were de-sensitized. The closed loop performance improvement (25.4 dB) was similar to that of the MIMO LQG compensator (25.3 dB). The limiting factor of this control design, therefore, was not closed loop stability problems, but phase delay in the system. Notice the higher frequency amplification as a result of the compensation for this delay, as in the previous designs.

A high authority, low authority control design (HAC/LAC) was then attempted. The low authority loop was Loop #2, u_2 to y_2, and the high authority loop was Loop #1, u_1 to y_1. Notice that the low authority loop, Loop #2, actually falls into the Topology III category, since the disturbance or input are not analogous, and the performance and output are not analogous. This is identical to MACE 4 design shown in Figure 5.18(a)-(c). The low authority loop was designed using rate feedback, and when Neo-Classical Design Rule 3 was used for MACE 3, the resulting

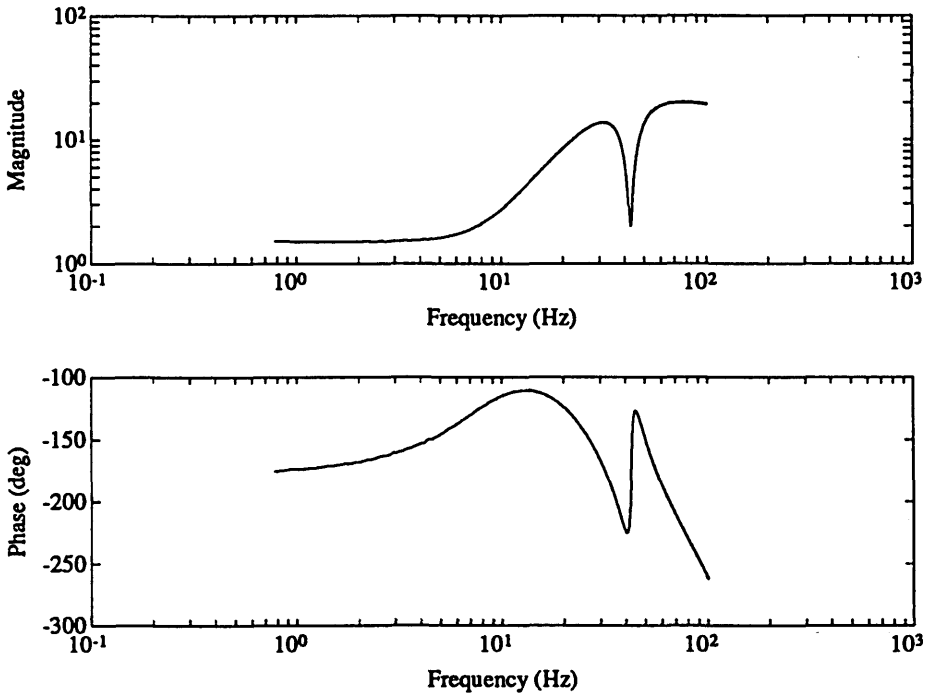

Figure 7.6. 7 state Neo-Classical compensator for the low authority loop, loop #2: 2 states for the high pass filter; 2 states for a lead filter; 2 states for the 36 Hz notch filter; 1 state for the 100 Hz rolloff.

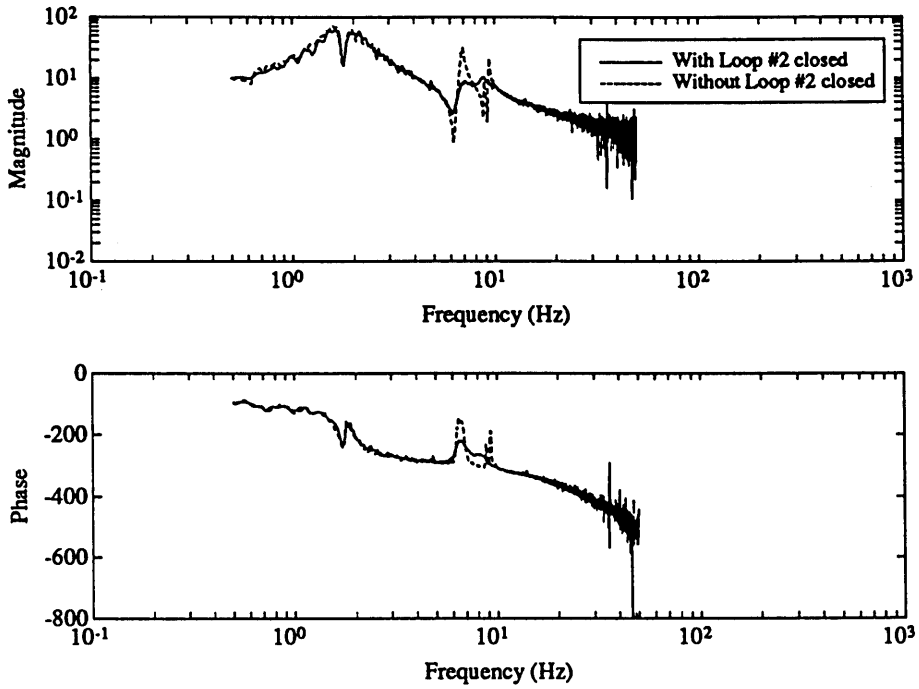

Figure 7.7. Measurement of the open loop transfer function for Loop #1 with and without the low authority loop closed for MACE 5A.

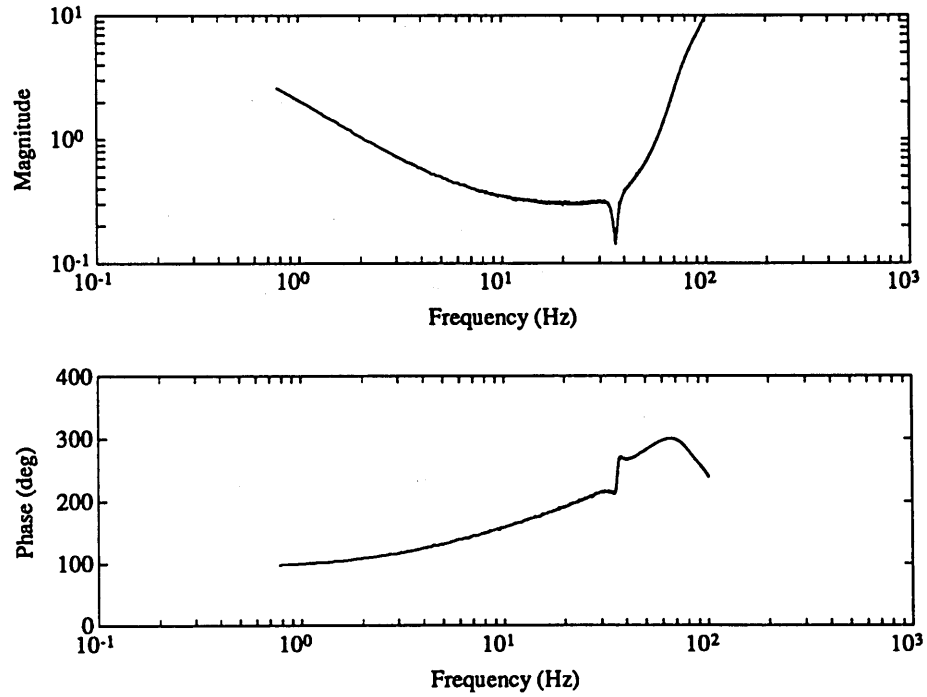

Figure 7.8. 12 state Neo-Classical compensator for the high authority loop, loop #1: 2 states for the stabilized integrator; 8 states for the lead filters; 2 states for the 36 Hz notch filter.

compensator used rate feedback at all frequencies. Therefore, the low authority controller is identical to the Neo-Classical design in Figures 5.18(a)-(c). The resulting 7 state Neo-Classical compensator is shown in Figure 7.6.

The design of the subsequent high authority loop for Loop #1, u_1 to y_1, is designed around the new plant, with Loop #2 closed. Figure 7.7 shows the open loop transfer function for Loop #1 with and without Loop #2 closed. Notice how the modes between 5 and 15 Hz are all damped by the low authority controller. The Neo-Classical design for Loop #1 falls into the Topology I category, since the disturbance and input are analogs, as are the performance and output. Therefore, Neo-Classical Design Rule 1 is used. This design is identical to the design created in for MACE 1A, except for the new open loop system is shown in Figure 7.7. Notice how the open loop transfer function in Figure 7.7 is identical around the crossover region (20 Hz) with or without Loop #2 closed. The high authority compensator is a Neo-Classical compensator, therefore, identical to that designed for MACE 1A shown in Figure 3.20(a) The resulting 12 state controller is shown in Figure 7.8.

Figure 7.9 shows the measurement of the open and closed loop disturbance to performance transfer functions for the HAC/LAC design for MACE 5A. The resulting closed loop transfer function is smoother within the closed loop bandwidth than the SISO Neo-Classical closed loop design for MACE 1A shown in Figure 3.20(c). The closed loop transfer function is also smooth, similar to the LQG and SWLQG compensators in Figures 7.4 and 7.5. Although the LAC does not add a lot of robustness to the closed loop system because the modes are not in the crossover region, the performance improvement did increase by a small amount, to 26.6 dB. Note that the HAC/LAC performance (26.6 dB) was better than that of the LQG (25.4 dB) and SWLQG (25.3 dB).

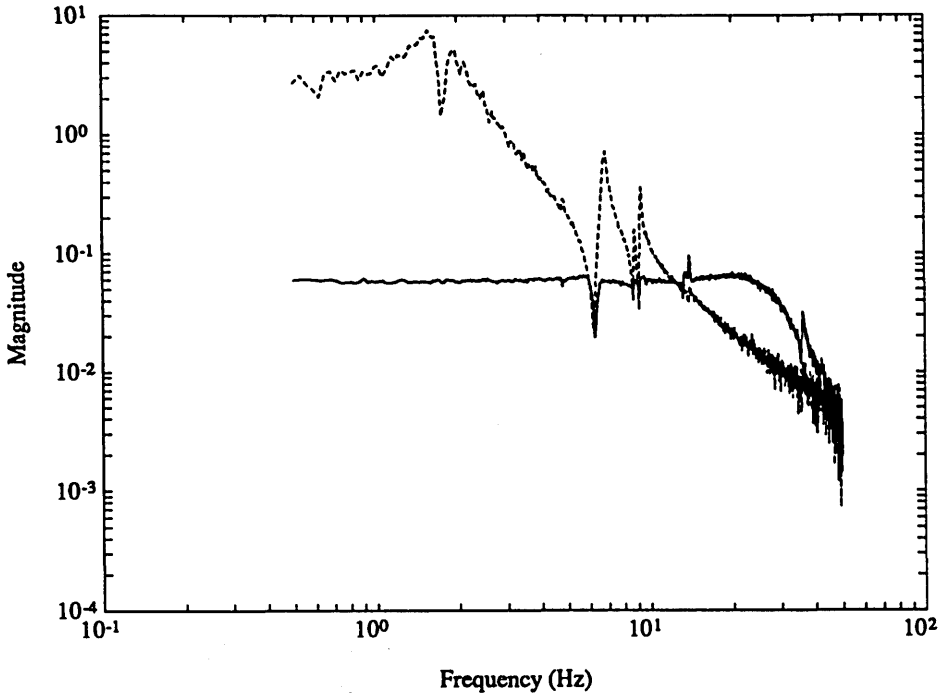

Figure 7.9. Measured open and closed loop disturbance to performance transfer functions with the 12/7 state HAC/LAC compensator for MACE 5A. Performance improvement was 26.6 dB.

MIMO Payload Pointing Loop with Torque Wheel Disturbance

The next MACE topology examined was similar to the first, except the disturbance was noncollocated from the performance at the payload. It was placed at the torque wheels. This topology, MACE 5B, shown in Figure 7.10, has the same disturbance and performance as the SISO MACE 2 topology in Figure 4.15.

A model based 36 state two input two output LQG compensator was first designed for this topology. The measured open and closed loop disturbance to performance transfer functions are shown in Figure 7.11. Notice how the MIMO compensator reduced the peaks at 6.8 and 9.4 Hz, where the SISO LQG compensator, in which only Loop #1 was closed, did not (Figure 4.18(c)). The low frequency disturbance rejection, however, is poor. This is a result of modelling

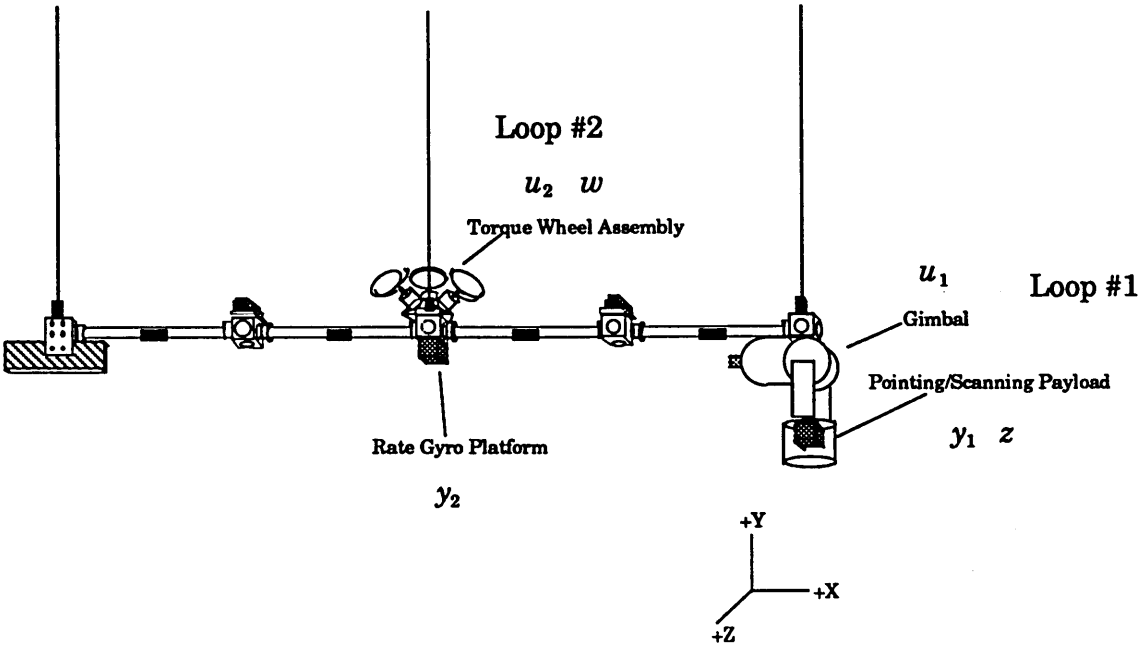

Figure 7.10. MACE 5B: Topology for the MIMO payload pointing loop topology, from the torque wheel disturbance.

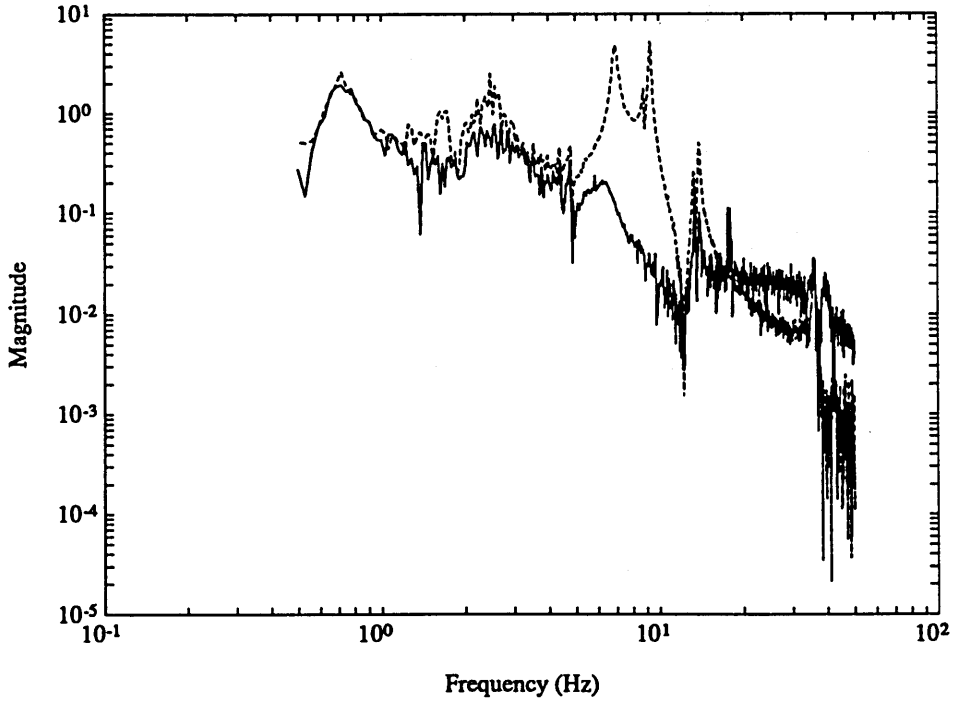

Figure 7.11. Measured open and closed loop disturbance to performance transfer functions with the model based 36 state MIMO LQG compensator for MACE 5B. Performance improvement was 11.2 dB.

errors. Figure C.3 shows the open loop transfer function from z-axis torque wheels to z-axis payload rate gyro. Notice that at low frequency, the magnitude of the model is in error by at least 10 dB. This error could affect the experimentally measured closed loop performance when using the model based compensator. The performance improvement of this design was 11.2 dB, equivalent to the SISO LQG closed loop system, with only Loop #1 closed, shown in Figure 4.18(c).

A model based SWLQG compensator was then designed for this topology. The modes at 1.2, 6.8, and 9.4 Hz were de-sensitized, in order to attempt to improve performance at lower frequency. Figure 7.12 shows the measurement of the open and closed loop disturbance to performance transfer functions. Notice the increased closed loop performance at low frequency. However, the reduction of the resonances at 6.8 and 9.4 Hz has been adversely affected. The performance improvement has

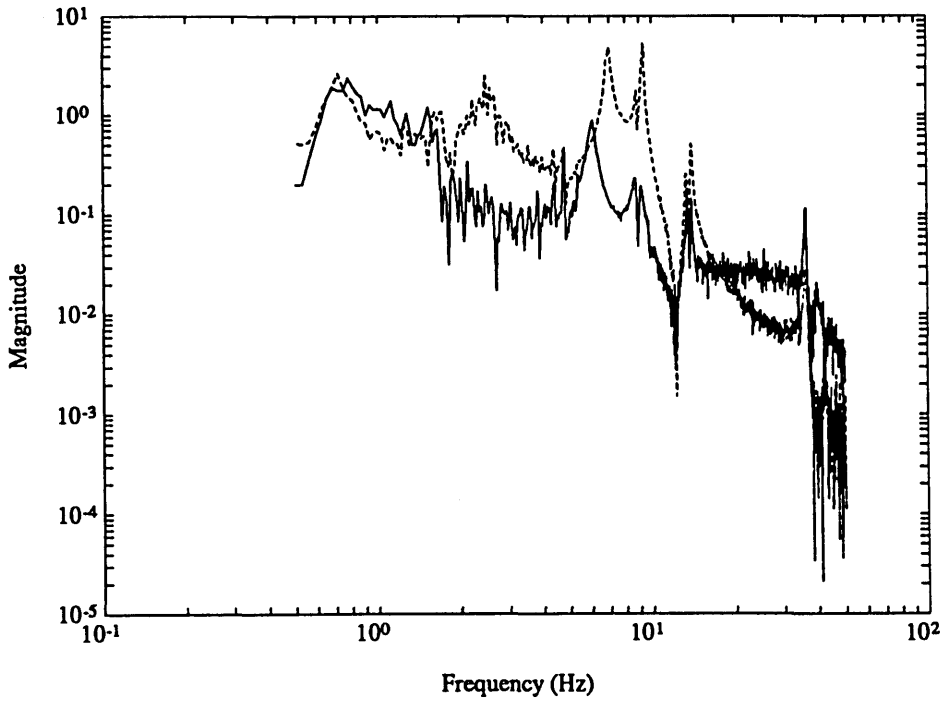

Figure 7.12. Measured open and closed loop disturbance to performance transfer functions with the model based 36 state MIMO SWLQG compensator MACE 5B. Performance improvement was 9.6 dB.

decreased from 11.2 dB (LQG) to 9.6 dB (SWLQG).

The final MIMO compensator design was a two input two output sequential loop closure design, for the same topology, MACE 5B. The two loops closed were the payload pointing loop, Loop #1, u_1 to y_1, and the bus loop, Loop #2, u_2 to y_2. These two loops, in comparison with the disturbance performance pair, both fall into the Topology II category. For Loop #1, the output y_1 and performance z are analogs, and for Loop #2, the input u_2 and disturbance w are analogs. Both loops were therefore designed using Neo-Classical Design Rule 2.

The first loop closed is the high bandwidth loop, Loop #1, was shown in the SISO case for MACE 2. The 16 state Neo-Classical design is shown in Figures 4.22(a)-(c). The bandwidth of this loop was 20 Hz. The 16 state Neo-Classical compensator designed for Loop #1 is shown in Figure 7.13.

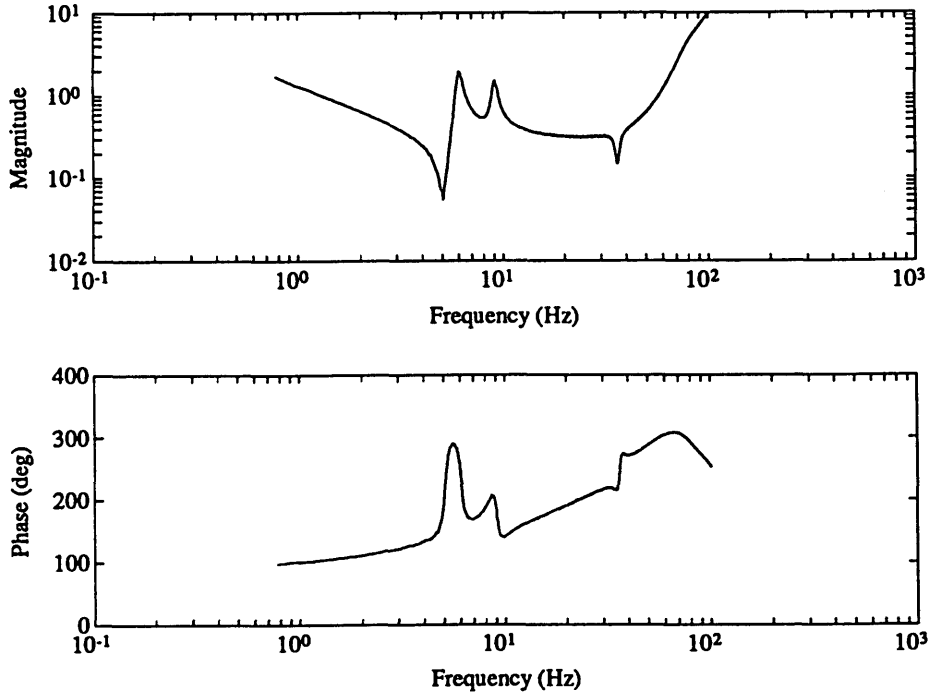

Figure 7.13. 16 state Neo-Classical compensator for loop #1 in MACE 5B: 2 states for the stabilized integrator; 8 states for the lead filters; 2 states for the 36 Hz notch filter; 4 states for filter dynamics.

With this loop closed, the compensator for Loop #2, was designed, also using Design Rule 2. The open loop plant, however, changed because Loop #1 was closed. Figure 7.14 shows the input output transfer function for Loop #2 with Loop #1 closed. Notice the low frequency dynamics have changed, but above 10 Hz, the dynamics were not affected.

The compensator designed for Loop #2, which contains 16 states, is very similar to the Neo-Classical compensator designed for the first loop. It is a 16 state compensator: 2 states for the stabilized integrator; 8 states for the lead filters; 2 states for the 36 Hz notch filter; and 4 states for the filter dynamics g_{zw}/g_{yu}. The resulting compensator is equivalent to the first Neo-Classical compensator, except for a deeper notch filter, and filter dynamics. This 16 state Neo-Classical compensator is shown in Figure 7.15. The bandwidth of this loop was approximately 15 Hz.

Although the bandwidths of the two loops were similar, there were no closed loop stability problems. Figure 7.16 shows the measurement of the open and closed loop disturbance to performance transfer functions for the sequential loop designs for MACE 5B. Notice how the sequential loop closure design (Figure 7.16) accomplished tasks that none of the other SISO or MIMO compensators have done (Figures 4.18(c), 4.20(c), 4.22(c), 7.11, 7.12), namely low frequency disturbance rejection and resonant peak reduction at 6.8 and 9.4 Hz. The closed loop performance improvement with this compensator was 19.9 dB, larger that of the previous MIMO compensators (11.2 dB for LQG, 9.6 dB for SWLQG).

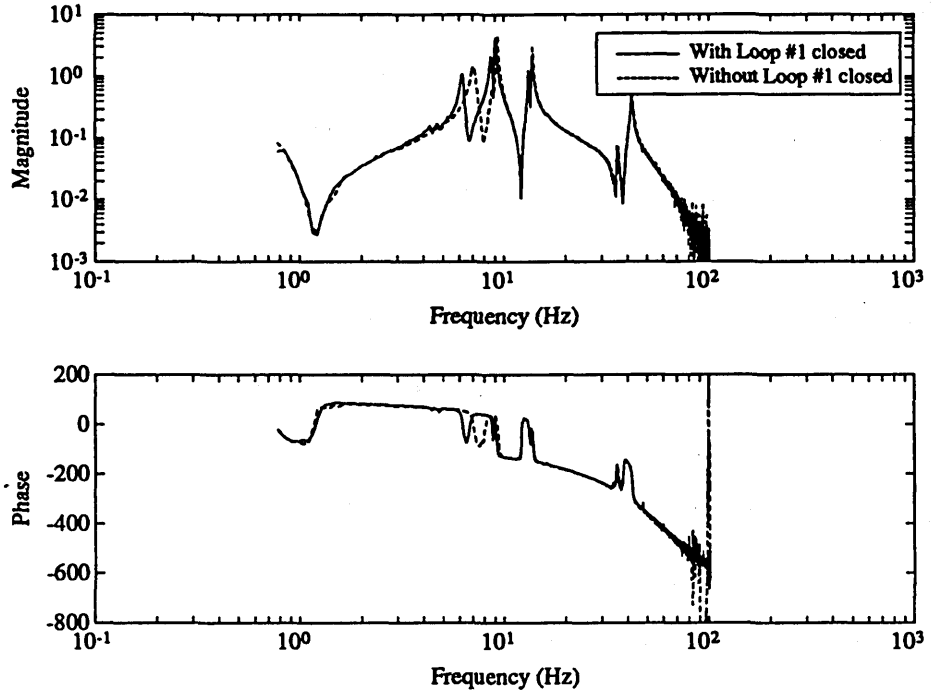

Figure 7.14. Measurement of the open loop transfer function of Loop #2 for MACE 5B with and without Loop #1 closed.

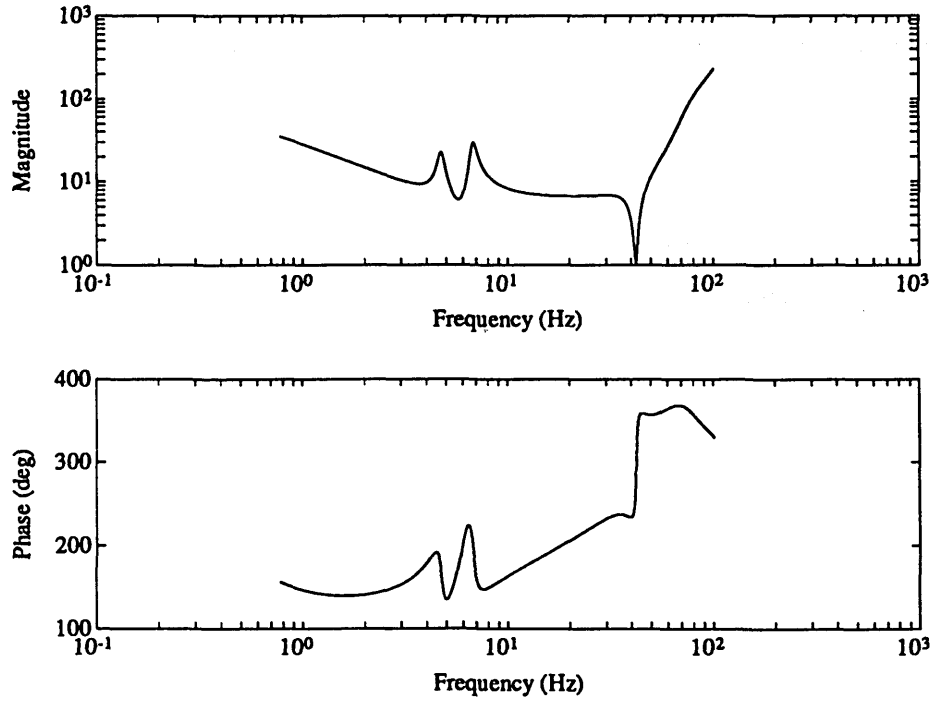

Figure 7.15. 16 state Neo-Classical compensator for loop #2 in MACE 5B: 2 states for the stabilized integrator; 8 states for the lead filters; 2 states for the 36 Hz notch filter; 4 states for filter dynamics.

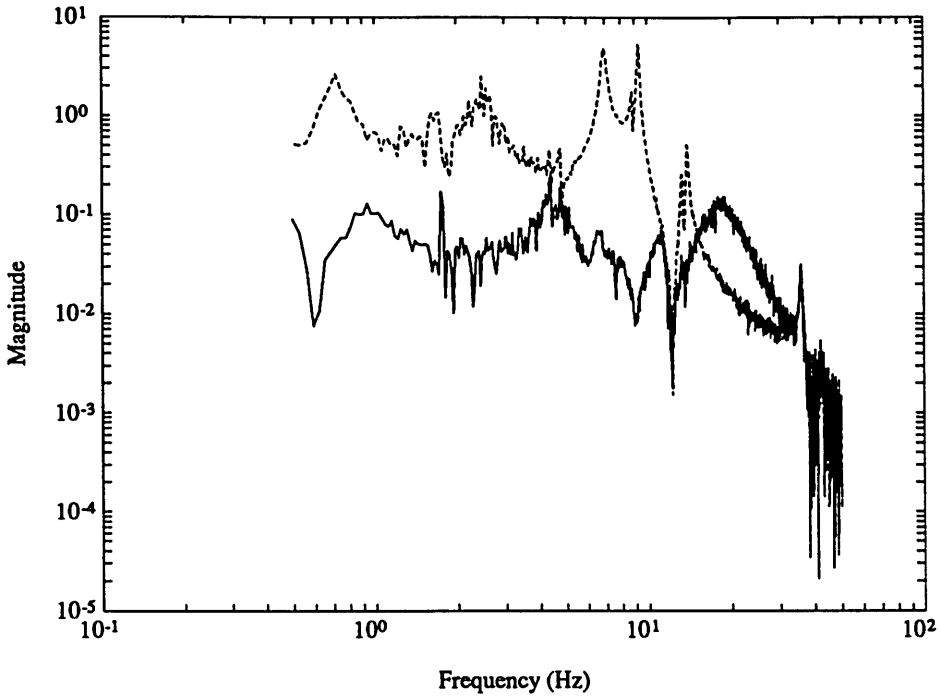

Figure 7.16. Measured open and closed loop disturbance to performance transfer functions for the 16/16 state sequential loop compensator MACE 5B. Performance improvement was 19.9 dB.

Chapter 8

Conclusions and Recommendations

Conclusions

Neo-Classical control design techniques have been developed for controlled structures. Neo-Classical Control combines the loop assignments and complex topological design of LQG controllers, the robustness of SWLQG controllers, and the lower order, robustness, and practical insight of classical controllers, into a control strategy for structures. For the problems examined, the Neo-Classical compensators were lower order, more robust, and deliver equal or superior performance when compensated to the optimal LQG and SWLQG techniques.

In order to understand the form of the optimal compensation used to motivate the Neo-Classical techniques, the asymptotic properties of the LQG compensator were examined. For low noise (small μ) and expensive control (large ρ), the SISO LQG compensator converges to a rate feedback, low gain inversion of the disturbance to output transfer function, except for the most dominant mode. If the disturbance to output transfer function has two dominant modes, the compensator

places a weighted zero pair between the two open pole pairs. For low noise (small μ) and cheap control (small ρ), the SISO LQG compensator converged to a high gain compensator, where the zeros are the zeros of the disturbance to performance transfer function, and the poles are a weighted average of the zeros of the disturbance to output and input to performance transfer functions. Making the assumption that the Kalman Filter weighting is smaller than the LQR weighting, the poles of the high gain asymptote are identical to those of the low gain asymptote, i.e. the zeros of the disturbance to output transfer function.

The low gain asymptote is dependent upon the disturbance to output transfer function being minimum phase, and the high gain asymptote is dependent upon both the disturbance to output and input to performance transfer functions being minimum phase. The rate convergence of the asymptotes is also affected by regularity of the pole zero patterns of these transfer functions as well.

The SISO disturbance rejection problem can divided into three categories, depending upon the relationship between the performance and output, and disturbance and input. If the performance and output are collocated and dual, they are said to be analogs. If the disturbance and input are collocated and dual, they are said to be analogs.

For the case where the performance and output are analogs, and the disturbance and input are analogs, and the input and output are collocated, dual, and complementary extreme, the types of compensation for the structural modes depends upon their location in the loop transfer function. For Region 1, at low frequency within the bandwidth, the LQG compensator is a high gain controller, with the temporal relationship between the performance and output, and pole zero cancellations. This compensator is also identical to the disturbance to performance transfer function minimizing compensator. For Region 4, at high frequency, the LQG compensator is an inversion of the input output transfer function, except for

the dominant mode. For Regions 2 and 3, which make up the region of the loop transfer function before and after loop crossover, the LQG compensator is a combination of both the open loop inversion, and open loop pole zero cancellation.

For this same topology, if the SWLQG compensator is de-sensitized to mode in Region 2, the compensator pole and zero pairs in that region damp, and migrate together, creating pole zero cancellations. If the SWLQG compensator is de-sensitized to mode in Region 3, the compensator pole pairs damp quickly, however the zero pairs do not, thus creating a controller resembling a notch filter.

The design rule for Topology I was created, based upon the analysis of the LQG and SWLQG compensators. In Region 1, the compensator is a high gain compensator, with the temporal relationship between the performance and output. In Region 2, no dynamics are added because the SWLQG compensator suggests they are nonrobust. In Region 3, the SWLQG compensator robustifies the compensator pole zero inversions by creating notch filters. And in Region 4, the dynamics are superfluous because they do not affect the closed loop stability or robustness of the system.

If the open loop input output transfer function contains multiple dominant modes, the LQG compensator is very similar to that of the compensator of a single dominant mode. If the multiple dominant modes lie in Region 2, the LQG compensator creates a weak pole zero inversion, similar in the single mode case. And if the modes are in Region 1, the compensator contains pole zero cancellations, identical to that of the single dominant mode case.

For the topology where the disturbance and input are analogs, but the performance and output are not, and the input output pair is collocated, dual, and complementary extreme, Topology IIA, the LQG and SWLQG analysis is very similar to that of the first case. The only difference is that in Regions 1 and 2, the LQG compensator creates a high gain filter, g_{zw}/g_{yu} instead of only the temporal

relationship between the performance and output. This high gain compensator is also identical to the disturbance to performance transfer function minimizing compensator.

For the topology where the performance and output are analogs, but the disturbance and input are not, and the input output pair is collocated, dual, and complementary extreme, Topology IIB, the LQG and SWLQG analysis is not very similar to either Topology I or Topology IIA. The LQG compensators, for most values of the Kalman Filter and LQR weightings are unstable and nonminimum phase. These compensation techniques are shown to be nonrobust by comparison with the SWLQG compensator. The LQG compensator, which should create the high gain LQG asymptote in Region 1, does not because the pole zero pattern of the disturbance to output transfer function is not alternating poles and zeros. The magnitude of the compensator in Region 1, instead of creating the high gain LQG asymptote with the filter g_{zw}/g_{yw}, creates the magnitude of the disturbance to performance transfer function minimizing compensator, g_{zw}/g_{yu}.

Because the transfer function minimizing compensator and closed loop system for Topology IIB is identical to that of Topology IIA, the Neo-Classical design rule is generalized for both cases. For this design rule, the filter dynamics g_{zw}/g_{yu} are split into the temporal relationship between the performance and output, and a structural filter. The design rule then is identical to those in Topology I, except the final step is to add stable, minimum phase dynamics representing the structural filter to the compensator in Regions 1 and 2.

For the general SISO disturbance rejection case, where the performance and output are nonanalogous, and the disturbance and input are nonanalogous Topology III, the LQG compensators do not match the asymptotes, as a result of the pole zero patterns of the disturbance to output and input to performance transfer functions not being alternating poles and zeros. The LQG compensator, instead, converges to

the disturbance to performance transfer function minimizing compensator. This compensator, in certain cases, creates a subtraction in the closed loop disturbance to performance transfer function, which is nonrobust as far as practical implementation. This occurs when a test for the ability of a high gain compensator to loop shape is not satisfied. The test is satisfied for a frequency range if the magnitude of the closed loop disturbance to performance transfer function (assuming a high gain compensator), is less than the open loop disturbance to performance magnitude. For Neo-Classical control, if the test is satisfied, then the design rule for Topology II is used. If it is not satisfied, then a rate feedback controller is designed for all frequencies, as it is the best practical compensator.

For noncollocated input output pairs, the Neo-Classical design rules are similar to those previously. However, they are dependent on the pole zero pattern of the input output transfer function. If the pole zero pattern is alternating in the frequency range of interest, the optimal and Neo-Classical compensators are the same as in the previous topologies. If there is a high frequency nonminimum phase zero, the optimal and Neo-Classical compensators are the same as in the previous topologies, up to a bandwidth limited by the nonminimum phase zero. If there is a low frequency nonminimum phase zero, the optimal and Neo-Classical compensators are similar to the previous topologies, with disturbance rejection occurring at higher frequencies. If there is a missing zero pair in the pole zero pattern, the LQG compensator places a zero pair, and higher frequency pole pair, to create a region of alternating poles and zeros. The Neo-Classical design rule also uses this technique.

As the Kalman Filter weighting is made larger, thus adding sensor noise to the compensator design, certain compensation occurred in each topology. The Region 1 controller became high pass filtered. The high frequency rolloff also is steeper, and occurs at a lower frequency than the low noise case.

The Neo-Classical design rules were applied to a variety of topologies on the

MACE test article. The compensators were designed and implemented experimentally as a validations of the rules. Optimal LQG and SWLQG compensators were also designed and implemented on the same topologies. In general, the Neo-Classical compensators were lower order, more robust, and achieved similar or better performance improvement.

The Neo-Classical design rules were adapted to a MIMO experiment on the MACE test article. The Neo-Classical MIMO compensators designed and implemented on the MACE test article had better performance improvement and compensator dimension when compared to the LQG and SWLQG compensators.

Recommendations

The LQG asymptotic analysis compares very well with the LQG compensators when the open loop transfer functions contain alternating poles and zeros. However, when the open loop transfer functions contain nonminimum phase zeros or missing zero pairs, the comparisons are not as easy. The LQG compensators become unstable and/or nonminimum phase. And the rate of convergence to the asymptote is also dependent upon the open loop pole zero patterns. Therefore, this asymptotic analysis should be examined further.

A few MIMO compensators were designed and experimentally implemented on the MACE test article. The MIMO control design problem, however, is a very complex issue. The evidence is not presented to encompass the field of MIMO control design. A few techniques were presented to shown the adaptability of Neo-Classical control design to the MIMO problem, and two types of optimal MIMO compensators, LQG and SWLQG, were used for comparison. This issue is still an area of active research, and should be investigated more thoroughly.

Bibliography

AC-100 Users Guide: Using the AC-100 v.2.4.03A. Integrated Systems Inc., November, 1990.

Ashkenazi, A. and Bryson, A. E. Jr., "Control Logic for Parameter Insensitivity and Disturbance Attenuation," *AIAA J. of Guid., Control, and Dyn.*, Vol. 5, No. 4, July 1982, pp. 383-388.

Aubrun, J.-N., "Theory of the Control of Structures by Low-Authority Controllers," *AIAA Journal of Guidance and Control*, Vol. 13., No. 5, Sept.-Oct. 1980, pp. 444-451.

Balas, M. J., "Modal Control of Certain Flexible Dynamic Systems," *SIAM Journal on Control and Optimization*, Vol. 16, No. 3, pp. 450-462.

Bathe, K. J., *Finite Element Procedures in Engineering Analysis*, Prentice-Hall, Inc., Englewood Cliffs New Jersey, 1982.

Bernstein, D. S. and Haddad, W. M., "The Optimal Projection Equations with Petersen-Hollet Bounds: Robust Stability and Performance via Fixed-order Dynamic compensation for Systems with Structured Real-valued Parameter Uncertainty," *IEEE Trans. on Auto. Control*, Vol. AC-33, 1988, pp. 578-582.

Bernstein, D. S. and Hyland, D. C., "Optimal Projection for Uncertain Systems (OPUS): A Unified Theory of Reduced Order, Robust Control Design," in *Large Space Structures: Dynamics and Control* (Atluri, S. N. and Amos, A. K., eds.), pp. 263-302, Springer-Verlag, New York, 1988.

Bernstein, D. S. and Hyland, D. C., "The Optimal Projection Approach to Robust, Fixed-Structure Control Design," in *Mechanics and Control of Space Structures* (Junkins, J. L. ed.), pp. 237-293, AIAA, Washington D.C., 1990.

Blelloch, P. A., and Mingori, D. L., "Robust Linear Quadratic Gaussian Control of Flexible Structures," *AIAA J. of Guid., Control, and Dyn.*, Vol. 13, No. 1, Jan.-Feb. 1990, pp. 66-72.

Bryson, A. E. Jr., and Ho, Y.-C., *Applied Optimal Control*, Blaisdell Publishing Co., Waltham, MA, 1969.

Crawley, E. F. and Hall, S. R., "The Dynamics of Controlled Structures," Tech. Rep. SERC #10-91-I, M.I.T. Space Engineering Research Center, July 1991.

D'Azzo, J. J., and Houpis, C. H., *Linear Control System Analysis & Design: Conventional and Modern*, McGraw-Hill, Inc. 1988.

Doyle J. C., "Guaranteed Margins for LQG Regulators," *IEEE Trans. on Auto. Control*, Vol. 23, No. 4, August 1978, pp. 756-757.

Doyle, J. C., "Analysis of Feedback Systems with Structured Uncertainties," *IEE Proceedings*, Vol. 129, Part D, No. 6, Nov. 1982, pp. 242-250.

Doyle, J. C., Stein, G., "Multivariable Feedback Design: Concepts for a Classical /Modern Synthesis," *IEEE Trans. on Auto. Control*, Vol. AC-26, 1982, pp. 4-16.

Doyle, J. C., "Structured Uncertainty in Control System Design," *Proceedings, IEEE Conference on Decision and Control*, Ft. Lauderdale, FL, 1985, pp. 260-265

Fan, M. K. H., Tits, A. L., and Doyle, J. C., "Robustness in the Presence of Mixed Parametric Uncertainty and Unmodelled Dynamics," *IEEE Trans. on Auto. Control*, Vol. AC-36, No. 1, Jan. 1991, pp. 25-38.

Fleming, F. M. and Crawley, E. F., "The Zeroes of Controlled Structures: Sensor /Actuator Attributes and Structural Modelling," AIAA Paper No. 91-0984 presented at the *AIAA/ASME/ASCE/AMS 32nd Structures, Structural Dynamics and Materials Conference*, Baltimore, MD, April 1991.

Fleming, F. M., *The Effect of Structure, Actuator and Sensor on the Zeroes of Controlled Structures*, Master's Thesis, Massachusetts Institute of Technology. M.I.T. SERC report #18-90, Dec., 1990.

Freudenberg and Looze, "Right Half Plane Poles and Zeroes and Design Tradeoffs in Feedback Systems," *IEEE Trans. on Automatic Control*, Vol. AC-30, No. 6,

Jan. 1985.

Gevartner, W. B., "Basic Relations of Flexible Vehicles, *AIAA Journal*, Vol. 8, No. 4, April, 1970, pp. 666-672.

Grocott, S. C. O., MacMartin, D. G., and Miller, D. W., "Experimental Implementation of a Multiple Model Technique for Robust Control of the MACE Test Article," to appear in the *Third International Conference on Adaptive Structures*, Nov. 1992.

Grocott, S., Sesak, J., "Sensitivity Weighted LQG controllers," Lockheed Summer Report, August 14, 1992.

Gupta, N., Lyons, M., Aubrun, J., Marguiles, G., "Modelling, Control, and Identification Methods for Flexible Structures," *Spacecraft Pointing and Position Control Conference*, No. 260, 1982, pp. 12-1 - 12-41.

Haddad, W. M., Bernstein, D. S., "Generalized Riccati Equations for the Full- and Reduced-Order Mixed Norm $\mathcal{H}_2/\mathcal{H}_\infty$ Standard Problem," *Systems and Control Letters*, Vol. 14, 1990.

How, J. P., *Robust Control Design with Real Parameter Uncertainty using Absolute Stability Theory*, Master's Thesis, Massachusetts Institute of Technology, 1993.

Hung, Y. S. and MacFarlane, A. G. J., "Multivariable Feedback: A Quasi-classical Approach", *Lecture Notes in Control and Information Sciences*, Vol. 40., Berlin: Springer-Verlag, 1982.

Hyland, D. C. and Richter, S., "On Direct Versus Indirect Methods for Reduced-Order Controller Design," *IEEE Trans. on Auto. Control*, Vol. 35, 1990.

Hyland, D. C., "Maximum Entropy Stochastic Approach to Controller Design for Uncertain Systems," *Proceedings, American Control Conference*, Arlington, VA, June, 1982, pp. 680-688.

Kaileth, T., *Linear Systems*, Prentice-Hall, Inc., Englewood Cliffs, NJ, 1980.

Kalman, R. E., "A new approach to Linear Filtering and Prediction Theory," *Transactions of the ASME (J. Basic Engineering)*, Vol. 82D, No. 1, March, 1960, pp. 35-45.

Kalman, R. E., and Bucy, R. S., "New Results in Linear Filtering and Prediction Theory," *Transactions of the ASME (J. Basic Engineering*, Vol. 83D, No. 1,

March, 1961, pp. 95-108.

Kharitonov, V. L., "Asymptotic Stability of an Equilibrium Position of a Family of Systems of Linear Differential Equations," *Differencial'nye Uravenija*, Vol. 14, No. 11, 1978, pp. 2086-2088.

Kienholz, D. A., "A Pneumatic/Electric Suspension System for Simulating O-Orbit Conditions," 90-WA/Aero-8, presented at the *Winter Annual Meeting of the American Society of Mechanical Engineers*, Dallas, TX, Nov. 1990.

Kuvaritakis, B., "Theory and Practice of the Characteristic Locus Design Method," *Proc. of the Inst. of Elec. Engineers*, Vol. 126, 1979, pp. 542-548.

Kwakernaak and Sivan, *Linear Optimal Control Systems,* Wiley-Interscience, 1972.

Lazarus, K. B., Crawley, E. F., Lin, C. Y., "Fundamental Mechanismsof Aeroelastic Control With Control Surface and Strain Actuation," AIAA paper No. 91-0985, Proc. of the *32nd AIAA/ASME/ASCE/AHS Structures, Structural Dynamics and Materials Conference*, Baltimore MD, April, 1991, pp. 1817-1831.

Ly, U.-L., "A Design Algorithm for Robust Low-Order Controllers," Tech. Rep. SUDAAR 536, Stanford University., Nov. 1982.

MACE Document No. MACE-1-101, Experimental Requirements Document, M.I.T. Space Engineering Research Center, Oct. 1991.

Maciejowski, J. M., *Multivariable Feedback Design*, Addison-Wesley Publishers Ltd., 1989.

MacMartin, D. G., "*An $\mathcal{H}_\infty$ Power Flow Approach to the Control of Uncertain Systems*," S.M. Thesis, Department of Aeronautics and Astronautics, M.I.T., Cambridge MA, Feb. 1990. SERC Report # 5-92.

MacMartin, D. G., Hall, S. R., Bernstein, D. S., "Fixed Order Multi-Model Estimation and Control," *Proc. American Control Conference*, Boston, MA, June 1991, pp. 2113-3118.

Matrixx User's Guide, v.2.03, April, 1990, Integrated Systems Inc.

Mayne, D. Q., "Sequential Design of Linear Multivariable Systems," *Proc. of the Inst. of Elec. Engineers*, Vol. 126, 1979, pp. 568-572.

Mercadel, M. *$\mathcal{H}_2$ Fixed Architecture, Control Design for Large Scale Systems,* Ph.D. Thesis, Department of Aeronautics and Astronautics, M.I.T., Cambridge, MA,

June 1990.

Miller, D. W., and Hall, S. R., "Experimental Results Using Travelling Wave Power Flow Technique," Proc. *ASME Winter Annual Meeting*, AD-Vol. 15, San Francisco, CA, Dec. 1989, pp. 35-42.

Miller, D. W., Jacques, R. N., de Luis, J., "Typical Section Problems for Structural Control Applications," AIAA Paper 90-1255, pres. at the *Dynamics Specialists Conference*, Long Beach, CA, April, 1990.

Miller, D. W., Saarmaa, E., Jacques, R. J., "Preliminary Structural Control Results from the Middeck Active Control Experiment (MACE)," in *AIAA Dynamics and Specialist Conference*, Dallas TX, April 1992, pp. 566-576. Paper AIAA-92-2138-CP.

Miller, D. W., Sepe, R. S., Rey, D., Saarmaa, E., Crawley, E. F., "The Middeck Active Control Experiment (MACE)," pres. at the *CSI Conference*, Lake Tahoe, CA, March 3-6, 1992.

Moore, B., Principal Component Analysis in Linear Systems: Controllability, Observability, and Model Reduction," *IEEE Trans. on Auto. Control*, 26-1, Feb. 1981.

Morton, B. G., and McAfoos, R. M., "A Mu-Test for Robustness Analysis of Real Parameter Variation Problem," *Proceedings, American Control Conference*, May, 1985, pp. 135-138.

Pro-Matlab User's Guide, The Mathworks, July, 1992.

Rey, D., Crawley, E. F., and Glaese, R., "Finite Element Model of the Middeck Active Control Experiment," Preprint, submitted to the 1993 *AIAA Structures, Structural Dynamics, and Materials Conference*, April 1993.

Rosenbrock, H. H., *State-Space and Multivariable Theory*, Nelson, London, 1970.

Saarmaa, E., "Sensor/Actuator Specifications Document," Tech. Rep. MACE Document 1-370, Massachusetts Institute of Technology, October 1991.

Sesak, J. R. and Likins, D. D., "Model Error Sensitivity Suppression: Quasistatic Optimal Control for Flexible Structures," *Proceedings, IEEE Conference on Decision and Control*, Ft. Lauderdale FL, Dec. 1988.

Skelton, R. E., Hughes, P. C., and Hablani, H. B., "Order Reduction for Models of Space Structures Using Modal Cost Analysis," *J. of Guidance, Control, and*

Dyn., Vol. 5, 1982, pp 351-357.

Steiber, M. E., "Sensors, Actuators, and Hyperstability of Structures," *AIAA Guidance, Navigation, and Control Conference*, 1988. Paper No. 88-4047.

Stein, G. and Athens, M., "The LQG/LTR Procedure for Multivariable Feedback Control Design," *IEEE Trans. on Auto. Control*, Vol. AC-32, No. 2, February 1984.

Strang, G., *Linear Algebra and Its Applications*, 2nd ed., Academic Press, 1980.

Wie, B. and Byun, K.-W., "New Generalized Structural Filtering Concept for Active Vibration Control Synthesis,", *J. Guidance, Control, and Dyn.*, Vol. 12, No. 2, March-April 1989, pp. 147-154.

Wie, B. and Gonzalez, M., "Active Control Synthesis for Flexible Space Structures Excited by Persistent Disturbances," AIAA Paper 90-3427, Aug. 1990.

Wie, B., Horta, L., and Sulla, J., "Classical Control System Design and Experiment for the Mini-Mast Truss Structure," *J. Guidance, Control, and Dyn.*, Vol. 14, No. 4, July-August 1991, pp. 778-784.

Yousuff, A. and Skelton, R. E., "Controller Reduction by Component Cost Analysis," *IEEE Trans. on Automatic Control*, Vol. AC-29, 1984, pp. 520-530.

Appendix A

Asymptotic Properties of the SISO LQG Compensator

Doyle and Stein (1982) showed that when the sensor noise is small, or the Kalman Filter weighting μ is small, and there are no nonminimum phase zeros in the transfer function from disturbance G, then the LQR loop is recovered.

$$\lim_{\mu \to 0} K(s) = G(sI - A)^{-1}B\Big(C(sI - A)^{-1}B\Big)^{-1} = G_{LQ}(G_{OL})^{-1} \tag{A.1}$$

where the LQR loop transfer function G_{LQ}, and the open loop transfer function G_{OL}, are given by

$$G_{LQ} = G(sI - A)^{-1}B \tag{A.2}$$

$$G_{OL} = C(sI - A)^{-1}B \tag{A.3}$$

For the general disturbance rejection problem, where the disturbance is not the same as the input, the resulting compensator does not simplify as easily. In this

analysis, a matrix inversion lemma will be used [Kailath (1980)]

$$(A+BCD)^{-1} = A^{-1} - A^{-1}B\left(C^{-1} + DA^{-1}B\right)^{-1}DA^{-1} \tag{A.4}$$

The LQG compensator is given by

$$K(s) = G\left(sI - A + B_u G + HC_y\right)^{-1}H = G\left(\overline{\Phi}^{-1} + HC_y\right)^{-1}H \tag{A.5}$$

where

$$\overline{\Phi} = \left(sI - A + B_u G\right)^{-1} \tag{A.6}$$

Using the matrix inversion lemma twice,

$$K(s) = G\left[\overline{\Phi} - \overline{\Phi}H\left(I + C_y\overline{\Phi}H\right)^{-1}C_y\overline{\Phi}\right]H \tag{A.7}$$

$$K(s) = G\overline{\Phi}H\left[I - \left(I + C_y\overline{\Phi}H\right)^{-1}C_y\overline{\Phi}H\right] \tag{A.8}$$

$$K(s) = G\overline{\Phi}H\left(I + C_y\overline{\Phi}H\right)^{-1} \tag{A.9}$$

The above compensator is then split into two parts. The first of which is again simplified using the matrix inversion lemma twice.

$$G\overline{\Phi}H = G\left(\Phi^{-1} + B_u G\right)^{-1}H \tag{A.10}$$

$$G\overline{\Phi}H = G\left[\Phi - \Phi B_u\left(I + G\Phi B_u\right)^{-1}G\Phi\right]H \tag{A.11}$$

$$G\overline{\Phi}H = \left[I - G\Phi B_u\left(I + G\Phi B_u\right)^{-1}\right]G\Phi H \tag{A.12}$$

$$G\overline{\Phi}H = \left[I + G\Phi B_u\right]^{-1}G\Phi H \tag{A.13}$$

The second part of the problem is simplified in a similar manner.

$$I + C_y \bar{\Phi} H = I + C_y \left(\Phi^{-1} + B_u G\right)^{-1} H \tag{A.14}$$

$$I + C_y \bar{\Phi} H = I + C_y \left[\Phi - \Phi B_u (I + G\Phi B_u)^{-1} G\Phi\right] H \tag{A.15}$$

$$I + C_y \bar{\Phi} H = I + C_y \Phi \left[I - B_u (I + G\Phi B_u)^{-1} G\Phi\right] H \tag{A.16}$$

$$I + C_y \bar{\Phi} H = I + C_y \Phi \left[I + G\Phi B_u\right]^{-1} H \tag{A.17}$$

Substituting the results from Equations A.13 and A.17 into A.9, the LQG compensator becomes

$$K(s) = \left[I + G\Phi B_u\right]^{-1} G\Phi H \left(I + C_y \Phi \left[I + G\Phi B_u\right]^{-1} H\right)^{-1} \tag{A.18}$$

This compensator can be further simplified by assuming the compensator is single input, single output (SISO), or there is one performance, disturbance, input, and output.

$$K(s) = \frac{G\Phi H}{1 + G\Phi B_u} \left[1 + \frac{C_y \Phi H}{1 + G\Phi B_u}\right]^{-1} \tag{A.19}$$

$$K(s) = \frac{G\Phi H}{1 + G\Phi B_u} \left[\frac{1 + G\Phi B_u + C_y \Phi H}{1 + G\Phi B_u}\right]^{-1} \tag{A.20}$$

$$K(s) = \frac{G\Phi H}{1 + G\Phi B_u + C_y \Phi H} \tag{A.21}$$

Equation A.21 shows the SISO LQG compensator for given LQR and Kalman Filter gain matrices G and H.

For the low noise result of the SISO Kalman Filter, or as the Kalman Filter

weighting μ tends to zero, the optimal gains are given by [Kwakernaak and Sivan (1972)]

$$\underset{\mu\to 0}{LIM}\, H = \frac{1}{\sqrt{\mu}} B_w W_H = \frac{\pm 1}{\sqrt{\mu}} B_w \tag{A.22}$$

where W_H is an orthonormal matrix, or ±1 in the SISO case.

$$W_H^T W_H = I = 1 \tag{A.23}$$

This result is dependent upon the disturbance to output transfer function $C_y \Phi B_w$ being minimum phase.

Similarly, for cheap control in the LQR problem, or as the LQR weighting ρ tends to zero, the optimal LQR gains are given by

$$\underset{\rho\to 0}{LIM}\, G = \frac{1}{\sqrt{\rho}} W_G C_z = \frac{\pm 1}{\sqrt{\rho}} C_z \tag{A.24}$$

whereW_G is an orthonormal matrix, or ±1 in the SISO case.

$$W_G^T W_G = I = 1 \tag{A.25}$$

This result is dependent upon the input to performance transfer function $C_z \Phi B_u$ being minimum phase.

This leads to the following simplified SISO LQG compensator, for low noise and cheap control.

$$\underset{\substack{\mu\to 0\\ \rho\to 0}}{LIM}\, K(s) = \frac{\pm \frac{1}{\sqrt{\rho}} \frac{1}{\sqrt{\mu}} C_z \Phi B_w}{\pm \frac{1}{\sqrt{\rho}} C_z \Phi B_u \pm \frac{1}{\sqrt{\mu}} C_y \Phi B_w} \tag{A.26}$$

For the expensive control, low noise SISO compensator, the asymptotic optimal gain matrix of the LQR problem is used. MacMartin (1990) showed that for

the expensive LQR problem, the optimal gain matrix G is

$$\underset{\rho\to\infty}{LIM}\, G = \frac{1}{\sqrt{\rho}} \sum_i \sqrt{v_i^H Q v_i} \left[\frac{\left(w_i^H B_u\right)^H}{\left|w_i^H B_u\right|} \right] w_i^H \tag{A.27}$$

where v_i and w_i are the right and left eigenvectors of the system matrix A, and the superscript H denotes a complex conjugate transpose.

For single input single output systems, the entire quantity is a constant, except for the last term, w_i^H. This states that the optimal LQR feedback gains are a weighted combination of the left eigenvectors. Lazarus (1991) showed that in the expensive control case, the gains are nonzero only for the rate states. The LQR compensator is equivalent to a rate feedback sensor. The expensive control, low noise LQG compensator is then given by

$$\underset{\substack{\mu\to 0\\ \rho\to\infty}}{LIM}\, K(s) = \frac{G\Phi B_w}{C_y \Phi B_w} \tag{A.28}$$

where G is the expensive control, LQR gain matrix given in Equation A.27.

Note that if in the MIMO case, the low noise, expensive LQG asymptote can be shown to be

$$\underset{\substack{\mu\to 0\\ \rho\to\infty}}{LIM}\, K(s) = G\Phi B_w \left[C_y \Phi B_w\right]^{-1} \tag{A.29}$$

The low noise, cheap control LQG asymptote for the MIMO problem does not simplify.

Appendix B

Typical Section Model

The typical section model was made using a Rayleigh-Ritz analysis [Bathe (1982)] of a cantilever beam. First, the beam was segmented into four beam elements, each with the same properties. Figure B.1 shows a beam element, with four generalized degrees of freedom, i.e. the vertical position of each end, u_i, and rotation of each end, v_i, and with four generalized loads, i.e. a vertical force, r_i, and torque, t_i, at each end.

For each beam element, there is a generalized mass and stiffness matrix, given by

$$k_i = \frac{EI}{L}\begin{bmatrix} 12 & 6L & -12 & 6L \\ 6L & 4L^2 & -6L & 2L^2 \\ -12 & -6L & 12 & -6L \\ 6L & 2L^2 & -6L & 4L^2 \end{bmatrix} \tag{B.1}$$

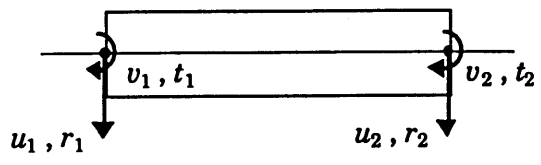

Figure B.1. Generalized beam element.

$$m_i = \rho AL \begin{bmatrix} 1 & 0 & 0 & 0 \\ 0 & 0 & 0 & 0 \\ 0 & 0 & 1 & 0 \\ 0 & 0 & 0 & 0 \end{bmatrix} \tag{B.2}$$

The properties of this model are given in Table B.1.

Table B.1. Properties of the typical section model.

Parameter	Value
EI	10
L	0.5
ρA	1

The four beam elements are then assembled into a global system, with 10 generalized degrees of freedom, U_i and V_i, and 10 generalized loads, R_i and T_i. These are shown in Figure B.2.

Applying the boundary conditions of the cantilever beam, and condensing out the two degrees of freedom and two loads at node 5, the global mass and stiffness matrices can then be put in matrix form.

$$\begin{bmatrix} M_{UU} & M_{UV} \\ M_{VU} & M_{VV} \end{bmatrix} \begin{Bmatrix} \ddot{U} \\ \ddot{V} \end{Bmatrix} + \begin{bmatrix} K_{UU} & K_{UV} \\ K_{VU} & K_{VV} \end{bmatrix} \begin{Bmatrix} U \\ V \end{Bmatrix} = \begin{Bmatrix} R \\ T \end{Bmatrix} \tag{B.3}$$

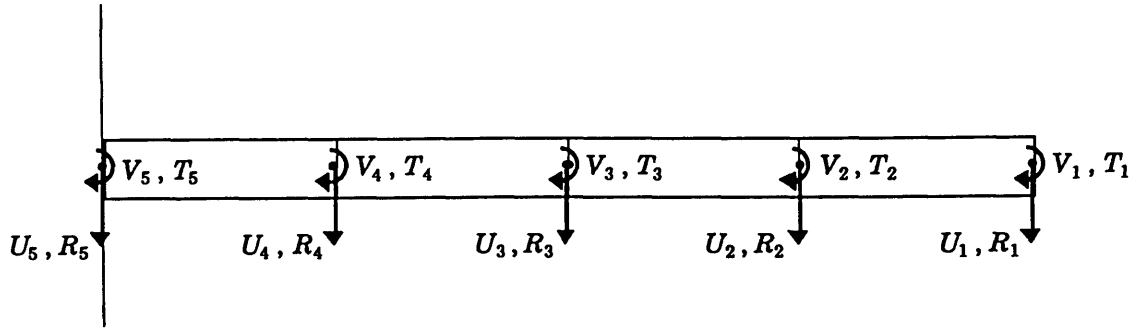

Figure B.2. Cantilever beam made up of four beam elements.

where U and V are the 8 degrees of freedom, and R and T are the 8 loads.

$$U^T = [U_1 \quad U_2 \quad U_3 \quad U_4] \tag{B.4}$$

$$V^T = [V_1 \quad V_2 \quad V_3 \quad V_4] \tag{B.5}$$

$$R^T = [R_1 \quad R_2 \quad R_3 \quad R_4] \tag{B.6}$$

$$T^T = [T_1 \quad T_2 \quad T_3 \quad T_4] \tag{B.7}$$

Four static load patterns, q_i, are then used to generate four Ritz vectors.

$$Q = [q_1 \quad q_2 \quad q_3 \quad q_4] = \begin{Bmatrix} I_{4x4} \\ 0_{4x4} \end{Bmatrix} \tag{B.8}$$

The four load patterns are vectors of all zeros, with a value of one at the ith vertical force R_i, shown in Figure B2. The Ritz vectors, Ψ, are then found by solving the static problem

$$K\Psi = Q \tag{B.9}$$

These 8x4 Ritz vectors are then used to create the mass and stiffness matrices which span the subspace of the Ritz vectors, or

$$\tilde{K} = \Psi^T K \Psi \tag{B.10}$$

$$\tilde{M} = \Psi^T M \Psi \tag{B.11}$$

Next, an eigenvalue problem is made, using the new mass and stiffness matrices.

$$\tilde{K}\Phi = \Lambda \tilde{M}\Phi \tag{B.12}$$

The approximation of the eigenvectors for the system are now given by projecting

these eigenvectors over the subspace of Ritz vectors, or

$$\hat{\Phi} = \Psi\Phi \tag{B.13}$$

These eigenvectors are then used to find diagonal 4x4 mass and stiffness matrices, giving the modal form of the system.

$$\hat{K} = \hat{\Phi}^T \tilde{K} \hat{\Phi} \tag{B.14}$$

$$\hat{M} = \hat{\Phi}^T \tilde{M} \hat{\Phi} \tag{B.15}$$

The mass and stiffness matrices are then put into state space form, with 1% damping added to each of the four modes. The resulting system has 8 states , 4 inputs and disturbances as the vertical force at each degree of freedom, and 4 outputs as vertical velocity at each degree of freedom, and 4 performances as the vertical position at each degree of freedom. The state space system is given by

$$\dot{x} = Ax + B_u u + B_w w \tag{B.16}$$

$$y = C_y x \tag{B.17}$$

$$z = C_z x \tag{B.18}$$

where the system matrices are

$$A = \begin{bmatrix} 0 & I \\ -M^{-1}K & -(2)(0.01)\sqrt{(M^{-1}K)} \end{bmatrix} \tag{B.19}$$

$$B_u = \begin{bmatrix} 0 \\ M^{-1}\hat{\Phi}^T R \end{bmatrix} \tag{B.20}$$

$$C_y = \begin{bmatrix} 0 & R^T\hat{\Phi} \end{bmatrix} \tag{B.21}$$

$$C_z = \begin{bmatrix} R^T\hat{\Phi} & 0 \end{bmatrix} \tag{B.22}$$

Appendix C

Open Loop Transfer Functions: Finite Element Model and Data

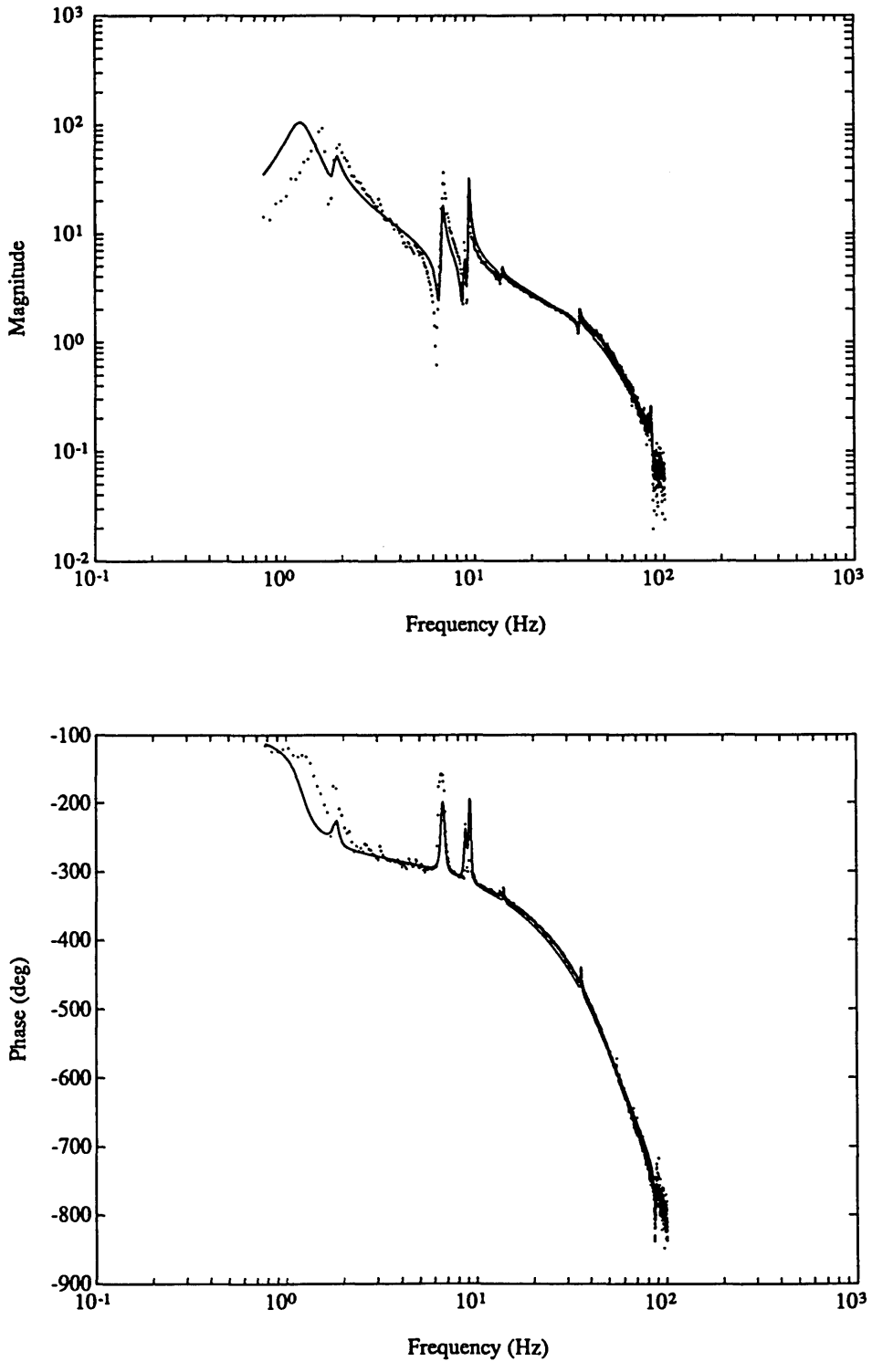

Figure C.1. Transfer function from z-axis gimbal to z-axis payload rate gyro.

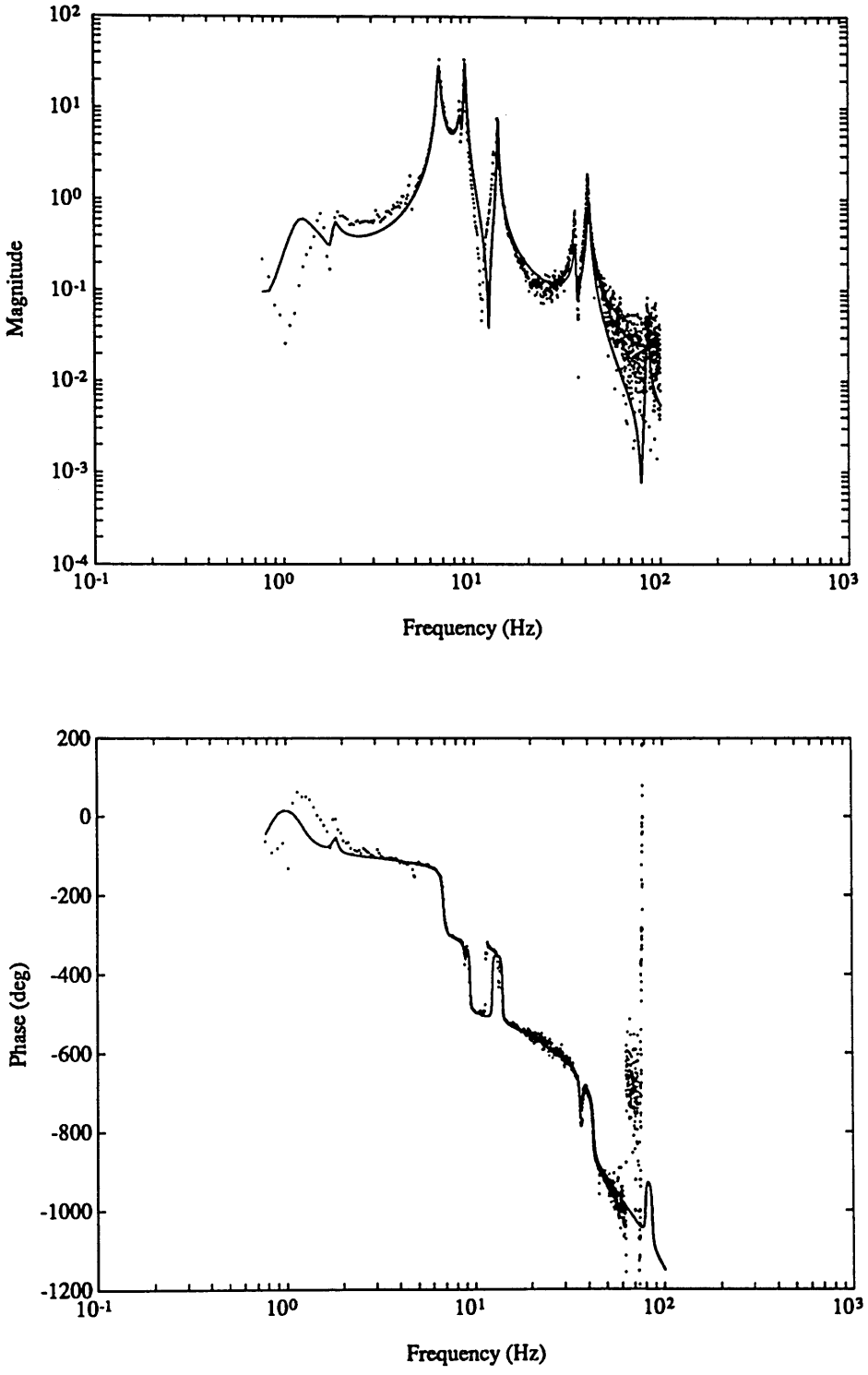

Figure C.2. Transfer function from z-axis gimbal to z-axis bus rate gyro.

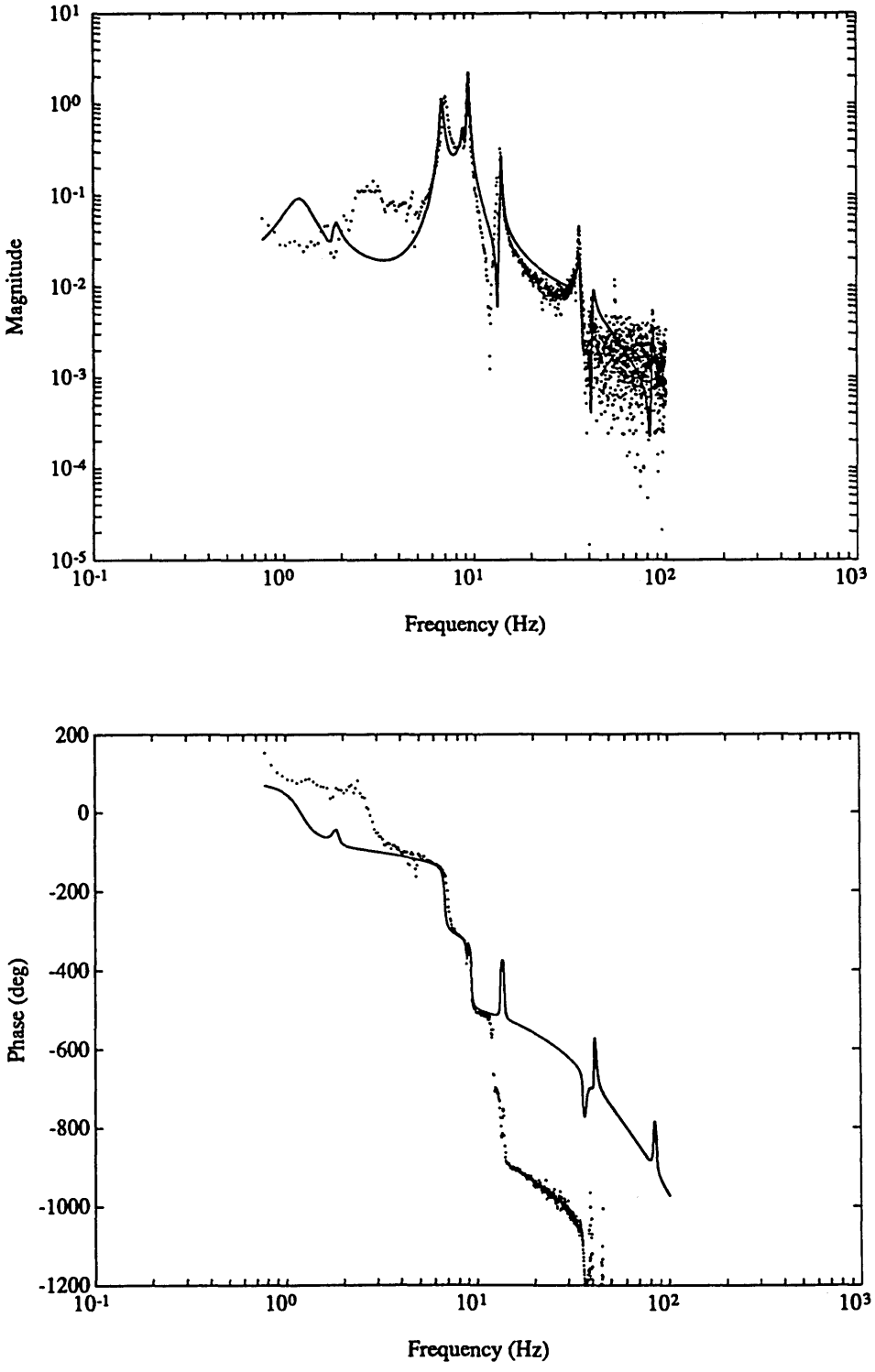

Figure C.3. Transfer function from z-axis torque wheels to z-axis payload rate gyro.

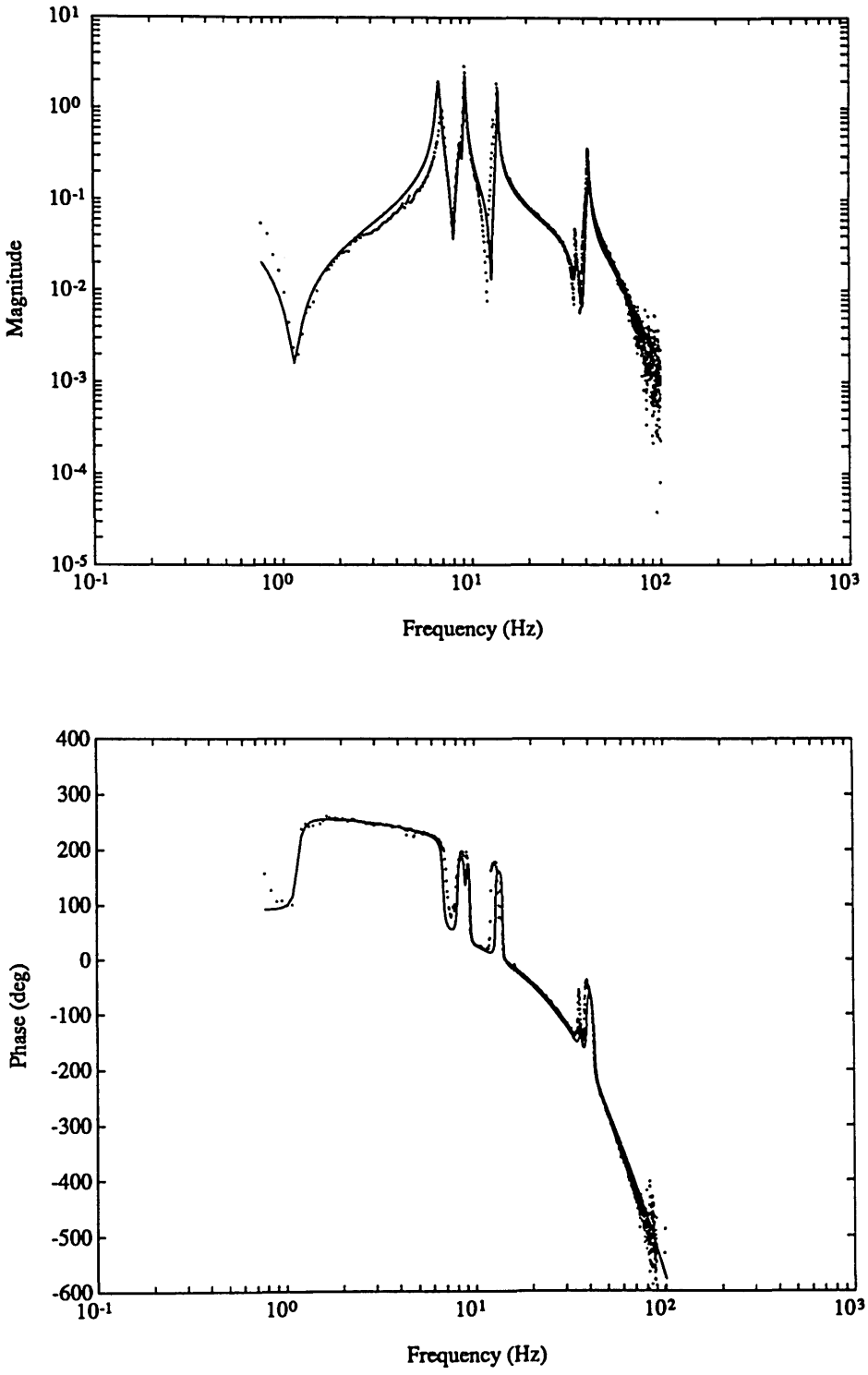

Figure C.4. Transfer function from z-axis torque wheels to z-axis bus rate gyro.

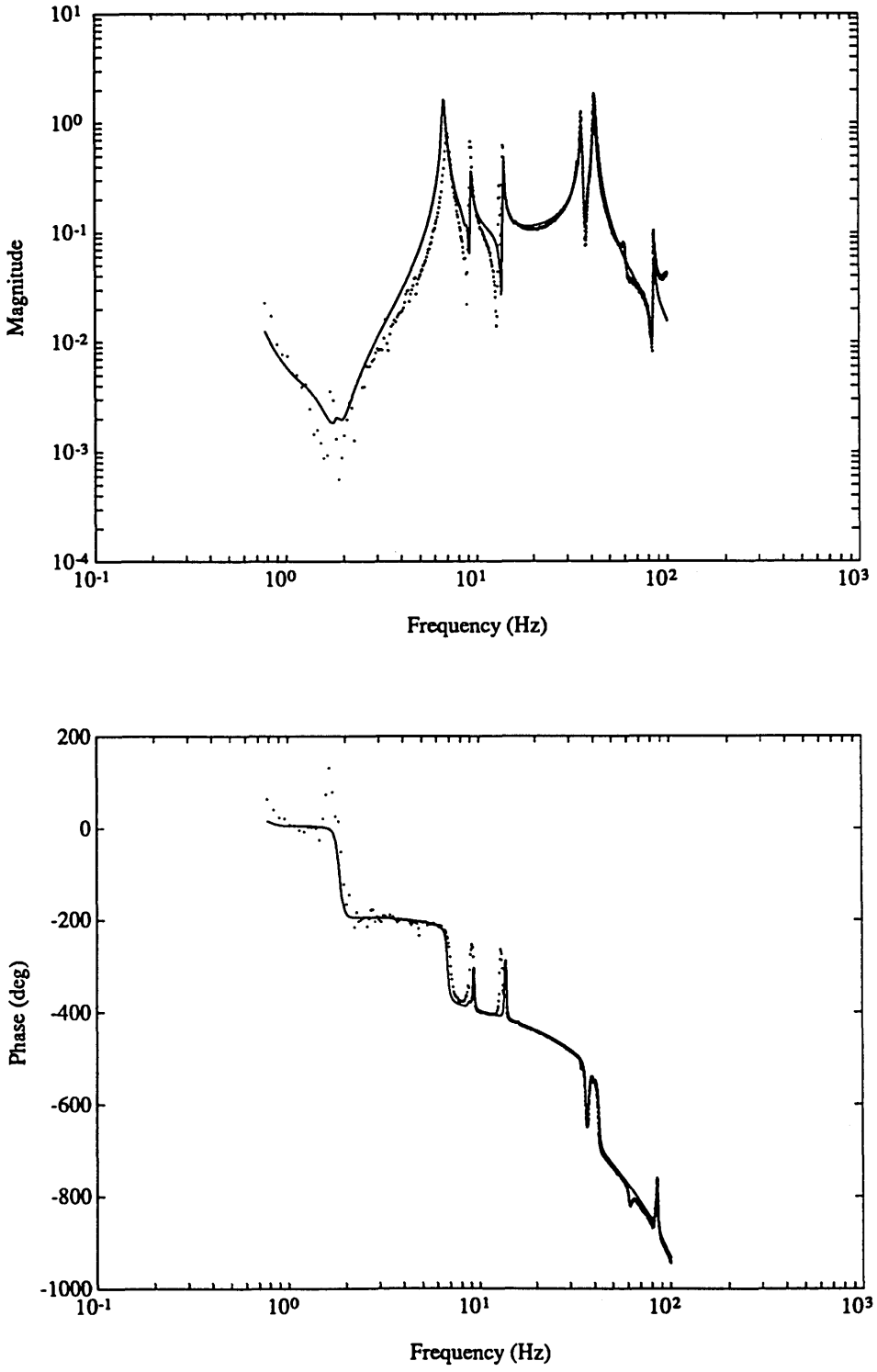

Figure C.5. Transfer function from z-axis torque wheels to y-axis accelerometer.